Dynamics and Design of Nonholonomic Robotic Mechanical Systems

by

Subir Kumar Saha

B. E. (REC, Durgapur, India), 1983

M. Tech. (IIT, Kharagpur, India), 1985

Department of Mechanical Engineering

McGill University, Montreal

Canada

A thesis submitted to the Faculty of Graduate Studies and Research
in partial fulfillment of the requirements for the degree of
Doctor of Philosophy

September 23, 1991

Abstract

This thesis presents a novel approach in formulating kinematic constraints and a methodology for the dynamic modelling of mechanical systems with nonholonomic couplings. The method presented here is based on the natural orthogonal complement (NOC) of the kinematic constraint matrix associated with the linear homogeneous form of the kinematic constraints. The method of the NOC is used to model mechanical systems consisting of multiple-loop kinematic chains with nonholonomic constraints. Moreover, the method of the NOC, when coupled with an optimization technique, can be used for the feedforward control of redundantly actuated systems, as shown here.

The method of the NOC is first discussed in detail with the aid of an example of a two-wheeled mechanical system. Then, nonholonomic robotic mechanical systems, for example, automatic guided vehicles (AGVs), are analysed for simulation purposes. As a result, general-purpose software is developed for the kinematic and dynamic analyses of three-degree-of-freedom (3-DOF) AGVs. These AGVs use omnidirectional wheels which, in contrast to conventional wheels, e.g., the wheels in an automobile, result in 3-DOF motion of the vehicle. Isotropic designs of 3-DOF AGVs for direct kinematics are proposed, which should enhance the control of the vehicle.

With advanced computer graphics, a common trend is to use motion animation in assessing the time response of the systems under study. This brought about issues of algorithmic complexity that are inherent to motion animation. These issues are addressed with an example involving the attitude representation of a rigid body and the choice of a suitable coordinate frame in representing the dynamic equations of motion.

Résumé

Cette thèse presente une approche originale à la formulation des contraintes cinématiques et une méthode pour modeler la dynamique de systèmes à couples non-holonomes. La méthode est basée sur l'idée générale du complément orthogonal naturel de la matrice correspondant à la forme linéaire homogène des contraintes cinématiques. La méthode du complément orthogonal naturel se prête bien à la simulation de systèmes comprenant plusieurs boucles cinématiques. En outre, en la liant à des méthodes d'optimisation, la commande en boucle ouverte de systèmes à motorisation redondante est obtenue.

La méthode du complément orthogonal naturel est présentée en détail avec l'aide d'un exemple d'un système mécanique à deux roues. Puis, les systèmes robotiques non-holonomes, tel que les véhicules autonomes, font l'objet d'une étude approfondie. Un logiciel à usage général est donc mis au point pour permettre l'analyse cinématique et dynamique des véhicules autonomes à trois degré de liberté (3 ddl) Ces derniers sont munis de roues omnidirectionnelles qui, contrairement aux roues d'une automobile, permettent au véhicule un mouvement à 3 ddl . La conception d'un véhicules autonomes isotrope et à 3 ddl est presentée, a fin de faciliter la commande du véhicule.

L'animation graphique devient de plus en plus répandue comme outil servant à l'analyse de systèmes mécano-robotiques. La question de complexité algorithmique des méthodes d'analyse devient alors importante et est donc adressée Comme illustration, un exemple traitant de la représentation de l'orientation d'un corps rigide est présenté, l'importance du choix d'un repère convenable pour la représentation des équations dynamiques étant démontré.

Claim of Originality

The author claims the originality of the items listed below:

- A new criterion is developed to classify kinematic constraints of mechanical systems. In order to detect the holonomicity of kinematic constraints, two lemmas are provided along with their proofs.
- The dynamic modelling of nonholonomic mechanical systems based on the natural orthogonal complement (NOC) of the kinematic constraint matrix, that results from the linear homogeneous kinematic constraints, is developed.
- The degree-of-freedom (DOF) and controllability information of a system may be obtained as a part of the dynamic model of a mechanical system using the NOC. Thus, the time required to separately determine the DOF of a system and to test its controllability is eliminated.
- The developed dynamic modelling technique, mentioned in the second item above, is coupled with an optimization technique to analyse the dynamics of nonholonomic systems with redundant actuation and inequality constraints.
- Computer software for the kinematic and dynamic analyses of 3-DOF automatic guided vehicles (AGVs) of arbitrary architecture consisting of omnidirectional wheels is developed.
- A concept of isotropic design for the direct kinematics of 3-DOF AGVs is introduced that will ease the control of these vehicles.
- The dependence of efficiency and accuracy of the simulation and animation code on coordinate frames in representing the dynamic model of a system is extensively analysed.
- Alternative approaches of attitude representation of rigid bodies for simulation purposes are introduced with a discussion on their merits and demerits. Suggestions are made for the motion animation of mechanical systems.

This research work has been partially reported by Saha and Angeles (1989, 1991a, 1991b, 1991c, 1991d) in journals and conference proceedings.

Acknowledgements

I would like to extend my sincere thanks and deep gratitude to my supervisor, Prof. Jorge Angeles, for his continuous guidance, assistance and inspiration without which this thesis could not have been completed. His depth of knowledge, clear explanations and elegant presentations have always helped me to understand, analyse and solve a problem in a unified way. Needless to say, this thesis has greatly benefited from the comments that he made after reading the manuscript.

I am thankful to the McGill University faculty with whom I have taken several graduate-level courses, particularly, Prof. M. P. Paidoussis, Prof. A. K. Mista, Dr. G. X. Li, of the Department of Mechanical Engineering and Prof. C. C. Paige, of the School of Computer Science, for their well organized presentations of the state-of-the-art course materials. These courses helped me in quickly understanding the publications related to the research on dynamics of mechanical systems and robotics.

I am grateful to the Government of India for their scholarship under the "Scheme of Scholarship for Studying Abroad" without which this work would have never been possible. Moreover, the research work reported in this thesis was possible under NSERC (Natural Science and Engineering Research Council, of Canada) Research Grant No. A4532, Equipment Grant No. EQP00-92729, FCAR (Fonds pour la formation de chercheurs et l'aide à la recherche, of Quebec) Grant No. 88AS2517, along with the partial support from the Institute for Robotics and Intelligent Systems, a network of Canadian centres of excellence.

My Master's supervisor Prof. A. B. Chattopadhyay and my cousin Prof. S. C. Ray, both at Indian Institute of Technology (IIT), Kharagpur, India, have provided me with invaluable help, suggestions and inspiration, both before and after coming to Canada.

The love and care of my parents Nitya Gopal Saha and Hiramati Saha have always been a constant source of my enthusiasm to complete this work. My brother's and sister's families, Prabir, Swapna, Pratik, and Chandralekha, Aveek, Averi and Avishek have also encouraged me in doing this research.

I am indebted to my friends Simon Dancose, *IBM Inc.*, Montreal, Ou Ma and Saumyendra Mathur, *SPAR Aerospace Ltd.*, Toronto, Roger Cormier, Jr., *NISSAN Motors Co. Ltd.*, Japan, Clément Gosselin, *Laval University*, Quebec City, Meyer

Nahon, *University of Victoria*, Victoria, Xavier Cyril, *CAE Electronics*, Montreal, who graduated from McGill University, and my fellow graduate students John Darcovich, Liu Zheng and Robert Lucyshyn for the invaluable discussions I had with them and their warm amicability.

The immense patience of my friend Slobodan Lazar in proofreading my thesis is honestly appreciated and my hearty thanks go to Meyer Nahon for translating the abstract of my thesis into French. Moreover, the well-equipped and pleasant environment of the McGill Research Centre for Intelligent Machines has made my work and stay enjoyable. Also, the assistance from the Department of Mechanical Engineering is truly acknowledged. Last but not least, I would like to recall all my friends at IIT, Kharagpur and in Montreal, my relatives, and many others whose direct or indirect contribution made this research possible.

Dedicated to
My parents

Contents

List of Figures

List of Tables

Chapter 1

Introduction

A mechanical system consists of rigid bodies coupled by kinematic pairs. Rigid bodies in a mechanical system are called *links*. Kinematic pairs that restrict the independent motion of the links are known as *joints* or *couplings*. In a mechanical system, a set of links coupled by joints forms a *kinematic chain*. Kinematic chains may be *simple* or *complex*. Simple chains are defined here as kinematic chains containing links having a *degree of connectivity* smaller than or equal to two. It is recalled that the degree of connectivity of a link is the number of rigid bodies that are coupled to the said link by joints. Therefore, simple kinematic chains encompass both serial manipulators and closed single-loop linkages. On the other hand, complex kinematic chains are those containing at least one link having a degree of connectivity greater than or equal to three, for example, automatic guided vehicles and parallel manipulators. A joint that allows a restrictive motion of the rigid bodies in a kinematic chain, thus, leads to *kinematic constraints*. The characteristics of kinematic constraints, apart from the type of a kinematic pair, i.e., a joint or a coupling, depend on the *topology* of the system. The topology of a kinematic chain is defined as a description of the number of links and joints in a system and their interconnections, disregarding geometric details such as link lengths and shapes.

In dynamic analyses of mechanical systems, i.e., design, simulation and control of mechanical systems, kinematic constraints play a vital role. While deriving the

dynamic model of a mechanical system, these constraints are treated differently, depending on the modelling techniques, as in Kane (1968), Meirovitch (1970), Huston and Passerello (1974) and Muir and Neuman (1988). The kinematic formulation affects the complexity of the derivation of the dynamic equations of motion, as discussed in Chapters 2 and 3, where several approaches are presented for the dynamic modelling of mechanical systems.

A review of kinematic constraints is given in the section below. Their definitions, characteristics and differences are illustrated in order to provide a clear understanding of the forms of kinematic constraints, to address the associated difficulties due to the physics of the joints and to decide upon the mathematical tools necessary in coping with such difficulties. This will also help in understanding the terminology and the methods used in this thesis.

1.1 Classification of Mechanical Systems According to their Kinematic Constraints

In mechanical systems, kinematic constraints are represented by a set of algebraic or differential equations. The existence of algebraic constraints means that a set of corresponding differential equations exists. However, the reverse is not true, i.e., the existence of differential kinematic constraints does not mean that a corresponding set of algebraic equations exists. In the former case, where a set of algebraic equations exists, the constraint equations are called *holonomic* constraints, whereas, in the latter case, the differential constraint equations that do not have equivalent algebraic equations are known as *nonholonomic* constraints. Thus, based on the type of constraints, mechanical systems may be classified as *holonomic* or *nonholonomic* systems. A mechanical system in which all joints lead to holonomic constraints is called a holonomic mechanical system. On the contrary, if the mechanical system has at least one nonholonomic constraint, it is known as a nonholonomic mechanical system. Throughout this thesis, a mechanical system is assumed to consist of m

independent constraints, of which h are holonomic and n are nonholonomic. Thus,

$$m = h + n$$

Moreover, p denoting the number of *generalized coordinates* that are defined as those variables which give an unambiguous representation of the configuration of the system, i.e., with the help of these coordinates, a unique configuration of the system in the 3-dimensional Cartesian space is possible, is greater than m.

1.1.1 Holonomic Constraints

A *holonomic*[1] constraint may be defined as a constraint that can be expressed by an algebraic, usually nonlinear, relation amongst the generalized coordinates and, possibly, time. The set of generalized coordinates is not unique, as there is more than one set of coordinates capable of describing the configuration of the system uniquely. However, the sets of generalized coordinates must be finite, single-valued and continuous functions that are twice differentiable with respect to time. Now, the constraints arising due to the presence of the joints and the topology of the kinematic chains of the holonomic system are expressed as

$$\mathbf{f}(\boldsymbol{\theta}, t) = \mathbf{0} \tag{1.1}$$

where $\mathbf{f}$ is a vector function of class C^2 (Rudin, 1976), $\boldsymbol{\theta}$ is a p-dimensional vector whose components are the generalized coordinates and t denotes time. It is assumed here that the mechanical system at hand consists of h holonomic constraints only, i.e., it is assumed that $n = 0$. Thus, $\mathbf{f}$ is an h-dimensional vector that is defined, along with $\boldsymbol{\theta}$, as

$$\mathbf{f} \equiv [f_1, \cdots, f_h]^T \quad \text{and} \quad \boldsymbol{\theta} \equiv [\theta_1, \cdots, \theta_p]^T$$

Furthermore, the holonomic constraints of eq.(1.1) can be differentiated with respect to time, which yields a linear relation amongst the *generalized speeds*, $\dot{\boldsymbol{\theta}}$, namely,

$$\mathbf{J}\dot{\boldsymbol{\theta}} + \mathbf{b} = \mathbf{0} \tag{1.2}$$

[1]The word *holonomic* is derived from the Greek word *holos*, which means whole.

where $\mathbf{J}$ is an $h \times p$ matrix and $\mathbf{b}$ is an h-dimensional vector, both, in general, being functions of the generalized coordinates and time. Note that the left-hand side of eq (1.2) is the total derivative of $\mathbf{f}(\boldsymbol{\theta}, t)$ with respect to time, i.e.,

$$\mathbf{J} = \frac{\partial \mathbf{f}}{\partial \boldsymbol{\theta}} \quad \text{and} \quad \mathbf{b} = \frac{\partial \mathbf{f}}{\partial t} \tag{1.3}$$

and hence, one can obtain eq.(1.1) by integrating the expression given in eq.(1.2). What follows is that, for holonomic systems, the kinematic constraints in the form of eq.(1.2) are *integrable* and eq.(1.3) forms the basis for the necessary and sufficient conditions for integrability of differential equations in the form of eq.(1.2) (Ince, 1956; Spiegel, 1985). These holonomicity conditions for the kinematic constraint equations of a mechanical system can be stated as: all $p \times p$ matrices, each of which is derived as the gradient of $\mathbf{j}_i$ with respect to $\boldsymbol{\theta}$, i.e., $\partial \mathbf{j}_i / \partial \boldsymbol{\theta}$, for $i = 1, \cdots, h$, where $\mathbf{j}_i$ is the ith column of matrix $\mathbf{J}^T$, must be symmetric. In addition,

$$\frac{\partial b_i}{\partial \boldsymbol{\theta}} = \frac{\partial \mathbf{j}_i}{\partial t}, \qquad \text{for} \quad i = 1, \cdots, h$$

where b_i is the ith element of vector $\mathbf{b}$.

Alternatively, integrability conditions can be obtained, as in Isidori (1985) and Nakamura and Mukherjee (1990), by using the definitions below and a theorem from nonlinear control theory.

Definition 1.1 Lie bracket: If vector $\mathbf{x}$, and two vector fields $\mathbf{f}_1(\mathbf{x})$ and $\mathbf{f}_2(\mathbf{x})$ belong to an open subset U of $\mathbf{R}^n$, then the Lie bracket or Lie product of $\mathbf{f}_1$ and $\mathbf{f}_2$, denoted by $[\mathbf{f}_1, \ \mathbf{f}_2]$, is a third vector field defined by

$$[\mathbf{f}_1, \ \mathbf{f}_2](\mathbf{x}) = \frac{\partial \mathbf{f}_2}{\partial \mathbf{x}} \mathbf{f}_1(\mathbf{x}) - \frac{\partial \mathbf{f}_1}{\partial \mathbf{x}} \mathbf{f}_2(\mathbf{x})$$

Definition 1.2 Involutive distribution: A linearly independent set of vector fields $\{\mathbf{f}_1, \cdots, \mathbf{f}_m\}$ is said to be involutive if, and only if, there exist scalar functions α_{ijk} such that

$$[\mathbf{f}_i, \ \mathbf{f}_j] = \sum_{k=1}^{m} \alpha_{ijk} \mathbf{f}_k$$

Theorem 1.1 Frobenius's Theorem: Let $\{\mathbf{f}_1, \cdots, \mathbf{f}_m\}$ be a set of vector fields that are linearly independent at each point $\mathbf{x}$. Then, the set of vector fields is said to be completely integrable if, and only if, it is involutive.

The presence of *integral forms* of kinematic constraints in a holonomic system, as in eq.(1.1), allows the dimension of the vector of generalized coordinates to be reduced to a minimal set of generalized coordinates. In fact, by solving for h of the p generalized variables from the h constraints, the number of generalized coordinates is reduced to q, where $q \equiv p - h$. Moreover, these q coordinates are now independent and any arbitrary infinitesimal change in these q coordinates represents a *possible* displacement of the system. Note that the degree-of-freedom (DOF) of a system is defined as the number of *independent generalized coordinates* that are necessary and sufficient to *control* the system such that, given a certain configuration, any arbitrary change of these coordinates will move the system to another configuration. That is, using q independent coordinates, it is possible to move the system from a known configuration to another desired configuration. Thus, the DOF of the holonomic system at hand is q. This leads to a result for holonomic systems: In a holonomic system, the *minimum* number of generalized coordinates required to completely specify the configuration of the system is equal to the DOF of the system.

In dynamics, the motion of a system can be treated in terms of the motion of a point in a multi-dimensional space termed the *configuration space* (Neĭmark and Fufaev, 1967). For a holonomic system, the dimension of the configuration space is equal to its DOF, i.e., q, and hence, at any instant, the system can be described by a vector $\boldsymbol{\theta}$ in a q-dimensional space.

Finally, a holonomic constraint may be distinguished as either *scleronomic* or *rheonomic*[2], as described below:

[2] *scleronomic* and *rheonomic* owe their names to the Greek words *sklerós* and *rheo*, whose meanings are *hard* and *to flow*, hence changeable, respectively.

- *scleronomic*: Holonomic constraints in which time t does not appear explicitly are known as scleronomic constraints, i.e., the constraints can be expressed as

$$\mathbf{f}(\boldsymbol{\theta}) = \mathbf{0} \quad \text{or} \quad \mathbf{J}\dot{\boldsymbol{\theta}} = \mathbf{0}$$

- *rheonomic*: Contrary to scleronomic constraints, if one of the holonomic constraints in a set of constraint equations contains t explicitly, as in eq.(1.1) or eq.(1.2), then they are referred to as rheonomic constraints, i.e.,

$$\mathbf{f}(\boldsymbol{\theta}, t) = \mathbf{0} \quad \text{or} \quad \mathbf{J}\dot{\boldsymbol{\theta}} = -\mathbf{b}$$

1.1.2 Nonholonomic Constraints

Nonholonomic constraints, first identified by Hertz in 1894 (Neĭmark and Fufaev, 1967), restrict the *kinematically possible* motions, i.e., the possible values of the velocities of the individual links, of the system. For simplicity, it is assumed that the h holonomic constraints allow the elimination of h generalized coordinates, the number of generalized coordinates needed to describe the system thus being reduced to $p - h$.

Unlike holonomic constraints, eq.(1.2), for nonholonomic systems, is *nonintegrable*, i.e., the differential expression involved does not amount to the total time derivative of any vector function $\mathbf{f}(\boldsymbol{\theta}, t)$. Moreover, since no algebraic function of the generalized coordinates can be derived from nonholonomic constraints, n generalized coordinates cannot be expressed in terms of other generalized coordinates. Thus, a nonholonomic system can be defined as *a mechanical system in which the minimum number of the generalized coordinates required to specify the configuration of the system at any time is greater than the DOF of the system.*

A distinguishing property of a nonholonomic system is that not all variations of its generalized coordinates, irrespective of how they are chosen, correspond to a motion of the system satisfying its constraints. Moreover, contrary to holonomic constraints, the constraints on the admissible velocities of the individual parts of a

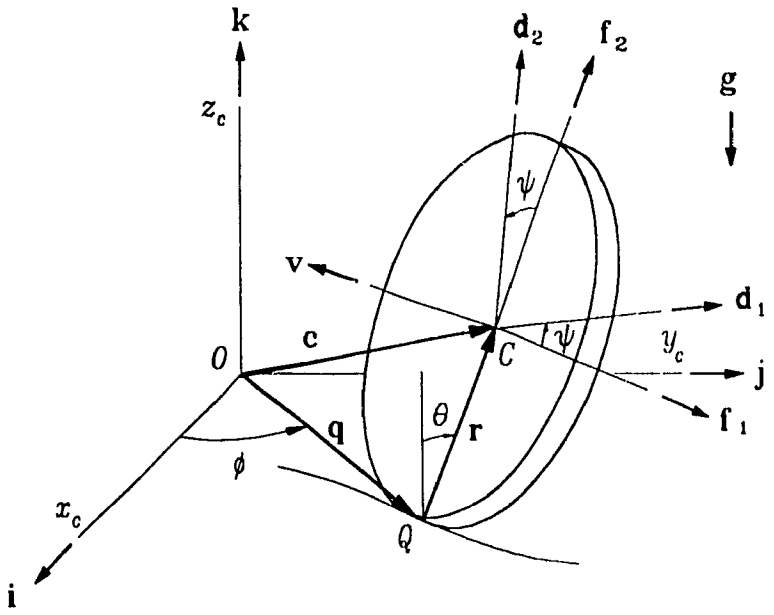

Fig. 1.1 A disk rolling on a plane

nonholonomic system do not lead to restrictions on their admissible configurations Furthermore, the existence of a single nonintegrable constraint does not always guarantee the system to be nonholonomic, since this constraint may prove to be integrable by virtue of the remaining constraint equations. For an example of such a case, the reader is referred to Neĭmark and Fufaev (1967).

As mentioned before, the dimension of the configuration space, which can also be defined as the *minimum* number of generalized coordinates necessary to specify the configuration of a system completely, is different from its DOF if the system is nonholonomic. In fact, the dimension of the configuration space of a nonholonomic system is always larger than its DOF. Moreover, a distinction is made here between the minimum number of coordinates required to *specify* the configuration of a system completely, i.e., the dimension of its configuration space, and the minimum number of coordinates necessary to *control* the system, i.e., the DOF of the system

To exemplify a nonholonomic system, a rigid disk rolling on a horizontal plane without slippage, as shown in Fig. 1.1, is considered. Thus, a *pure rolling* motion of the disk is assumed. The configuration of this disk at any instant is completely

specified by five generalized coordinates, namely, two rectangular coordinates of the mass centre of the disk, say, x_c and y_c, and three angles representing the orientation of the body with respect to the inertial frame, say, the Euler angles θ, ϕ and ψ. The pure rolling condition may, alternatively, be stated by saying that the disk moves in contact with a *perfectly rough* fixed horizontal plane. A rough surface, in contrast to a *perfectly smooth* surface, does not allow arbitrary changes of the five generalized coordinates. If the surface is smooth, the disk can take on any position, i.e., slippage occurs, as long as it remains in contact with the plane. The five coordinates can, therefore, have any arbitrary values representing a possible displacement of the body, which, then, implies that the system has five DOF. However, when the plane is rough, the condition that the displacement of the point of contact be zero must be satisfied, and this implies that the quantities representing any arbitrary configuration of the disk on the plane are not independent. In fact, the velocity of the mass centre of the disk must satisfy two scalar constraints. These constraints can be written in the form of eq.(1.2) where vector $\mathbf{b}$ vanishes. The expressions for $\mathbf{J}$ and $\boldsymbol{\theta}$ are:

$$\mathbf{J} \equiv \begin{bmatrix} \mathbf{j}_1^T \\ \mathbf{j}_2^T \end{bmatrix} \tag{1.4}$$

and

$$\boldsymbol{\theta} \equiv [\theta, \quad \phi, \quad \psi, \quad x_c, \quad y_c]^T \tag{1.5}$$

while vectors $\mathbf{j}_1$ and $\mathbf{j}_2$ are given as

$$\mathbf{j}_1 = [r\cos\theta\sin\phi, \quad r\sin\theta\cos\phi, \quad r\cos\phi, \quad 1, \quad 0]^T$$
$$\mathbf{j}_2 = [-r\cos\theta\cos\phi, \quad r\sin\theta\sin\phi, \quad r\sin\phi, \quad 0, \quad 1]^T$$

where r is the radius of the disk. Now, it can be readily verified that $\partial\mathbf{j}_1/\partial\boldsymbol{\theta}$ and $\partial\mathbf{j}_2/\partial\boldsymbol{\theta}$, two 5×5 matrices, are nonsymmetric. Thus, the resulting constraint equations are nonholonomic and the DOF of this system turns out to be three.

Note that, while pure rolling conditions are satisfied, the five coordinates may take on arbitrary values as the disk rolls on the plane, i.e., the disk can take on any position relative to the plane. To justify this assertion, it is shown in Neĭmark

and Fufaev (1967) how the disk can be brought from a given position denoted by vector $\boldsymbol{\theta}_0 \equiv [\theta_0, \ \phi_0, \ \psi_0, \ x_0, \ y_0]^T$ to any other prescribed position given by $\boldsymbol{\theta}_1 \equiv [\theta_1, \ \phi_1, \ \psi_1, \ x_1, \ y_1]^T$. First, the disk is rolled from a point C_0 on the plane whose coordinates are (x_0, y_0) to a point C_1 that is given by (x_1, y_1) along any curve of length $r(\psi_1 - \psi_0 + 2\pi k)$, where k is an arbitrary constant. Then, the disk is rotated around the axis perpendicular to the plane at point C_1 until the angle ϕ takes the desired value ϕ_1. Finally, the disk is tilted to the position where $\theta = \theta_1$. This verifies that the dimension of the configuration space is five, whereas the DOF of the disk rolling on the plane is three. A similar situation arises in everyday life when parking a car, which requires a set of complex manoeuvres to place the car in a space between two other parked cars.

Further classifications of mechanical systems are possible that are based on the values of the components of vector $\mathbf{b}$, as in eq.(1.2). These are:

- *catastatic*: If all components of $\mathbf{b}$ vanish, i.e., if vector $\mathbf{b}$ does not appear in eq.(1.2), the constraints are called catastatic. A disk rolling on a plane is a catastatic nonholonomic system. It is pointed out here that a mechanical system containing catastatic integrable constraint equations is not always a scleronomic system because, upon integration of eq.(1.2), time may appear explicitly in its algebraic forms, i.e., the system is rheonomic.
- *acatastatic*: Acatastatic constraints have at least one nonzero component of $\mathbf{b}$.

1.2 Robotic Mechanical Systems

A mechanical system may be either controlled or uncontrolled. A disk rolling on a plane is an example of the latter, but most engineering systems are controlled. An example of a controlled system is the 6-DOF manipulator developed during World War II, which was meant to reproduce the motion of the arm of a manned master manipulator by means of electronic amplifiers. A system under digital con-

trol is much more versatile because it allows for *programming*. Thus, a computer-controlled mechanical system is referred to here as a *robotic mechanical system*, popularly known as a *robot*. A *robot*[3], according to the International Standard Organization (Poole, 1989), is defined as *an automatically controlled, reprogrammable, multi-purpose manipulative machine, with or without locomotion, for use in industrial automation applications*. However, modern robots are not only restricted to industrial applications. They are also used in unstructured environments like hospitals and military applications. To use robots in an unstructured environment, the autonomous nature of the robots is important, which essentially depends on accurate sensors and on-line computations allowing robots to make decisions. In any case, robots can be either holonomic or nonholonomic. This allows one to classify robotic mechanical systems as (a) holonomic robotic mechanical systems (HRMS) and (b) nonholonomic robotic mechanical systems (NHRMS). Examples of HRMS are serial and parallel manipulators whose kinematic constraints are holonomic. On the other hand, automatic guided vehicles (AGVs) and snake-like articulated mobile robots with crawler tracks (Hirose and Morishima, 1990) are NHRMS, since nonholonomic constraints arise due to rolling of wheels and crawler movements. Yet another example of a NHRMS is RoboTRAC (Hiller and Schmitz, 1990), a system supported with wheels and legs.

Although the first industrial robot was built in 1954, the research in dynamics of serial manipulators started in the late seventies and has been considered an almost accomplished subject. In this area, the problem of dynamic simulation for real-time control of manipulators has been addressed by Luh et al. (1980), Walker and Orin (1982), Kane and Levinson (1983), Khalil et al. (1986), Lee and Chang (1986), Angeles and Ma (1988) and Balafoutis et al. (1988), just to mention a few.

With the introduction of flexible manufacturing cells in factory automation, the necessity of increasing mobility in fixed robotic manipulators was felt. In effect,

[3]The term *robot* is derived from the Czech word *robota*, which means forced labour or compulsory service. It was first used in two plays written by the Czech author Karel Čapek. The more popular one is *Rossum's Universal Robots*

the research on mobile robotic systems is receiving more and more attention. In this context, walking machines and rolling robots are well-known mobile robots. Walking machines are *legged mobile robots*. They offer independent control of their joints and have the greatest capability of going over unstructured terrain. However, due to the presence of complex kinematic chains and their time-varying topology, they are difficult to control and the computations required for leg control and balance are prohibitive. Also, power drain is large (Waldron, 1985; Poole, 1989) and their payload capability is quite restricted (Hirose and Morishima, 1990). On the other hand, AGVs are *wheeled mobile robots* and perform well if the terrain is horizontal or has only a limited slope. The motions of AGVs are reasonably smooth and their wheels have good traction (Poole, 1989). They are favoured in the shop floors, because they are more energy efficient (Muir and Neuman, 1987a) than others on rigid, horizontal surfaces. An AGV with a serial manipulator mounted on top is believed to find wide applications in factories, offices, hospitals, supermarkets and houses. However, AGVs are nonholonomic systems and their kinematic properties demand a special treatment for their dynamic analysis, which is a motivation for the research work reported here.

1.3 A Survey of Nonholonomic Robotic Mechanical Systems

Since the development of AGVs in the sixties, they have mostly been used in factories. These models are like driverless forklift trucks and can handle large loads from one area of the factory to another, but are generally constrained to follow a fixed path. These paths are usually physical guidepaths such as inductive or wire-guided, optical and magnetic guidepaths (Premi and Besant, 1983; Boegli, 1985; Hammond, 1986; Tsumura, 1986). They are fairly simple and reliable. However, these systems have severe drawbacks as paths are not easily alterable, which leads to limited control over vehicle paths and stopping points, higher installation cost in the case of the wire-guided systems and high maintenance costs due to the wear and

tear of the paint or the reflective tape of optical systems. The use of *virtual guide-paths* (Boegli, 1985) leads to a new generation of AGVs, also known as *autonomous robots* (Poole, 1989), i.e., autonomous wheeled mobile robots. In these systems, the actual configuration of the vehicle is obtained from indirect information, which is processed using its on-board computer. This information may be obtained from indicators like inertial navigation systems, dead-reckoning systems, sonic or laser beacons, corner-cube and laser-scanning (Tsumura, 1986), computer vision systems (Boegli, 1985; Hammond, 1986) and free-wheel techniques (Culley and Baldur, 1988). These navigation systems extend the application of AGVs to space and undersea explorations (Tanaka, 1985), nuclear and explosive handling (Maki, 1985; Meieran and Gelhaus, 1986), security (Kajiwara et al., 1985), military (Lindauer and Hill, 1985), mobility for the disabled (Tachi et al., 1981), patient care (Nakano et al., 1981; Borenstein and Koren, 1985) and construction work (Saito et al., 1985; Kangari and Yoshida, 1990). Besides, AGVs have been developed for research purposes as in Iijima et al. (1981), Moravec (1983), Dillmann and Rembold (1985), Cheng et al. (1989) and others.

Mobility is an essential feature of AGVs that is achieved by wheel locomotion systems. Locomotion of AGVs with three or four wheels is more common, although six or more wheels are also possible. Some configurations even have sets of double wheels. Four wheels offer more stability, more traction when all wheels are driven, and slightly better clearance capabilities. Three wheels offer less complex steering, the elimination of suspension mountings, less weight for the wheel assembly, and some navigational improvements. However, there are many ways to construct, mount and steer the wheels. Figure 1.2 illustrates some popular wheel configurations. Figure 1.2(a) shows a wheel configuration where two rear wheels are independently driven and also used for steering purposes. For stability, a free- or caster-wheel is attached to the front. This wheel configuration is used in the YAMABICO 3.1 AGV (Iijima et al., 1981), a similar vehicle being analysed in Chapter 4 of this thesis. The approach of Cybermation, Inc., USA, is that all wheels are driven and

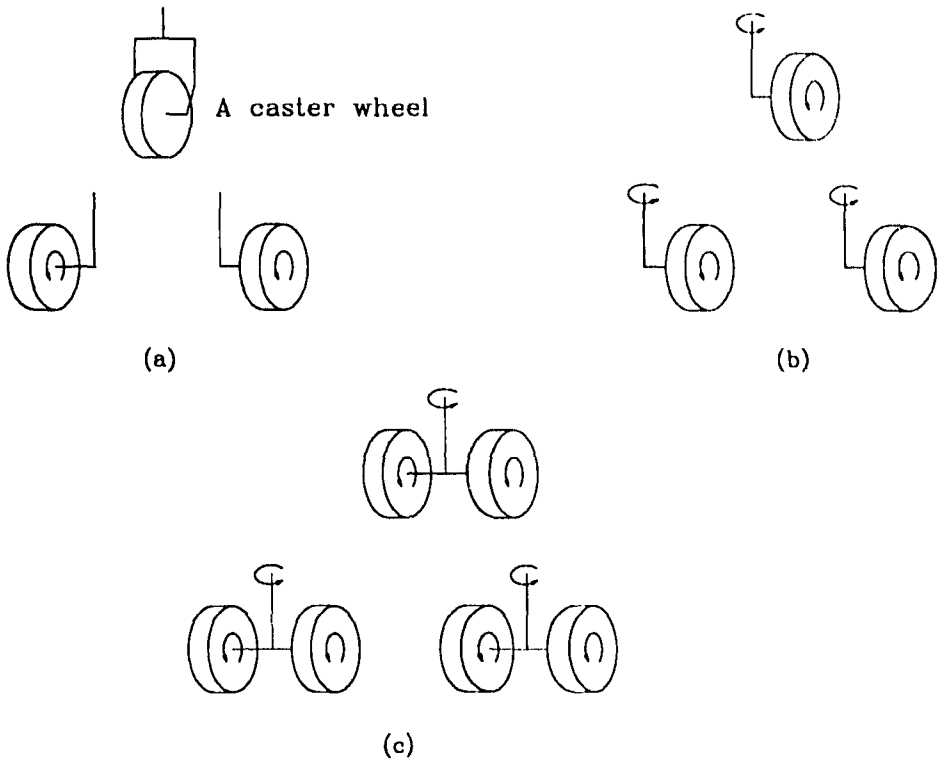

Fig. 1.2 (a) Two rear wheels are driven, (b) Three wheels are synchronously driven and steered, (c) Three sets of double-wheels are driven and steered.

steered, as shown in Fig. 1.2(b), in total synchronisation. In both cases, as shown in Figs. 1.2(a) and (b), the systems have 2-DOF. In the former case, the system can move in a straight path that is parallel to the wheel velocities and can rotate about an axis perpendicular to the floor, while, in the latter, the system can move anywhere on the floor but cannot rotate about a vertical axis, resulting in two possible independent motions of the vehicles. Carnegie Mellon's PLUTO (Moravec, 1983; Bortz, 1984) has a set of two wheels on each of the three support legs of a triangular platform, as shown in Fig 1.2(c), which leads to a 3-DOF AGV. Concordia's CONCIC-2 (Cheng et al., 1989; Rajagopalan and Huard, 1989) operates as either a 2- or a 3-DOF AGV. A modifiable wheelbase configuration of CONCIC-2 is very useful in studying different kinematic, dynamic and control aspects of the AGV. Its driven or driven and steered wheels may be assembled in the vertices of a triangular Figs. 1.2(a) and (c)—, rectangular or rhombic platform. Although some of the AGVs mentioned above have 3-DOF, their control is difficult because they have redundant

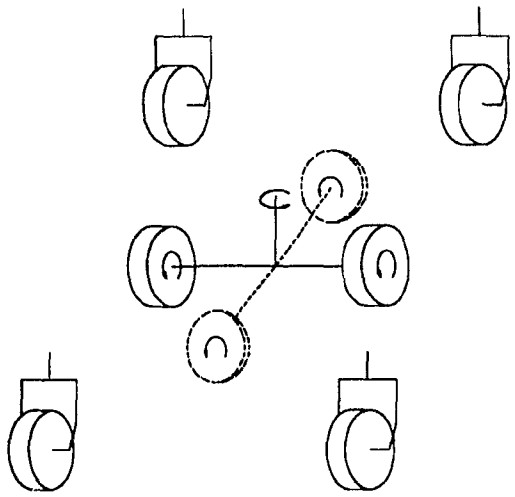

Fig. 1.3 Wheel configuration of a centre-driven AGV.

actuation, i.e., the number of driven wheels is greater than their DOF. One way of avoiding redundant actuation in a 3-DOF AGV is to have a centre-driven vehicle (Carlisle, 1984), in which lateral movements of the vehicle are possible by steering the two driven wheels together, as shown in Fig. 1.3. For stability of the vehicle, four caster wheels are attached at the four vertices of a rectangular platform. This system has the disadvantage that, to change its direction of motion from longitudinal to lateral, it has to come to a complete stop to orient the driven wheels from the former to the latter direction, as shown in Fig. 1.3. The invention of the Mecanum wheel (Jonsson, 1985) or Omnidirectional wheel (Carlisle, 1984; Adams, 1984; Muir and Neuman, 1987a) or Ilonator (Daniel et al., 1985), shown in Fig. 1.4, allows for a 3-DOF mobility in a vehicle without redundant actuation. Contrary to the conventional wheels, Figs. 1.2 and 1.3, an omnidirectional wheel consists of a wheel hub about which rollers are mounted at an angle α, as shown in Fig. 1.4(b), such that their spin axes, vectors $\mathbf{e}'$, are not parallel to the axis of the wheel hub, which in turn is parallel to vector $\mathbf{e}$. If vectors $\mathbf{e}$ and $\mathbf{e}'$ are parallel then the assembly will lead to a kinematic structure of a conventional wheel and hence, the wheel is no longer omnidirectional. The rotation of these rollers adds another DOF to the wheel and hence, to the system. However, this wheel is difficult to manufacture. Moreover, if the inertial properties of the rollers are not negligible, then the computational

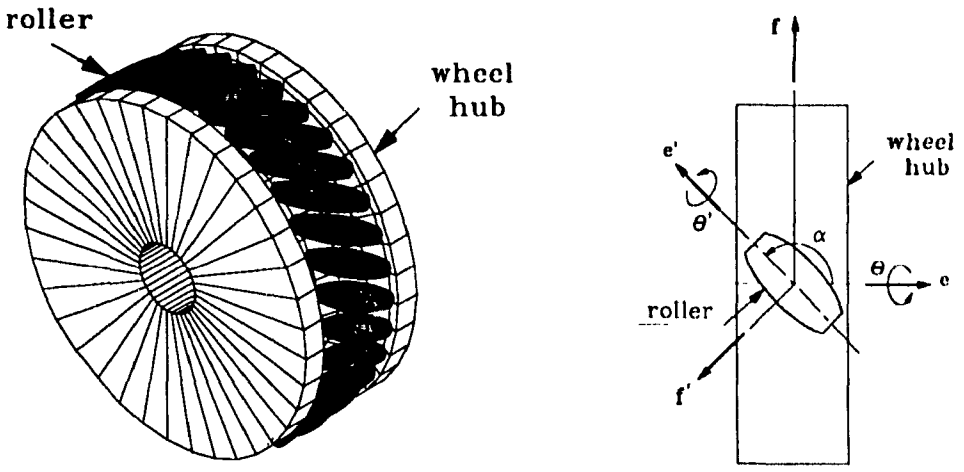

Fig. 1.4 (a) An omnidirectional wheel, (b) A schematic diagram.

complexity increases in the dynamic modelling of AGVs with this type of wheels.

Generally, AGVs are popular NHRMS. However, NHRMS that are more complex than AGVs also exist: a 16-DOF snake-like articulated mobile KR I robot (Hirose and Morishima, 1990)—a hybrid configuration consisting of six articulated body and crawler tracks that has excellent terrain adaptability, sufficient payload capacity and high mobility—has been developed to satisfy the requirements of a nuclear reactor plant in Japan; a space vehicle (Nakamura and Mukherjee, 1990) that has been conceived by NASA for performing various tasks in space; and RoboTRAC (Hiller and Schmitz, 1990), a wheeled-and-legged mobile system for rough-terrain locomotion.

1.4 Research Objectives

Literature investigations reveal that, since the invention of AGVs, attention has mostly been paid to navigation systems, path-planning and obstacle avoidance algorithms. The problems of kinematics and dynamics pertaining to AGVs for analysis, design, simulation and control purposes have been recently addressed by a few researchers. The kinematic modelling of AGVs was reported by Agulló et al. (1987), Muir and Neuman (1987a, 1987b), Cheng and Rajagopalan (1988) and Alexander and Maddocks (1989), while dynamic analysis by Cyril et al. (1989), Muir and New-

man (1988) and Agulló et al. (1989), and control by d'Andréa-Novel et al. (1991) and Samson and Ait-Abderrahim (1991). A method based on *the natural orthogonal complement* (NOC) (Angeles and Lee, 1988) is devised in the present research for the dynamic modelling of NHRMS. AGVs of various architectures are modelled to test the performance of the modelling technique developed here.

Closely related design problems associated with the 3-DOF AGVs with omnidirectional wheels are the optimum selection of the total number of wheels, the number of driven wheels, wheel size, steering method, orientation of the wheels, profile and orientation of the rollers, number of rollers in a wheel, etc., some of which are addressed here for the first time. Kinematic designs of the 3-DOF AGVs based on the transformation matrix for direct kinematics are done, where the optimum orientation of the rollers relative to the wheel hub and the optimum positions and orientations of the wheel hubs with respect to the platform are found.

Finally, simulation is recognized as an important tool that can be used in the design and control of mechanical systems and, consequently, simulation of NHRMS is given due attention.

1.5 Thesis Contributions

The present research focuses on the development and application of a dynamic modelling technique for nonholonomic systems, known as the method of the NOC. This technique is based on a novel formulation of kinematic constraints arising from different types of kinematic pairs and a suitably defined orthogonal complement of the associated kinematic constraint matrix. Here, two lemmas are given in §3.1 with regard to the classification of kinematic constraints that avoid the necessity of finding the gradients of the rows of the kinematic constraint matrix, generally required to determine the integrability of first-order differential equations arising from the constraints in the kinematic pairs. A mechanical system consisting of multiple kinematic chains or loops, multi-loop systems for brevity, even in the presence of re-

dundant actuation, can be analysed with this method, as described in §3.3 and §3.6. The DOF of a mechanical system can be determined with the adopted methodology, which then allows the prediction of the controllability of the system. The duality between kinematic constraints and nonworking constraint wrenches can be exploited for design purposes. To this end, since a nonholonomic mechanical system consists of both holonomic and nonholonomic couplings, the developed method can be suitably applied to a holonomic system as well.

The method of the NOC is then applied to the dynamic simulation of different NHRMS, which leads to suitable simulation algorithms. First, the simulation of a 3-wheeled 2-DOF AGV is reported, the results showing that the method of the NOC is an accurate simulation tool. A general-purpose computer program, OMNI, is developed that allows users to perform inverse kinematics, dynamics and forward dynamics leading to the simulation of 3-DOF AGVs consisting of any number of omnidirectional wheels. Redundant actuation in 3-DOF vehicles is also considered where the dynamic modelling is done using the method of the NOC coupled with an optimization technique. With the methodology developed in this thesis, limitations on the motor torques can be taken into account in the inverse dynamics and simulation of 3-DOF AGVs. Moreover, kinematic designs are reported, whereby an accurate and efficient scheme for direct kinematics, and hence, control, can be achieved.

Finally, a current important feature in design and real-time control, namely, animation, is thoroughly addressed. Here, the frequency at which the configuration of a system is computed must match the speed at which the system moves. However, a fast algorithm with poor accuracy is useless. Thus, it is being shown with an example that the representation of a dynamic model in different coordinate systems affects the efficiency and accuracy of the simulation algorithm thus produced. The results are followed by some suggestions which can be helpful when one attempts to derive a simulation algorithm for animation purposes.

1.6 Thesis Outline

A review of classification of mechanical systems and all pertinent definitions are presented in this chapter. Related issues are also discussed, as pertaining to holonomic, nonholonomic and robotic mechanical systems. Objectives of the research and the thesis contributions are included as well.

A review of the existing methodologies for the dynamic modelling of nonholonomic mechanical systems that have been used since 1894 is given in Chapter 2. With the advent of computers, it has become a natural tendency to derive algorithms leading to the automatic development of dynamic models of systems consisting of complex kinematic chains. This led to some methods based on orthogonal complements of kinematic constraints that are briefly described in Chapter 2.

The dynamic modelling of nonholonomic robotic mechanical systems using a special class of orthogonal complements, namely, the NOC, is presented in Chapter 3 as a dynamic modelling method, in six steps. The crucial step in this formulation is finding the NOC of the kinematic constraint matrix. The independence of the kinematic constraint equations arising from a holonomic or a nonholonomic coupling is discussed in Chapter 3 and two lemmas associated with holonomic and nonholonomic constraints that help in identifying the nature of kinematic constraints, as in §3.1, are proven. Moreover, the methodology for multi-loop systems is described in §3.3. An optimization technique coupled with the method of the NOC is given for mechanical systems with redundant actuations.

Chapter 4 deals with the modelling of nonholonomic robotic mechanical systems. The method of the NOC is, first, exemplified with a system consisting of an axle coupled to two wheels, as in §4.1. Then, a simulation algorithm of a 3-wheeled 2-DOF AGV is developed that has been tested when the vehicle is moving in a circular trajectory and in a path consisting of two straight lines connected by a smooth curve. The dynamic analysis of a 3-DOF AGV with all wheels driven may be ob-

tained by a direct application of the NOC. However, if more than three wheels are actuated then the system becomes redundantly actuated. A natural choice in finding a motor-torque setpoint for the controller is to use optimization techniques. Thus, a method described in §3.6, applied to redundantly actuated 3-DOF AGVs, is derived.

In Chapter 5, kinematic designs for 3-DOF AGVs that are based on the isotropic matrices associated with the inverse and direct kinematics are addressed. It has been shown that a matrix related to the inverse kinematics of the 3-DOF AGVs cannot be made isotropic. On the other hand, geometrical parameters of the vehicles corresponding to the isotropic matrix for direct kinematics are suggested which will increase the accuracy and efficiency of the control algorithms of the vehicles.

Some aspects of animation, like rigid-body attitude representation and the choice of a coordinate frame to represent the dynamic equations of motion of a system that affect the efficiency of a simulation algorithm leading, possibly, to an unrealistic animation of the system, are studied in Chapter 6. A case study of a disk rolling on a plane is included and guidelines are provided for animation purposes.

Finally, Chapter 7 concludes with a general discussion on the achievements in this research and suggestions for further research work.

Several appendices are included for completeness of this thesis. Appendix A contains some detailed derivations that would distract the reader if included within the main body of the thesis. Appendix B gives the detailed description of the derivations of equations of motion of a disk rolling on a plane in the disk-fixed and inertial frames, the results being used in Chapter 6.

Chapter 2

Dynamic Modelling of Nonholonomic Systems. A Review

The existence of kinematic constraints in the differential form of eq.(1.2), that impose no restrictions on the possible configurations of a mechanical system, was recognized at the end of the nineteenth century. Lagrange, in his celebrated *Mécanique Analytique* (1788), did not suspect the existence of such constraints (Neĭmark and Fufaev, 1967). Thus, he assumed that independent coordinates with independent variations could be chosen for any mechanical system, once allowance had been made for the conditions imposed by the nature of the system, which is equivalent to saying that it is always possible to find a set of independent coordinates defining the configuration of the system at any instant. This oversight was discovered after a considerable amount of time had elapsed, in connection with the study of various cases of motion of rigid bodies constrained to roll without slipping either on a plane or on a smooth warped surface.

In regard to the dynamics of multibody mechanical systems, the primary interest is in motion study or simulation. Simulation is defined as, *given the present state of a system, say at time* $t = 0$, *and the history of the external moments and forces, find the state variables in the future, i.e., at any time* $t > 0$. Here, terms like *state*

and *state variable* are understood in the usual sense (Kailath, 1980). Thus, a set of state variables of a system of l particles can be defined as the set of position and velocity vectors of all the particles. Alternatively, the set of position and momentum vectors of all the particles can play the role of state variables as well. In simulation, internal or reaction forces at the interconnection of the joints need not be found, because they do not contribute to the motion of the system. However, the constraint reaction forces are important in design, for they produce stress, strain, wear and, eventually, failure. In simulation, to obtain a dynamic model of a system using Newton's Second Law compels one to introduce and eliminate the reaction forces from the equations of motion. But, since the minimum number of generalized coordinates that are necessary and sufficient to describe the configuration of a holonomic system are independent, the application of variational principles like the *principle of virtual work* and the *principle of stationary action* lead to a set of dynamic equations which do not include the kinematic constraints. Thus, for holonomic systems, dynamic equations which are free of constraint forces may be obtained. On the contrary, due to the nonintegrability of some kinematic constraints of nonholonomic systems, the minimum number of generalized coordinates required to define its configuration completely is not independent. Therefore, the use of a similar methodology, as adopted in modelling holonomic systems, employing variational principles, forces one to introduce the kinematic constraints into the dynamic equations of motion of nonholonomic systems via a set of Lagrange multipliers, which do not vanish in general. However, it will be seen that the different treatment of kinematic constraints, as explained in some of the formulations of §2.2, and Chapter 3, results in constraint force-free dynamic models of nonholonomic systems, irrespective of the principle used to obtain the models.

Pertaining to the dynamic analysis of mechanical systems, several general-purpose software packages like MEDUSA (Dix and Lehman, 1972), IMP (Sheth and Uicker, 1972), DRAM (Chace and Sheth, 1973), VECENT (Andrews and Kesa-

van, 1975), DADS (Crosheck and Ford, 1988)[1] etc., have been developed to generate dynamic equations of motion automatically, to integrate the differential equations numerically and to solve for the internal reaction forces at the joints of the mechanical system under study. The objective behind general-purpose software is to use the ability of the processor for the dynamic analyses of mechanical systems, i.e., to obtain an economic and reliable design of a system in a considerably short time since neither investment nor time are required to build the prototype and to test its performance. Moreover, when a software package is used, the design variables of the system can be varied interactively to investigate the changes in its performance. Furthermore, using these packages, dynamic models can be generated without knowing much about the formulation techniques or the theory behind them. In dynamics, it is always desirable to have a symbolic representation of the governing equations of motion in order to gain insight into the behaviour of the system. Sometimes, the symbolic representation of equations of motion increases the efficiency of computer simulations, as intermediate steps are not required. Software like AUTOLEV (Schaechter et al., 1988), an interactive symbolic dynamics package based on Kane's method (Kane, 1968; Kane and Levinson, 1985), provides a symbolic formulation of the dynamic model, implementing FORTRAN code for simulation results. However, AUTOLEV runs currently in personal computers and does not provide animations of the simulated motions.

In §2.1, some definitions will be introduced which will be used throughout this thesis. Then, a brief review of different formulations of the dynamic modelling of nonholonomic systems is given.

[1] MEDUSA: Machine Dynamics Universal System Analyzer; IMP: Integrated Mechanisms Program; DRAM Dynamic Response of Articulated Machinery; VECENT: Vector Network; DADS Dynamic Analysis and Design System

2.1 Some Definitions

Let a nonholonomic mechanical system possess q DOF and be composed of l links. Moreover, a p-dimensional generalized coordinate vector $\boldsymbol{\theta}$ is defined as

$$\boldsymbol{\theta} \equiv [\boldsymbol{\theta}_I^T, \ \boldsymbol{\theta}_D^T]^T \tag{2.1}$$

where $\boldsymbol{\theta}_I$ and $\boldsymbol{\theta}_D$ are q- and m-dimensional vectors of *independent generalized coordinates* and *dependent generalized coordinates*, respectively, which are expressed as

$$\boldsymbol{\theta}_I \equiv [\theta_1, \cdots, \theta_q]^T \quad \text{and} \quad \boldsymbol{\theta}_D \equiv [\theta_{q+1}, \cdots, \theta_p]^T \tag{2.2}$$

Note that, since nonholonomic constraints are nonintegrable, no explicit relation exists between $\boldsymbol{\theta}_I$ and $\boldsymbol{\theta}_D$ and, thus, no set of independent generalized coordinates can be chosen which will completely describe a configuration of the nonholonomic system. Now, a vector of *generalized speeds* is defined as the time rate of change of $\boldsymbol{\theta}$, namely,

$$\dot{\boldsymbol{\theta}} \equiv [\dot{\boldsymbol{\theta}}_I^T, \ \dot{\boldsymbol{\theta}}_D^T]^T \tag{2.3}$$

where vectors $\dot{\boldsymbol{\theta}}_I$ and $\dot{\boldsymbol{\theta}}_D$ are the time rates of change of vectors $\boldsymbol{\theta}_I$ and $\boldsymbol{\theta}_D$, respectively. It is pointed out here that, as in eq.(1.2), the kinematic constraints can always be expressed as linear functions of the generalized speeds. Thus, using the constraint equations, eq.(1.2), vector $\dot{\boldsymbol{\theta}}_D$ can be evaluated in terms of $\dot{\boldsymbol{\theta}}_I$.

Furthermore, vector $\boldsymbol{\phi}$ is introduced as a p-dimensional vector of *generalized forces*, and is expressed as

$$\boldsymbol{\phi} \equiv \boldsymbol{\phi}_I + \boldsymbol{\phi}_D \tag{2.4}$$

where the q- and m-dimensional vectors $\boldsymbol{\phi}_I$ and $\boldsymbol{\phi}_D$ are called the *independent* and *dependent generalized force* vectors, respectively.

Also, pertaining to the motion of a mechanical system, the *twist* of the ith rigid link of the kinematic chain of the system under study, $\mathbf{t}_i$, undergoing an arbitrary motion in the 3-dimensional space, is defined in terms of its angular velocity $\boldsymbol{\omega}_i$ and

the velocity of the corresponding mass centre $\dot{\mathbf{c}}_i$, although any other point of the body could be used, both being, in general, 3-dimensional vectors. Hence, $\mathbf{t}_i$ is the 6-dimensional vector defined as

$$\mathbf{t}_i \equiv \begin{bmatrix} \boldsymbol{\omega}_i \\ \dot{\mathbf{c}}_i \end{bmatrix} \tag{2.5}$$

Moreover, if $\mathbf{I}_i$ denotes the *inertia tensor* of the ith link about its mass centre and this, as well as all vector quantities involved, are referred to the ith link-fixed coordinate system, whose angular velocity is $\boldsymbol{\sigma}_i$, then the 6×6 matrices of *extended angular velocity* of the coordinate system, $\mathbf{W}_i$, of *extended mass* and its time derivative, $\mathbf{M}_i$ and $\dot{\mathbf{M}}_i$, respectively, are defined as

$$\mathbf{W}_i \equiv \begin{bmatrix} \boldsymbol{\Omega}_i & \mathbf{O} \\ \mathbf{O} & \boldsymbol{\Omega}_i \end{bmatrix}, \qquad \mathbf{M}_i \equiv \begin{bmatrix} \mathbf{I}_i & \mathbf{O} \\ \mathbf{O} & m_i\mathbf{1} \end{bmatrix} \quad \text{and} \quad \dot{\mathbf{M}}_i \equiv \begin{bmatrix} \dot{\mathbf{I}}_i & \mathbf{O} \\ \mathbf{O} & \mathbf{O} \end{bmatrix} \tag{2.6}$$

where m_i, $\mathbf{O}$ and $\mathbf{1}$ denote the mass of the ith link, the zero and the identity 3×3 tensors, respectively. The *cross-product* tensor $\boldsymbol{\Omega}_i$, as in eq.(2.6), is defined as

$$\boldsymbol{\Omega}_i \equiv \frac{\partial(\boldsymbol{\sigma}_i \times \mathbf{x})}{\partial \mathbf{x}} \equiv \boldsymbol{\sigma}_i \times \mathbf{1} \tag{2.7}$$

for an arbitrary 3-dimensional vector $\mathbf{x}$. Henceforth, the *cross-product* tensor of any 3-dimensional vector $\mathbf{z}$ will be denoted by $\mathbf{Z}$, unless otherwise indicated. Furthermore, if $\mathbf{n}_i$ and $\mathbf{f}_i$ are the resultant moment and the resultant force acting on the ith link, respectively, the latter being applied at the mass centre of this link, then the *wrench* $\mathbf{w}_i$ acting on the ith link is defined in accordance with the definition of $\mathbf{t}_i$, as a 6-dimensional vector, i.e.,

$$\mathbf{w}_i \equiv \begin{bmatrix} \mathbf{n}_i \\ \mathbf{f}_i \end{bmatrix} \tag{2.8}$$

Finally, for a mechanical system composed of l links, the $6l$-dimensional vectors of *generalized twist* and *generalized wrench*, $\mathbf{t}$ and $\mathbf{w}$, respectively, are defined as

$$\mathbf{t} \equiv \begin{bmatrix} \mathbf{t}_1 \\ \vdots \\ \mathbf{t}_l \end{bmatrix} \quad \text{and} \quad \mathbf{w} \equiv \begin{bmatrix} \mathbf{w}_1 \\ \vdots \\ \mathbf{w}_l \end{bmatrix} \tag{2.9}$$

and the $6l \times 6l$ matrices of *generalized angular velocity*, $\mathbf{W}$, of *generalized mass*, $\mathbf{M}$, and the time rate of change of the latter, $\dot{\mathbf{M}}$, are given by

$$\mathbf{W} \equiv \mathrm{diag}[\mathbf{W}_1, \cdots, \mathbf{W}_l] \tag{2.10a}$$

$$\mathbf{M} \equiv \text{diag}[\mathbf{M}_1, \cdots, \mathbf{M}_l] \tag{2.10b}$$

$$\dot{\mathbf{M}} \equiv \text{diag}[\dot{\mathbf{M}}_1, \cdots, \dot{\mathbf{M}}_l] \tag{2.10c}$$

2.2 A Review of Different Formulations

Earlier attempts to obtain dynamic models of nonholonomic systems, free of constraint forces, were based on the principle of virtual work and the variational principle of stationary action. The principle of virtual work which is based upon virtual displacements has found almost universal acceptance. In fact, the analyst can dispense with virtual displacements by formally differentiating the generalized coordinates and suitably identifying the velocities and angular velocities involved. Nevertheless, the principle of virtual work is included in this review for completeness. Thus, a *virtual displacement* of a system is defined as a displacement undergone by the system as the result of *virtual variations* of its generalized coordinates. A virtual variation, in general, is imagined as an arbitrary infinitesimal variation of a coordinate, which is compatible with the constraints imposed on the system. All links of the system thus undergo physically possible virtual displacements at no time at all. Now, in dynamics, the principle of virtual work is based on both the principle of virtual work of statics and the d'Alembert principle (Meirovitch, 1970; Greenwood, 1977), which is stated as, "the work done by the external, internal or reaction and inertia forces associated with the virtual displacement, is zero, i.e., the total virtual work vanishes." Thus, the principle of virtual work yields the d'Alembert-Lagrange equations of the system under study, namely,

$$[\frac{d}{dt}(\frac{\partial T}{\partial \dot{\boldsymbol{\theta}}}) - \frac{\partial T}{\partial \boldsymbol{\theta}} - (\boldsymbol{\phi} - \frac{\partial V}{\partial \boldsymbol{\theta}})]^T \delta\boldsymbol{\theta} = 0 \tag{2.11}$$

where $\delta\boldsymbol{\theta}$ is the virtual variation of $\boldsymbol{\theta}$ and T is a scalar function denoting the kinetic energy of the system. The kinetic energy of a system of rigid bodies is simply the sum of the kinetic energies of all l rigid bodies of the system. Thus, T can be expressed as

$$T = \sum_{i=1}^{l} T_i = \sum_{i=1}^{l} \frac{1}{2} \mathbf{t}_i^T \mathbf{M}_i \mathbf{t}_i = \frac{1}{2} \mathbf{t}^T \mathbf{M} \mathbf{t}$$

Moreover, $V \equiv V(\boldsymbol{\theta}, t)$ is the potential energy of the system and $-\partial V/\partial \boldsymbol{\theta}$ represents the generalized force due to the potential V. Furthermore, $\boldsymbol{\phi}$ can be expressed by

$$\boldsymbol{\phi} \equiv \frac{\partial \pi^S}{\partial \dot{\boldsymbol{\theta}}} - \frac{\partial \pi^D}{\partial \dot{\boldsymbol{\theta}}}$$

in which π^S and π^D are the power supplied to and the power dissipated by the system, respectively. Equation (2.11) may be rewritten as

$$[\frac{d}{dt}(\frac{\partial L}{\partial \dot{\boldsymbol{\theta}}}) - \frac{\partial L}{\partial \boldsymbol{\theta}} - \boldsymbol{\phi}]^T \delta\boldsymbol{\theta} = 0 \tag{2.12}$$

where $L \equiv T - V$ is the Lagrangian of the system.

2.2.1 Lagrange's Equations

In the presence of holonomic constraints only, a set of independent generalized coordinates, vector $\boldsymbol{\theta}_I$, may be chosen. Hence, $\delta\boldsymbol{\theta}$ in eq.(2.12) may be replaced by $\delta\boldsymbol{\theta}_I$ and, correspondingly, $\boldsymbol{\phi}$ by $\boldsymbol{\phi}_I$. Since the components of $\delta\boldsymbol{\theta}_I$ are independent, eq.(2.12) leads to the q independent scalar Lagrange equations of motion of a holonomic system (Meirovitch, 1970; Greenwood, 1977), i.e.,

$$\frac{d}{dt}(\frac{\partial L}{\partial \dot{\boldsymbol{\theta}}_I}) - \frac{\partial L}{\partial \boldsymbol{\theta}_I} = \boldsymbol{\phi}_I \tag{2.13}$$

In modelling nonholonomic systems that consist of holonomic and nonholonomic constraints, it is possible to choose a set of p generalized coordinates such that no holonomic constraints appear in the set of constraint equations, i.e., $h = 0$. In turn, constraint equations consist of only n nonholonomic constraints, i.e., the number of scalar constraints is $m = n$. Thus, recalling the definition of the virtual variation, it is seen from eq.(1.2) that the variations of $\boldsymbol{\theta}$ satisfy a system of linear homogeneous equations which is as follows:

$$\mathbf{J}\delta\boldsymbol{\theta} = \mathbf{0} \tag{2.14}$$

where $\mathbf{J}$ is an $n \times p$ matrix and $\delta\boldsymbol{\theta}$ is a p-dimensional vector. Nonholonomic constraints are now incorporated into the d'Alembert-Lagrange equations, eq.(2.12), via

an n-dimensional vector $\boldsymbol{\lambda}$ of Lagrange multipliers (Meirovitch, 1970), which leads to

$$[\frac{d}{dt}(\frac{\partial L}{\partial \dot{\boldsymbol{\theta}}}) - \frac{\partial L}{\partial \boldsymbol{\theta}} - \boldsymbol{\phi} - \mathbf{J}^T\boldsymbol{\lambda}]^T\delta\boldsymbol{\theta} = 0 \tag{2.15}$$

In eq.(2.15), the components of $\delta\boldsymbol{\theta}$ are not independent. However, vector $\boldsymbol{\lambda}$ can be chosen in such a way that the expression in brackets of eq.(2.15) vanishes for the given n components of vector $\delta\boldsymbol{\theta}$. The remaining q components being independent, they can be chosen arbitrarily, as in the case of a holonomic system. It follows that

$$\frac{d}{dt}(\frac{\partial L}{\partial \dot{\boldsymbol{\theta}}}) - \frac{\partial L}{\partial \boldsymbol{\theta}} = \boldsymbol{\phi} + \mathbf{J}^T\boldsymbol{\lambda} \tag{2.16}$$

which yields the p scalar equations of motion of the nonholonomic system (Meirovitch, 1970; Greenwood, 1977) under discussion. Moreover, eq.(2.16) together with eq.(1.2), forms a complete system of $p+n$ scalar equations with p unknown generalized coordinates and n unknown Lagrange multipliers. The necessity of introducing Lagrange multipliers in the dynamic models of nonholonomic systems is a major drawback in the study of these systems. However, vector $\boldsymbol{\lambda}$ has a physical meaning: the components of $\boldsymbol{\lambda}$ are the generalized nonworking reaction forces due to nonholonomic constraints.

2.2.2 Čaplygin's Equations

Čaplygin (Neĭmark and Fufaev, 1967) pointed out that, in certain conservative nonholonomic systems, kinematic constraints can be expressed as homogeneous equations which are linear in $\dot{\boldsymbol{\theta}}$. In other words, it is possible to obtain $\dot{\boldsymbol{\theta}}_D$ in terms of $\dot{\boldsymbol{\theta}}_I$, i.e.,

$$\dot{\boldsymbol{\theta}}_D = \mathbf{U}\dot{\boldsymbol{\theta}}_I \tag{2.17}$$

where $\mathbf{U}$ is an $n \times q$ matrix. According to Čaplygin, in these systems, $\boldsymbol{\theta}_D$ appears neither in $\mathbf{U}$ nor in the Lagrangian L, such systems being known nowadays as Čaplygin systems. Moreover, Neĭmark and Fufaev (1967) extended the definition of Čaplygin systems to those nonconservative nonholonomic systems in which none of $\mathbf{U}$, L, π^S and π^D contain $\boldsymbol{\theta}_D$. Čaplygin systems are remarkable in that their dynamic equa-

tions of motion can be separated from the nonintegrable constraint equations. It is evident from the form of eq.(2.17) that $\delta\boldsymbol{\theta}_I$ may be assumed to be independent and $\delta\boldsymbol{\theta}_D$ can be written as

$$\delta\boldsymbol{\theta}_D = \mathbf{U}\delta\boldsymbol{\theta}_I$$

Now, the d'Alembert-Lagrange equations, eq.(2.12), in terms of the variation of $\boldsymbol{\theta}_I$ is given as

$$[\frac{d}{dt}(\frac{\partial L}{\partial \dot{\boldsymbol{\theta}}_I}) - \frac{\partial L}{\partial \boldsymbol{\theta}_I} - \boldsymbol{\phi}_I + \mathbf{U}^T \frac{d}{dt}(\frac{\partial L}{\partial \dot{\boldsymbol{\theta}}_D})]^T \delta\boldsymbol{\theta}_I = 0$$

from which, by virtue of the independence of $\delta\boldsymbol{\theta}_I$, the equation below is obtained

$$\frac{d}{dt}(\frac{\partial L}{\partial \dot{\boldsymbol{\theta}}_I}) - \frac{\partial L}{\partial \boldsymbol{\theta}_I} + \mathbf{U}^T \frac{d}{dt}(\frac{\partial L}{\partial \dot{\boldsymbol{\theta}}_D}) = \boldsymbol{\phi}_I \tag{2.18}$$

A new Lagrange function L^* is introduced such that the dependent generalized speeds $\dot{\boldsymbol{\theta}}_D$ are eliminated from the original Lagrange function L by means of eq.(2.17). Thus, using the *chain rule*, the useful relations shown below are readily obtained:

$$\frac{\partial L^*}{\partial \boldsymbol{\theta}_I} = \frac{\partial L}{\partial \boldsymbol{\theta}_I} + (\frac{\partial \dot{\boldsymbol{\theta}}_D}{\partial \boldsymbol{\theta}_I})^T \frac{\partial L}{\partial \dot{\boldsymbol{\theta}}_D} \tag{2.19a}$$

$$\frac{\partial L^*}{\partial \dot{\boldsymbol{\theta}}_I} = \frac{\partial L}{\partial \dot{\boldsymbol{\theta}}_I} + (\frac{\partial \dot{\boldsymbol{\theta}}_D}{\partial \dot{\boldsymbol{\theta}}_I})^T \frac{\partial L}{\partial \dot{\boldsymbol{\theta}}_D} \tag{2.19b}$$

Substituting eqs.(2.19a) and (2.19b) into eq.(2.18), one obtains

$$\frac{d}{dt}[\frac{\partial L^*}{\partial \dot{\boldsymbol{\theta}}_I} - (\frac{\partial \dot{\boldsymbol{\theta}}_D}{\partial \dot{\boldsymbol{\theta}}_I})^T \frac{\partial L}{\partial \dot{\boldsymbol{\theta}}_D}] - \frac{\partial L^*}{\partial \boldsymbol{\theta}_I} + (\frac{\partial \dot{\boldsymbol{\theta}}_D}{\partial \boldsymbol{\theta}_I})^T \frac{\partial L}{\partial \dot{\boldsymbol{\theta}}_D} + \mathbf{U}^T \frac{d}{dt}(\frac{\partial L}{\partial \dot{\boldsymbol{\theta}}_D}) = \boldsymbol{\phi}_I \tag{2.20}$$

In eq.(2.20), the $n \times q$ matrices $\partial\dot{\boldsymbol{\theta}}_D/\partial\boldsymbol{\theta}_I$ and $\partial\dot{\boldsymbol{\theta}}_D/\partial\dot{\boldsymbol{\theta}}_I$ can be expressed using eq.(2.17) as

$$\frac{\partial \dot{\boldsymbol{\theta}}_D}{\partial \boldsymbol{\theta}_I} = \dot{\boldsymbol{\Theta}}^T \frac{\partial \mathbf{U}}{\partial \boldsymbol{\theta}_I} \tag{2.21a}$$

$$\frac{\partial \dot{\boldsymbol{\theta}}_D}{\partial \dot{\boldsymbol{\theta}}_I} = \mathbf{U} \tag{2.21b}$$

where $\partial\mathbf{U}/\partial\boldsymbol{\theta}_I$ is defined in such a way that each $\partial\mathbf{u}_i/\partial\boldsymbol{\theta}_I$, for $i = 1, \cdots, n$, is a $q \times q$ matrix, $\mathbf{u}_i$ being the ith column of matrix $\mathbf{U}^T$. Now, the $nq \times n$ matrix $\dot{\boldsymbol{\Theta}}$ and the $nq \times q$ matrix $\partial\mathbf{U}/\partial\boldsymbol{\theta}_I$ are defined as

$$\dot{\boldsymbol{\Theta}} \equiv \begin{bmatrix} \dot{\boldsymbol{\theta}}_I & \cdots & \mathbf{0} \\ \vdots & \ddots & \vdots \\ \mathbf{0} & \cdots & \dot{\boldsymbol{\theta}}_I \end{bmatrix} \quad \text{and} \quad \frac{\partial \mathbf{U}}{\partial \boldsymbol{\theta}_I} \equiv \begin{bmatrix} \partial \mathbf{u}_1/\partial \boldsymbol{\theta}_I \\ \vdots \\ \partial \mathbf{u}_n/\partial \boldsymbol{\theta}_I \end{bmatrix} \tag{2.22}$$

where **0** is the q-dimensional zero vector. Moreover, $(\partial \mathbf{u}_i/\partial \boldsymbol{\theta}_I)^T \dot{\boldsymbol{\theta}}_I$ gives the ith column of matrix $(\partial \dot{\boldsymbol{\theta}}_D/\partial \boldsymbol{\theta}_I)^T$. Furthermore, using eqs.(2.21a) and (2.21b), eq.(2.20) is rewritten as

$$\frac{d}{dt}(\frac{\partial L^*}{\partial \dot{\boldsymbol{\theta}}_I}) - \frac{\partial L^*}{\partial \boldsymbol{\theta}_I} - [\frac{d\mathbf{U}^T}{dt} - (\frac{\partial \mathbf{U}}{\partial \boldsymbol{\theta}_I})^T \dot{\boldsymbol{\Theta}}] \frac{\partial L}{\partial \dot{\boldsymbol{\theta}}_D} = \boldsymbol{\phi}_I \tag{2.23}$$

with $d\mathbf{U}^T/dt$ being calculated as

$$\frac{d\mathbf{U}^T}{dt} = \frac{\partial \mathbf{U}^T}{\partial \boldsymbol{\theta}_I} \dot{\boldsymbol{\Theta}} \tag{2.24}$$

where the $q \times nq$ matrix $\partial \mathbf{U}^T/\partial \boldsymbol{\theta}_I$ is such that $(\partial \mathbf{u}_i/\partial \boldsymbol{\theta}_I)\dot{\boldsymbol{\theta}}_I$ represents the ith column of $d\mathbf{U}^T/dt$. Matrix $\partial \mathbf{U}^T/\partial \boldsymbol{\theta}_I$ is defined by

$$\frac{\partial \mathbf{U}^T}{\partial \boldsymbol{\theta}_I} \equiv [\frac{\partial \mathbf{u}_1}{\partial \boldsymbol{\theta}_I}, \quad \cdots, \quad \frac{\partial \mathbf{u}_n}{\partial \boldsymbol{\theta}_I}]$$

Finally, using eq.(2.24), Čaplygin's equations of motion (Neĭmark and Fufaev, 1967; Dolapchiev, 1969) are obtained from eq.(2.23) as

$$\frac{d}{dt}(\frac{\partial L^*}{\partial \dot{\boldsymbol{\theta}}_I}) - \frac{\partial L^*}{\partial \boldsymbol{\theta}_I} - [\frac{\partial \mathbf{U}^T}{\partial \boldsymbol{\theta}_I} - (\frac{\partial \mathbf{U}^T}{\partial \boldsymbol{\theta}_I})^T] \dot{\boldsymbol{\Theta}} (\frac{\partial L}{\partial \dot{\boldsymbol{\theta}}_D})' = \boldsymbol{\phi}_I \tag{2.25}$$

where the symbol $(\partial L/\partial \dot{\boldsymbol{\theta}}_D)'$ means that all the dependent generalized speeds in the expression $\partial L/\partial \dot{\boldsymbol{\theta}}_D$ have been eliminated using eq.(2.17). Thus, eq.(2.25) leads to q independent constraint-free equations of motion of a nonholonomic system in terms of the independent generalized coordinates and its time derivatives. Note that one of the integrability conditions for a set of velocity constraint equations, eq.(1.2), that is given in the previous chapter, is that all $q \times q$ matrices $\partial \mathbf{u}_i/\partial \boldsymbol{\theta}_I$ for $i = 1, \cdots, n$ be symmetric. Therefore, in the presence of only holonomic constraints, the holonomicity conditions are written as

$$\frac{\partial \mathbf{u}_i}{\partial \boldsymbol{\theta}_I} = (\frac{\partial \mathbf{u}_i}{\partial \boldsymbol{\theta}_I})^T, \qquad \text{for} \quad i = 1, \cdots, n \tag{2.26}$$

Moreover, the ith column of the expression in brackets of eq.(2.25), by virtue of eq.(2.26), vanishes, i.e.,

$$\frac{\partial \mathbf{u}_i}{\partial \boldsymbol{\theta}_I} \dot{\boldsymbol{\theta}}_I - (\frac{\partial \mathbf{u}_i}{\partial \boldsymbol{\theta}_I})^T \dot{\boldsymbol{\theta}}_I = \mathbf{0} \tag{2.27}$$

Hence, Čaplygin's equations reduce to the Lagrange equations of motion for holonomic systems.

2.2.3 Gibbs-Appell's Equations

Gibbs-Appell's equations of motion of nonholonomic systems are based on the concept of *acceleration energy* S, similar to the kinetic energy T. These equations were first discovered by Gibbs in 1879 (Gibbs, 1879, 1961) and independently discovered in 1899 and studied in detail by Appell. Gibbs-Appell's equations (Gibbs, 1879, 1961; Appell, 1899; Neĭmark and Fufaev, 1967; Desloge, 1986a, 1986b) are given in terms of *quasi-coordinates* as

$$\frac{\partial S}{\partial \ddot{\mathbf{q}}} = \boldsymbol{\phi}_q \tag{2.28}$$

where S is the *acceleration energy* or the *Gibbs-Appell function* for a system of rigid bodies in motion. A general form of the Gibbs-Appell function for rigid-body motion can be found in Ginsberg (1988). Moreover, $\mathbf{q}$ and $\boldsymbol{\phi}_q$ are the q-dimensional vectors of quasi-coordinates and generalized forces, respectively. Quasi-coordinates, as defined in Neĭmark and Fufaev (1967) and Greenwood (1977), are motion variables that are of a differential nature, but are not integrable. For example, as illustrated in Ginsberg (1988), the equations of motion may be obtained in terms of the angular velocity, as the equations of motion of a disk rolling on a plane, derived in Chapter 6, but there is no orientation vector that may be used to form a corresponding set of generalized coordinates. Moreover, quasi-coordinates are introduced by means of linear relations between the derivatives of quasi-coordinates and the generalized speeds as

$$\dot{\mathbf{q}} = \mathbf{U}_q \dot{\boldsymbol{\theta}} + \mathbf{q}' \tag{2.29}$$

where $\mathbf{U}_q$ is a $p \times p$ matrix, and $\mathbf{q}$ and $\mathbf{q}'$ are p-dimensional vectors but the prime does not denote differentiation here. The dimensions of $\mathbf{U}_q$, $\mathbf{q}$ and $\mathbf{q}'$ may vary depending on the formulation technique. For example, in the derivation of Gibbs-Appell's equations, $\mathbf{U}_q$, $\mathbf{q}$ and $\mathbf{q}'$ are a $q \times p$ matrix and q-dimensional vectors, respectively. The form of Gibbs-Appell's equations is very simple, but in many complex problems it is much harder to write down the acceleration energy than the expression for the kinetic energy. However, it is pointed out in Neĭmark and

Fufaev (1967) that the acceleration energy completely characterizes the dynamics of a nonholonomic system in the sense that, having an expression for the function S only, and no further information about the system (in particular, not knowing anything about the constraints imposed on the system), the equations of motion can be derived. This assertion is proven by showing that it is possible to find two different dynamic systems for which the expression T is the same but the function S is different.

Simultaneously, Volterra (1898) derived the equations of motion in variables which he called *motion characteristics*. Later, Voronec (1901) who is one of the founders of the mechanics of nonholonomic systems, derived the equations of motion, similar to eq.(2.25), without making the restrictive assumptions which lead to Čaplygin systems. Voronec's equations can, therefore, be applied to a larger class of nonholonomic systems. Moreover, Maggi (1901) showed that Volterra's and Gibbs-Appell's equations may be derived from his method, first proposed in 1896. Furthermore, Papstavridis in his recent papers (Papstavridis, 1988, 1990) derived geometrically the constraint-free equations of Maggi for mechanical systems with linear nonholonomic and/or holonomic constraints and the most general Gibbs-Appell's equations of motion for systems under nonlinear nonholonomic constraints. He also showed how to calculate the constraint reaction forces.

2.2.4 The Principle of Stationary Action

The principle of stationary action considers the motion of an entire system between two times t_1 and t_2. It is an integral principle that reduces the problems of dynamics to the investigation of the stationary values of a definite integral. According to this principle, the actual motion of the system is such that

$$\int_{t_1}^{t_2} (\delta T + \delta W) dt = 0 \tag{2.30}$$

where δT is the variation of the kinetic energy and δW is the virtual work done by the system due to potential fields, applied external actions and dissipation. For

conservative systems, $\delta W = -\delta V$, where δV is the variation of the potential energy, and eq.(2.30) takes on the form

$$\int_{t_1}^{t_2} \delta L dt = 0 \tag{2.31}$$

Equation (2.31), when applied to a holonomic system, leads to the familiar Hamilton principle, namely,

$$\delta \int_{t_1}^{t_2} L dt = 0 \tag{2.32}$$

where L is the Lagrangian of the system. Hamilton's principle, as given in eq.(2.32), can be stated as, "the actual path in the configuration space of a system renders the value of the definite integral in eq.(2.32) stationary with respect to all arbitrary variations of the path between the two instants t_1 and t_2, provided that the path variations vanish at these two end points." It can be shown that, for conservative holonomic systems, Hamilton's principle leads to the well-known Euler-Lagrange[2] equations of motion of a conservative holonomic system (Meirovitch, 1970; Greenwood, 1977):

$$\frac{d}{dt}\left(\frac{\partial L}{\partial \dot{\boldsymbol{\theta}}_I}\right) - \frac{\partial L}{\partial \boldsymbol{\theta}_I} = \mathbf{0} \tag{2.33}$$

However, using eq.(2.30) and introducing the Lagrange multipliers, the equations of motion of nonholonomic systems in the presence of external moments and forces can be readily obtained in the form of eq.(2.16), as derived in Meirovitch (1970), Greenwood (1977) and others.

2.2.5 Hamilton's Canonical Equations

A different procedure of replacing q second-order equations by $2q$ first-order ones can be obtained by writing Hamilton's canonical equations of motion. To obtain such equations, a new function $H(\boldsymbol{\theta}_I, \mathbf{p}, t)$, known as the Hamiltonian, is defined as

$$H(\boldsymbol{\theta}_I, \mathbf{p}, t) \equiv \mathbf{p}^T \dot{\boldsymbol{\theta}}_I - L^* \tag{2.34}$$

[2]This equation was first derived by Euler in 1744 and was later applied to mechanical systems by Lagrange

where $\mathbf{p}$ is the vector of the generalized momenta which is given as

$$\mathbf{p} \equiv \sum_{i=1}^{l} \frac{\partial T_i}{\partial \dot{\boldsymbol{\theta}}_I} = \sum_{i=1}^{l} \mathbf{M}_i \mathbf{t}_i = \mathbf{M}\mathbf{t} = \frac{\partial L^*}{\partial \dot{\boldsymbol{\theta}}_I} \tag{2.35}$$

Moreover,

$$\frac{\partial H}{\partial \boldsymbol{\theta}_I} = -\frac{\partial L^*}{\partial \boldsymbol{\theta}_I} \tag{2.36}$$

Hamilton's canonical equations may be obtained by varying both sides of eq.(2.34) and comparing the coefficients of the same variations. However, using the identities in eqs.(2.35) and (2.36), Hamilton's canonical equations can be obtained from Čaplygin's equations of motion (Neĭmark and Fufaev, 1967), eq.(2.25), as

$$\dot{\boldsymbol{\theta}}_I = \frac{\partial H}{\partial \mathbf{p}} \tag{2.37a}$$

$$\dot{\mathbf{p}} = \boldsymbol{\phi}_I - \frac{\partial H}{\partial \boldsymbol{\theta}_I} - [\frac{\partial \mathbf{U}^T}{\partial \boldsymbol{\theta}_I} - (\frac{\partial \mathbf{U}}{\partial \boldsymbol{\theta}_I})^T]\dot{\boldsymbol{\Theta}}'(\frac{\partial L}{\partial \dot{\boldsymbol{\theta}}_D})' \tag{2.37b}$$

where $\dot{\boldsymbol{\Theta}}'$ is $\dot{\boldsymbol{\Theta}}$ of eq.(2.22) in which $\dot{\boldsymbol{\theta}}_I$ is substituted by $\partial H/\partial \mathbf{p}$. The meaning of the expression $(\partial L/\partial \dot{\boldsymbol{\theta}}_D)'$ was explained in §2.2.2, when deriving Čaplygin's equations of motion.

2.2.6 Kane's Equations

Kane's equations, also referred to as Lagrange's form of d'Alembert's Principle in Huston, Passerello and Harlow (1978) and Huston and Passerello (1979, 1980), are derived by considering that, for a q-DOF nonholonomic mechanical system, a set of q independent parameters exists which are linear combinations of $\dot{\boldsymbol{\theta}}$, i.e., an expression similar to eq.(2.29) exists where $\dot{\boldsymbol{\theta}}$ is substituted by $\dot{\boldsymbol{\theta}}_I$ and $\mathbf{U}_q$, $\mathbf{q}$ and $\mathbf{q}'$ are a $q \times q$ matrix and q-dimensional vectors, respectively. Therefore, $\dot{\mathbf{q}}$ is given by

$$\dot{\mathbf{q}} = \mathbf{U}_q \dot{\boldsymbol{\theta}}_I + \mathbf{q}' \tag{2.38}$$

Moreover, matrix $\mathbf{U}_q$ and vector $\mathbf{q}'$ are chosen in such a way that eq.(2.38) can be solved uniquely for $\dot{\boldsymbol{\theta}}_I$. Furthermore, the components of $\dot{\mathbf{q}}$ are defined in Kane (1983) as *generalized speeds*. Now, the twist of the ith link is written as

$$\mathbf{t}_i = \mathbf{V}_i \dot{\mathbf{q}} + \mathbf{v}_i \tag{2.39}$$

where the 6-dimensional vector $\mathbf{v}_i$ and the $6 \times q$ matrix $\mathbf{V}_i$ are both functions of $\boldsymbol{\theta}$ and time. Moreover, matrix $\mathbf{V}_i$ is given as

$$\mathbf{V}_i \equiv \begin{bmatrix} \mathbf{V}_i^{\omega} \\ \mathbf{V}_i^{c} \end{bmatrix}$$

where the $3 \times q$ matrices $\mathbf{V}_i^{\omega}$ and $\mathbf{V}_i^{c}$ are defined as

$$\mathbf{V}_i^{\omega} \equiv [\boldsymbol{\omega}_i^1, \cdots, \boldsymbol{\omega}_i^q] \quad \text{and} \quad \mathbf{V}_i^{c} \equiv [\dot{\mathbf{c}}_i^1, \cdots, \dot{\mathbf{c}}_i^q]$$

while vectors $\boldsymbol{\omega}_i^j$ and $\dot{\mathbf{c}}_i^j$ for $j = 1, \cdots, q$, are the jth *partial angular velocity* and jth *partial velocity* (Kane, 1983; Levinson, 1987) of the ith link, respectively. Then, from d'Alembert's principle, Kane's equations of motion (Kane, 1961; Kane and Wang, 1965; Kane, 1983) are derived as

$$\boldsymbol{\phi}_I + \boldsymbol{\phi}_I^* = \mathbf{0} \tag{2.40}$$

which leads to q independent equations of motion of the nonholonomic system at hand, $\boldsymbol{\phi}_I$ and $\boldsymbol{\phi}_I^*$ being calculated as the q-dimensional vectors of *generalized active forces* and *generalized inertia forces* (Kane, 1983), respectively. Moreover, vectors $\boldsymbol{\phi}_I$ and $\boldsymbol{\phi}_I^*$ are calculated as

$$\boldsymbol{\phi}_I = \mathbf{V}^T \mathbf{w} \quad \text{and} \quad \boldsymbol{\phi}_I^* = \mathbf{V}^T \mathbf{w}^* \tag{2.41}$$

where the $6l \times q$ matrix $\mathbf{V}$ is defined as

$$\mathbf{V} \equiv [\mathbf{V}_1^T, \cdots, \mathbf{V}_l^T]^T \tag{2.42}$$

and $\mathbf{w}$ is a $6l$-dimensional vector of the generalized wrench acting on the system of l links. The generalized wrench of inertia moments and forces, a $6l$-dimensional vector $\mathbf{w}^*$, is given by

$$\mathbf{w}^* = -\mathbf{M}\dot{\mathbf{t}} - (\dot{\mathbf{M}} + \mathbf{W}\mathbf{M})\mathbf{t} \tag{2.43}$$

The expression for $\mathbf{w}^*$, as in eq.(2.43), will be obvious from Chapter 3 of this thesis, where the uncoupled Newton-Euler equations of motion of the l links are derived. Note that, in eq.(2.41), $\mathbf{w}$ contains external and constraint wrenches. However,

since constraint wrenches do not contribute to the motion of the system, they automatically vanish from Kane's formulation. Thus, it is not necessary to consider the constraint moments and forces while evaluating the generalized active forces in eq.(2.40).

Passerello and Huston (1973) extended Kane's formulation which, contrary to eq.(2.38), is based on the original definition of $\dot{\mathbf{q}}$, i.e., eq.(2.29). According to Passerello and Huston, vector $\dot{\mathbf{q}}$ in eq.(2.29) is defined in such a way that the last n scalar equations of eq.(2.29) are equivalent to eq.(1.2) and the remaining equations are left arbitrary, such that $\mathbf{U}_q^{-1}$ exists. Moreover, to be compatible with the nonholonomic constraints, eq.(1.2), the last n components of vector $\dot{\mathbf{q}}$ are all zero. It is pointed out in Passerello and Huston (1973) that, for holonomic systems, the generalized inertia force $\boldsymbol{\phi}_I^*$ of Kane's equations may be evaluated from the kinetic energy of the system, which is the left-hand side of eq.(2.13). This derivation avoids the computation of the acceleration of the bodies in the system. However, in order to obtain Kane's equations of motion of nonholonomic systems, the computation of the acceleration components is required. Passerello and Huston (1973) showed that the burden of computing the acceleration terms of the bodies in nonholonomic systems can be eliminated. In their method, the term $\boldsymbol{\phi}_I^*$ of a nonholonomic system is evaluated from the kinetic energy of the system and by inverting matrix $\mathbf{U}_q$. Thus, the dynamic equations which appeared in Passerello and Huston (1973) may not be the most convenient for all types of problems. However, by appropriately choosing the first q components of $\dot{\mathbf{q}}$, a set of equations of motion can be obtained, which amounts to a simplified version of Čaplygin's equations.

In dynamics, an independent set of dynamic equations is preferable since the dimension of the problem is minimum, which, in turn, enhances the speed of the simulation algorithm. Moreover, if the set of generalized coordinates is not independent, the solution of a dynamics problem involves the solution of a set of differential and algebraic equations, which is far more complex than the numerical integration of purely differential equations (Gear and Petzold, 1984; Park and Haug, 1986). Thus,

an important consideration here is the choice of independent coordinates in reducing the dimension of the dynamics problem. An arbitrary selection of independent coordinates often results in ill-conditioned matrices. To cope with such a situation, Wehage and Haug (1982) presented a method of partitioning the set of generalized coordinates using the LU factorization of the matrix **J**. On the other hand, Mani et al. (1985), Singh and Likins (1985), Kim and Vanderploeg (1986) and Liang and Lance (1987) used numerical techniques whereby matrix **J** was decomposed to determine a set of independent coordinates.

2.3 The Use of Orthogonal Complements in Dynamics

Recent developments in fast mathematical processors attracted researchers to automatically develop dynamic models of complex mechanical systems and to efficiently integrate the resulting differential equations of motion for simulation and animation purposes. The use of an orthogonal complement of the velocity constraint matrix, for example, **J** in eq.(1.2), that allows one to obtain constraint-free equations of motion, has been reported by many researchers. Some of these approaches will be reviewed below with a discussion of their merits and demerits.

2.3.1 Derivation of Dynamic Equations

One of the early research works in developing dynamic models of mechanical systems using an orthogonal complement is reported in Huston and Passerello (1974). In their paper, the equations of motion were first written in terms of p generalized coordinates as

$$\mathbf{I}\ddot{\boldsymbol{\theta}} + \mathbf{C}\dot{\boldsymbol{\theta}} = \boldsymbol{\phi}^W + \boldsymbol{\phi}^N \tag{2.44}$$

where **I** is a $p \times p$ positive-definite symmetric matrix, $\mathbf{C}\dot{\boldsymbol{\theta}}$ is a p-dimensional vector of generalized forces due to convective inertia terms, $\boldsymbol{\phi}^W$ and $\boldsymbol{\phi}^N$ are p-dimensional vectors of generalized working forces and generalized nonworking constraint forces,

respectively. The kinematic constraints are assumed to be holonomic, i.e., of the form

$$\mathbf{f}(\boldsymbol{\theta}) = \mathbf{0} \tag{2.45}$$

Note that, in eq.(2.45), the constraints are functions of $\boldsymbol{\theta}$ only. Therefore, only scleronomic constraints were considered. Hence, this method, in its present form, precludes its application to nonholonomic systems. However, the principle used to eliminate the constraint forces from the dynamic equations can be extended to nonholonomic systems. Let the system consist of h ($h < p$) scleronomic constraints and, hence, $\mathbf{f}$ is an h-dimensional vector. Differentiation of eq.(2.45) leads to

$$\mathbf{J}\dot{\boldsymbol{\theta}} = \mathbf{0} \tag{2.46}$$

where $\mathbf{J}$ is the $h \times p$ Jacobian matrix of $\mathbf{f}$ with respect to $\boldsymbol{\theta}$. According to this formulation, eq.(2.44), along with eq.(2.45), leads to $p + h$ scalar equations in $2p$ unknowns, $\boldsymbol{\theta}$ and $\boldsymbol{\phi}^N$, which admit an infinity of solutions, for $p > h$. However, given suitable initial conditions, the solution of eq.(2.44) is bound to be unique, based on the causality principle of dynamic systems (Vidyasagar, 1978). Moreover, the solution for $\boldsymbol{\theta}$ does not involve $\boldsymbol{\phi}^N$, and a question arises, namely, what are the conditions on $\boldsymbol{\phi}^N$ such that vector $\boldsymbol{\theta}$ is uniquely determined? To answer this question, both sides of eq.(2.44) are premultipied by $\dot{\boldsymbol{\theta}}^T$ and integrated, which leads to a quadratic form, as in Huston and Passerello (1974), namely,

$$\dot{\boldsymbol{\theta}}^T \mathbf{I}\dot{\boldsymbol{\theta}} = 2\int \dot{\boldsymbol{\theta}}^T \boldsymbol{\phi}^W dt + 2\int \dot{\boldsymbol{\theta}}^T \boldsymbol{\phi}^N dt$$

Now, since $\boldsymbol{\phi}^W$ is arbitrary, $\dot{\boldsymbol{\theta}}^T \boldsymbol{\phi}^N$ must be zero for $\dot{\boldsymbol{\theta}}$ to be independent of $\boldsymbol{\phi}^N$ Furthermore, this condition and eq.(2.46) must hold for all values of $\boldsymbol{\theta}$ and $\dot{\boldsymbol{\theta}}$. Thus, $\boldsymbol{\phi}^N$ must lie in the range of $\mathbf{J}^T$, i.e., an h-dimensional vector $\boldsymbol{\lambda}$ exists such that

$$\boldsymbol{\phi}^N = \mathbf{J}^T \boldsymbol{\lambda} \tag{2.47}$$

Alternatively, by definition, the generalized nonworking constraint force $\boldsymbol{\phi}^N$ does not produce any power. Hence,

$$\dot{\boldsymbol{\theta}}^T \boldsymbol{\phi}^N = 0$$

Since $\mathbf{J}\dot{\boldsymbol{\theta}} = \mathbf{0}$ from eq.(2.46), there exists an undetermined vector $\boldsymbol{\lambda}$ such that eq.(2.47) is true.

To satisfy the condition that $\dot{\boldsymbol{\theta}}^T\boldsymbol{\phi}^N$ must be zero, a $p \times q$ matrix $\mathbf{T}$ is defined in such a way that the matrix $\mathbf{T}$ is an orthogonal complement of $\mathbf{J}$, i.e., $\mathbf{JT} = \mathbf{O}$, where $\mathbf{O}$ is the $h \times q$ zero matrix. Then, premultiplication of both sides of eq.(2.44) by $\mathbf{T}^T$ yields

$$\mathbf{T}^T\mathbf{I}\ddot{\boldsymbol{\theta}} + \mathbf{T}^T\mathbf{C}\dot{\boldsymbol{\theta}} = \mathbf{T}^T\boldsymbol{\phi}^W \tag{2.48}$$

where $\boldsymbol{\phi}^N$ vanishes in the equations of motion. Moreover, q scalar equations of motion, as in eq.(2.48), along with h scalar equations of constraints, eq.(2.45), are sufficient to solve for the p unknowns in vector $\boldsymbol{\theta}$. It is pointed out here that, although this method is elegant, no guidelines are provided for the calculation of the matrix $\mathbf{T}$ and thus, it might be difficult to obtain $\mathbf{T}$ for large systems. Furthermore, the system has q-DOF and q coordinates are sufficient to control and describe the configuration of holonomic systems. With this methodology, the evaluation of extra h coordinates becomes redundant and the time required for their computation can be saved.

A similar approach has appeared in Hemami and Weimer (1981) which, unlike the approach of Huston and Passerello (1974), is applicable to nonholonomic systems. Here, also, no formal construction procedure of an orthogonal matrix is mentioned. However, it is suggested in Hemami and Weimer (1981) that, since $\mathbf{T}$ is not unique, some transformations such as premultiplication of eq.(2.44) by $\mathbf{I}^{-1}$ or premultiplication of eq.(2.46) by a nonsingular $h \times h$ matrix might ease the problem of finding $\mathbf{T}$.

2.3.2 The Computation of an Orthogonal Complement

The general concept of formulating constrained dynamic equations of motion using an orthogonal complement of a velocity constraint matrix is the same, i.e., to eliminate the constraint forces from the dynamic models of constrained mechanical systems.

Kamman and Huston (1984) used the *zero-eigenvalue theorem* in this context. The theorem is based on the zero eigenvalues of matrix $\mathbf{J}^T\mathbf{J}$, which are nothing but the zero singular values of $\mathbf{J}$. In this approach, a $p \times q$ matrix $\mathbf{T}$ is constructed whose columns are the independent eigenvectors associated with the zero eigenvalues of the $p \times p$ matrix $\mathbf{J}^T\mathbf{J}$. Thus,

$$\mathbf{J}^T\mathbf{J}\mathbf{T} = \mathbf{O} \tag{2.49}$$

where $\mathbf{O}$ is now the $p \times q$ zero matrix. Premultiplication of both sides of eq.(2.49) by $\mathbf{T}^T$, under the assumption that both $\mathbf{J}$ and $\mathbf{T}$ are of full rank, leads to

$$\mathbf{J}\mathbf{T} = \mathbf{O}$$

and the equations of motion may be obtained from eq.(2.48).

Alternative approaches for obtaining the orthogonal complement of matrix $\mathbf{J}$ are available. The singular-value-decomposition, the QR decomposition and the Gram-Schmidt orthogonalization procedure (Stewart, 1973; Golub and Van Loan, 1983) of the velocity constraint matrix $\mathbf{J}$ are suggested by Mani et al. (1985) and Singh and Likins (1985), Kim and Vanderploeg (1986), and Liang and Lance (1987), respectively. These algorithms involve numerical schemes of a complex nature. To avoid this difficulty, an alternative approach of finding an orthogonal complement is proposed by reformulating the kinematic constraints and choosing a *natural* set of generalized coordinates. The proposed technique involves neither eigenvalue calculations nor requires any decomposition schemes which are undesirable for the development of fast and accurate simulation algorithms.

Chapter 3

The Method of the Natural Orthogonal Complement (NOC)

The method of the natural orthogonal complement (NOC) relies on a novel formulation of kinematic constraints. An orthogonal complement of the kinematic constraint matrix, derived in the present approach, arises *naturally* from the definition of the velocity field of the system at hand as a linear transformation of the independent generalized speeds, which are usually the time derivatives of the joint displacements of kinematic pairs or couplings, i.e., the joint rates. The resulting orthogonal complement is termed the *natural orthogonal complement* and thus, the adopted methodology is called the method of the NOC, as first introduced in Angeles and Lee (1988). It has successfully been applied to systems with holonomic couplings (Angeles and Ma, 1988; Angeles and Lee, 1989; Ma and Angeles, 1989) and systems with flexible bodies (Cyril et al., 1989; Darcovich, 1991). In this thesis, the dynamic modelling of mechanical systems based on the NOC has been extended to nonholonomic systems. The NOC method is presented here in a unified manner, which helps to systematically develop a dynamic model of a mechanical system containing holonomic and nonholonomic couplings, as well as serial and multi-loop kinematic chains. Moreover, while developing a dynamic model, the method is capable of detecting the DOF and the controllability of the system, as pointed out in §3.3. Thus, prior to the dynamic analysis of a proposed design, it is not necessary

to perform separate analyses for the determination of the system's DOF and its controllability. Also, if the design is suitable, a part of the dynamic analysis is already done. Hence, the determination of the DOF of a system, along with the test for its controllability, can be performed as a part of the dynamic analysis. Furthermore, it will be apparent from subsequent chapters, in which the method is used to derive the equations of motion of different mechanical systems, that the NOC is evaluated without any complex computations. It is also shown in §3.6 how the method of the NOC can be used in the presence of redundant actuation.

3.1 Formulation of the Kinematic Constraints

The crucial step in successfully modelling a broad class of mechanical systems with the NOC is the representation of the kinematic constraints. Generally, as shown in Chapters 1 and 2, the form taken on by these constraints is such that they are linear in the generalized speeds and linearly independent among them. Within the framework of this methodology, both holonomic and nonholonomic constraints are expressed as a system of equations that are *linear* and *homogeneous* in the *twists* of all the bodies of the system, and, most frequently, linearly dependent among them. The twist of the ith rigid link, which contains the necessary and sufficient information for determining the velocity field of this ith link, is defined in §2.1. Moreover, it is assumed that the ith body of the system under study that comprises l rigid links and k kinematic pairs is coupled to the jth link through either a holonomic or a nonholonomic coupling, which is denoted as the (i,j) joint. Now, mechanical couplings that produce holonomic and nonholonomic constraints on the twists of the coupled bodies—velocity constraints—are represented as a system of linear homogeneous equations in the twists of the two coupled bodies, say $\mathbf{t}_i$ and $\mathbf{t}_j$, defined as in eq.(2.5), namely,

$$\mathbf{A}_{i,i}\mathbf{t}_i + \mathbf{A}_{i,j}\mathbf{t}_j = \mathbf{0}, \quad \text{for } (i,j) = 1,\cdots,k;\ i,j \in [1,\ l] \text{ and } i \neq j \tag{3.1}$$

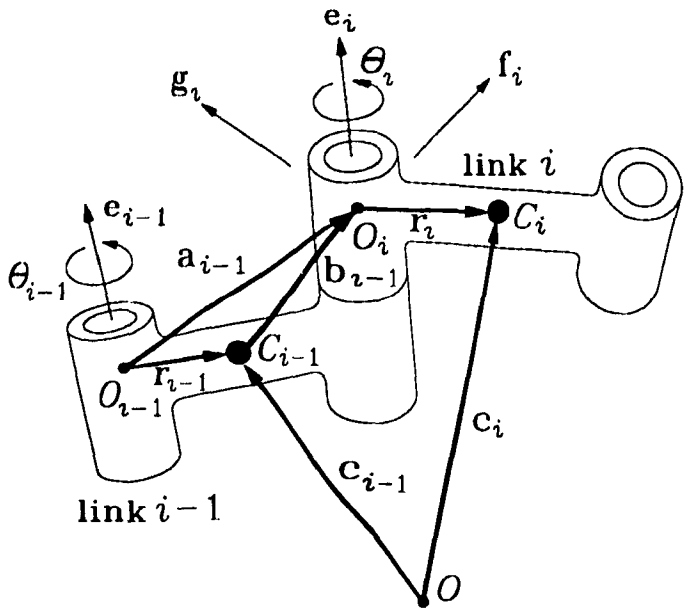

Fig. 3.1 Two links coupled by a revolute joint.

Furthermore, for m' scalar constraints, the $m' \times 6$ coefficient matrices $\mathbf{A}_{t,t}$ and $\mathbf{A}_{t,j}$ are, in general, configuration-dependent, i.e., they are functions of the generalized coordinates. Here m' denotes the total number of kinematic constraint equations, which are usually linearly dependent. The forms of matrices $\mathbf{A}_{t,t}$ and $\mathbf{A}_{t,j}$, for holonomic and nonholonomic couplings, are derived below.

3.1.1 Holonomic Constraints

The *fundamental* lower kinematic pairs, namely, the prismatic and revolute pairs, always lead to holonomic constraints. These pairs are called fundamental because the other four lower kinematic pairs—the screw, the cylindrical, planar and spherical pairs—can be derived as a combination of these. Mechanical couplings other than the lower kinematic pairs, that produce holonomic constraints are, among others, pulley-belt, cam-follower and gear-train transmissions.

As an example shown in Fig. 3.1, the kinematic constraints of two links coupled by a revolute joint are derived as follows: If $\dot{\theta}_i$ is the joint rate for the $(i, i-1)$st revolute pair coupled to the ith and the $(i-1)$st links, then, referring to Fig. 3.1, the

relative angular velocity of the ith link with respect to the $(i-1)$st link, $\boldsymbol{\omega}_i - \boldsymbol{\omega}_{i-1}$, is $\dot{\theta}_i \mathbf{e}_i$, where vector $\mathbf{e}_i$ is the unit vector parallel to the axis of the $(i, i-1)$st revolute pair. Thus, the equation constraining the angular velocities of two successive links is given by:

$$\mathbf{e}_i \times (\boldsymbol{\omega}_i - \boldsymbol{\omega}_{i-1}) = \mathbf{0}$$

or

$$\mathbf{E}_i(\boldsymbol{\omega}_i - \boldsymbol{\omega}_{i-1}) = \mathbf{0} \tag{3.2}$$

where $\mathbf{E}_i$ is the cross-product tensor, as defined in eq.(2.7), associated with vector $\mathbf{e}_i$. Moreover, from Fig. 3.1 it is clear that

$$\dot{\mathbf{c}}_i = \dot{\mathbf{c}}_{i-1} + \boldsymbol{\omega}_{i-1} \times \mathbf{b}_{i-1} + \boldsymbol{\omega}_i \times \mathbf{r}_i \tag{3.3}$$

where the 3-dimensional vectors $\mathbf{c}_{i-1}$ and $\mathbf{c}_i$ denote the position of the mass centres of links $i-1$ and i, respectively. Moreover, vectors $\mathbf{b}_{i-1}$ and $\mathbf{r}_i$ are shown in Fig. 3.1. Equations (3.2) and (3.3) are now written in terms of the link twists, which readily produces an equation of the form of eq.(3.1), namely,

$$\mathbf{A}_{i,i}\mathbf{t}_i + \mathbf{A}_{i,i-1}\mathbf{t}_{i-1} = \mathbf{0} \tag{3.4}$$

where the 6×6 matrices $\mathbf{A}_{i,i}$ and $\mathbf{A}_{i,i-1}$ are as shown below:

$$\mathbf{A}_{i,i} = \begin{bmatrix} \mathbf{E}_i & \mathbf{O} \\ \mathbf{R}_i & \mathbf{1} \end{bmatrix}, \qquad \mathbf{A}_{i,i-1} = \begin{bmatrix} -\mathbf{E}_i & \mathbf{O} \\ \mathbf{B}_{i-1} & -\mathbf{1} \end{bmatrix} \tag{3.5}$$

with $\mathbf{R}_i$ and $\mathbf{B}_{i-1}$ being the cross-product tensors associated with vectors $\mathbf{r}_i$ and $\mathbf{b}_{i-1}$, respectively.

3.1.2 Nonholonomic Constraints

This subsection will be limited to nonholonomic pure rolling, and hence, no slippage is considered. As an example of this type of nonholonomic coupling, a rigid body rolling on a plane without slipping is shown in Fig. 3.2, the non-slip condition in linear homogeneous form being derived below. If the rigid body is considered as

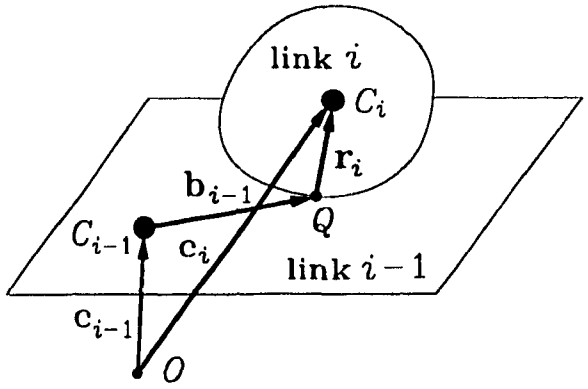

Fig. 3.2 A rigid body rolling on a plane.

the ith link of a system and the plane is a part of the boundary of the $(i-1)$st link, then, referring to Fig. 3.2, the resulting nonholonomic constraint is stated as

$$\dot{\mathbf{c}}_i = \dot{\mathbf{c}}_{i-1} + \boldsymbol{\omega}_{i-1} \times \mathbf{b}_{i-1} + \boldsymbol{\omega}_i \times \mathbf{r}_i \tag{3.6}$$

where the vectors appearing in eq.(3.6) are shown in Fig. 3.2. Moreover, eq.(3.6) can also be written in the form of eq.(3.4), with the 3×6 matrices $\mathbf{A}_{i,i}$ and $\mathbf{A}_{i,i-1}$ defined as

$$\mathbf{A}_{i,i} = [\mathbf{R}_i \quad \mathbf{1}] \quad \text{and} \quad \mathbf{A}_{i,i-1} = [\mathbf{B}_{i-1} \quad -\mathbf{1}] \tag{3.7}$$

and the cross-product tensors $\mathbf{R}_i$ and $\mathbf{B}_{i-1}$ are associated with the vectors $\mathbf{r}_i$ and $\mathbf{b}_{i-1}$, respectively, as shown in Fig. 3.2.

From eqs.(3.4), (3.5) and (3.7), it is apparent that kinematic constraints, whether holonomic or nonholonomic, can be written in the form of linear homogeneous equations in the twists of every pair of coupled bodies of a mechanical system. An essential difference between the holonomic and nonholonomic constraints previously derived is stated in the form of lemmas.

Lemma 3.1 Holonomic kinematic constraints written in the form of eqs.(3.4) and (3.5) always lead to six linearly dependent scalar constraint equations, i.e., $m' = 6$.

Proof: Let a matrix $\mathbf{A}_h$ be defined as

$$\mathbf{A}_h = \begin{bmatrix} \mathbf{E}_i & \mathbf{O} & -\mathbf{E}_i & \mathbf{O} \\ \mathbf{R}_i & \mathbf{1} & \mathbf{B}_{i-1} & -\mathbf{1} \end{bmatrix} \tag{3.8}$$

where the first two column blocks of matrix $\mathbf{A}_h$ amount to the 6×6 matrix $\mathbf{A}_{i,i}$ in eq.(3.5) and the last two column blocks correspond to the 6×6 matrix $\mathbf{A}_{i,i-1}$ in eq.(3.5). To prove that these six holonomic constraints are dependent, it is sufficient to show that the matrix $\mathbf{A}_h$ in eq.(3.8) is rank deficient. This is done as follows: matrix $\mathbf{A}_h$ is a 6×12 matrix, its rank thus being at most six, i.e., the matrix has at most six independent rows. To find its rank, elementary operations can be performed on the columns of $\mathbf{A}_h$, as shown in §A.1, that do not change its rank, thereby producing a reduced 6×6 matrix $\mathbf{A}'_h$, as shown below:

$$\mathbf{A}'_h = \begin{bmatrix} \mathbf{E}_i & \mathbf{O} \\ \mathbf{O} & \mathbf{1} \end{bmatrix} \tag{3.9}$$

It is clear from eq.(3.9) that three eigenvalues of the 6×6 matrix $\mathbf{A}'_h$ are those of the 3×3 identity tensor, $\mathbf{1}$, the other three eigenvalues of the same matrix being those of $\mathbf{E}_i$, which, as proven in §A.3, has exactly one zero eigenvalue, associated with the unit eigenvector $\mathbf{e}_i$. Thus, the rank of matrix $\mathbf{A}'_h$ is five and, hence, of the six constraint equations, only five are independent. When uncoupled, a rigid body in the 3-dimensional Cartesian space has six DOF. Therefore, a revolute pair that allows only one DOF motion of the coupled bodies leads to five independent scalar constraints, as reflected by the rank of matrix $\mathbf{A}'_h$. Moreover, if the six constraint equations were independent, the DOF of a revolute joint would be zero, i.e., the coupled bodies would be rigidly connected. Hence, any joint, possessing one or more DOF, leading to holonomic constraints, has six dependent constraint equations. Moreover, among kinematic pairs, an increase in the DOF means an elimination of an independent constraint equation.

Lemma 3.2 Nonholonomic kinematic constraints, as given in eqs.(3.4) and (3.7), always result in three linearly independent scalar constraint equations.

Proof: In a similar way to the holonomic case, a matrix $\mathbf{A}_n$ is constructed as follows:

$$\mathbf{A}_n = [\mathbf{R}_i \quad \mathbf{1} \quad \mathbf{B}_{i-1} \quad -\mathbf{1}] \tag{3.10}$$

where the four column blocks of the 3×12 matrix $\mathbf{A}_n$ are those of the matrices $\mathbf{A}_{i,i}$ and $\mathbf{A}_{i,i-1}$, given in eq.(3.7). Now, matrix $\mathbf{A}_n$ is reduced, as explained in §A.2, and amounts to the 3×3 identity tensor, namely,

$$\mathbf{A}_n^r = \mathbf{1} \tag{3.11}$$

which shows that the three constraint equations in eq.(3.7) are linearly independent.

3.2 Dynamic Modelling of Mechanical Systems Using the NOC

The method of the NOC, as pertaining to mechanical systems composed of constrained rigid bodies, first introduced in Angeles and Lee (1988). is described in six steps, namely,

Step 1: The Euler equations of motion, describing the rotational motion of the ith link, are given by

$$\frac{d}{dt}(\mathbf{I}_i\boldsymbol{\omega}_i) + \boldsymbol{\sigma}_i \times \mathbf{I}_i\boldsymbol{\omega}_i = \mathbf{n}_i$$

or

$$\mathbf{I}_i\dot{\boldsymbol{\omega}}_i + \dot{\mathbf{I}}_i\boldsymbol{\omega}_i + \boldsymbol{\sigma}_i \times \mathbf{I}_i\boldsymbol{\omega}_i = \mathbf{n}_i \tag{3.12}$$

where $\mathbf{I}_i$ is the 3×3 inertia tensor of the ith link about its mass centre and $\boldsymbol{\omega}_i$, $\boldsymbol{\sigma}_i$ and $\mathbf{n}_i$ are the 3-dimensional vectors of angular velocity of the ith link, angular velocity of the ith coordinate frame fixed to the ith link and the resultant moment acting on the ith link, respectively. Moreover, Newton's Second Law, describing the motion of the mass centre of the ith link, is expressed as

$$\frac{d}{dt}(m_i\dot{\mathbf{c}}_i) + \boldsymbol{\sigma}_i \times (m_i\dot{\mathbf{c}}_i) = \mathbf{f}_i$$

or

$$m_i\ddot{\mathbf{c}}_i + m_i\boldsymbol{\sigma}_i \times \dot{\mathbf{c}}_i = \mathbf{f}_i \tag{3.13}$$

where m_i and $\mathbf{f}_i$ are the mass of the ith link and the resultant force acting on the mass centre of the ith link, respectively. Now, recalling the definitions of the twist, $\mathbf{t}_i$, wrench, $\mathbf{w}_i$, extended angular velocity matrix, $\mathbf{W}_i$, extended mass matrix, $\mathbf{M}_i$ of the ith link, and the rate of change of the latter, $\dot{\mathbf{M}}_i$, as defined in §2.1, the Newton-Euler equations, eqs.(3.12) and (3.13), governing the motion of the ith body, can be written in a compact form as:

$$\mathbf{M}_i\dot{\mathbf{t}}_i = -(\dot{\mathbf{M}}_i + \mathbf{W}_i\mathbf{M}_i)\mathbf{t}_i + \mathbf{w}_i^W + \mathbf{w}_i^N \tag{3.14}$$

where the resultant wrench vector $\mathbf{w}_i$ has been decomposed as

$$\mathbf{w}_i = \mathbf{w}_i^W + \mathbf{w}_i^N$$

with $\mathbf{w}_i^W$ and $\mathbf{w}_i^N$ being defined, in accordance with the definition of $\mathbf{w}_i$, as the working wrench and the nonworking constraint wrench, both acting on the ith body, respectively. The former represents working moments and forces supplied by actuators or arising from gravity or dissipation, whereas the latter denotes nonworking moments and forces whose sole role is that of keeping the bodies together.

Step 2: It is assumed that the mechanical system under study is composed of l rigid links. Then, the Newton–Euler equations for all the individual links can be written as

$$\mathbf{M}_i\dot{\mathbf{t}}_i = -(\dot{\mathbf{M}}_i + \mathbf{W}_i\mathbf{M}_i)\mathbf{t}_i + \mathbf{w}_i^W + \mathbf{w}_i^N, \quad \text{for} \quad i = 1,...,l \tag{3.15}$$

Next, by virtue of the definitions given in §2.1, of the $6l$-dimensional vectors of generalized twist $\mathbf{t}$ and the $6l \times 6l$ matrices of generalized angular velocity $\mathbf{W}$, generalized mass $\mathbf{M}$, and its time-rate of change, $\dot{\mathbf{M}}$, the l dynamic equations, eq.(3.15), can now be expressed as

$$\mathbf{M}\dot{\mathbf{t}} = -(\dot{\mathbf{M}} + \mathbf{W}\mathbf{M})\mathbf{t} + \mathbf{w}^W + \mathbf{w}^N \tag{3.16}$$

where $\mathbf{w}^W$ and $\mathbf{w}^N$ are defined, similar to $\mathbf{w}$, as the $6l$-dimensional vectors of generalized working wrench and generalized nonworking constraint wrench, respectively. They are given as

$$\mathbf{w}^W \equiv \begin{bmatrix} \mathbf{w}_1{}^W \\ \vdots \\ \mathbf{w}_l{}^W \end{bmatrix} \quad \text{and} \quad \mathbf{w}^N \equiv \begin{bmatrix} \mathbf{w}_1{}^N \\ \vdots \\ \mathbf{w}_l{}^N \end{bmatrix}$$

Equation (3.16) is formally identical to eq.(3.14), and constitutes a set of $6l$ unconstrained scalar dynamic equations. Moreover, if eq.(3.16) is rewritten as

$$\mathbf{w}^W + \mathbf{w}^N = \mathbf{M}\dot{\mathbf{t}} + (\dot{\mathbf{M}} + \mathbf{W}\mathbf{M})\mathbf{t} \tag{3.17}$$

then the negative of the right-hand side of eq.(3.17) is recognized as the generalized inertia wrench, denoted in eq.(2.43) by $\mathbf{w}^*$. This is equivalent to the inertia force in d'Alembert's equations of motion of a moving particle, which is defined as the negative of the product of the mass of the particle and its acceleration. The right-hand side of eq.(3.17) is used in §2.2.6 to find the generalized inertia forces of Kane's equations of motion.

Step 3: The kinematic constraints produced by holonomic and nonholonomic couplings are derived in a differential form. Within the methodology adopted here, as proven in §3.1, every holonomic coupling gives rise to six linearly dependent scalar equations. Also, every nonholonomic coupling, in the absence of slippage, gives rise to three linearly independent scalar equations. These constraints can be written as a system of linear homogeneous equations in the twists of the l links of the system, which is equivalent to the following linear homogeneous system in the vector of generalized twist:

$$\mathbf{A}\mathbf{t} = \mathbf{0} \tag{3.18}$$

Here, $\mathbf{A}$ is a $(6\gamma + 3\nu) \times 6l$ matrix, γ and ν being the numbers of holonomic and nonholonomic pairs or couplings, respectively, so that the total number of kinematic pairs k is equal to $\gamma + \nu$.

Step 4: Under the assumption that the DOF of the system is q, the q-dimensional vector $\dot{\boldsymbol{\theta}}_I$ of independent generalized speeds is recalled from eq.(2.3). Then, the vector of generalized twist can be represented as the following linear transformation of $\dot{\boldsymbol{\theta}}_I$:

$$\mathbf{t} = \mathbf{T}\dot{\boldsymbol{\theta}}_I \tag{3.19}$$

where $\mathbf{T}$ is a $6l \times q$ matrix that is, in general, a function of the generalized coordinates, $\boldsymbol{\theta}_I$, and time. Upon substitution of $\mathbf{t}$, as given by eq.(3.19), into eq.(3.18), the relation

below is obtained:

$$\mathbf{A}\mathbf{T}\dot{\boldsymbol{\theta}}_I = \mathbf{0} \tag{3.20}$$

Since all the components of vector $\dot{\boldsymbol{\theta}}_I$ are independent, the relation below can be readily derived:

$$\mathbf{A}\mathbf{T} = \mathbf{O} \tag{3.21}$$

where $\mathbf{O}$ is the $(6\gamma + 3\nu) \times q$ zero matrix. Equation (3.21) shows that $\mathbf{T}$ is an orthogonal complement of $\mathbf{A}$. Because of the particular form of choosing this complement, eq.(3.19), $\mathbf{T}$ is termed the *natural orthogonal complement* (NOC) of $\mathbf{A}$. It is pointed out here that, to obtain the NOC of the kinematic constraint matrix $\mathbf{A}$, as shown in eq.(3.21), the choice of eq.(3.19) is important, because for matrix $\mathbf{T}$ to be the NOC, the generalized twist must be written as a linear combination of the independent generalized speeds. In serial-type mechanical systems, for example, a q-axes q-DOF serial robotic manipulator, where all the joint rates can be considered as the independent generalized speeds, an expression for $\mathbf{t}$ in the form of eq.(3.19) is readily available. However, in the presence of unactuated joints that occur in a multi-loop mechanical system, e.g., in a parallel robotic manipulator, where not all joints are actuated, deriving the expression appearing in eq.(3.19) is not straightforward. Thus, in §3.3, a method is given to find the NOC for mechanical systems with unactuated joints.

Step 5: Since the role of the nonworking constraint wrenches is limited to keeping the coupled links together, they do not contribute to changes in the energy of the system. Hence, the power π^N developed by the constraint wrenches vanishes, i.e.,

$$\pi^N = \mathbf{t}^T\mathbf{w}^N = 0 \tag{3.22}$$

Substitution of eq.(3.19) into eq.(3.22) leads to

$$\dot{\boldsymbol{\theta}}_I^T\mathbf{T}^T\mathbf{w}^N = 0 \tag{3.23}$$

and, due to the independence of the components of vector $\dot{\boldsymbol{\theta}}_I$, eq.(3.23) leads to

$$\mathbf{T}^T\mathbf{w}^N = \mathbf{0} \tag{3.24}$$

where $\mathbf{0}$ is the q-dimensional zero vector. Now, it is apparent from eq.(3.24) that $\mathbf{w}^N$ lies in the nullspace of matrix $\mathbf{T}^T$. Moreover, by virtue of the definition of matrix $\mathbf{A}$, $\mathbf{T}$ is an orthogonal complement of $\mathbf{A}$. Thus, the vector of nonworking constraint wrench, $\mathbf{w}^N$, lies in the range of the transpose of $\mathbf{A}$, i.e.,

$$\mathbf{w}^N = \mathbf{A}^T\boldsymbol{\lambda} \tag{3.25}$$

where $\boldsymbol{\lambda}$ is a $(6\gamma + 3\nu)$-dimensional vector of undetermined scalars which are nothing but the Lagrange multipliers discussed in §2.2.1. It is pointed out here that the duality between kinematic constraints and nonworking constraint wrenches (Saha and Angeles, 1991d), as evident from eqs.(3.18) and (3.25), can be exploited in order to determine the constraint torques and forces which are needed for design purposes.

Step 6: Upon multiplication of both sides of the $6l$-dimensional Newton-Euler uncoupled equations of the system, eq.(3.16), by the transpose of $\mathbf{T}$, the vector of nonworking constraint wrench is eliminated from the said equation, which is obvious from eq.(3.24), the equation thus obtained being reduced to:

$$\mathbf{T}^T\mathbf{M}\dot{\mathbf{t}} = -\mathbf{T}^T(\dot{\mathbf{M}} + \mathbf{W}\mathbf{M})\mathbf{t} + \mathbf{T}^T\mathbf{w}^W \tag{3.26}$$

Now, both sides of eq.(3.19) are differentiated with respect to time, which yields

$$\dot{\mathbf{t}} = \mathbf{T}\ddot{\boldsymbol{\theta}}_I + \dot{\mathbf{T}}\dot{\boldsymbol{\theta}}_I \tag{3.27}$$

Note that the entities of $\dot{\mathbf{T}}$ are not, in general, simply the time derivatives of the corresponding entities of $\mathbf{T}$, because the vector bases on which $\mathbf{T}$ is expressed are usually time-varying.

Furthermore, $\mathbf{w}^W$ is decomposed as follows:

$$\mathbf{w}^W = \mathbf{w}^A + \mathbf{w}^G + \mathbf{w}^D \tag{3.28}$$

where $\mathbf{w}^A$ represents the generalized wrench due to torques and forces applied by the actuators, if any, whereas $\mathbf{w}^G$ and $\mathbf{w}^D$ account for gravity and dissipative effects, respectively.

Substituting eqs.(3.19), (3.27) and (3.28) into eq.(3.26), a system of q independent dynamic equations are derived for a constrained mechanical system, namely,

$$\mathbf{T}^T\mathbf{M}(\mathbf{T}\ddot{\boldsymbol{\theta}}_I + \dot{\mathbf{T}}\dot{\boldsymbol{\theta}}_I) = -\mathbf{T}^T(\dot{\mathbf{M}} + \mathbf{W}\mathbf{M})\mathbf{T}\dot{\boldsymbol{\theta}}_I + \mathbf{T}^T(\mathbf{w}^I + \mathbf{w}^G + \mathbf{w}^D)$$

or

$$\mathbf{I}(\boldsymbol{\theta}_I)\ddot{\boldsymbol{\theta}}_I = \mathbf{C}(\boldsymbol{\theta}_I, \dot{\boldsymbol{\theta}}_I)\dot{\boldsymbol{\theta}}_I + \boldsymbol{\tau} + \boldsymbol{\gamma} + \boldsymbol{\delta} \tag{3.29}$$

where

$\mathbf{I} \equiv \mathbf{T}^T\mathbf{M}\mathbf{T}$: $q \times q$ matrix of generalized inertia.

$\mathbf{C} \equiv -\mathbf{T}^T[\mathbf{M}\dot{\mathbf{T}} + (\dot{\mathbf{M}} + \mathbf{W}\mathbf{M})\mathbf{T}]$: $q \times q$ matrix of convective inertia terms

$\boldsymbol{\tau} \equiv \mathbf{T}^T\mathbf{w}^A$: q-dimensional vector of generalized driving force

$\boldsymbol{\gamma} \equiv \mathbf{T}^T\mathbf{w}^G$: q-dimensional vector of generalized force due to gravity

$\boldsymbol{\delta} \equiv \mathbf{T}^T\mathbf{w}^D$: q-dimensional vector of generalized dissipative force

From the foregoing discussion, then, it becomes apparent that eq.(3.29) represents the Euler-Lagrange dynamic equations of the system at hand, free of non working generalized constraint forces. Moreover, the dynamic model thus derived is applicable to mechanical systems consisting of both holonomic and nonholonomic couplings. Furthermore, the dynamic equations have been derived without resorting to lengthy partial differentiations, which would be the case if either a straightforward or a recursive derivation of the Euler-Lagrange equations had been attempted.

3.3 Derivation of the NOC in the Presence of Unactuated Joints

The presence of unactuated joints is very common in multi-loop mechanical systems, an example of such a system being an automatic guided vehicle. In order to obtain the dynamic equations of motion in the presence of unactuated joints with the aid of the NOC method, it is necessary to rederive eq.(3.19) in Step 4 and eq.(3.27) in Step 6 of the adopted methodology given in §3.2. In any mechanical system, the

generalized twist of all the links can be written as a linear transformation of the p-dimensional vector of the generalized speeds which need not be independent, i.e.,

$$\mathbf{t} = \mathbf{T}_m \dot{\boldsymbol{\theta}} \tag{3.30}$$

where the $6l \times p$ matrix $\mathbf{T}_m$ is a function of vector $\boldsymbol{\theta}$ and time. Substitution of eq.(3.30) into eq.(3.18) yields

$$\mathbf{A}\mathbf{T}_m \dot{\boldsymbol{\theta}} = \mathbf{0} \tag{3.31}$$

Since the components of $\dot{\boldsymbol{\theta}}$, in general, are not independent,

$$\mathbf{A}\mathbf{T}_m \neq \mathbf{O} \tag{3.32}$$

which has already been pointed out in Step 4 of §3.2. However, a set of independent generalized speeds which are, normally, a set of actuated joint rates, grouped in the q-dimensional vector $\dot{\boldsymbol{\theta}}_I$, can be chosen, where q is the DOF of the system, in the absence of redundant actuations. Moreover, $\dot{\boldsymbol{\theta}}_D$ is defined as the vector of rates of the remaining joints in the system, i.e., as the vector of unactuated joint rates. Thus, vector $\dot{\boldsymbol{\theta}}$ can be expressed according to eq.(2.3), while eq.(3.30) can be rewritten as

$$\mathbf{t} = \mathbf{T}_I \dot{\boldsymbol{\theta}}_I + \mathbf{T}_D \dot{\boldsymbol{\theta}}_D \tag{3.33}$$

where

$$\mathbf{T}_m \equiv [\mathbf{T}_I, \quad \mathbf{T}_D]$$

and $\mathbf{T}_I$ and $\mathbf{T}_D$ are $6l \times q$ and $6l \times m$ matrices, respectively. Furthermore, to write $\mathbf{t}$ as a linear transformation of vector $\dot{\boldsymbol{\theta}}_I$, an expression of $\dot{\boldsymbol{\theta}}_D$ in terms of $\dot{\boldsymbol{\theta}}_I$, similar to eq.(2.17), is derived as follows: an $m \times p$ matrix $\mathbf{J}$ is first derived, whose rows are the m independent rows of the $(6\gamma + 3\nu) \times p$ matrix $\mathbf{A}\mathbf{T}_m$. These independent constraint equations are expressed as

$$\mathbf{J}\dot{\boldsymbol{\theta}} = \mathbf{0} \tag{3.34}$$

where eq.(3.34) is eq.(1.2) in which the m-dimensional vector $\mathbf{b}$ does not appear. Thus, with the approach introduced here, no distinction needs to be made between

catastatic, acatastatic, scleronomic and rheonomic constraints, for all are treated as catastatic ones. Note that it is not recommended to compute matrix $\mathbf{J}$ from eq.(3.31), since such computation will involve decomposition techniques similar to those mentioned in §2.3.2, which, due to their complexity, are not recommended for the development of fast simulation algorithms. In fact, a scheme based on independent loop equations of the whole kinematic chain (Gosselin, 1988; Nahon, 1990) is presented in §3.4, which also allows one to obtain the DOF of the mechanical system at hand using the relation given in Angeles and Gosselin (1988) as

$$q = \dim[\mathcal{N}(\mathbf{J})] \tag{3.35}$$

where $\mathcal{N}(\mathbf{J})$ is the nullspace of $\mathbf{J}$.

Now, eq.(3.34) is rewritten as

$$\mathbf{J}_I\dot{\boldsymbol{\theta}}_I + \mathbf{J}_D\dot{\boldsymbol{\theta}}_D = \mathbf{0} \tag{3.36}$$

where

$$\mathbf{J} \equiv [\mathbf{J}_I, \ \mathbf{J}_D]$$

$\mathbf{J}_I$ and $\mathbf{J}_D$ being $m \times q$ and $m \times m$ matrices, respectively. If the mechanical system at hand is controllable by its minimal set of actuated joints, then $\mathbf{J}_D$ is of full rank. Thus, $\mathbf{J}_D^{-1}$ exists and, hence, the dependent generalized speeds are computed as given by eq.(2.17), namely,

$$\dot{\boldsymbol{\theta}}_D = \mathbf{U}\dot{\boldsymbol{\theta}}_I \tag{3.37}$$

where the $m \times q$ matrix $\mathbf{U}$ is derived from eq.(3.36) as

$$\mathbf{U} = -\mathbf{J}_D^{-1}\mathbf{J}_I$$

Upon substitution of eq.(3.37) into eq.(3.33), an expression for $\mathbf{t}$ is obtained as,

$$\mathbf{t} = (\mathbf{T}_I + \mathbf{T}_D\mathbf{U})\dot{\boldsymbol{\theta}}_I \tag{3.38}$$

Since $\dot{\boldsymbol{\theta}}_I$ is defined as the vector of independent generalized speeds, the NOC of matrix $\mathbf{A}$, in the presence of unactuated joints and in the absence of redundant

actuation, is given by

$$\mathbf{T} = \mathbf{T}_I + \mathbf{T}_D\mathbf{U} = \mathbf{T}_I - \mathbf{T}_D\mathbf{J}_D^{-1}\mathbf{J}_I \tag{3.39}$$

Matrix $\dot{\mathbf{T}}$ is now obtained as

$$\dot{\mathbf{T}} = \dot{\mathbf{T}}_I + \dot{\mathbf{T}}_D\mathbf{U} + \mathbf{T}_D\dot{\mathbf{U}}$$

or

$$\dot{\mathbf{T}} = \dot{\mathbf{T}}_I - \dot{\mathbf{T}}_D\mathbf{J}_D^{-1}\mathbf{J}_I + \mathbf{T}_D\mathbf{J}_D^{-1}\dot{\mathbf{J}}_D\mathbf{J}_D^{-1}\mathbf{J}_I - \mathbf{T}_D\mathbf{J}_D^{-1}\dot{\mathbf{J}}_I \tag{3.40}$$

Knowing matrices $\mathbf{T}$ and $\dot{\mathbf{T}}$ from eqs.(3.39) and (3.40), a set of constrained Euler-Lagrange dynamic equations of motion of mechanical systems in the presence of unactuated joints is written as

$$\mathbf{I}(\boldsymbol{\theta})\ddot{\boldsymbol{\theta}}_I = \mathbf{C}(\boldsymbol{\theta}, \dot{\boldsymbol{\theta}}_I)\dot{\boldsymbol{\theta}}_I + \boldsymbol{\tau} + \boldsymbol{\gamma} + \boldsymbol{\delta} \tag{3.41}$$

where $\mathbf{I}$, $\mathbf{C}$, $\boldsymbol{\tau}$, $\boldsymbol{\gamma}$ and $\boldsymbol{\delta}$ are defined in Step 6 of §3.2. It is pointed out that, contrary to eq.(3.29), matrix $\mathbf{I}$ in eq.(3.41) is a function of all generalized coordinates. Moreover, matrix $\mathbf{C}$ is, in general, a nonlinear function of the generalized coordinates and linear in the independent generalized speeds.

It is apparent from eqs.(3.39) and (3.40), that matrices $\mathbf{T}$ and $\dot{\mathbf{T}}$ entail cumbersome expressions. Thus, for multi-loop systems where matrix $\mathbf{T}$ is time-varying, the derivation of $\mathbf{T}$ and $\dot{\mathbf{T}}$ at any instant using these equations will lead to expensive algorithms. Efficient methods of calculating both $\mathbf{T}$ and $\dot{\mathbf{T}}$, while avoiding the cumbersome expressions, are shown in §3.5.

3.4 A Relation between the Actuated and Unactuated Joint Rates

In the present formulation, the derivation of matrix $\mathbf{J}$, as in eq.(3.34), is necessary in order to find a relation between the actuated and unactuated joint rates which, in turn, allows one to determine the dependent generalized speeds in terms of

the independent generalized speeds. In fact, in the absence of redundant actuation, the unactuated and actuated joint rates can play the roles of the dependent and independent generalized speeds, respectively. The presence of unactuated joints is very common in mechanical systems with kinematic loops. In a multi-loop system, a set of m independent constraint relations can be conveniently obtained from the independent kinematic loops of the kinematic chains. The independent kinematic loops are recognized here from the graph representation of mechanical systems.

3.4.1 Graph Representation of Kinematic Chains

The concept of a mechanical network, derived from that of an electrical network, allows one to systematically describe kinematic chains (Davies, 1981). Topologically, a mechanical network containing joints and links is analogous to an electrical network made up of nodes and impedances. Hence, *graph theory* offers a systematic way of representing the topology of kinematic chains. The graph representation of kinematic chains has been used by, among others, Dobrjanskyj and Freudenstein (1967) and Baker (1981). It consists of a diagram where each link is represented by a point and each joint by an edge. Thus, the graph representation of a kinematic chain of a mechanical network is a collection of points connected by edges. Pertinent definitions of terms and results to be used in this thesis can be found in (Harary, 1969), and hence, they are not included here.

The number of independent kinematic loops in a mechanical system is found by counting the number of independent cycles, C, in the associated graph. The number C in a connected graph is given in turn by Euler's formula for graphs (Harary, 1969), namely,

$$C = Q - P + 1 \tag{3.42}$$

where Q is the number of edges and P is the number of points. Moreover, C is an invariant of the graph $\mathcal{G}$. The determination of the independent loops in a multi loop system is illustrated with an example pertaining to a 3-wheeled 2-DOF AGV.

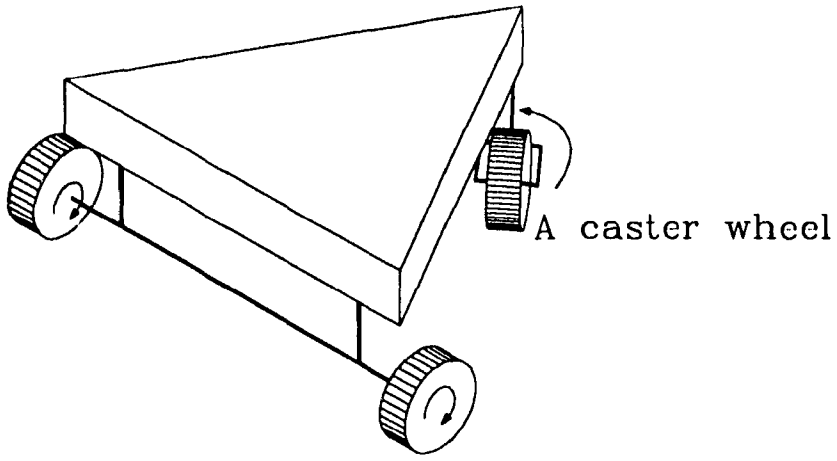

Fig. 3.3 A 3-wheeled 2-DOF AGV

The result will be used later in Chapter 4. The graph for this AGV, as shown in Fig. 3.3, is drawn in Fig. 3.4(a) where points B, P, R_1, R_2, F and L represent, respectively, the base, i.e., the floor on which the AGV moves, the platform, the left rear wheel, the right rear wheel, the front caster wheel and the fork connecting the platform with the front wheel. A spanning tree is shown in Fig. 3.4(b). The spanning tree is not unique and thus, other spanning trees could have been chosen. The chords corresponding to this spanning tree are shown in Fig. 3.4(c) and finally, the two resulting cycle bases, i.e., the two independent kinematic loops of the system at hand, are shown in Fig. 3.4(d).

3.5 Calculation of the NOC and its Time Derivative

The derivation of the NOC, particularly using eq.(3.39) is, in general, costly, except for very simple systems such as a disk rolling on a plane or a planar four-bar linkage. An efficient method of calculating $\mathbf{T}$ (Ma and Angeles, 1989) can be readily derived by noticing that $\mathbf{T}$ depends on generalized coordinates only. Moreover, the jth column of $\mathbf{T}$ equals $\partial \mathbf{t}/\partial \dot{\theta}_j$, for $j = 1, \cdots, q$. Thus, $\mathbf{T}$ can be found as follows:

$$\mathbf{T} = [\mathbf{t}|_{\dot{\theta}_1=1}, \mathbf{t}|_{\dot{\theta}_2=1}, \cdots, \mathbf{t}|_{\dot{\theta}_q=1}]_{\text{other } \theta_j\text{s of } \boldsymbol{\theta}_I \text{ are zero}} \tag{3.43}$$

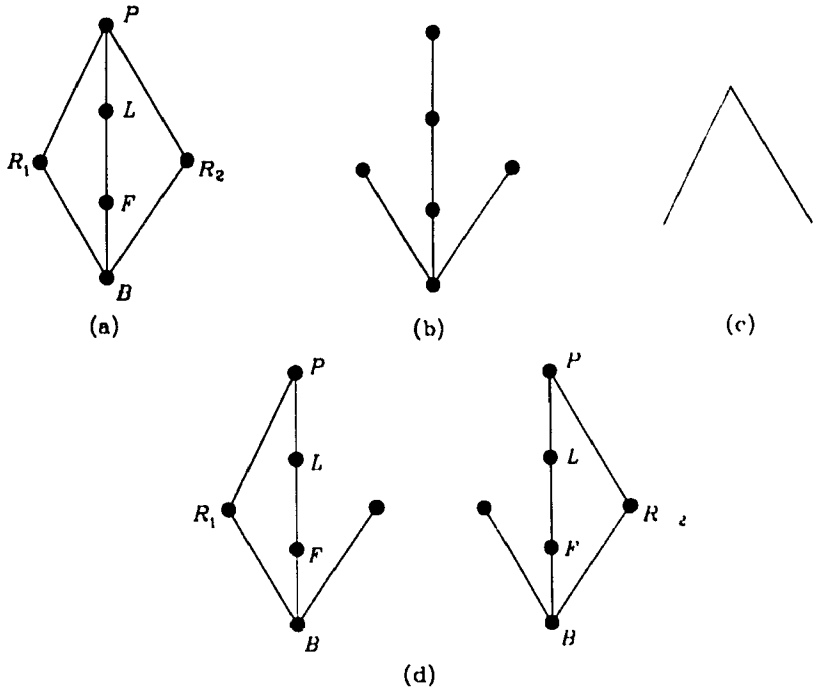

Fig. 3.4 (a) A connected graph, (b) A spanning tree, (c) Chords, (d) Independent loops.

i.e., the jth column of $\mathbf{T}$ is calculated as the generalized twist of the system assuming that all the independent speeds except the jth one are zero, which has a value of unity.

The inverse dynamics problem in robotics is defined as, *given a task, for example, to follow a path by an AGV, find the required joint torques and forces, i.e., the motor torques at the wheels of the AGV.* In this problem, matrix $\dot{\mathbf{T}}$ does not appear in the dynamic equations, because the driving torques are obtained as

$$\boldsymbol{\tau} = \mathbf{T}^T[\mathbf{M}\dot{\mathbf{t}} + (\dot{\mathbf{M}} + \mathbf{W}\mathbf{M})\mathbf{t} - \mathbf{w}^G - \mathbf{w}^D] \tag{3.41}$$

where $\dot{\mathbf{t}}$ may be calculated recursively from a known twist rate of a link in a kinematic chain, which is required to perform the given task. However, in forward dynamics, which arises in simulation studies, $\dot{\mathbf{T}}$ appears, but its direct calculation can be avoided. In fact, the generalized inertia terms that are quadratic in $\dot{\boldsymbol{\theta}}_I$, $\mathbf{C}(\boldsymbol{\theta}, \dot{\boldsymbol{\theta}}_I)\dot{\boldsymbol{\theta}}_I$ in eq.(3.41), can be evaluated efficiently using the technique introduced by Walker and Orin (1982) for serial manipulators and which has later been extended by Ma

and Angeles (1989) for parallel manipulators. With this technique, the foregoing quadratic terms are calculated as

$$\mathbf{C}(\boldsymbol{\theta}, \dot{\boldsymbol{\theta}}_I)\dot{\boldsymbol{\theta}}_I = -(\boldsymbol{\tau} + \boldsymbol{\gamma} + \boldsymbol{\delta})|_{\ddot{\boldsymbol{\theta}}_I = \mathbf{0}} \tag{3.45}$$

i.e., the first term of the right-hand side of eq.(3.41) is computed from inverse dynamics (Walker and Orin, 1982) as the negative of the sum of the remaining three terms when $\ddot{\boldsymbol{\theta}}_I$ is set equal to $\mathbf{0}$. Equation (3.45) can be readily implemented in dynamic simulations of mechanical systems.

3.6 Application of the Method of the NOC in the Presence of Redundant Actuation

Redundant actuation occurs when the number of driven actuators in a system exceeds the DOF of the system at hand. The *degree of redundant actuation* is given by the difference between the number of driven actuators and the DOF of the system. Moreover, since the number of equations governing the dynamics of the system is always equal to its DOF, in inverse dynamics, defined in §3.5, the dynamic equations cannot uniquely yield the required torques of the actuators, because an underdetermined system of equations arises. Furthermore, the set of kinematic equations relating the twist of the end-effector, for example, the gripper of a serial-type manipulator, or the platform of an AGV, and the actuated joints, is also underdetermined. The underdeterminacy in the kinematic and dynamic equations, resulting from redundant actuation, can easily be avoided by 'feathering' the redundant actuators, i.e., not driving the redundant actuators while leaving the corresponding joints free to move. However, in feathering, unless the choice of the driven actuators is based on some suitable performance criterion the system may function poorly. On the other hand, redundant actuation allows greater safety in case of breakdown of individual actuators. For example, if a mechanical system is redundantly actuated, it can still be controlled if one or more actuators break down – up to the degree of redundant actuation. Redundant actuation may be applied to parallel-architecture

robots, e.g., parallel manipulators and AGVs, in order to make them lighter and faster, although the advantage obtained through redundant actuation might be offset by the weight of the extra actuators. In many instances the use of redundant actuation is advisable and a common approach to address such a problem is through constrained optimization, which is outlined in the subsection below.

3.6.1 Constrained Optimization

A general constrained optimization problem is stated as

$$\min_{\mathbf{x}} \quad f(\mathbf{x}) \tag{3.46a}$$

$$\text{subject to} \quad h_i(\mathbf{x}) = 0, \qquad \text{for} \quad i = 1, \ldots, c_e \tag{3.46b}$$

$$g_j(\mathbf{x}) \geq 0, \qquad \text{for} \quad j = 1, \ldots, c_n \tag{3.46c}$$

where $\mathbf{x}$ is a μ-dimensional vector of *design variables*, while c_e and c_n denote the number of equality and inequality constraints, respectively. Function $f(\mathbf{x})$ is normally called the *objective function*, while eq.(3.46b) represents a set of equality constraints and eq.(3.46c) represents a set of inequality constraints. For convenience, the discussion is limited to objective functions which are twice continuously differentiable throughout the region of interest.

The constraints given by eqs.(3.46b) and (3.46c) are nonlinear in general. However, the constraints of interest that arise from the dynamics of a mechanical system with redundant actuation are linear. Thus, only linear constraints are considered here and, hence, the optimization problem is redefined as

$$\min_{\mathbf{x}} \quad f(\mathbf{x}) \tag{3.47a}$$

$$\text{subject to} \quad \mathbf{A}_1\mathbf{x} = \mathbf{b}_1 \tag{3.47b}$$

$$\mathbf{A}_2\mathbf{x} \geq \mathbf{b}_2 \tag{3.47c}$$

where $\mathbf{A}_1$ is a matrix of dimension $c_e \times \mu$, while $\mathbf{A}_2$ is a matrix of dimension $c_n \times \mu$. The conditions for a minimum $f(\mathbf{x})$ can be found in any book on optimization, for example, Gill et al., (1981), and hence, are not given here. An optimization problem

subject to linear constraints can be solved by *linear* or *quadratic programming* (Gill et al., 1981), if the objective function $f(\mathbf{x})$ is linear or, correspondingly, quadratic.

An optimization problem in the form of either eqs.(3.46a)-(3.46c) or eqs.(3.47a)-(3.47c) can be readily solved by using any standard procedure. For instance, in this research, an IMSL[1] (IMSL, 1990a) subroutine, DQ2ROG, is used. This subroutine is based on Powell's implementation of the dual quadratic programming algorithm by Goldfarb and Idnani (1983), for convex quadratic programming subject to constraints, as given in eqs.(3.47b) and (3.47c).

3.6.2 System Dynamics Under Redundant Actuation

A nonholonomic mechanical system possessing q-DOF requires at least q actuators for its control. It is now assumed that, under redundant actuation, μ actuators are driven to control the q-DOF of the system, where $\mu > q$, thus leading to an optimization problem. Let $\mathbf{t}_C$ be the q-dimensional twist vector representing the angular velocity of the end-effector and the velocity of its mass centre, C. It is assumed here that the dimension of the twist vector $\mathbf{t}_C$ coincides with the DOF of the system, q. Moreover, $\dot{\boldsymbol{\theta}}_A$ is defined as the μ-dimensional vector of actuated joint rates. Note that, in §3.2 and §3.3, since the number of actuators is equal to the DOF of the system, a set of actuated joint rates is always taken as the set of independent generalized speeds. In the present case, the joint rates are not independent, but the q components of the twist of the end-effector are independent, and hence, they can play the role of the independent generalized speeds. Thus, using the method of the NOC, a set of dynamic equations is obtained in terms of the angular velocity of the end-effector and the velocity of the mass centre, namely,

$$\mathbf{I}(\boldsymbol{\theta})\dot{\mathbf{t}}_C = \mathbf{C}(\boldsymbol{\theta}, \mathbf{t}_C)\mathbf{t}_C + \mathbf{w}_C^A + \mathbf{w}_C^G + \mathbf{w}_C^D \tag{3.48}$$

where the $q \times q$ matrices $\mathbf{I}$ and $\mathbf{C}$, and the q-dimensional vectors $\mathbf{w}_C^A$, $\mathbf{w}_C^G$ and $\mathbf{w}_C^D$ are defined in a similar way to the definitions of the matrices and vectors associated

[1]IMSL Mathematical Library consists of FORTRAN subroutines for mathematical applications.

with the dynamic equations given in eq.(3.29). However, in inverse dynamics, it is necessary to calculate the joint variables, their time derivatives and the corresponding torques to perform a certain task. This is done as follows: First, an expression relating the twist of the end-effector $\mathbf{t}_C$ and the actuated joint rates $\dot{\boldsymbol{\theta}}_A$ is written in a similar way to eq.(3.30), i.e.,

$$\mathbf{t}_C = \mathbf{T}_A \dot{\boldsymbol{\theta}}_A \tag{3.49}$$

where $\mathbf{T}_A$ is a $q \times \mu$ matrix. Then, the wrench of the end-effector $\mathbf{w}_C^A$, required to perform a task, is obtained from the equations of motion, eq.(3.48). Moreover, the power supplied to the system can be calculated as

$$\pi^S = \mathbf{t}_C^T \mathbf{w}_C^A \tag{3.50}$$

Furthermore, when μ joints are driven, the power supplied by the actuators, π^A, is given as

$$\pi^A = \dot{\boldsymbol{\theta}}_A^T \boldsymbol{\tau}_A \tag{3.51}$$

where $\boldsymbol{\tau}_A$ is the μ-dimensional vector of actuated joint torques. Now, since the power supplied by the actuators must be equal to the power input to the system, i.e., $\pi^A = \pi^S$, a relation between the actuator torques and the wrench of the end-effector is readily derived, namely,

$$\dot{\boldsymbol{\theta}}_A^T \boldsymbol{\tau}_A = \mathbf{t}_C^T \mathbf{w}_C^A \tag{3.52}$$

Again, to solve the problem of inverse dynamics, defined in §3.5, the joint rate vector $\dot{\boldsymbol{\theta}}_A$ must be known. Thus, eq.(3.49) must be solved for $\dot{\boldsymbol{\theta}}_A$ to obtain the required joint torques $\boldsymbol{\tau}_A$. But eq.(3.49) leads to an underdetermined system of linear equations that does not define $\dot{\boldsymbol{\theta}}_A$ uniquely. However, using an optimization approach under the equality constraints, eq.(3.49), a unique solution can be found, namely, as

$$\dot{\boldsymbol{\theta}}_A = \mathbf{L}\mathbf{t}_C \tag{3.53}$$

which minimizes $1/2(\dot{\boldsymbol{\theta}}_A^T \dot{\boldsymbol{\theta}}_A)$ if matrix $\mathbf{L}$ is defined as the *pseudo-inverse* of $\mathbf{T}_A$ (Rao and Mitra, 1971), i.e.,

$$\mathbf{L} \equiv \mathbf{T}_A^T (\mathbf{T}_A \mathbf{T}_A^T)^{-1} \tag{3.54}$$

Now, substitution of eq.(3.53) into eq.(3.52) leads to

$$\mathbf{t}_C^T \mathbf{w}_C^A = \mathbf{t}_C^T \mathbf{L}^T \boldsymbol{\tau}_A$$

or

$$\mathbf{t}_C^T (\mathbf{w}_C^A - \mathbf{L}^T \boldsymbol{\tau}_A) = 0 \tag{3.55}$$

One possible way of verifying that eq.(3.55) holds is by equating the expression in the brackets to zero, i.e.,

$$\mathbf{w}_C^A - \mathbf{L}^T \boldsymbol{\tau}_A = 0$$

or

$$\mathbf{w}_C^A = \mathbf{L}^T \boldsymbol{\tau}_A \tag{3.56}$$

Equation (3.56) is also an underdetermined system of linear equations and can be solved for $\boldsymbol{\tau}_A$ in a similar way to eq.(3.49), i.e.,

$$\boldsymbol{\tau}_A = (\mathbf{L}^T)^I \mathbf{w}_C^A = \mathbf{L}(\mathbf{L}^I \mathbf{L})^{-1} \mathbf{w}_C^A \tag{3.57}$$

in which the solution vector $\boldsymbol{\tau}_A$ minimizes $1/2(\boldsymbol{\tau}_A^T \boldsymbol{\tau}_A)$. Using eq.(3.54), eq.(3.57) is simplified as

$$\boldsymbol{\tau}_A = \mathbf{T}_A^T \mathbf{w}_C^A \tag{3.58}$$

Note that in solving eqs.(3.49) and (3.56), only the linear constraints are considered. However, if there are any limitations on the motions and available power of the actuators, they can be accounted for through inequality constraints, as in eq.(3.47c).

Dynamic simulation, defined in the preamble of Chapter 2, under redundant actuation, can be readily done by using eq.(3.56) and integrating the dynamic equations of motion of the system under study, eq.(3.48).

Chapter 4

Dynamics of Nonholonomic Robotic Mechanical Systems (NHRMS)

Nonholonomic robotic mechanical systems (NHRMS), as defined in §1.2, are nonholonomic mechanical systems under computer control. Well-known examples of such systems are automatic guided vehicles (AGVs). AGVs are widely used in modern factories, particularly in flexible manufacturing cells, and, more recently, in houses, offices, as well as in space applications. Most of the industrial AGVs use only kinematic models for their control purposes. However, the smooth and accurate control of state-of-the-art AGVs requires that their dynamics be considered. Moreover, fast algorithms are needed for the on-line computations of the required motor torques that enable the vehicle to decide upon the course of action at any instant. Thus, the systematic approach to dynamic modelling, namely, the method of the NOC for the modelling of nonholonomic mechanical systems that has been proposed in Chapter 3, is used to model a 3-wheeled 2-DOF AGV and a few 3-DOF AGVs with omnidirectional wheels. The method is first exemplified with a simple nonholonomic system, a 2-wheeled mechanical system, where all necessary calculations are given in order to explain the different steps in modelling the nonholonomic system. Then, the dynamic model of a 3-wheeled 2-DOF AGV is obtained. Finally, a general-purpose code, OMNI, is written for the inverse kinematics, dynamics and

simulation of 3-DOF AGVs consisting of λ omnidirectional wheels. The developed software is tested for 3-, 4- and 6-wheeled vehicles.

4.1 A Two-Wheeled Mechanical System

A 2-wheeled mechanical system moving on a floor, as shown in Fig. 4.1, is assumed to consist of an axle that is coupled by two revolute pairs to two wheels. The system at hand is nothing but the axle of the 3-wheeled 2-DOF AGV connected by two driving wheels, as shown in Fig. 3.3. Here, pure rolling of the wheels on the floor is assumed and hence, nonholonomic constraints arise, as derived in §3.1.2. The dynamic analysis of the 2-wheeled system forms the basis of modelling the AGV of Fig. 3.3. Since the system has 2-DOF, two wheels in the system are considered to be driven or actuated by two independent motors. The kinematic analysis of the system is done separately in §4.1.1, the results of which are used in the dynamic analysis of the system.

4.1.1 Velocity and Acceleration Analyses

For analysis, a coordinate frame of unit vectors $\mathbf{i}, \mathbf{j}$ and $\mathbf{k}$ is fixed at the centre of the axle, C. According to Fig. 4.1, the velocity of point C can be written as

$$\mathbf{v}_C \equiv \qquad + \mathbf{v}_{C/O_1}$$

where $\mathbf{v}_1$ is the velocity of point O_1 and $\mathbf{v}_{C/O_1}$ is the relative velocity of C with respect to O_1. Velocity $\mathbf{v}_1$ can be written in terms of the radius r of the wheels and

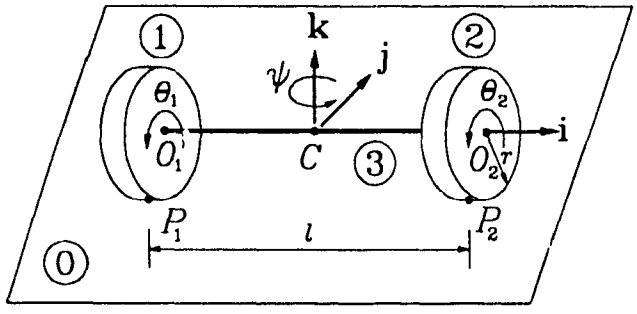

Fig. 4.1 A 2-wheeled mechanical system

the actuated joint rate of the first wheel, $\dot{\theta}_1$, namely,

$$\mathbf{v}_1 = -\dot{\theta}_1 r\mathbf{j} \tag{4.1}$$

and $\mathbf{v}_{C/O_1}$ can be expressed as the cross product of the angular velocity, $\boldsymbol{\omega}$, of the system with vector $\mathbf{a}_1$, a vector from point O_1 to point C, i.e.,

$$\mathbf{v}_{C/O_1} = \boldsymbol{\omega} \times \mathbf{a}_1 \tag{4.2}$$

The angular velocity of the 2-wheeled mechanical system may be written from the joint rates of the driving wheels as

$$\boldsymbol{\omega} = \dot{\psi}\mathbf{k} = \eta(\dot{\theta}_1 - \dot{\theta}_2)\mathbf{k} \tag{4.3}$$

where $\dot{\psi}$ is the angular velocity component of $\boldsymbol{\omega}$ about $\mathbf{k}$, while $\eta = r/l$, l being the length of the axle, as shown in Fig. 4.1. Now, using eqs.(4.1) and (4.2), a relation between the velocity of point C and the actuated joint rates, θ_1 and θ_2, is given by

$$\mathbf{v}_C \equiv \dot{\mathbf{c}} = -\frac{r}{2}(\dot{\theta}_1 + \dot{\theta}_2)\mathbf{j} \tag{4.4}$$

Combining eqs.(4.3) and (4.4), the twist, $\mathbf{t}_C$, of the centre of the axle or the end effector of the system, is written as a linear transformation of the independent joint rates, vector $\dot{\boldsymbol{\theta}}_I$, namely,

$$\mathbf{t}_C = \mathbf{T}_C\dot{\boldsymbol{\theta}}_I \tag{4.5}$$

where $\mathbf{t}_C$ is a 6-dimensional vector, $\dot{\boldsymbol{\theta}}_I$ is a 2-dimensional vector and $\mathbf{T}_C$ is a 6×2 matrix. These are defined as

$$\mathbf{t}_C \equiv [\boldsymbol{\omega}^T, \ \mathbf{c}^T]^T, \qquad \dot{\boldsymbol{\theta}}_I \equiv [\dot{\theta}_1, \ \dot{\theta}_2]^T \tag{4.6}$$

and

$$\mathbf{T}_C = \frac{\eta}{2}\begin{bmatrix} 2\mathbf{k} & -2\mathbf{k} \\ -l\mathbf{j} & -l\mathbf{j} \end{bmatrix}$$

The same relation, eq.(4.5), can also be obtained from

$$\mathbf{v}_C \equiv \dot{\mathbf{c}} = \mathbf{v}_2 + \mathbf{v}_{C/O_2} \tag{4.7}$$

where $\mathbf{v}_2$ is the velocity of point O_2. In order to obtain the relation between the twist rate of the centre of the axle and the actuated joint accelerations and rates, the relation given in eq.(4.5) is differentiated with respect to time, thereby obtaining

$$\dot{\mathbf{t}}_C = \mathbf{T}_C\ddot{\boldsymbol{\theta}}_I + \dot{\mathbf{T}}_C\dot{\boldsymbol{\theta}}_I \tag{4.8}$$

where

$$\dot{\mathbf{t}}_C \equiv [\dot{\boldsymbol{\omega}}^T, \quad \ddot{\mathbf{c}}^T]^T, \qquad \ddot{\boldsymbol{\theta}}_I \equiv [\ddot{\theta}_1, \quad \ddot{\theta}_2]^T \tag{4.9}$$

and $\dot{\mathbf{T}}_C$, producing the centrifugal and Coriolis acceleration terms, is given by

$$\dot{\mathbf{T}}_C = \frac{1}{2}\eta\dot{\psi}\begin{bmatrix}\mathbf{0} & \mathbf{0}\\ l\mathbf{i} & l\mathbf{i}\end{bmatrix} = \frac{1}{2}r\dot{\psi}\begin{bmatrix}\mathbf{0} & \mathbf{0}\\ \mathbf{i} & \mathbf{i}\end{bmatrix} \tag{4.10}$$

where the expression for $\dot{\psi}$ in terms of the actuated joint rates is available from eq.(4.3). Thus, upon substitution of the expression for $\dot{\psi}$ into eq.(4.10), matrix $\dot{\mathbf{T}}_C$ is rewritten as

$$\dot{\mathbf{T}}_C = \frac{1}{2}\eta r(\dot{\theta}_1 - \dot{\theta}_2)\begin{bmatrix}\mathbf{0} & \mathbf{0}\\ \mathbf{i} & \mathbf{i}\end{bmatrix} \tag{4.11}$$

4.1.1.1 Inverse Kinematics

Inverse kinematics is defined as, *given the Cartesian positions of the system at hand and their time derivatives, determine the joint histories, i.e., joint angles, rates and accelerations.*

Since the motion of the axle is planar, a 6-dimensional twist vector is unnecessary, for a *reduced* 3-dimensional twist vector will suffice. If vector $\mathbf{t}_C$ is replaced by a 3-dimensional twist vector, $\mathbf{t}'_C$, defined in terms of the angular velocity component about $\mathbf{k}$, $\dot{\psi}$, the velocity along $\mathbf{i}$, $\dot{x}$, and the velocity along $\mathbf{j}$, $\dot{y}$, of the system, then eq.(4.5) can be rewritten in the moving coordinate frame **i-j-k** as indicated below, provided the matrix $\mathbf{T}_C$ is replaced by a corresponding 3×2 matrix $\mathbf{T}'_C$, namely,

$$\mathbf{t}'_C = \mathbf{T}'_C\dot{\boldsymbol{\theta}}_I \tag{4.12}$$

where

$$\mathbf{t}'_C \equiv [\dot{\psi}, \quad \dot{x}, \quad \dot{y}]^T \quad \text{and} \quad \mathbf{T}'_C = \frac{1}{2}\eta\begin{bmatrix}1 & -1\\ 0 & 0\\ -l & -l\end{bmatrix} \tag{4.13}$$

Note that the second row of matrix $\mathbf{T}'_C$ is zero, thus, the velocity component along i for the 2-wheeled system vanishes, which is obvious due to the pure rolling constraints in the wheels. Thus, eq.(4.12) leads to a system of two equations in two unknowns Hence, vector $\dot{\boldsymbol{\theta}}_I$ is calculated as

$$\dot{\boldsymbol{\theta}}_I = \mathbf{S}\mathbf{t}'_C \tag{4.14}$$

where the 2×2 matrix $\mathbf{S}$ is as follows:

$$\mathbf{S} = \frac{1}{2}\eta \begin{bmatrix} 1 & -2/l \\ -1 & -2/l \end{bmatrix}$$

It is to be noted that, as pointed out in Step 6 of §3.2, since $\mathbf{T}'_C$ of eq.(4.13) is represented in a moving coordinate frame the time derivative of $\mathbf{T}'_C$ cannot be obtained by simply differentiating the elements of $\mathbf{T}'_C$ with respect to time. Thus, the expression for the acceleration inversion is derived from eq.(4.8). Now, if the 6-dimensional twist rate vector $\mathbf{t}_C$ of eq.(4.8) is replaced by a 3 dimensional vector $\dot{\mathbf{t}}'_C$, and the 6×2 matrix $\dot{\mathbf{T}}_C$ is replaced by a 3×2 matrix $\dot{\mathbf{T}}'_C$, then eq.(4.8) is rewritten as

$$\dot{\mathbf{t}}'_C = \mathbf{T}'_C \ddot{\boldsymbol{\theta}}_I + \dot{\mathbf{T}}'_C \boldsymbol{\theta}_I \tag{4.15}$$

where

$$\dot{\mathbf{t}}'_C \equiv [\ddot{\psi}, \quad \ddot{x}, \quad \ddot{y}]^T \quad \text{and} \quad \dot{\mathbf{T}}'_C = \frac{1}{2}\eta r(\dot{\theta}_1 - \dot{\theta}_2) \begin{bmatrix} 0 & 0 \\ 1 & 1 \\ 0 & 0 \end{bmatrix} \tag{4.16}$$

Moreover, eq.(4.15) that has been derived from eq.(4.8) can also be obtained by differentiating eq.(4.12) as

$$\dot{\mathbf{t}}'_C = \mathbf{T}'_C \dot{\boldsymbol{\theta}}_I + \mathbf{W}_C \mathbf{T}'_C \boldsymbol{\theta}_I \tag{4.17}$$

where $\mathbf{W}_C$ is a 3×3 transformation matrix which takes into account the motion of the coordinate frame i-j-k and is given by

$$\mathbf{W}_C = \begin{bmatrix} 0 & 0 & 0 \\ 0 & 0 & -\dot{\psi} \\ 0 & \dot{\psi} & 0 \end{bmatrix} \tag{4.18}$$

Now, the actuated joint accelerations can be obtained by regarding eq.(4.15) as an overdetermined system of three equations in two unknowns The least-squares

approximation of this system is given as

$$\ddot{\boldsymbol{\theta}}_I = \mathbf{T}_C'^{\,I}(\dot{\mathbf{t}}_C' - \mathbf{T}_C'\dot{\boldsymbol{\theta}}_I) \tag{4.19}$$

where $\mathbf{T}_C'^{\,I} \equiv [(\mathbf{T}_C')^T(\mathbf{T}_C')]^{-1}(\mathbf{T}_C')^T$ is the Moore-Penrose generalized inverse of $\mathbf{T}_C'$ (Rao and Mitra, 1971). Matrix $\mathbf{T}_C'^{\,I}$ is readily calculated as

$$\mathbf{T}_C'^{\,I} = \frac{1}{2}\eta \begin{bmatrix} 1 & 0 & -2/l \\ -1 & 0 & -2/l \end{bmatrix}$$

and for consistent input values of the components of vector $\dot{\mathbf{t}}_C'$, the solution for $\ddot{\boldsymbol{\theta}}_I$ given by eq.(4.19) is exact, i.e., the least-squares error is zero. Alternatively, the independent joint accelerations can also be found from the time derivative of eq.(4.14).

To obtain the independent actuated joint angles, $\boldsymbol{\theta}_I$, eq.(4.14), which relates the Cartesian velocities with joint rates can be integrated, with known initial conditions, using any standard integration scheme.

4.1.1.2 Direct Kinematics

As opposed to inverse kinematics, direct kinematics is defined as, *given the independent generalized coordinates of the system at hand and their time derivatives, determine the positions, velocities and accelerations of the end-effector of the system.*

Velocities and accelerations of the axle can be easily computed from eqs.(4.12) and (4.15), respectively. In order to determine the configuration of the system, the orientation of the system in the inertial frame, i.e., the orientation between the moving frame and the inertial frame, ψ, and the Cartesian coordinates of the system, x_c and y_c, need to be evaluated. First, ψ is obtained by integrating the expression for $\dot{\psi}$, as given by the first scalar relation of eq.(4.12), namely,

$$\psi = \eta(\theta_1 - \theta_2) \tag{4.20}$$

Then, the Cartesian velocities, $\dot{x}_c$ and $\dot{y}_c$, of point C in the inertial frame are written as

$$\dot{x}_c = -\dot{y}\sin\psi, \qquad \dot{y}_c = \dot{y}\cos\psi \tag{4.21}$$

Clearly, the scalar equations in eq.(4.21) are the nonholonomic constraints of the system which are nonintegrable and thus, do not lead to algebraic equations as functions of ψ, x_c and y_c. However, in direct dynamics, since the actuated joint rates are specified, the expression for $\dot{y}$ in eq.(4.21) is readily obtained using eq.(4.12), $\dot{y}$ being the third component of vector $\mathbf{t}'_C$. Also, angle ψ is known from eq.(4.20) Hence, eq.(4.21) can be integrated to obtain the positions of the system, i.e., the Cartesian coordinates x_c and y_c, with the known initial position of the centre of the axle.

4.1.2 Dynamic Modelling

The dynamic modelling of the 2-wheeled mechanical system is done using the method of the NOC, whereby the system is assumed to consist of three rigid links, as denoted by the encircled numbers of Fig. 4.1. Note that, since the angular velocity of the wheels $\boldsymbol{\omega}_i = \boldsymbol{\omega} + \dot{\theta}_i \mathbf{i}$, for $i = 1, 2$, have nonzero horizontal components, i.e., $\dot{\theta}_i \mathbf{i}$, the definitions of 3-dimensional reduced twist vectors are not sufficient to describe the twists of the wheels. Thus, to develop the dynamic model of the 2-DOF 2-wheeled mechanical system in a unified way, the 6-dimensional vectors of twist and twist rate are used.

The kinematic constraint equations of the 2-wheeled system in the form of eq.(3.18) are derived as follows: First, the nonholonomic kinematic constraints between links 1 and 0 are written using the methodology described in §3.1 as

$$\mathbf{A}_{11}\mathbf{t}_1 = \mathbf{0} \tag{4.22}$$

where the 3×6 matrix $\mathbf{A}_{11}$ is given by

$$\mathbf{A}_{11} = [r\boldsymbol{\Psi} \quad \mathbf{1}]$$

the 3×3 cross-product tensor $\boldsymbol{\Psi}$ being associated with vector $\mathbf{k}$. Then, the constraints due to the revolute coupling at point O_1 are written as

$$\mathbf{A}_{33}\mathbf{t}_3 + \mathbf{A}_{31}\mathbf{t}_1 = \mathbf{0} \tag{4.23}$$

with the 6×6 kinematic constraint matrices $\mathbf{A}_{33}$ and $\mathbf{A}_{31}$ being given by

$$\mathbf{A}_{33} = \begin{bmatrix} \boldsymbol{\Upsilon} & \mathbf{O} \\ (l/2)\boldsymbol{\Upsilon} & \mathbf{1} \end{bmatrix} \quad \text{and} \quad \mathbf{A}_{31} = \begin{bmatrix} -\boldsymbol{\Upsilon} & \mathbf{O} \\ \mathbf{O} & -\mathbf{1} \end{bmatrix}$$

where $\boldsymbol{\Upsilon}$ is the cross-product tensor associated with vector $\mathbf{i}$. Kinematic constraint matrices arising from the couplings between links 2 and 0, and 3 and 2 are obtained in a similar way to eqs.(4.22) and (4.23), respectively. Thus, the 18×18 matrix $\mathbf{A}$, appearing in eq.(3.18), for the 2-wheeled system, is as follows:

$$\mathbf{A} = \begin{bmatrix} r\boldsymbol{\Psi} & \mathbf{1} & \mathbf{O} & \mathbf{O} & \mathbf{O} & \mathbf{O} \\ -\boldsymbol{\Upsilon} & \mathbf{O} & \mathbf{O} & \mathbf{O} & \boldsymbol{\Upsilon} & \mathbf{O} \\ \mathbf{O} & -\mathbf{1} & \mathbf{O} & \mathbf{O} & (l/2)\boldsymbol{\Upsilon} & \mathbf{1} \\ \mathbf{O} & \mathbf{O} & r\boldsymbol{\Psi} & \mathbf{1} & \mathbf{O} & \mathbf{O} \\ \mathbf{O} & \mathbf{O} & -\boldsymbol{\Upsilon} & \mathbf{O} & \boldsymbol{\Upsilon} & \mathbf{O} \\ \mathbf{O} & \mathbf{O} & \mathbf{O} & -\mathbf{1} & -(l/2)\boldsymbol{\Upsilon} & \mathbf{1} \end{bmatrix} . \tag{4.24}$$

In order to obtain the generalized twist of the system at hand as a linear transformation of the actuated joint rates, i.e., eq.(3.19), the twist of the left wheel (body 1) is written as

$$\mathbf{t}_1 = [\boldsymbol{\omega}^T + \dot{\theta}_1 \mathbf{i}^T, \quad -r\dot{\theta}_1 \mathbf{j}^T]^T \tag{4.25}$$

The relations for the other links are similarly obtained as

$$\mathbf{t}_2 = [\boldsymbol{\omega}^T + \dot{\theta}_2 \mathbf{i}^T, \quad -r\dot{\theta}_2 \mathbf{j}^T]^T \quad \text{and} \quad \mathbf{t}_3 = [\boldsymbol{\omega}^T, \quad \dot{\mathbf{c}}^T]^T \tag{4.26}$$

and the 18-dimensional vector $\mathbf{t}$ is given by

$$\mathbf{t} \equiv [\mathbf{t}_1^T, \quad \mathbf{t}_2^T, \quad \mathbf{t}_3^T]^T \tag{4.27}$$

Now, upon substitution of the expressions for the components of vector $\mathbf{t}'_C$, as in eq.(4.12), into eqs.(4.25) and (4.26) leads to an expression in the form of eq.(3.19) where the 18×2 NOC matrix for the the system is obtained as

$$\mathbf{T} = \begin{bmatrix} \mathbf{i} + \eta\mathbf{k} & -\eta\mathbf{k} \\ -r\mathbf{j} & \mathbf{0} \\ \eta\mathbf{k} & \mathbf{i} - \eta\mathbf{k} \\ \mathbf{0} & -r\mathbf{j} \\ \eta\mathbf{k} & -\eta\mathbf{k} \\ -(r/2)\mathbf{j} & -(r/2)\mathbf{j} \end{bmatrix} \tag{4.28}$$

Matrix $\mathbf{T}$ of eq.(4.28) is easily verified as the NOC of matrix $\mathbf{A}$ of eq.(4.24) by noting that $\mathbf{AT} = \mathbf{O}$.

The equations of motion in absence of dissipation are derived as

$$\mathbf{I}\ddot{\boldsymbol{\theta}}_I = \boldsymbol{\tau} \tag{4.29}$$

where the generalized matrix consisting of the convective inertia terms $\mathbf{C}$ and the generalized force due to gravity acceleration $\boldsymbol{\gamma}$, both of eq.(3.29), vanish. Note that the dissipation, which would damp out the simulation errors, prohibits one from assessing the accuracy of the simulation algorithms. Henceforth, dissipation is not included in the models. The 2×2 matrix $\mathbf{I}$ and the 2-dimensional vector $\boldsymbol{\tau}$ are as follows:

$$\mathbf{I} = \frac{mr^2}{2}\begin{bmatrix} 3+\eta^2 & -\eta^2 \\ -\eta^2 & 3+\eta^2 \end{bmatrix}, \qquad \boldsymbol{\tau} = \begin{bmatrix} \tau_1 \\ \tau_2 \end{bmatrix}$$

with m being the mass of each wheel. The scalars τ_1 and τ_2 are the applied torques at the motors of the wheels. Moreover, in deriving the dynamic model of the 2-wheeled mechanical system, the mass of the axle (body 3) is considered negligible compared to the mass of the wheels. Furthermore, it has been shown in §A.1 that the derived dynamic model of the system at hand is the same as the one developed using Kane's formulation.

It is pointed out here that, while developing the dynamic equations of motion for the 2-wheeled system, eq.(4.29), the derivation of matrix $\mathbf{A}$, as in eq.(4.24), is redundant. Thus, the evaluation of the kinematic constraint matrices for a 3-wheeled 2-DOF AGV and 3-DOF AGVs are not shown in §4.2.2 and §4.4.2.

4.1.3 Trajectory Planning

For planar rigid-body motion, three coordinates specifying the orientation and position of the system are necessary. However, due to nonholonomic constraints at the wheel-floor interface, the system at hand possesses only 2-DOF. Thus, the orientation and position of the system cannot be specified arbitrarily, the reasons

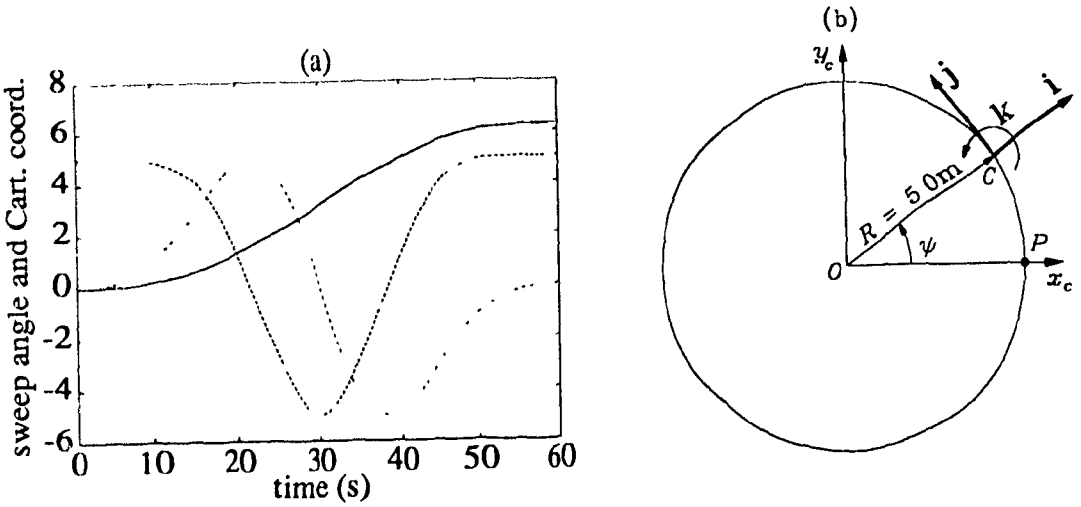

– ψ (rad), - - x_c (m), - · - y_c (m).

Fig. 4.2 A circular trajectory: Variations of (a) sweep angle, ψ, and Cartesian coordinates, x_c and y_c, with time, and (b) y_c vs. x_c.

being explained in §1.1.2. Hence, proper trajectory planning is required for smooth motion of the system, without which the relations of eq.(4.12) may be violated.

4.1.3.1 A Circular Trajectory

The 2-wheeled system is considered to traverse a circular path of radius R in t_f seconds. The sweep angle, ψ, which is also the orientation of the moving coordinate frame attached to the centre of the axle, point C, with respect to the inertial frame fixed at point O, is assumed to be a fifth-order polynomial function of time, such that it satisfies the zero velocity and acceleration conditions at the starting ($t = 0$) and finishing points ($t = t_f$), i.e. point P of Fig. 4.2(b). This is given as

$$\psi(t) = a_0 + a_1 t + \ldots + a_5 t^5 \tag{4.30a}$$

$$\text{subject to } \psi(0) = 0, \quad \dot{\psi}(0) = 0, \quad \ddot{\psi}(0) = 0 \tag{4.30b}$$

$$\text{and } \psi(t_f) = 2\pi, \quad \dot{\psi}(t_f) = 0, \quad \ddot{\psi}(t_f) = 0 \tag{4.30c}$$

Using the six conditions at the two ends, eqs.(4.30b) and (4.30c), the coefficients are calculated as follows:

$$a_0 = 0.0 \text{ rad}, \qquad a_1 = 0.0 \text{ rad/s}, \qquad a_2 = 0.0 \text{ rad/s}^2,$$

$$a_3 = (20\pi/t_f^3)\ \text{rad/s}^3, \quad a_4 = -(30\pi/t_f^4)\ \text{rad/s}^4, \quad a_5 = (12\pi/t_f^5)\ \text{rad/s}^5.$$

The Cartesian coordinates of the centre of the axle for the 2-wheeled system are now given as

$$x_c = R\cos\psi \quad \text{and} \quad y_c = R\sin\psi \tag{4.31}$$

The time derivatives of angle ψ and the Cartesian coordinates are obtained by differentiating the expressions in eqs.(4.30a) and (4.31), respectively, with respect to time, which are then used to specify the required twists and twist rates of the system in the moving coordinate frame, as in the left-hand sides of eqs.(4.12) and (4.15). The variations of ψ, x_c and y_c with time for $R = 5.0$ m and $t_f = 60.0$ s are shown in Fig. 4.2(a), whereas the circular trajectory is shown in Fig. 4.2(b).

4.1.4 Inverse Kinematics and Dynamics Results

For numerical purposes, the geometrical and inertial parameters of the system are considered as

the radius of the wheels,	$r = 0.05$ m,
the length of the axle,	$l = 0.4$ m,
the mass of the wheels,	$m = 2.0$ kg

The required joint rates and accelerations to traverse the circular path, as shown in Fig. 4.2(b), are calculated from eqs.(4.14) and (4.19), respectively, whose plots are shown in Figs. 4.3(b) and (c)[1], respectively. The required joint angles, as shown in Fig. 4.3(a), to traverse the same path, are calculated by integrating the expressions in eq.(4.14) with given initial conditions. Integration is performed with the help of the DIVPRK, a subroutine of the IMSL package (IMSL, 1990b), which solves first-order differential equations by the Runge-Kutta 5th/6th order method for

[1]Note that, due to lack of space along the abscissae and ordinates of the plots of Figs. 4.2 and 4.3, 'Cart. coord.', 'jt.' and 'accn.' are substituted for words Cartesian coordinate, joint and acceleration, respectively. These abbreviations will be used throughout this thesis whenever necessary.

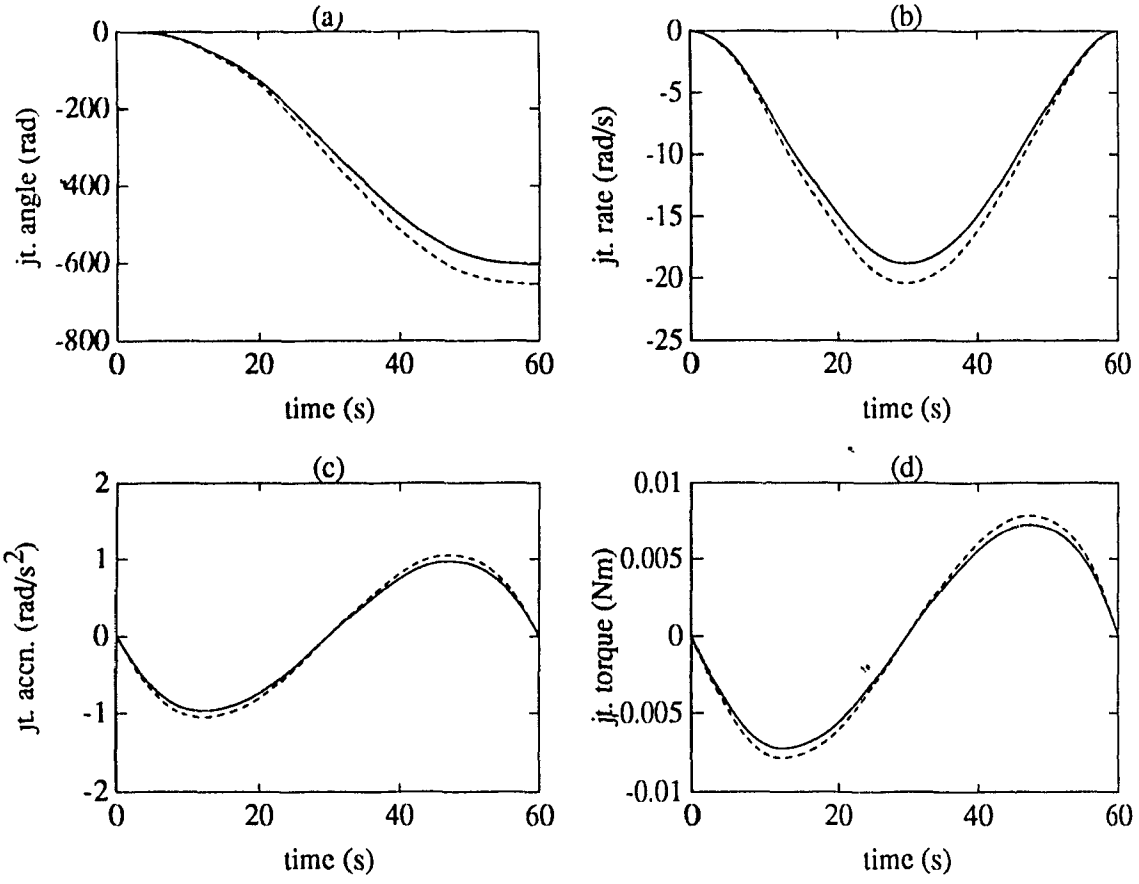

$-\ \theta_1,\ \dot{\theta}_1,\ \ddot{\theta}_1,\ \tau_1;\ -\ -\ \theta_2,\ \dot{\theta}_2,\ \ddot{\theta}_2,\ \tau_2.$

Fig. 4.3 Required joint (a) angles, (b) rates, (c) accelerations and (d) torques.

a specified step size and tolerance. Note that the tolerance has no units, because the DIVPRK subroutine attempts to control the norm of the local error in the solution of a differential equation in such a way that the global error is proportional to the specified tolerance and the global error is defined as

$$\max[|\varepsilon(1)|, \ldots, |\varepsilon(\nu)|]$$

where $\varepsilon(i) = [x(i) - x_t(i)]/\max[1, |x(i)|]$. The parameters $x_t(i)$ and $x(i)$ are, respectively, the true and computed solutions of a differential equation at the desired value i of the independent variable, e.g., time for the present study, for $i = 1, \ldots, \nu$. The results of joint angles are obtained with a step size of 0.6 s and tolerance of 0.001, and are shown in Fig. 1.3(a). The joint torques required to follow the circular path are obtained from the equations of motion of the system, eq.(4.29), and are

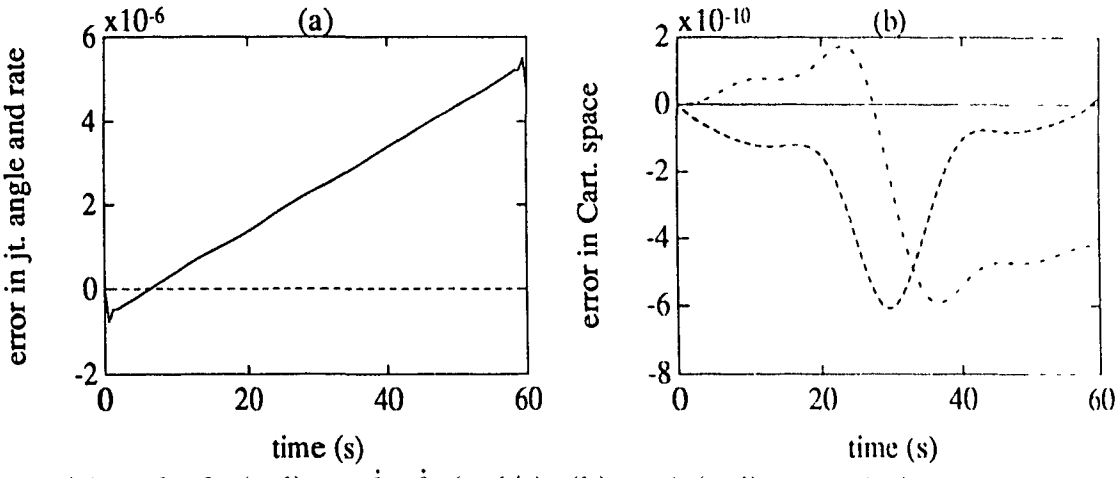

(a) — θ_1, θ_2 (rad); - - $\dot{\theta}_1$, $\dot{\theta}_2$ (rad/s). (b) - ψ (rad), - - x_c (m), - - - y_c (m)

Fig. 4.4 Simulation errors in joint and Cartesian spaces.

shown in Fig. 4.3(d). It is apparent form Figs. 4.3(c) and (d) that the plots for joint torques are proportional to the plots for joint accelerations which show that there is no convective inertia term in the dynamic model of the system at hand.

4.1.5 Simulation Results

Simulation involves direct dynamics via integration of the dynamic equations of motion. For the 2-wheeled system under study integration of eq.(4.29) may be obtained in closed-form, but, in general, numerical integration is essential in solving nonlinear differential equations, as derived for AGVs in §4.2 and §4.1. Thus, a numerical integration scheme, the subroutine DIVPRK of the IMSL package, is used in order to obtain the simulation results for the 2-wheeled mechanical system. The use of this subroutine allowed the author to get acquainted with the software by testing the effect of different variable arguments of the program and giving several inputs for which the results could be predicted intuitively.

To obtain the first-order differential equations, as required by the DIVPRK subroutine, from the second-order differential equations of motion, eq.(4.29) is written in the state-space form, namely,

$$\dot{\mathbf{x}} = \mathbf{H}\mathbf{x} + \mathbf{u} \tag{4.32}$$

where the 4×4 matrix $\mathbf{H}$ and the 4-dimensional vectors $\mathbf{x}$ and $\mathbf{u}$ are given by

$$\mathbf{H} \equiv \begin{bmatrix} \mathbf{O} & \mathbf{1} \\ \mathbf{O} & \mathbf{O} \end{bmatrix}, \quad \mathbf{x} \equiv \begin{bmatrix} \boldsymbol{\theta}_I \\ \dot{\boldsymbol{\theta}}_I \end{bmatrix} \quad \text{and} \quad \mathbf{u} \equiv \begin{bmatrix} \mathbf{0} \\ \mathbf{I}^{-1}\boldsymbol{\tau} \end{bmatrix}$$

where $\boldsymbol{\theta}_I \equiv [\theta_1, \quad \theta_2]^T$ is the vector of actuated joint angles θ_1 and θ_2. Moreover, once the joint rates are obtained from the integration of the dynamic model, the orientation of the system and the position of the mass centre of the system can be readily available from the direct kinematics. Simulation was carried out with a step size of 0.6 s and tolerance of 0.001. The corresponding simulation errors in the joint angles and joint rates, $\boldsymbol{\theta}_I$ and $\dot{\boldsymbol{\theta}}_I$, defined as the difference between the desired variables and the variables that were obtained after integration of the equations of motion, are shown in Fig. 4.4(a), whereas the errors in the sweep angle ψ, and in the Cartesian coordinates, x_c and y_c, are shown in Fig. 4.4(b). The higher errors in joint angles may be attributed to the fact that the desired joint angles were calculated from the integration of the required joint rates, whereas the required joint rates, along with the sweep angle and the Cartesian coordinates, were calculated from the algebraic expressions, eqs.(4.14), (4.30a) and (4.31), respectively. It is well-known that numerical integration accumulates errors. Thus, to calculate the joint angles, errors are introduced twice, during inverse kinematics and during simulation. On the other hand, errors in $\dot{\boldsymbol{\theta}}_I$, ψ, x_c and y_c result from simulation only. However, the errors in both joint angles and joint rates, the sweep angle and the Cartesian coordinates are very small. Hence, the deviation of the simulated trajectory from the actual circular path is not noticeable.

4.2 A Two-Degree-of-Freedom (DOF) Automatic Guided Vehicle (AGV)

The architecture of a 3-wheeled 2-DOF AGV is shown in Fig. 3.3, whereas a schematic diagram of the vehicle is shown in Fig. 4.5(a), that has been in use for different purposes, for example, as a mobile platform for nursing robots (Borenstein and Koren, 1985) and for artificial intelligence research (Iijima et al., 1981). A

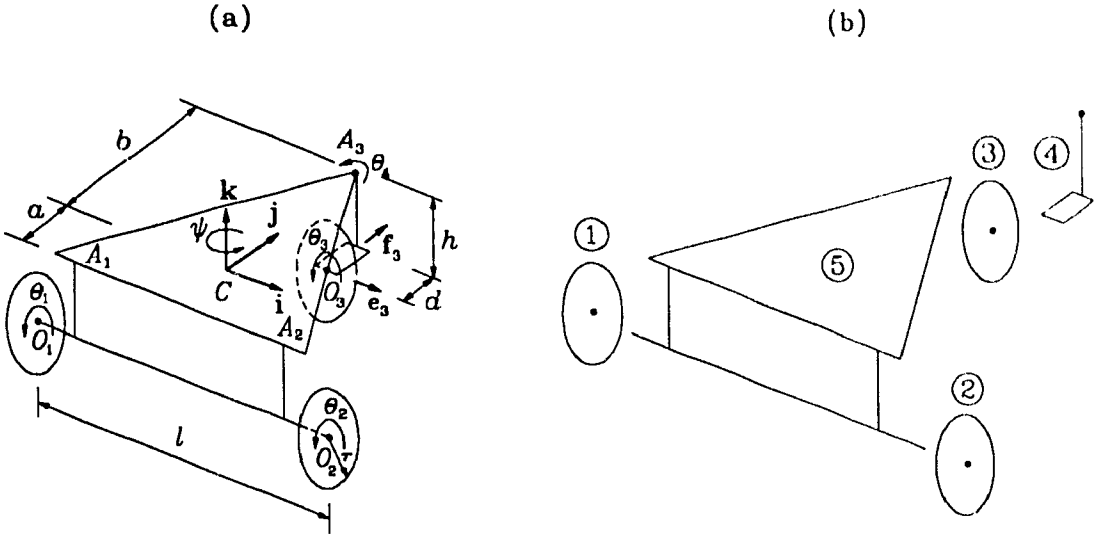

Fig. 4.5 (a) A schematic diagram of a 3-wheeled 2-DOF AGV, (b) Disassembled vehicle.

dynamic model of the 3-wheeled 2-DOF AGV is obtained here using the method of the NOC. It is assumed that the AGV under study contains three wheels and a platform. Moreover, the platform is coupled by revolute pairs to the two rear wheels. Furthermore, only the two rear wheels are driven or actuated by independent motors and, since, the vehicle has two degrees of freedom, no redundant actuation is present. Thus, the angular displacements of the actuated joints can be considered as the independent joint variables. For stability purposes, a caster wheel is attached at the front of the platform, as shown in Figs. 3.3 and 4.5(a), which is free to attain any orientation according to the motion of the vehicle. A coordinate frame of unit vectors **i**, **j** and **k** is fixed at the centroid C of the platform, as shown in Fig. 4.5(a), and unit orthogonal vectors $\mathbf{e}_i$, $\mathbf{f}_i$ ($i = 1, 2, 3$) are attached to the centres of the wheels, numbered 1, 2 and 3. Here, according to the definition of the architecture of the vehicle, $\mathbf{e}_i$ and $\mathbf{f}_i$, for $i = 1, 2$, are parallel to **i** and **j**, respectively.

4.2.1 Velocity and Acceleration Analyses

From Fig. 4.5(a), the angular velocity of the vehicle can simply be written using the joint rates of the driving wheels and can be expressed by eq (4.3). An equation relating the velocity of the platform with the actuated joint rates is obtained by

writing eqs.(4.1) and (4.2) for the AGV as

$$\mathbf{v}_C \equiv \dot{\mathbf{c}} = -a\eta(\dot{\theta}_1 - \dot{\theta}_2)\mathbf{i} - \frac{r}{2}(\dot{\theta}_1 + \dot{\theta}_2)\mathbf{j} \tag{4.33}$$

where $\eta = r/l$, while the radius of the wheels is r, and distances l and a are shown in Fig. 4.5(a). These parameters define the architecture of the vehicle. Combining eq.(4.3) for the 2-DOF AGV and eq.(4.33), the twist of the platform, i.e., the end-effector of the AGV, denoted by $\mathbf{t}_C$ is written as a linear transformation of the independent joint rate vector $\dot{\boldsymbol{\theta}}_I$, namely,

$$\mathbf{t}_C = \mathbf{T}_C\dot{\boldsymbol{\theta}}_I \tag{4.34}$$

where $\mathbf{t}_C$ and $\dot{\boldsymbol{\theta}}_I$ are 6- and 2-dimensional vectors, respectively, which are defined in eq.(4.6). Moreover, the 6×2 matrix $\mathbf{T}_C$ is given by

$$\mathbf{T}_C = \eta \begin{bmatrix} \mathbf{k} & -\mathbf{k} \\ -a\mathbf{i} - (l/2)\mathbf{j} & a\mathbf{i} - (l/2)\mathbf{j} \end{bmatrix} \tag{4.35}$$

The same relations, eq.(4.33), can also be obtained from a relation given in eq.(4.7).

To find the twist rate of the platform, the twist relation obtained in eq.(4.34) is differentiated with respect to time, which is given by eq.(4.8). The resultant 3×2 matrix $\dot{\mathbf{T}}_C$ for the 2-DOF AGV is given by

$$\dot{\mathbf{T}}_C = \eta^2(\dot{\theta}_1 - \dot{\theta}_2) \begin{bmatrix} \mathbf{0} & \mathbf{0} \\ (l/2)\mathbf{i} - a\mathbf{j} & (l/2)\mathbf{i} + a\mathbf{j} \end{bmatrix} \tag{4.36}$$

4.2.1.1 Inverse and Direct Kinematics

Since the motion of the platform is planar, a reduced 3-dimensional twist vector, $\mathbf{t}'_C$, as defined in eq.(4.13) of §4.1.1.1, is invoked again for the kinematic analysis of the 3-wheeled 2-DOF AGV. Then, eq.(4.34) can be written in the moving coordinate frame **i-j-k**, as shown in eq.(4.12), provided that matrix $\mathbf{T}_C$ is replaced by a corresponding 3×2 matrix $\mathbf{T}'_C$, namely,

$$\mathbf{T}'_C = \eta \begin{bmatrix} 1 & -1 \\ -a & a \\ -l/2 & -l/2 \end{bmatrix} \tag{4.37}$$

The actuated joint rates can now be obtained by solving the overdetermined system of equations resulting from eq.(4.34), namely, eq.(4.12) for the 2-DOF AGV. This is given by

$$\dot{\boldsymbol{\theta}}_I = \mathbf{T'}_C{}^I \mathbf{t}'_C \tag{4.38}$$

where $\mathbf{T'}_C{}^I$ is the well-known Moore-Penrose generalized inverse of matrix $\mathbf{T}'_C$ and is defined in eq.(4.19).

Acceleration inversion is performed by substituting the 6-dimensional twist rate vector $\dot{\mathbf{t}}_C$ with the 3-dimensional vector $\dot{\mathbf{t}}'_C$ and the 6×2 matrix $\dot{\mathbf{T}}_C$ is replaced by a 3×2 matrix $\dot{\mathbf{T}}'_C$. Three scalar equations relating the twist rate of the platform and the actuated joint rates and accelerations are shown in eq.(4.15) where vectors $\dot{\mathbf{t}}'_C$ and $\ddot{\boldsymbol{\theta}}_I$ are the time derivatives of vectors $\mathbf{t}'_C$ and $\boldsymbol{\theta}_I$, respectively. Matrix $\dot{\mathbf{T}}'_C$ is given as

$$\dot{\mathbf{T}}'_C = \eta^2(\dot{\theta}_1 - \dot{\theta}_2) \begin{bmatrix} 0 & 0 \\ l/2 & l/2 \\ -a & a \end{bmatrix}$$

Note that the expression for $\dot{\mathbf{t}}'_C$ of the 2-DOF AGV can also be obtained from eq.(4.17), where the 3×3 transformation matrix $\mathbf{W}_C$ takes into account the motion of the **i-j-k** frame. The actuated joint accelerations are then computed from eq.(4.19) for the AGV.

To obtain the actuated joint angles $\boldsymbol{\theta}_I$, the expressions for the joint rates, eq.(4.38), are integrated, with known initial conditions, using any standard integration scheme. Direct kinematics results may be obtained by following the outline given in §4.1.1.2.

4.2.2 Dynamic Modelling

It is assumed that the system at hand consists of five rigid bodies, which are numbered 1 to 5, as shown in Fig. 4.5(b). The 2-DOF AGV under study is a multi-loop mechanical system, its vectors of unactuated or dependent joint angles and rates

being defined as

$$\boldsymbol{\theta}_D \equiv [\theta_3, \ \theta_4]^T \quad \text{and} \quad \dot{\boldsymbol{\theta}}_D \equiv [\dot{\theta}_3, \ \dot{\theta}_4]^T \tag{4.39}$$

where θ_3, θ_4 and $\dot{\theta}_3$, $\dot{\theta}_4$ are joint angles and their time rates of change of the front caster wheel (body 3) and of the fork (body 4) connecting the caster wheel assembly with the platform (body 5), respectively. The generalized twist for the whole system is obtained by writing the twists of the five individual bodies as a linear transformation of all the joint rates. Now, the generalized twist $\mathbf{t}$, as in eq.(3.30), is defined as a 30-dimensional vector, namely,

$$\mathbf{t} \equiv [\mathbf{t}_1{}^T, \ldots, \mathbf{t}_5{}^T]^T \tag{4.40}$$

where $\mathbf{t}_i$ for $i = 1, \ 2$, $\mathbf{t}_3$ and $\mathbf{t}_4$ are given as

$$\mathbf{t}_i = \begin{bmatrix} \dot{\psi}\mathbf{k} + \dot{\theta}_i\mathbf{i} \\ -r\dot{\theta}_i\mathbf{j} \end{bmatrix}, \ \mathbf{t}_3 = \begin{bmatrix} (\dot{\psi} + \dot{\theta}_4)\mathbf{k} + \dot{\theta}_3\mathbf{e}_3 \\ -r\dot{\theta}_3\mathbf{f}_3 \end{bmatrix} \text{ and } \mathbf{t}_4 = \begin{bmatrix} (\dot{\psi} + \dot{\theta}_4)\mathbf{k} \\ \dot{\mathbf{c}} - b\dot{\psi}\mathbf{i} + (\dot{\psi} + \dot{\theta}_4)\mathbf{k} \times \mathbf{d}_4 \end{bmatrix} \tag{4.41}$$

where $\mathbf{d}_3$ represents the vector directed from point A_3 to the mass centre of the fork connecting the caster wheel assembly with the platform and $\mathbf{t}_5$ is nothing but the twist of the platform. The generalized twist rate vector can be obtained from the time derivative of $\mathbf{t}$. Since the latter contains dependent joint rates, a relation between these, vector $\dot{\boldsymbol{\theta}}_D$ and the independent joint rates $\dot{\boldsymbol{\theta}}_I$, is required, which is obtained in §4.2.2.1. Moreover, the dependent joint accelerations appear in the time rate of the generalized twist vector. Thus, an expression relating the dependent joint accelerations with the independent joint rates and accelerations is obtained from the time derivative of eq.(4.51). Once vector $\dot{\boldsymbol{\theta}}_D$ is obtained in terms of $\dot{\boldsymbol{\theta}}_I$, and $\ddot{\boldsymbol{\theta}}_D$ as a function of $\ddot{\boldsymbol{\theta}}_I$ and $\dot{\boldsymbol{\theta}}_I$, the equations of motion can be readily derived from eq.(3.29) using either the scheme given in §3.3 or §3.5, namely,

$$\mathbf{I}(\boldsymbol{\theta})\ddot{\boldsymbol{\theta}}_I = \mathbf{C}(\boldsymbol{\theta}, \dot{\boldsymbol{\theta}}_I)\dot{\boldsymbol{\theta}}_I + \boldsymbol{\tau} \tag{4.42}$$

where $\mathbf{I}$ and $\mathbf{C}$ are 2×2 generalized inertia matrix and matrix of convective inertia terms, respectively. The 2-dimensional vector $\boldsymbol{\tau}$ is given as

$$\boldsymbol{\tau} \equiv [\tau_1, \ \tau_2]^T$$

with τ_1 and τ_2 being the applied motor torques at the left and right actuated wheels, respectively. Note that the generalized force due to gravity acceleration vanishes and, in the absence of dissipation, vector $\boldsymbol{\delta}$ of eq.(3.29) does not appear. An explicit derivation of the equations of motion of the 2-DOF AGV based on the methodology given in §3.3 is attempted using MACSYMA (1983), a symbolic manipulation package. The symbolic calculations result in cumbersome expressions for the elements of the 2×2 matrices $\mathbf{I}$ and $\mathbf{C}$ of eq.(4.42). The two simplest expressions among all the elements of matrices $\mathbf{I}$ and $\mathbf{C}$, one from each matrix, are shown in §A.5. The cumbersome expressions are due to the system architecture and to the expressions for matrices $\mathbf{T}$ and $\dot{\mathbf{T}}$, eqs.(3.39) and (3.40), respectively. Thus, an efficient algorithmic approach is necessary to generate a dynamic model of the system, which has been done using the methodology outlined in §3.5.

4.2.2.1 A Relation between the Actuated and Unactuated Joint Rates

In order to find a relation between the actuated and unactuated joint rates, eq.(3.34) for the 3-wheeled 2-DOF AGV is desired. Thus, matrix $\mathbf{J}$ is obtained from the independent loops of the multi-loop system. As shown in §3.4.1, the system contains two independent loops. Since pure rolling of the wheels is considered the velocities of the contact points of the wheels with the floor are zero. Hence, using the left loop BR_1PLFB of Fig. 3.4(d), the velocity of point O_3, $\mathbf{v}_3$, is derived from the velocity of point O_1, namely,

$$\mathbf{v}_3 = \mathbf{v}_1 + \dot{\psi}\mathbf{k} \times \mathbf{a}_1 + (\dot{\psi} + \dot{\theta}_4)\mathbf{k} \times \mathbf{a}_3 \tag{4.43}$$

where $\mathbf{a}_1$ and $\mathbf{a}_3$ are the vectors from O_1 to A_3 and A_3 to O_3, respectively. A vector relation similar to eq.(4.43) can also be obtained using the right loop of Fig. 3.4(d), i.e., loop BR_2PLFB. To this end, six scalar constraints are obtained from the two loop equations that can be written in the form of eq.(3.34), i.e.,

$$\mathbf{J}\dot{\boldsymbol{\theta}} = \mathbf{0} \tag{4.44}$$

where the 6×5 matrix $\mathbf{J}$ and the 5-dimensional vector $\dot{\boldsymbol{\theta}}$ are given below:

$$\mathbf{J} = \begin{bmatrix} r\mathbf{j} & \mathbf{0} & -r\mathbf{f}_3 & -d\mathbf{e}_3 & -(l/2)\mathbf{j} + (a+b)\mathbf{i} - d\mathbf{e}_3 \\ \mathbf{0} & r\mathbf{j} & -r\mathbf{f}_3 & -d\mathbf{e}_3 & (l/2)\mathbf{j} + (a+b)\mathbf{i} - d\mathbf{e}_3 \end{bmatrix} \tag{4.45}$$

and

$$\dot{\boldsymbol{\theta}} \equiv \begin{bmatrix} \dot{\boldsymbol{\theta}}_I \\ \dot{\boldsymbol{\theta}}' \end{bmatrix}$$

while $\dot{\boldsymbol{\theta}}'$ is given by

$$\dot{\boldsymbol{\theta}}' \equiv [\dot{\theta}_3, \quad \dot{\theta}_4, \quad \dot{\psi}]^T$$

in which θ_3, θ_4 and ψ, as shown in Fig. 4.5(a), are defined as the joint angle of the caster wheel about an axis parallel to vector $\mathbf{e}_3$, the joint angle of the fork about an axis parallel to $\mathbf{k}$, and the angle of rotation of the platform about $\mathbf{k}$, respectively. Moreover, the 2-dimensional unit vectors $\mathbf{e}_3$ and $\mathbf{f}_3$ are given as

$$\mathbf{e}_3 = [c\theta_4, \quad s\theta_4, \quad 0]^T, \qquad \mathbf{f}_3 = [-s\theta_4, \quad s\theta_4, \quad 0]^T \tag{4.46}$$

where $s(\cdot)$ and $c(\cdot)$ denote the sine and the cosine of angle $(\cdot)$, respectively. Furthermore, since all vectors in eq.(4.45) have two nonzero components, the six scalar constraints of eq.(4.44) are reduced to only four. However, explicit expressions of eq.(4.45) show that only three of these constraints are independent. Thus, the nullspace of $\mathbf{J}$ of eq.(4.44) is of dimension two, which is nothing but the DOF of the AGV under study. The independent constraints are now expressed in the form of eq.(3.36) as

$$\mathbf{J}_I \dot{\boldsymbol{\theta}}_I + \mathbf{J}_D \dot{\boldsymbol{\theta}}' = \mathbf{0} \tag{4.47}$$

where the 3×2 matrix $\mathbf{J}_I$ and the 3×3 matrix $\mathbf{J}_D$ are given by

$$\mathbf{J}_I = \begin{bmatrix} 0 & 0 \\ r & 0 \\ 0 & r \end{bmatrix} \quad \text{and} \quad \mathbf{J}_D = \begin{bmatrix} r\ s\theta_4 & -d\ c\theta_4 & a+b-d\ c\theta_4 \\ -r\ c\theta_4 & -d\ s\theta_4 & -l/2-d\ s\theta_4 \\ -r\ c\theta_4 & -d\ s\theta_4 & l/2-d\ s\theta_4 \end{bmatrix} \tag{4.48}$$

To test the controllability of the system, i.e., the invertibility of matrix $\mathbf{J}_D$, the determinant of $\mathbf{J}_D$ is calculated as $-ldr$, which means that the dependent variables, vector $\dot{\boldsymbol{\theta}}'$, can always be calculated in terms of $\dot{\boldsymbol{\theta}}_I$, namely,

$$\dot{\boldsymbol{\theta}}' = \mathbf{U}\dot{\boldsymbol{\theta}}_I \tag{4.49}$$

the 3×2 matrix $\mathbf{U}$ being given by

$$\mathbf{U} = \begin{bmatrix} c\theta_4/2 - (a+b)s\theta_4/l & c\theta_4/2 + (a+b)s\theta_4/l \\ r\, s\theta_4/(2d) + \eta[(a+b)c\theta_4/d - 1] & r\, s\theta_4/(2d) - \eta[(a+b)c\theta_4/d + 1] \\ \eta & -\eta \end{bmatrix} \tag{4.50}$$

Alternatively, three independent constraints relating the independent and the dependent variables, eq.(4.47), can also be obtained by using different independent loops, e.g., BR_1PLFB and BR_1PR_2B of Fig. 3.4(a). Note that the constraints arising from the loop BR_1PR_2B lead to an expression for the angular velocity of the platform in terms of the independent joint rates, eq.(4.3). Now, since the angular velocity of the vehicle, $\dot{\psi}$, the third component of vector $\dot{\boldsymbol{\theta}}'$, is available from the kinematic analysis of the system, namely, eq.(4.12) for the AGV, the calculation of $\dot{\psi}$ is redundant. Moreover, to obtain the dependent joint accelerations, $\ddot{\boldsymbol{\theta}}_D$, which are necessary for the dynamic analysis, eq.(4.47) needs to be differentiated with respect to time. Furthermore, since the frame in which the matrices $\mathbf{J}_I$ and $\mathbf{J}_D$ are represented is not stationary, the time derivative of eq.(4.48) will no longer lead to a determined set of equations, and hence, $\ddot{\boldsymbol{\theta}}_D$ must be found from an overdetermined system of equations using the Moore-Penrose generalized inverse of $\mathbf{J}_D$. To avoid redundant and generalized inverse calculations, the expression for $\dot{\psi}$, derived in the kinematic analysis, is substituted in the loop equations, eq.(4.44), the two vector equations from loops BR_1PLFB and BR_2PLFB becoming identical. Thus, only two independent scalar equations are obtained that relate the dependent and independent joint rates. The two independent scalar constraints which result either from the first or second row of eq.(4.44), where the expression for $\dot{\psi}$ is substituted from eq.(4.34), are given by

$$\mathbf{J}_I\dot{\boldsymbol{\theta}}_I + \mathbf{J}_D\dot{\boldsymbol{\theta}}_D = \mathbf{0} \tag{4.51}$$

where $\mathbf{J}_I$ are $\mathbf{J}_D$ are now reduced to

$$\mathbf{J}_I = [(r/2)\mathbf{j} + \eta(a+b)\mathbf{i} - d\eta\mathbf{e}_3 \quad (r/2)\mathbf{j} + \eta(a+b)\mathbf{i} + d\eta\mathbf{e}_3] \tag{4.52a}$$

$$\mathbf{J}_D = [-r\mathbf{f}_3 \quad -d\mathbf{e}_3] \tag{4.52b}$$

Since the vectors in eq.(4.52a) are 2-dimensional, $\mathbf{J}_I$ and $\mathbf{J}_D$ are 2×2 matrices. The 2-dimensional vectors $\dot{\boldsymbol{\theta}}_I$ and $\dot{\boldsymbol{\theta}}_D$ are defined in eqs.(4.6) and (4.39), respectively.

Now, eq.(4.51) again confirms that the DOF of the system at hand is two and the 2×2 matrix $\mathbf{J}_D$ of eq.(4.52b) is never singular because the two vectors $\mathbf{e}_3$ and $\mathbf{f}_3$ are orthogonal, and hence, linearly independent.

4.3 Numerical Results for the AGV

Numerical results for the 3-wheeled 2-DOF AGV are obtained based on the methodology adopted in §4.2.1 and §4.2.2. Since the AGV under study possesses 2-DOF, proper path planning is necessary for the smooth motion of the vehicle on the floor. This is done below.

4.3.1 Trajectory Planning

The performance of the vehicle is tested while traversing a circular path and two straight paths connected by a smooth curve. The former path is generated in §4.1.3.1 and the latter is planned below.

4.3.1.1 Two Straight Paths Connected by a Smooth Curve

In the industrial application of AGVs, for example, in production shops where AGVs carry raw materials, tools and other equipment, it is necessary to switch lanes while avoiding obstacles. Thus, from a practical point of view a path consisting of two straight lines connected by a smooth curve is planned, as shown in Fig. 4.6. For a smooth operation of the vehicle, the following conditions are imposed on two straight segments of the path, namely, segments P_0P_1 and P_2P_3: For the segment P_0P_1,

$$\begin{aligned}
&\text{at } t = 0: \\
&\quad \psi = 0,\ \dot{\psi} = 0,\ \ddot{\psi} = 0; \qquad x_c = x_0,\ \dot{x}_c = 0,\ \ddot{x}_c = 0; \\
&\quad y_c = y_0,\ \dot{y}_c = 0,\ \ddot{y}_c = 0. \qquad (4.53a) \\
&\text{at } t = t_1:
\end{aligned}$$

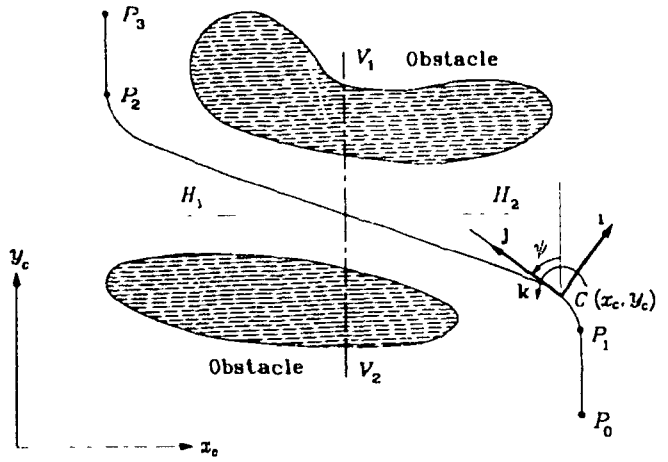

Fig. 4.6 Two straight lines connected by a smooth curve.

$$\psi = 0,\ \dot{\psi} = 0,\ \ddot{\psi} = 0; \qquad x_c = x_0,\ \dot{x}_c = 0,\ \ddot{x}_c = 0;$$
$$y_c = y_1,\ \dot{y}_c = \dot{y}_1,\ \ddot{y}_c = 0. \tag{4.53b}$$

where t denotes time and the time-dependent variables ψ, x_c and y_c are shown in Fig. 4.6. Moreover, t_1, x_0, y_0, y_1, $\dot{y}_1$ are user-specified constants. The other straight line, segment P_2P_3, is considered as the successive mirror image of the segment P_0P_1 about lines H_1H_2 and V_1V_2 or V_1V_2 and H_1H_2. Furthermore, a similar set of conditions given in eqs.(4.53a) and (4.53b) can be obtained for the segment P_2P_3. In eqs.(4.53a) and (4.53b), conditions on ψ and x_c are very simple and no calculations are required for path planning, while a cycloidal motion (Rothbart, 1956; Chen, 1982) is used to satisfy the conditions on y_c along P_0P_1. Now, two straight lines that are generated between segments P_0P_1 and P_2P_3 are connected by a polynomial which satisfies the conditions given below:

$$\text{at } y_c = y_1: \qquad x_c = x_1,\ x_c' = 0,\ x_c'' = 0,\ x_c''' = 0$$
$$\text{at } y_c = y_2: \qquad x_c = x_2,\ x_c' = 0,\ x_c'' = 0,\ x_c''' = 0 \tag{4.54}$$

where $(\cdot)'$ denotes $d(\cdot)/dy_c$ and x_1, x_2, y_1 and y_2 are user-specified constants. A seventh-order polynomial $x_c = f(y_c)$ is used to satisfy the conditions given in eq.(4.54) where y_c of $f(y_c)$ is calculated based on the assumption that $\dot{y}_c = \dot{y}_1$, which remains constant along segment P_1P_2, and hence, the value y_c is nothing but $(t - t_1)\dot{y}_1$ for $t \leq t_2$, t_2 being the travelling time along segment P_1P_2.

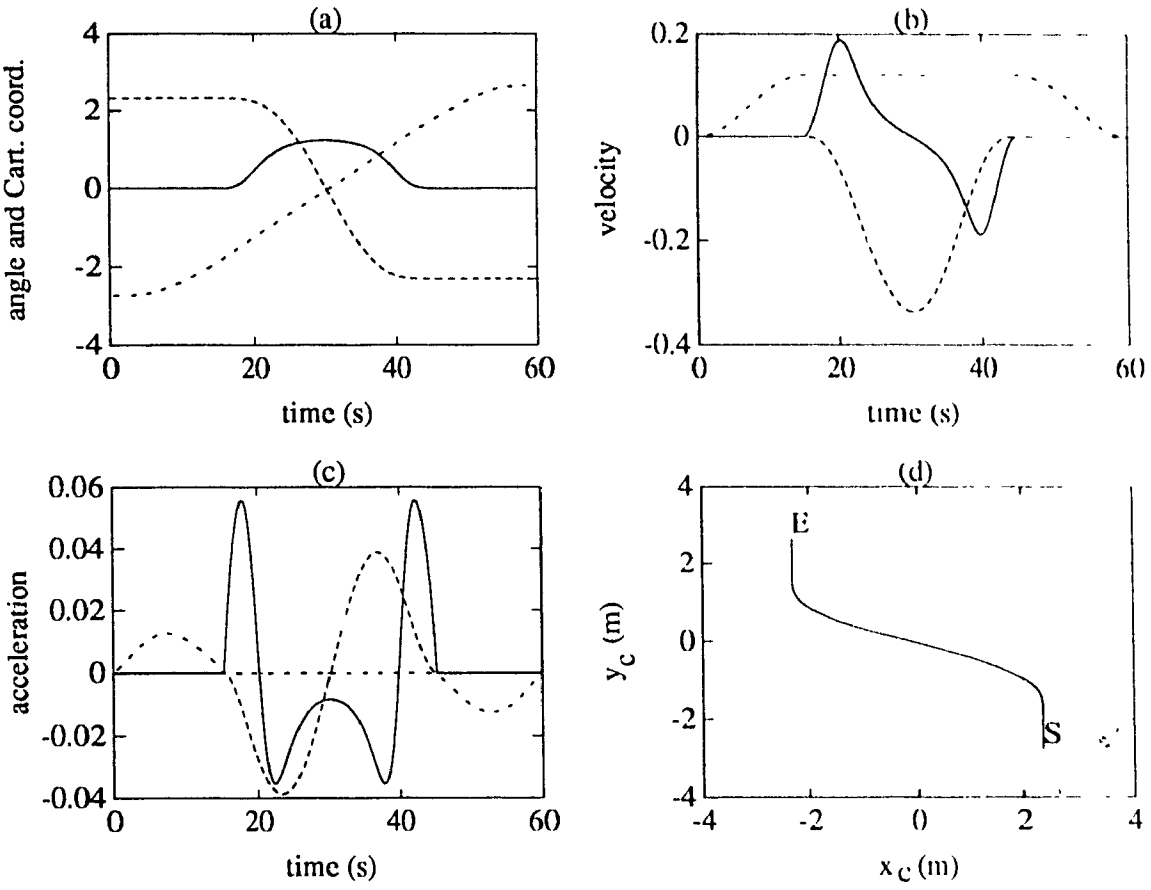

— ψ (rad), $\dot{\psi}$ (rad/s), $\ddot{\psi}$ (rad/s^2); - - x_c (m), $\dot{x}_c$ (m/s), $\ddot{x}_c$ (m/s^2);
- · - y_c (m), $\dot{y}_c$ (m/s), $\ddot{y}_c$ (m/s^2); S: start and E: end points

Fig. 4.7 Two straight paths connected by a smooth curve: Variation of (a) ψ, x_c and y_c vs. time, (b) ψ, $\dot{x}_c$ and $\dot{y}_c$ vs. time, (c) $\ddot{\psi}$, $\ddot{x}_c$ and $\ddot{y}_c$ vs. time, and (d) y_c vs x_c.

The variations of ψ, x_c, y_c and their time derivatives are shown in Fig. 4.7 for the total time of 60.0 s with $t_1 = 15.0$ s, $t_2 = 45.0$ s, $x_0 = x_1 = 2.32$ m, $x_2 = -2.32$ m, $y_0 = -2.75$ m, $y_1 = -1.85$ m, $y_2 = 1.75$ m and $\dot{y}_1 = 0.12$ m/s. 'S' and 'E' of Fig. 4.7(d) denote the start point P_0 and the end point P_3 of Fig. 4.6, respectively. Note that during the travel of the curved segment P_1P_2 of Fig. 4.6, the angular speed of the AGV is specified according to the time rate of change of the curvature. Moreover, the required velocity of the mass centre of the AGV is the velocity that is tangential to the curve joining P_1 and P_2. Since the AGV possesses only 2 DOF the specification of the required twist satisfies the relations given by eq.(4.12) for the

2-DOF AGV and, hence, the least-squares approximation $\dot{\theta}_I$ of the actuated joint rates of eq.(4.38) is the exact solution, i.e., the least-squares error is zero.

4.3.2 Numerical Example

For numerical results, the geometrical parameters of the vehicle are considered as

the radius of the wheels,	$r = 0.05$ m,
the length of the axle,	$l = 0.4$ m,
the distance from the edge A_1A_2 to point C,	$a = 0.101$ m,
the distance between the points C and A_3,	$b = 0.202$ m,
the height of the connecting link,	$h = 0.1$ m,
the offset of the caster wheel,	$d = 0.025$ m.

The inertial parameters are considered as:

the mass of each wheel,	$m_w = 2.0$ kg,
the mass of the platform,	$m = 20.0$ kg.

The inertia tensor for each wheel in the $\mathbf{e}_i$-$\mathbf{f}_i$-$\mathbf{k}$ frame, for $i = 1, 2, 3$, is given by

$$\mathbf{I}_i = \begin{bmatrix} 0.0025 & 0 & 0 \\ 0 & 0.00125 & 0 \\ 0 & 0 & 0.00125 \end{bmatrix} \text{kgm}^2$$

For symbolic manipulation, as in §A.5, the platform is assumed to be a triangular plate. However, an assumption where the platform is in the form of a box is more practical because an AGV needs to carry an on-board computer, batteries for the power supply and other necessary equipment. A similar architecture is used in YAMABICO 3.1 (Iijima et al., 1981), for which the dimensions of the platform are 0.35 m $\times$ 0.35 m $\times$ 0.55 m. Using the same dimensions and considering the mass of the platform as 20.0 kg, the inertia matrix of the platform (body 5) in the i-j-k

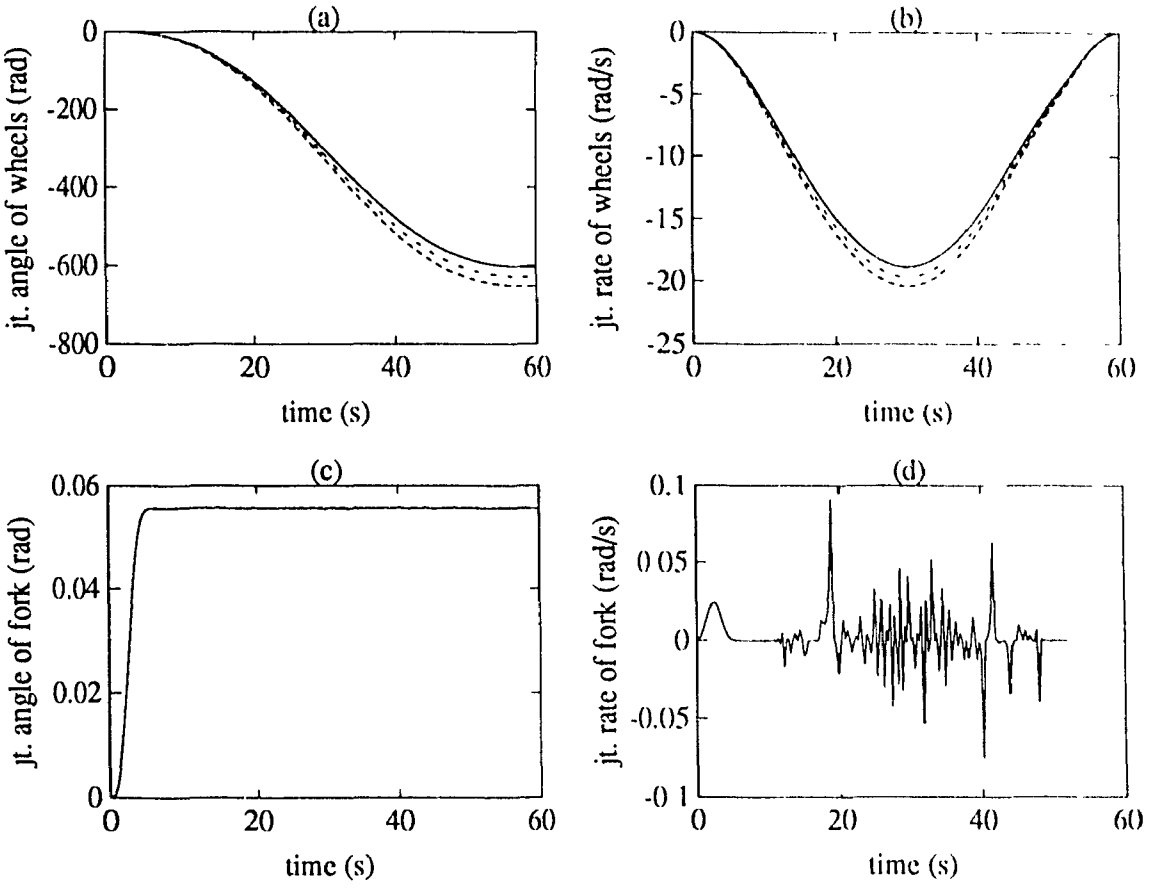

(a) & (b) — $\theta_1, \dot{\theta}_1$; - - $\theta_2, \dot{\theta}_2$; - - - $\theta_3, \dot{\theta}_3$. (c) & (d) $\theta_4, \dot{\theta}_4$.

Fig. 4.8 Required joint angles and rates to traverse a circular trajectory. Joint (a) angles and (b) rates of the wheels, (c) angle and (d) rate of the revolute pair that couples the fork of the caster wheel with the platform.

frame is calculated as

$$\mathbf{I}_5 = \begin{bmatrix} 0.7083 & 0 & 0 \\ 0 & 0.7083 & 0 \\ 0 & 0 & 0.4083 \end{bmatrix} \text{kgm}^2$$

Compared to the mass of the wheels and the platform, the mass of the fork (body 4) is assumed negligible.

4.3.3 Inverse Kinematics and Dynamics Results

The joint angles and their time rates of change required to traverse a circular path, as shown in Fig. 4.2, are calculated from inverse kinematics, as given in §4.2.1.1,

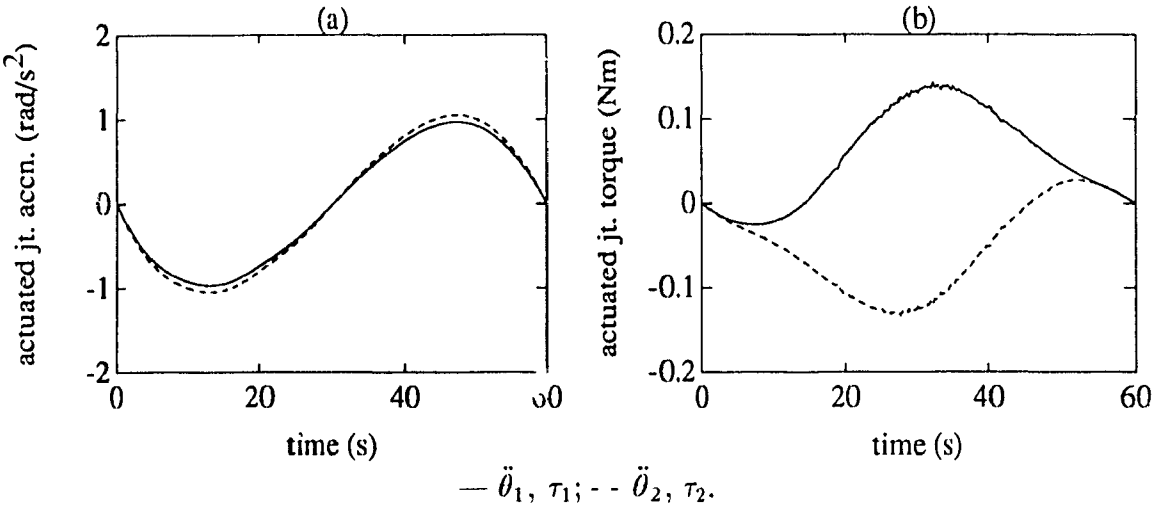

Fig. 4.9 Required actuated joint (a) accelerations and (b) torques to traverse a circular trajectory.

and plotted in Fig. 4.8. The actuated and unactuated joint angles are obtained by integrating eq.(4.38) together with the expression for $\dot{\theta}_D$, which is obtained from eq.(4.51), using the DIVPRK subroutine of the IMSL package. A step size of 0.3 s and tolerance of 0.001 is used for integration purposes. A different step size than the one used for the 2-wheeled mechanical system is chosen to obtain a faster convergence rate of the solutions of the differential equations. Note that, to traverse a circular path, angle θ_1 should be equal to the angle corresponding to the curvature of the circle, which is constant. The steady-state value of angle θ_4, as in Fig. 4.8(c), is the angle at which the caster wheel assembly of the vehicle should be oriented. The jump in Fig. 4.8(c) is due to zero initial condition for angle θ_4. On the other hand, if the initial value of θ_4 is calculated based on the curvature of the path, then this value does not vary over the travelling period of the vehicle, i.e., there is no jump. Moreover, for a constant θ_4, $\dot{\theta}_4$ should be zero, which is not the case in Fig. 4.8(d). The error in $\dot{\theta}_4$, which is a function of θ_1, θ_4 and the geometrical parameters of the vehicle, is mainly due to the integration errors in θ_4. The accuracy of $\dot{\theta}_4$ as well as θ_4 can be increased by providing a smaller tolerance to the integration scheme. The actuated joint accelerations and the corresponding joint torques are shown in Fig. 4.9. A comparison of Figs. 4.9(a) and (b) shows that the plots of the latter

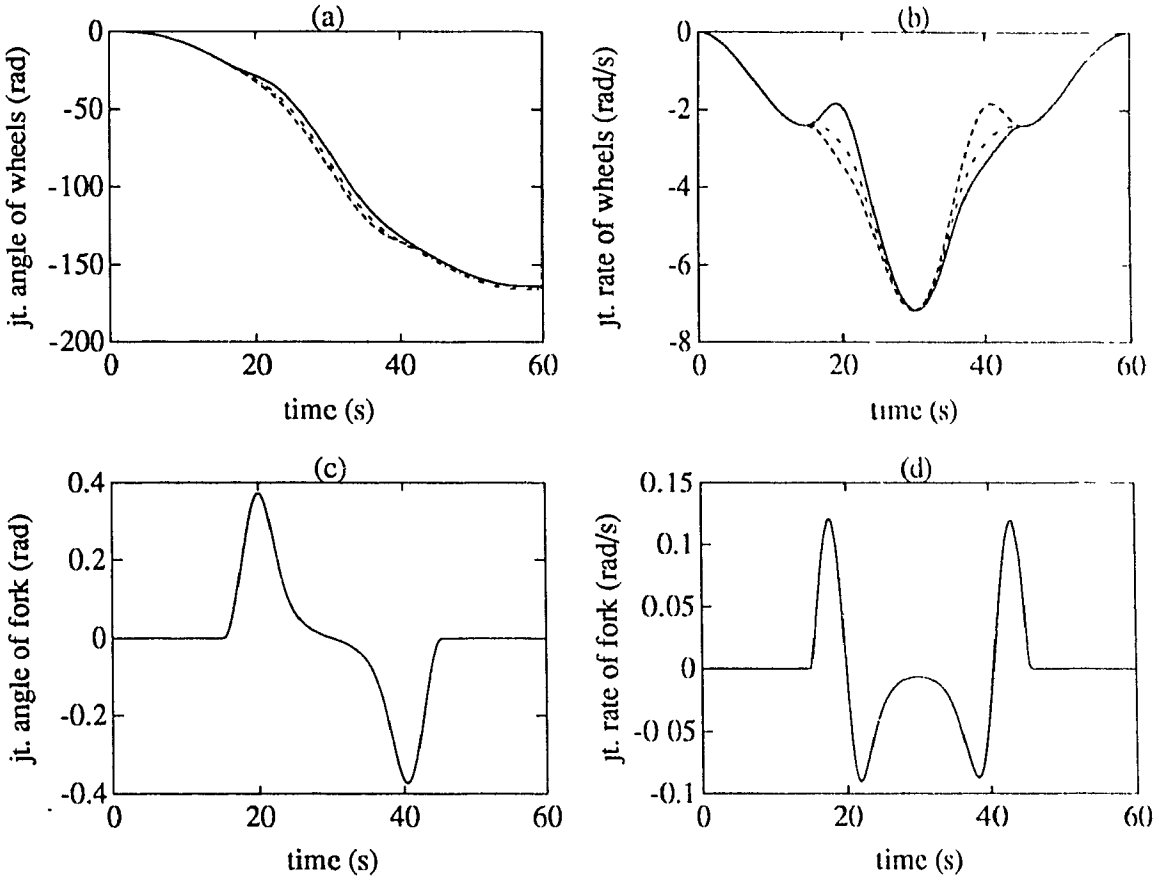

(a) & (b) — θ_1, $\dot{\theta}_1$; - - θ_2, $\dot{\theta}_2$; - · - θ_3, $\dot{\theta}_3$. (c) & (d) θ_4, $\dot{\theta}_4$.

Fig. 4.10 Required joint angles and rates to traverse a path consisting of two straight lines connected by a smooth curve: Joint (a) angles and (b) rates of the wheels, (c) angle and (d) rate of the revolute pair that couples the fork of the caster wheel with the platform.

are not proportional to those of the former, which is a clear indication of the effect of the convective inertia terms in the dynamic model of the vehicle. Moreover, a small discrepancy in the smoothness of the plots of the actuated joint torques, as in Fig. 4.9(b), is due to the variables θ_4 and $\dot{\theta}_4$, as evidenced in Figs. 4.8(c) and (d)

Inverse kinematics and dynamics results for the vehicle moving in a path consisting of two straight lines connected by a curve, as shown in Figs. 4.6 and 4.7, are shown in Fig. 4.10. To obtain the joint angles, the step size and tolerance are taken as 0.3 s and 10^{-5} for the DIVPRK subroutine. Here, a smaller tolerance is provided to enhance the accuracy. The required actuated joint accelerations and torques are

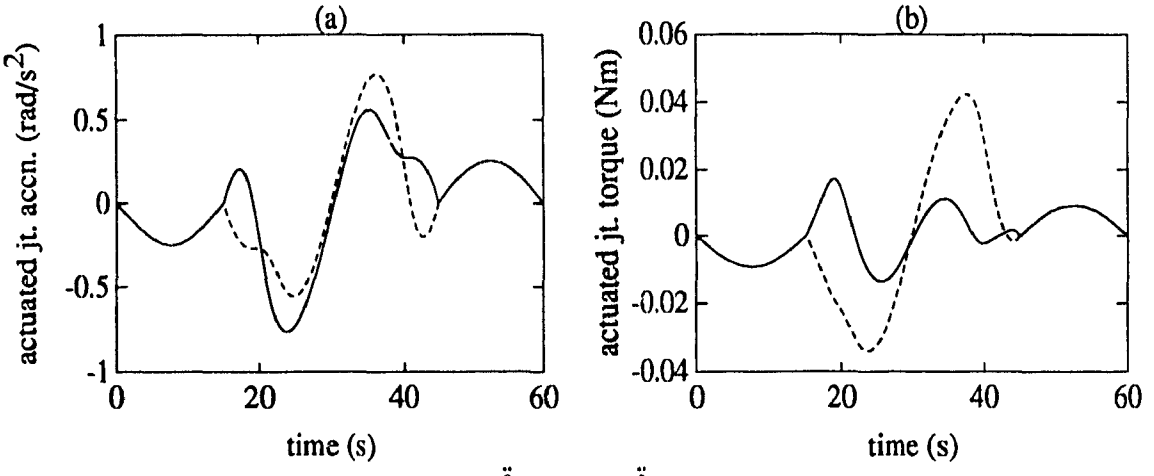

Fig. 4.11 Required actuated joint (a) accelerations and (b) torques to traverse a path consisting of two straight lines connected by a smooth curve.

plotted in Fig. 4.11.

4.3.4 Simulation Results

Simulation leading to direct dynamics involves the integration of the equations of motion, eq.(4.42). The first-order differential equations obtained from the state-space representation of eq.(4.42) are solved using the DIVPRK subroutine of the IMSL package. The state-space form of the equations of motion of the AGV is given by

$$\dot{\mathbf{x}} = \mathbf{H}\mathbf{x} + \mathbf{u} \tag{4.55}$$

where the 4×4 matrix $\mathbf{H}$ and the 4-dimensional vector $\mathbf{u}$ are given by

$$\mathbf{H} \equiv \begin{bmatrix} \mathbf{O} & \mathbf{1} \\ \mathbf{O} & \mathbf{I}^{-1}\mathbf{C} \end{bmatrix} \quad \text{and} \quad \mathbf{u} \equiv \begin{bmatrix} \mathbf{0} \\ \mathbf{I}^{-1}\boldsymbol{\tau} \end{bmatrix}$$

Vector $\mathbf{x} \equiv [\theta_1, \ \theta_2, \ \dot{\theta}_1, \ \dot{\theta}_2]^T$ is the 4-dimensional state vector. Simulation results are obtained from the integration of eq.(4.55) and direct kinematics. The integration step and tolerance are taken as 0.3 s and 0.001, respectively. When the vehicle traverses a circular path, simulation errors in joint and Cartesian spaces are plotted in Figs. 4.12(a)-(c). Since the simulation errors in both spaces are very small, the simulated trajectory in Fig. 4.12(d) cannot be distinguished from the planned circular

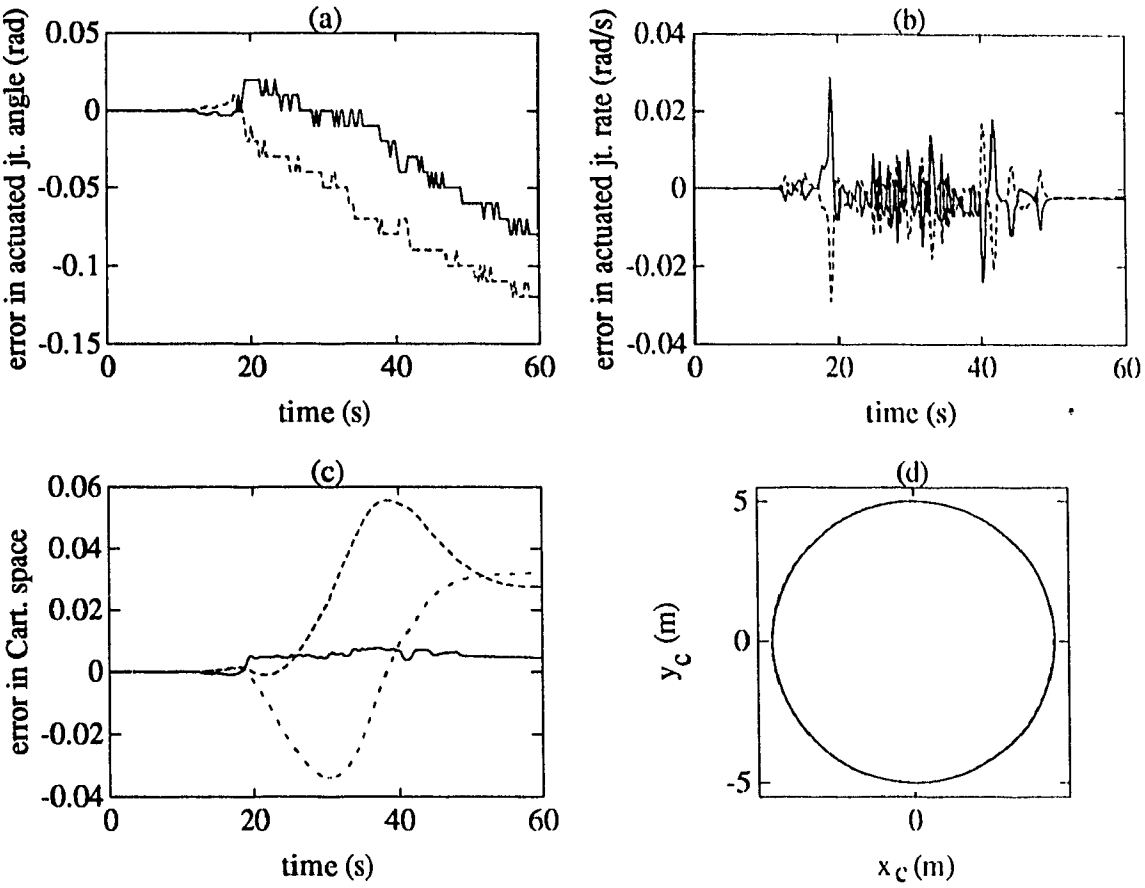

(a) & (b) — θ_1, $\dot{\theta}_1$; - - θ_2, $\dot{\theta}_2$. (c) — ψ (rad), - - x_c (m), - · - y_c (m).
(d) — planned and - - simulated trajectory.

Fig. 4.12 Simulation errors while traversing a circular trajectory.

path. On the other hand, when the vehicle traverses a path consisting of two straight lines connected by a curve, the simulation errors in the actuated joint angles, joint rates and in the Cartesian variables ψ, x_c and y_c are shown in Fig. 4.13. The step size and tolerance for the DIVPRK routine are taken as 0.3 s and 10^{-5}, respectively. Referring to Fig. 4.13(d), the simulated trajectory of the two straight lines connected by a curve cannot be distinguished from the original path due to small simulation errors.

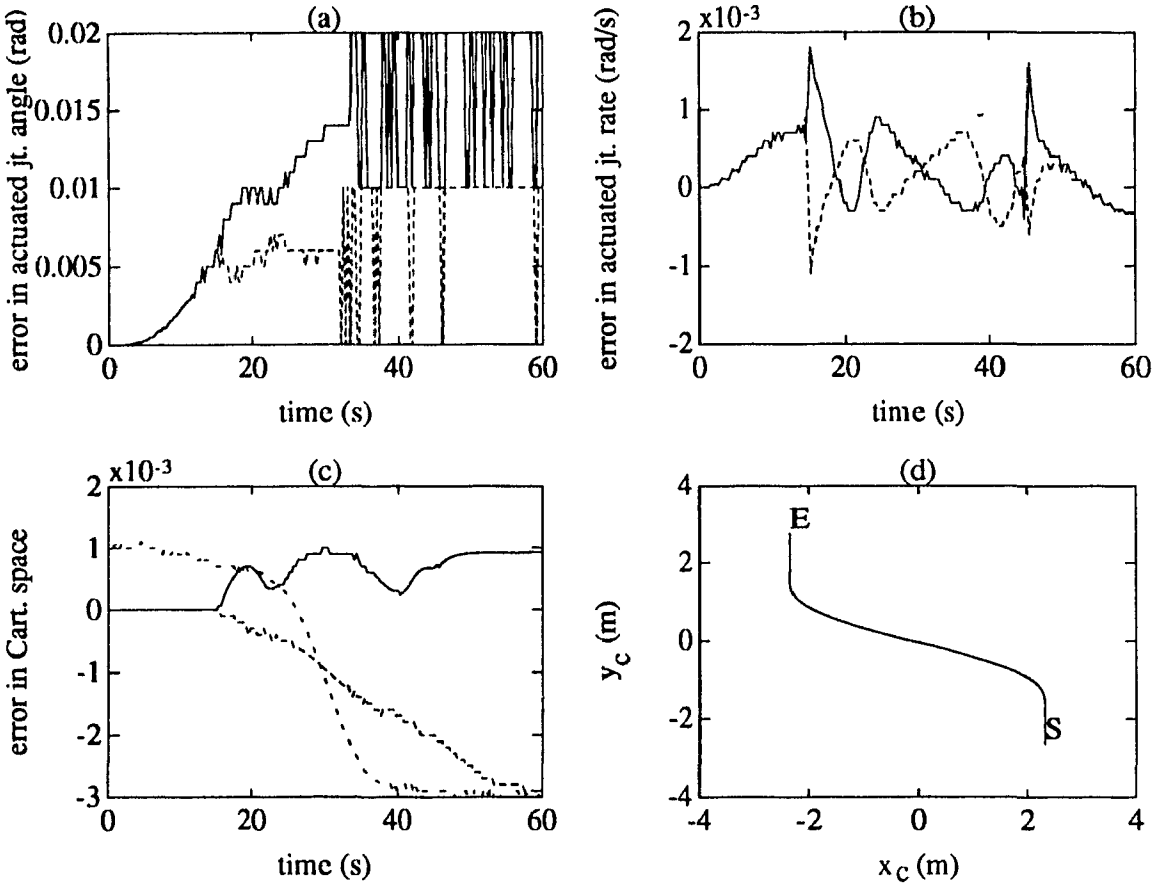

(a) & (b) — θ_1, $\dot{\theta}_1$; - - θ_2, $\dot{\theta}_2$. (c) — ψ (rad), - - x_c (m), - · - y_c (m).
(d) — planned and - - simulated trajectory; S: start and E: end points.

Fig. 4.13 Simulation errors while traversing a path consisting of two straight lines connected by a smooth curve.

4.4 Three-DOF Automatic Guided Vehicles

An automatic guided vehicle with omnidirectional wheels which allow a 3-DOF motion of the vehicle (Muir and Neuman, 1987a) is shown in Fig. 4.14(a). An omnidirectional wheel consisting of a wheel hub and several rollers mounted on it is shown in Figs. 1.4(a) and (b). A general architecture of a 3-DOF AGV, as shown in Fig. 4.14(a), is considered for analysis purposes. The vehicle is assumed to consist of λ omnidirectional wheels, of which μ are actuated, and a platform. The platform is coupled by revolute pairs to all the wheel hubs. To obtain a 3-DOF motion of the vehicle, at least three wheels must be driven or actuated, i.e.,

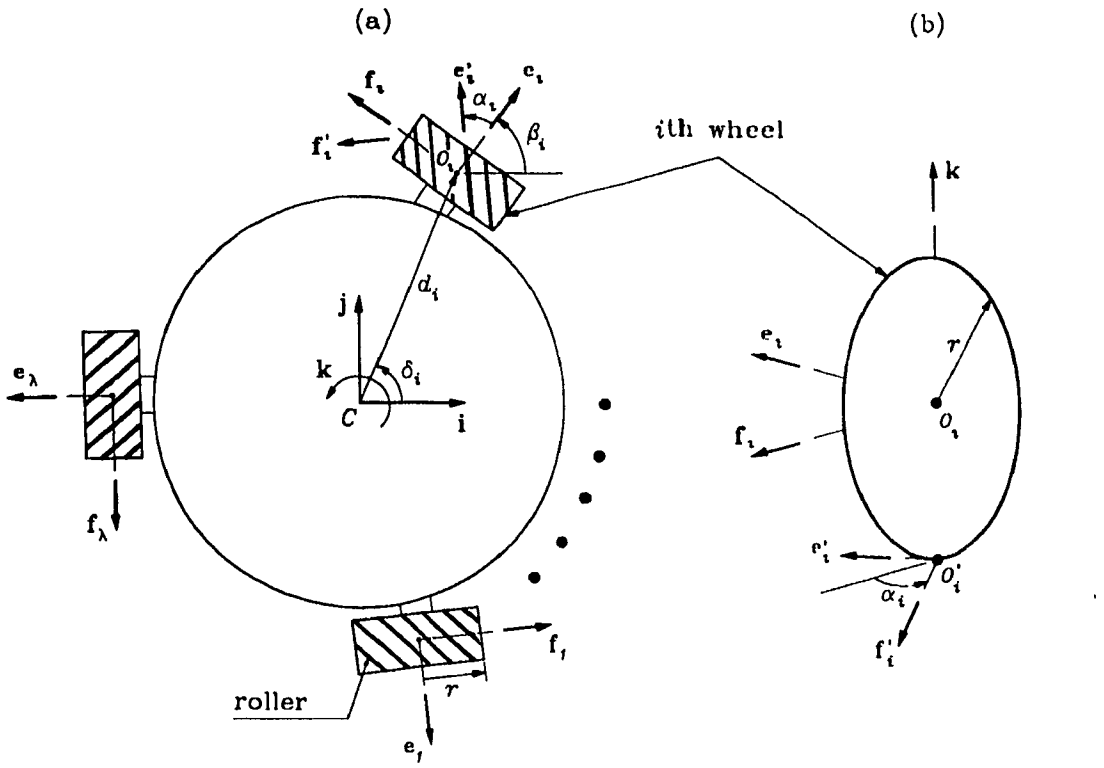

Fig. 4.14 A schematic diagram of (a) a λ-wheeled 3-DOF AGV and (b) an omnidirectional wheel.

$\mu \geq 3$. If more than three wheels are actuated, the system becomes redundantly actuated. Dynamic models of redundantly actuated AGVs are developed based on the methodology given in §3.6. The number of rollers in a wheel hub is such that the vehicle moves smoothly. Moreover, only one roller at a time is in contact with the floor. Furthermore, for analysis purposes, a coordinate frame of unit vectors $\mathbf{i}$, $\mathbf{j}$ and $\mathbf{k}$ is fixed at the centroid C of the platform, as shown in Fig. 4.14(a). According to Fig. 4.14(b), orthogonal unit vectors $\mathbf{e}_i$, $\mathbf{f}_i$ and $\mathbf{e}'_i$, $\mathbf{f}'_i$ ($i = 1, \cdots, \lambda$) are attached to the mass centre O_i of the ith wheel hub and to the mass centre O'_i of the roller mounted on the ith wheel and in contact with the floor, respectively. Note that the roller mounted on the ith wheel and in contact with the floor is termed here the ith active roller. Also, vector $\mathbf{e}_i$ is oriented at an angle β_i with respect to the unit vector $\mathbf{i}$ of the vehicle, as indicated in Fig. 4.14(a), and $\mathbf{e}'_i$ is oriented at α_i with respect to $\mathbf{e}_i$, which is shown in Figs. 1.4(b) and 4.14.

4.4.1 Velocity and Acceleration Analyses

Referring to Figs. 4.14(a) and (b), the velocity of the mass centre of the ith wheel, $\mathbf{v}_i$, can be derived from the velocity of the mass centre C of the platform, $\dot{\mathbf{c}}$, as

$$\mathbf{v}_i = \dot{\mathbf{c}} + \boldsymbol{\omega} \times \mathbf{d}_i \tag{4.56}$$

where $\boldsymbol{\omega}$ is the angular velocity of the platform and $\mathbf{d}_i$ is the vector directed from point C to point O_i. The velocity of point O_i can also be determined from the spinning of the rollers and wheel hubs, i.e.,

$$\mathbf{v}_i = -r_r\dot{\theta}'_i\mathbf{f}'_i - r\dot{\theta}_i\mathbf{f}_i \tag{4.57}$$

where r and r_r are the radii of the wheel hubs and rollers, respectively. The parameters $\dot{\theta}_i$ and $\dot{\theta}'_i$ are the joint rates of the ith wheel hub, or wheel, for brevity, and the ith active roller about the axes parallel to $\mathbf{e}_i$ and $\mathbf{e}'_i$, respectively. Using eqs.(4.56) and (4.57), an equation relating the joint rates of the ith wheel and the ith active roller with the twist of the platform is obtained as

$$\boldsymbol{\Theta}_i\dot{\boldsymbol{\theta}}_i = \boldsymbol{\Gamma}\mathbf{t}_C \tag{4.58}$$

where the 3×2 matrix $\boldsymbol{\Theta}_i$ and the 3×6 matrix $\boldsymbol{\Gamma}$ are given by

$$\boldsymbol{\Theta}_i = [\,-r\mathbf{f}_i \quad -r_r\mathbf{f}'_i\,], \quad \boldsymbol{\Gamma} = [\,-\mathbf{D}_i \quad \mathbf{1}\,] \tag{4.59}$$

and $\mathbf{D}_i$ is the 3×3 cross-product tensor associated with vector $\mathbf{d}_i$. The 2- and 6-dimensional vectors, $\dot{\boldsymbol{\theta}}_i$ and $\mathbf{t}_C$, respectively, are defined as

$$\dot{\boldsymbol{\theta}}_i \equiv [\dot{\theta}_i, \quad \dot{\theta}'_i]^T, \quad \mathbf{t}_C \equiv [\boldsymbol{\omega}^T, \quad \dot{\mathbf{c}}^T]^T \tag{4.60}$$

Note that, for planar motion of the platform, a 3-dimensional twist vector of the platform, as defined in eq.(4.13), is sufficient to describe the motion. Also, vectors $\mathbf{e}_i$, $\mathbf{e}'_i$, $\mathbf{f}_i$, $\mathbf{f}'_i$, in the **i**-**j**-**k** frame can be written as

$$\mathbf{e}_i = [c\beta_i, \quad s\beta_i, \quad 0]^T, \quad \mathbf{e}'_i = [c\gamma_i, \quad s\gamma_i, \quad 0]^T \tag{4.61a}$$

$$\mathbf{f}_i = [-s\beta_i, \quad c\beta_i, \quad 0]^T, \quad \mathbf{f}'_i = [-s\gamma_i, \quad c\gamma_i, \quad 0]^T \tag{4.61b}$$

where $\gamma_i \equiv \alpha_i + \beta_i$. Upon substitution of eqs.(4.61a) and (4.61b) into eq.(4.58) and introduction of the 3-dimensional twist vector $\mathbf{t}'_C$ of the platform, an expression relating $\dot{\boldsymbol{\theta}}_i$ with $\mathbf{t}'_C$ is derived, namely,

$$\boldsymbol{\Theta}_i \dot{\boldsymbol{\theta}}_i = \boldsymbol{\Gamma} \mathbf{t}'_C \tag{4.62}$$

where $\boldsymbol{\Theta}_i$ and $\boldsymbol{\Gamma}$ of eq.(4.59) are redefined as the 2×2 and the 2×3 matrices displayed below:

$$\boldsymbol{\Theta}_i = r \begin{bmatrix} s\beta_i & \rho s\gamma_i \\ -c\beta_i & -\rho c\gamma_i \end{bmatrix} \quad \text{and} \quad \boldsymbol{\Gamma} = \begin{bmatrix} -d_i s\delta_i & 1 & 0 \\ d_i c\delta_i & 0 & 1 \end{bmatrix} \tag{4.63}$$

with $\rho = r_r/r$ and d_i being the magnitude of the projection of vector $\mathbf{d}_i$ on the plane of the platform. Furthermore, angle δ_i appearing in eq.(4.63) is shown in Fig. 4.14(a) Vector $\mathbf{d}_i$ in the **i-j-k** frame can be expressed as

$$\mathbf{d}_i = [d_i c\delta_i, \quad d_i s\delta_i, \quad h]^T \tag{4.64}$$

where h is the perpendicular distance from the mass centre of the ith wheel, point O_i, to the plane of the platform containing point C. It is pointed out here that the parameter h does not appear in the kinematic and dynamic analyses of the 3-DOF AGVs.

Since eq.(4.62) is obtained by expressing all the vectors and matrices of eq.(4.58) in the moving **i-j-k** frame, the time derivatives of the elements of $\boldsymbol{\Theta}_i$ and $\boldsymbol{\Gamma}$ of eq.(4.63) do not lead to $\dot{\boldsymbol{\Theta}}_i$ and $\dot{\boldsymbol{\Gamma}}$. Thus, for acceleration analysis, the expression in eq.(4.58) is differentiated with respect to time, i.e.,

$$\boldsymbol{\Theta}_i \ddot{\boldsymbol{\theta}}_i + \dot{\boldsymbol{\Theta}}_i \dot{\boldsymbol{\theta}}_i = \boldsymbol{\Gamma} \mathbf{t}_C + \dot{\boldsymbol{\Gamma}} \mathbf{t}_C \tag{4.65}$$

Equation (4.65) is now rewritten using the 3-dimensional vectors of twist and twist rate of the platform, as defined in eqs.(4.13) and (4.16), respectively, namely,

$$\boldsymbol{\Theta}_i \ddot{\boldsymbol{\theta}}_i + \dot{\boldsymbol{\Theta}}_i \dot{\boldsymbol{\theta}}_i = \boldsymbol{\Gamma} \dot{\mathbf{t}}'_C + \dot{\boldsymbol{\Gamma}} \mathbf{t}'_C \tag{4.66}$$

Using the definitions given in eqs.(4.61a) and (4.61b), the 2×2 matrix $\dot{\boldsymbol{\Theta}}_i$ and the 2×3 matrix $\dot{\boldsymbol{\Gamma}}$ of eq.(4.66) are given as

$$\dot{\boldsymbol{\Theta}}_i = r\dot{\psi} \begin{bmatrix} c\beta_i & \rho\, c\gamma_i \\ s\beta_i & \rho\, s\gamma_i \end{bmatrix} \quad \text{and} \quad \dot{\boldsymbol{\Gamma}} = -d_i \dot{\psi} \begin{bmatrix} c\delta_i & 0 & 0 \\ s\delta_i & 0 & 0 \end{bmatrix} \tag{4.67}$$

Given eqs.(4.62) and (4.66), the inverse and direct kinematics of λ-wheeled 3-DOF AGVs are obtained below.

4.4.1.1 Inverse Kinematics

For inverse kinematics of the 3-DOF AGVs under study, the actuated joint angles and their time derivatives, which are not independent in the presence of redundant actuation, are determined from the required twist and twist rate of the platform traversing a desired path. Referring to eq.(4.62), the 2×2 matrix $\mathbf{\Theta}_i$ is nonsingular, unless angle α_i is equal to 0 or π, because $\det(\mathbf{\Theta}_i) = r^2\rho\ s\alpha_i \neq 0$. Note that the singularity of matrix $\mathbf{\Theta}_i$ at $\alpha_i = 0$ or π arises and then, the wheels become conventional, like the wheels in automobiles, which have two DOF. Thus, for any nonzero value of α_i, $\dot{\boldsymbol{\theta}}_i$ is obtained from eq.(4.62) as

$$\dot{\boldsymbol{\theta}}_i = \mathbf{\Theta}_i^{-1}\mathbf{\Gamma}\mathbf{t}_C' \tag{4.68}$$

where $\mathbf{\Theta}_i^{-1}\mathbf{\Gamma}$ is given by

$$\mathbf{\Theta}_i^{-1}\mathbf{\Gamma} = \frac{1}{r\rho\ s\alpha_i}\begin{bmatrix} -d_i\rho\ s(\gamma_i - \delta_i) & -\rho\ c\gamma_i & -\rho\ s\gamma_i \\ d_i\ s(\beta_i - \delta_i) & c\beta_i & s\beta_i \end{bmatrix} \tag{4.69}$$

From eq.(4.68), the joint rates of the ith wheel and the ith active roller, $\dot{\theta}_i$ and $\dot{\theta}_i'$, respectively, are given as

$$\dot{\theta}_i = -\frac{1}{r\ s\alpha_i}[d_i\dot{\psi}\ s(\gamma_i - \delta_i) + \dot{x}\ c\gamma_i + \dot{y}\ s\gamma_i] \tag{4.70}$$

and

$$\dot{\theta}_i' = \frac{1}{r_r\ s\alpha_i}[d_i\dot{\psi}\ s(\beta_i - \delta_i) + \dot{x}\ c\beta_i + \dot{y}\ s\beta_i] \tag{4.71}$$

Now, for a λ-wheeled vehicle, two λ-dimensional vectors, $\dot{\boldsymbol{\theta}}$ and $\dot{\boldsymbol{\theta}}'$ consisting of all the joint rates of the wheel hubs and the joint rates of the active rollers, respectively, are derived from eq.(4.68) as

$$\dot{\boldsymbol{\theta}} = \mathbf{L}\mathbf{t}_C' \quad \text{and} \quad \dot{\boldsymbol{\theta}}' = \mathbf{L}'\mathbf{t}_C' \tag{4.72}$$

where the $\lambda \times 3$ matrices $\mathbf{L}$ and $\mathbf{L}'$ are given as

$$\mathbf{L} = \begin{bmatrix} \eta_1 d_1 \; s(\gamma_1 - \delta_1) & \eta_1 \, c\gamma_1 & \eta_1 \, s\gamma_1 \\ \vdots & \vdots & \vdots \\ \eta_\lambda d_\lambda \; s(\gamma_\lambda - \delta_\lambda) & \eta_\lambda \, c\gamma_\lambda & \eta_\lambda \, s\gamma_\lambda \end{bmatrix} \tag{4.73}$$

and

$$\mathbf{L}' = \begin{bmatrix} \eta'_1 d_1 \; s(\beta_1 - \delta_1) & \eta'_1 c\beta_1 & \eta'_1 s\beta_1 \\ \vdots & \vdots & \vdots \\ \eta'_\lambda d_\lambda \; s(\beta_\lambda - \delta_\lambda) & \eta'_\lambda \, c\beta_\lambda & \eta_\lambda \, s\gamma_\lambda \end{bmatrix} \tag{4.74}$$

while $\eta_i = -1/(r \; s\alpha_i)$ and $\eta'_i = 1/(r_r \; s\alpha_i)$ for $i = 1, \cdots, \lambda$. In the presence of less actuated wheels than the total number of wheels in the vehicle, i.e., when $\mu < \lambda$, $\boldsymbol{\theta}$ and $\mathbf{L}$ are partitioned as

$$\dot{\boldsymbol{\theta}} \equiv \begin{bmatrix} \dot{\boldsymbol{\theta}}_A \\ \dot{\boldsymbol{\theta}}_N \end{bmatrix} \qquad \text{and} \qquad \mathbf{L} \equiv \begin{bmatrix} \mathbf{L}_A \\ \mathbf{L}_N \end{bmatrix} \tag{4.75}$$

where $\dot{\boldsymbol{\theta}}_A$ is the μ-dimensional vector consisting of the joint rates of the actuated wheel hubs and $\dot{\boldsymbol{\theta}}_N$ consists of the remaining joint rates, i.e., of the joint rates of the $\lambda - \mu$ nonactuated wheel hubs. Moreover, $\mathbf{L}_A$ and $\mathbf{L}_N$ are the $\mu \times 3$ and $(\lambda - \mu) \times 3$ matrices relating the twist of the platform with the joint rates of the actuated and nonactuated wheel hubs, respectively. Furthermore, a vector of unactuated joint rates $\dot{\boldsymbol{\theta}}_U$ is introduced, which contains all the joint rates of the active rollers for all the wheels and nonactuated wheel hubs. The $(2\lambda - \mu)$-dimensional vector $\dot{\boldsymbol{\theta}}_U$ and the $(2\lambda - \mu) \times 3$ matrix $\mathbf{L}_U$ are defined accordingly, i.e.,

$$\dot{\boldsymbol{\theta}}_U \equiv \begin{bmatrix} \dot{\boldsymbol{\theta}}' \\ \dot{\boldsymbol{\theta}}_N \end{bmatrix} \qquad \text{and} \qquad \mathbf{L}_U \equiv \begin{bmatrix} \mathbf{L}' \\ \mathbf{L}_N \end{bmatrix} \tag{4.76}$$

The relations required to obtain the actuated and unactuated joint rates are now readily available from eqs.(4.72)–(4.76) as

$$\dot{\boldsymbol{\theta}}_A = \mathbf{L}_A \mathbf{t}'_C \quad \text{and} \quad \dot{\boldsymbol{\theta}}_U = \mathbf{L}_U \mathbf{t}'_C \tag{4.77}$$

The actuated and unactuated joint accelerations are now written from eq.(4.66) by following the similar steps in obtaining eq.(4.77) from eq.(4.62), namely,

$$\ddot{\boldsymbol{\theta}}_A = \mathbf{L}_A \dot{\mathbf{t}}'_C + \dot{\mathbf{L}}_A \mathbf{t}'_C \tag{4.78a}$$

$$\ddot{\boldsymbol{\theta}}_U = \mathbf{L}_U \dot{\mathbf{t}}'_C + \dot{\mathbf{L}}_U \mathbf{t}'_C \tag{4.78b}$$

Since all the vectors and matrices of eq.(4.72) are represented in the moving coordinate **i-j-k** frame, the entries of the $\mu \times 3$ matrix $\dot{\mathbf{L}}_A$ and the $(2\lambda - \mu) \times 3$ matrix $\dot{\mathbf{L}}_U$ are not simply the time derivatives of the elements of $\mathbf{L}_A$ and $\mathbf{L}_U$ of eq.(4.77), respectively. Thus, eqs.(4.78a) and (4.78b) are derived using eq.(4.66). The actuated and unactuated joint angles required by the AGV to move in a specified path are obtained by integrating eq.(4.77), with known initial conditions.

4.4.1.2 Direct Kinematics

To obtain the twist of the platform from the given actuated joint rates, the relation between the twist of the platform and the actuated joint rates, as given in eq.(4.77), is used. Since the vehicle has three DOF, for a vehicle with three actuated wheels, matrix $\mathbf{L}_A$ is 3×3. Hence, for a nonsingular $\mathbf{L}_A$ matrix, the twist of the platform is obtained as

$$\mathbf{t}'_C = \mathbf{L}_A^{-1}\dot{\boldsymbol{\theta}}_A = \mathbf{T}_A\dot{\boldsymbol{\theta}}_A \tag{4.79}$$

where $\mathbf{T}_A \equiv \mathbf{L}_A^{-1}$. The singularity of matrix $\mathbf{L}_A$ will be pointed out in Chapter 5. However, for AGVs consisting of more than three wheels, the relation between the twist of the platform and the actuated joint rates leads to more equations than unknowns, i.e., to an overdetermined system of algebraic equations. For a consistent set of input data, i.e., vector $\dot{\boldsymbol{\theta}}_A$, vector $\mathbf{t}'_C$ can be calculated with the help of the Moore-Penrose generalized inverse, i.e.,

$$\mathbf{t}'_C = \mathbf{T}_A\dot{\boldsymbol{\theta}}_A \tag{4.80}$$

where $\mathbf{T}_A \equiv \mathbf{L}_A^I \equiv (\mathbf{L}_A^T\mathbf{L}_A)^{-1}\mathbf{L}_A^T$. The twist rate of the platform is now obtained from eq.(4.78a).

The orientation and the position of the mass centre of the platform in an inertial frame is found by integrating the following relation:

$$[\mathbf{t}'_C]_I = [\mathbf{Q}]_I\mathbf{t}'_C \tag{4.81}$$

where the 3-dimensional vector $[\mathbf{t}'_C]_I$ is the twist of the platform represented in an

inertial frame $\mathcal{I}$, whereas the 3×3 matrix $[\mathbf{Q}]_I$ is the orientation of the i-j-k frame with respect to the $\mathcal{I}$-frame. Vector $[\mathbf{t}'_C]_I$ and matrix $[\mathbf{Q}]_I$ are given by

$$[\mathbf{t}'_C]_I \equiv \begin{bmatrix} \dot{\psi} \\ \dot{x}_c \\ \dot{y}_c \end{bmatrix} \quad \text{and} \quad [\mathbf{Q}]_I = \begin{bmatrix} 1 & 0 & 0 \\ 0 & c\psi & -s\psi \\ 0 & s\psi & c\psi \end{bmatrix} \tag{4.82}$$

4.4.2 Dynamic Modelling

In order to develop the dynamic model of 3-DOF AGVs, it is assumed that the mass of the rollers is much smaller compared to the mass of the wheel hubs. Moreover, since the radius of the rollers is also much smaller than the radius of the wheel hubs, the moments of inertia of the rollers about their centroids are considerably small and hence, can be neglected. However, the moments of inertia of the rollers about the centroids of the wheel hubs may be significant. Thus, to account for the mass of the rollers and their moments of inertia about the centroids of the wheel hubs, an omnidirectional wheel is assumed to consist of a wheel hub in which the rollers are rigidly attached to the hub. Therefore, for dynamic modelling, the system can be assumed to consist of λ wheel hubs and the platform. Moreover, pure rolling is assumed at the roller-floor interface. Furthermore, the control of 3-DOF AGVs with more than three actuated wheels leads to redundant actuation, and thus, dynamic models of 3-DOF AGVs with redundant actuation are developed separately in §4.4.3. Note that the 3-dimensional reduced twist and twist rate vectors, as used in kinematics to denote the twist of the platform and its rate of change are not sufficient to represent the twist of the wheel hubs and, hence, the 6-dimensional twist vector and its rate of change are used for all bodies in developing the dynamic models of interest. Also, due to the reasons given in §4.1.2 the dissipation is not included in the model of 3-DOF AGVs. Thus, an assessment for accuracy of the simulation software, OMNI, that is developed in §4.5 is possible. Now, the generalized twist of the vehicle is given by a $6(\lambda + 1)$-dimensional vector, i.e.,

$$\mathbf{t} \equiv [\mathbf{t}_1^T, \quad \cdots, \quad \mathbf{t}_\lambda^T, \quad \mathbf{t}_C^T]^T \tag{4.83}$$

where the twist of the ith wheel is written as

$$\mathbf{t}_i = [\dot{\psi}\mathbf{k}^T + \dot{\theta}_i\mathbf{e}_i^T, \quad \dot{\mathbf{c}}^T + \dot{\psi}(\mathbf{k} \times \mathbf{d}_i)^T]^T, \quad \text{for } i = 1, \cdots, \lambda$$

In an AGV with three actuated joint rates, the latter can play the role of the independent generalized speeds, i.e., $\dot{\boldsymbol{\theta}}_I$ of eq.(3.29) can be substituted by $\dot{\boldsymbol{\theta}}_A$ of eq.(4.75). The unactuated or dependent joint rates and accelerations for the dynamic analysis can obtained from eqs.(4.77) and (4.78b), respectively, as in §4.4.1.1. The dynamic model of a λ-wheeled 3-DOF AGV with three actuated wheels is obtained based on the methodology given either in §3.2 for $\mu = \lambda = 3$ or in §3.3 for $\mu = 3$ and $\lambda > 3$. In both cases, i.e., $\mu = \lambda = 3$ and $\mu = 3$, $\lambda > 3$, a fast algorithm can be developed using the schemes described in §3.5. The equations of motion for 3-DOF AGV with 3-actuated wheels are written as

$$\mathbf{I}\ddot{\boldsymbol{\theta}}_I = \mathbf{C}\dot{\boldsymbol{\theta}}_I + \boldsymbol{\tau} \tag{4.84}$$

where $\mathbf{I}$ and $\mathbf{C}$ are the 3×3 matrices of generalized inertia and convective inertia terms, respectively, while $\boldsymbol{\tau}$ is the 3-dimensional vector containing the joint torques of the actuated wheels. In eq.(4.84), the generalized force due to gravity vanishes and the generalized inertia matrix is a constant matrix $\mathbf{I}$, i.e., $\mathbf{I}$ is independent of the generalized coordinates. The generalized vector due to dissipation does not appear, since no dissipation is considered.

4.4.3 Inverse Dynamics in the Presence of Redundant Actuation

Three-DOF AGVs with more than three actuated wheels lead to redundant actuation and the actuated joint rates can no longer be considered as the independent generalized speeds. However, the components of the reduced twist vector $\mathbf{t}_C'$ of the platform consisting of the angular velocity $\dot{\psi}$ of the platform and the two Cartesian velocities $\dot{x}$ and $\dot{y}$, i.e., $\mathbf{t}_C' \equiv [\dot{\psi}, \quad \dot{x}, \quad \dot{y}]^T$, are always independent. Thus, to apply the method of the NOC to redundantly actuated AGVs, vector $\mathbf{t}_C'$ can play the role

of the independent generalized speeds and an equation similar to eq.(4.81) is readily derived as

$$\mathbf{I}_C \dot{\mathbf{t}}'_C = \mathbf{C}_C \mathbf{t}'_C + \mathbf{w}_C^A \tag{4.85}$$

where $\mathbf{I}_C$ and $\mathbf{C}_C$ are the 3×3 matrices of inertia terms and convective inertia terms, respectively, associated with the vector of independent generalized speeds, $\mathbf{t}'_C$. Vector $\mathbf{w}_C^A$ is the 3-dimensional generalized wrench acting on the platform. Again the generalized wrench $\mathbf{w}_C^G$ due to gravity vanishes and $\mathbf{w}_C^D$ does not appear. For the control of a redundantly actuated vehicle, the actuator torques are obtained as follows: From the power balance of the system at hand, an expression relating the joint torques and the generalized wrench $\mathbf{w}_C^A$ of eq.(4.85), as in eq.(3.55) of §3.6, is obtained with the aid of the expression for $\dot{\boldsymbol{\theta}}_A$ of eq.(4.77), namely,

$$\mathbf{w}_C^A = \mathbf{L}_A^T \boldsymbol{\tau}_A \tag{4.86}$$

Equation (4.86) leads to an underdetermined system of three scalar equations in μ (> 3) unknown actuator torques, vector $\boldsymbol{\tau}_A$. Equation (4.86) can be solved for $\boldsymbol{\tau}_A$ resorting to an optimization approach. In fact, vector $\boldsymbol{\tau}_A$ can be obtained so that it optimizes an objective function $f(\boldsymbol{\tau}_A)$ subject to the equality constraints of eq.(4.86). For example, if $f(\boldsymbol{\tau}_A) = 1/2(\boldsymbol{\tau}_A^T \boldsymbol{\tau}_A)$, the joint torques are readily derived as

$$\boldsymbol{\tau}_A = \mathbf{L}_A (\mathbf{L}_A^T \mathbf{L}_A)^{-1} \mathbf{w}_C^A = \mathbf{T}_A^T \mathbf{w}_C^A \tag{4.87}$$

Moreover, linear inequality constraints arising from the motor torque limitations may be included, along with eq.(4.86), in optimizing $f(\boldsymbol{\tau}_A)$. The inequality constraints can be expressed as

$$\boldsymbol{\tau}_A \leq \boldsymbol{\tau}_A^L \tag{4.88}$$

where $\boldsymbol{\tau}_A^L$ is the vector containing the limiting values of the joint torques. The solutions of the actuated joint torques are obtained using the DQ2ROG subroutine of the IMSL package.

4.4.4 Simulation

A general-purpose code for the simulation of λ-wheeled 3-DOF AGVs, OMNI, leading to direct dynamics is developed in §4.5. For that, first, given the actuated joint torques, the generalized wrench acting on the platform is calculated using eq.(4.86). Then, differential equations, eq.(4.85), resulting from the dynamic model of a 3-DOF AGV, along with the relation given in eq.(4.81), are integrated in order to find the orientation and the position of the mass centre of the platform. A set of first-order differential equations required for the DIVPRK subroutine of the IMSL package is written as

$$\dot{\mathbf{x}} = \mathbf{H}\mathbf{x} + \mathbf{u} \tag{4.89}$$

where the 6×6 matrix $\mathbf{H}$ and the 6-dimensional vectors $\dot{\mathbf{x}}$ and $\mathbf{u}$ are given by

$$\mathbf{H} \equiv \begin{bmatrix} \mathbf{O} & [\mathbf{Q}]_I \\ \mathbf{O} & \mathbf{I}^{-1}\mathbf{C} \end{bmatrix}, \quad \dot{\mathbf{x}} \equiv \begin{bmatrix} [\dot{\mathbf{t}}'_C]_I \\ \dot{\mathbf{t}}'_C \end{bmatrix} \quad \text{and} \quad \mathbf{u} \equiv \begin{bmatrix} \mathbf{0} \\ \mathbf{I}^{-1}\mathbf{w}_C^A \end{bmatrix} \tag{4.90}$$

with the 3-dimensional vector $[\mathbf{t}'_C]_I$ and the 3×3 transformation matrix $[\mathbf{Q}]_I$ being defined in eq.(4.82). The set of first-order differential equations, eq.(4.89) is now integrated using the DIVPRK subroutine of the IMSL package with given initial condition, $\mathbf{x}_0$.

4.5 OMNI: A Software Package for the Analyses of Three-DOF AGVs

A general-purpose software package is developed based on the kinematic and dynamic analyses of 3-DOF AGVs with λ-wheels, of which μ are actuated, with μ, $\lambda \geq 3$. The software is based on the kinematic and dynamic models developed in §4.4. Given the number of wheels, the number of actuated wheels, the architecture of the vehicle and its inertial parameters, the software solves the kinematic and dynamic problems at four different levels, which are described below:

Level 1: Velocity and acceleration inversion.

Input:

- The total number of wheels, λ, in the vehicle, and the number of actuated wheels, μ.
- The radii of the wheel hubs and the rollers.
- The orientation of the rollers of the ith omnidirectional wheel with respect to its hub, i.e., α_i for $i = 1, \cdots, \lambda$.
- The orientation of the ith wheel with respect to the platform, i.e., the orientation β_i between $\mathbf{i}$ and $\mathbf{e}_i$ for $i = 1, \cdots, \lambda$.
- The position of the mass centre of the ith wheel hub, O_i, i.e., vector $\mathbf{d}_i$, for $i = 1, \cdots, \lambda$. Note that the third component of $\mathbf{d}_i$, h of eq.(4.64), neither appears in the kinematics nor in the dynamics relations. Thus, h is not required. Moreover, to compute the first two components of $\mathbf{d}_i$, angle δ_i and the distance d_i, as defined before in eq.(4.64), for $i = 1, \cdots, \lambda$, should be supplied.
- The travelling time and the number of intervals at which the results are required.
- The required twist of the platform and its time rate of change at every sampled point of the interval.

Output:

- The actuated and unactuated joint rates and accelerations, vectors $\dot{\boldsymbol{\theta}}_A$, $\dot{\boldsymbol{\theta}}_U$ and their time rate of change at the desired points.

Level 2: Position inversion.

Input:

- The total number of wheels, λ, in the vehicle, and the number of actuated wheels, μ, as in Level 1.
- The history of the joint rates, which are obtained from the output of Level 1.
- The initial conditions for all the joint angles, which include actuated as well as unactuated joints, i.e., vectors $\boldsymbol{\theta}_A$ and $\boldsymbol{\theta}_U$, at time $t = 0$.
- The travelling time and the number of time intervals.

Output:

- The joint angles, vectors $\boldsymbol{\theta}_A$ and $\boldsymbol{\theta}_U$, for $t > 0$.

Level 3: Inverse dynamics.

Input:

- The total number of wheels, λ, in the vehicle, and the number of actuated wheels, μ, as in Level 1.
- The architecture of the vehicle, as in Level 1.
- The mass and the inertia tensor of the ith wheel, for $i = 1, \cdots, \lambda$, and the mass and the inertia tensor of the platform.
- The travelling time and the sampled instants for which the torques are required.

Output:

- At the desired time, the actuated joint torques are calculated based on eq.(4.84) when $\mu = 3$. On the other hand, for $\mu > 3$, the actuated torques are obtained using the scheme given in §4.4.3.

Level 4: Dynamic simulation

Input:

- The total number of wheels, λ, in the vehicle, and the number of actuated wheels, μ, as in Level 1.
- The architecture of the vehicle, as in Level 1.
- The mass and the inertia tensor of the ith wheel for $i = 1, \cdots, \lambda$, and the mass and the inertia tensor of the platform.
- The history of the joint torques.
- The initial values for the configuration and the twist of the vehicle at $t = 0$.
- The travelling time and the sampled instants for which the simulation results are required.

Output:

- The configuration and twist of the platform at time $t > 0$.

The software that has been developed in this research, OMNI, is used in analysing several 3-DOF AGVs. Results are obtained for different vehicles traversing three different paths, as explained below.

4.6 Inverse Kinematics and Dynamics Results

OMNI is tested with 3-DOF AGVs of different architectures following different trajectories, which are planned in §4.6.1.

4.6.1 Trajectory Planning

Three different paths are chosen in testing the performance of the vehicles under study, namely,

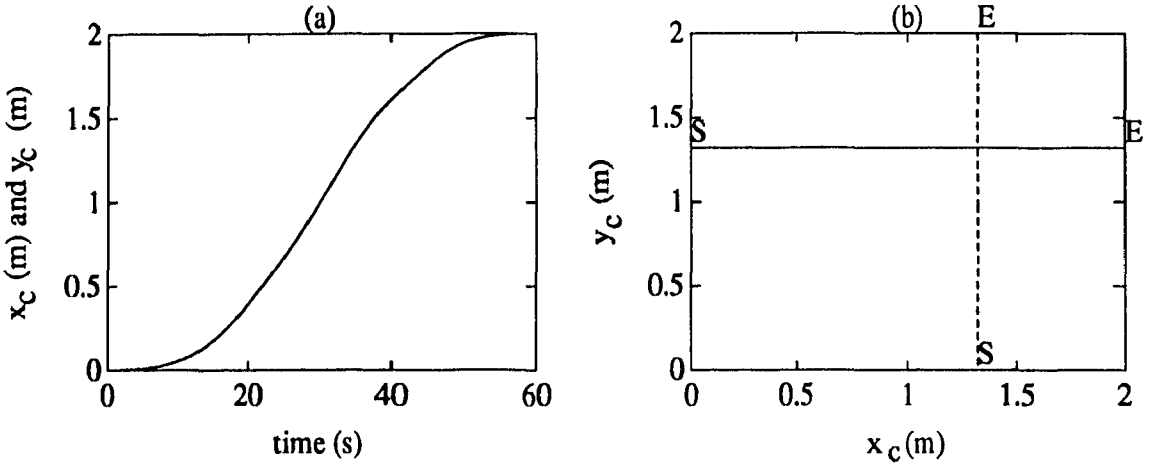

(a) — x_c for Path 1 and y_c for Path 2.
(b) — Path 1, - - Path 2; S: start and E: end points.

Fig. 4.15 Variation of (a) x_c vs. time for Path 1 and y_c vs. time for Path 2, and (b) y_c vs. x_c.

Path 1: The vehicle is assumed to move in a straight path parallel to the x_c-axis of Fig. 4.15(b) with a fixed orientation. The path is planned in such a way that the vehicle starts and stops with zero velocity and acceleration, which has been achieved with a cycloidal motion (Rothbart, 1956; Chen, 1982). The variation of x_c with time is shown in Fig. 4.15(a).

Path 2: This path is such that the vehicle moves along a path parallel to y_c of Fig. 4.15(b) with constant orientation. The variation of y_c with time is shown in Fig. 4.15(a).

Path 3: This path is the two straight lines connected by a smooth curve, as shown in Fig. 4.6, which is plotted in different scales. In contrast to the 2-DOF AGV, where angular velocities are specified depending on the curvature of the curved path, the three components of the required twist of the platform are specified independently, because the system has 3-DOF. Thus, a path is specified in such a way that the orientation of the platform remains fixed at $\psi = 0$, in the segment P_0P_1 of Fig. 4.6; then, it changes its value to $\pi/2$ following a cycloidal motion and, then, continues with constant orientation, i.e., at $\psi = \pi/2$, along the segment P_2P_3 of Fig. 4.6. The variation of angle ψ and the Cartesian coordinates, along with their time derivatives,

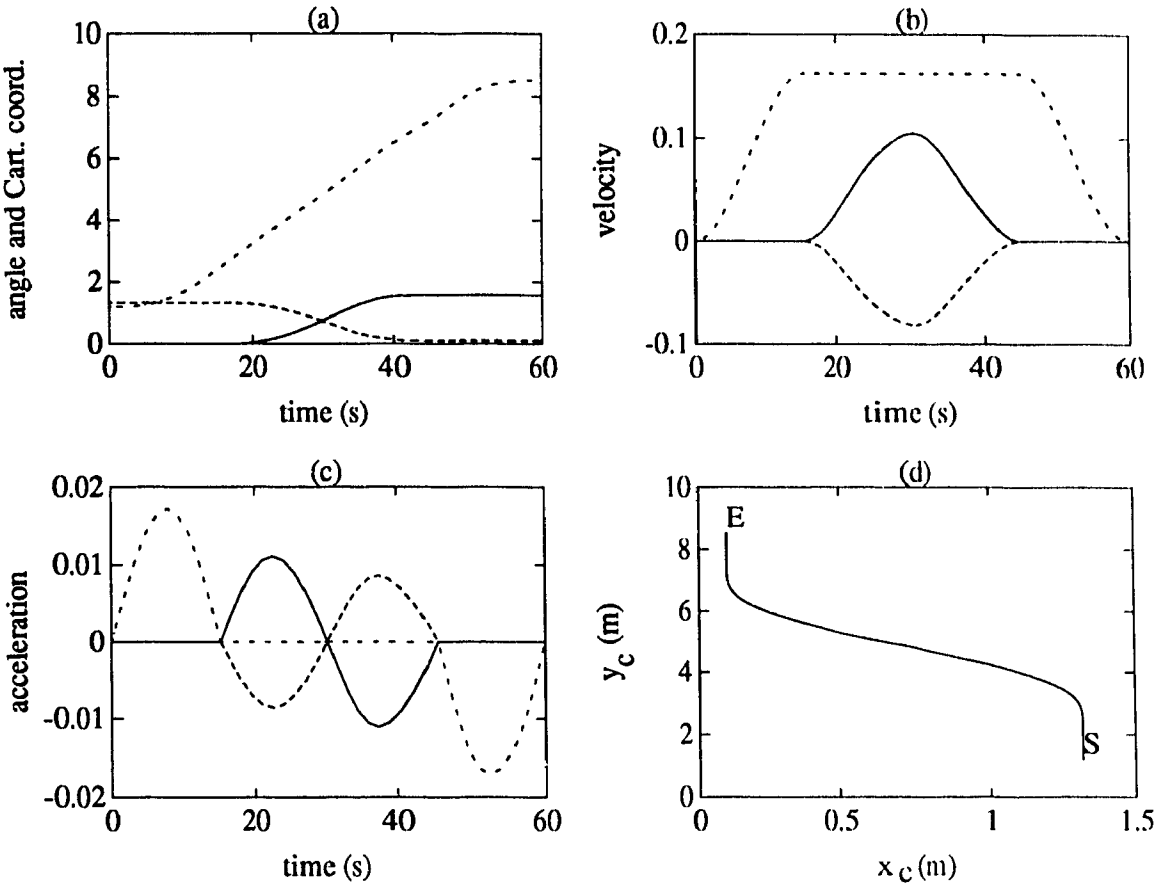

— ψ (rad), $\dot{\psi}$ (rad/s), $\ddot{\psi}$ (rad/s^2); - - x_c (m), $\dot{x}_c$ (m/s), $\ddot{x}_c$ (m/s^2);
- · - y_c (m), $\dot{y}_c$ (m/s), $\ddot{y}_c$ (m/s^2); S: start and E: end points.

Fig. 4.16 Two straight paths connected by a smooth curve: Variation of (a) ψ, x_c and y_c vs. time, (b) $\dot{\psi}$, $\dot{x}_c$ and $\dot{y}_c$ vs. time, (c) $\ddot{\psi}$, $\ddot{x}_c$ and $\ddot{y}_c$ vs. time, and (d) y_c vs. x_c.

are shown in Figs. 4.16(a)-(c). The path is shown in Fig. 4.16(d). The plots of the inverse kinematics and dynamics results obtained for different vehicles moving in Paths 1, 2 and 3 are given in Figs. 4.20-4.32.

4.6.2 A Three-Wheeled AGV: All Wheels are Actuated

The kinematic and dynamic analyses of the 3-wheeled 3-DOF AGV shown in Fig. 4.17 are performed using OMNI. For numerical computations, the geometrical parameters of the vehicle are given in Table 4.1.

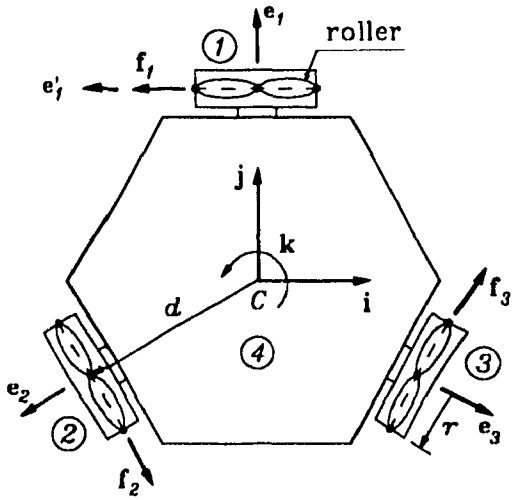

Fig. 4.17 A 3-wheeled 3-DOF AGV.

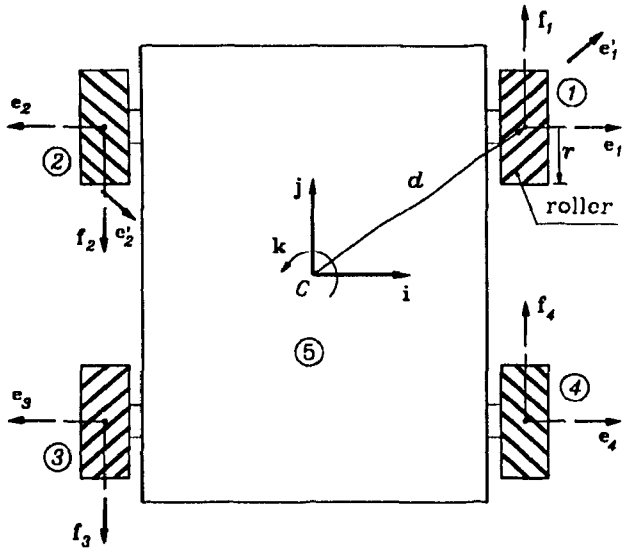

Fig. 4.18 A 4-wheeled 3-DOF AGV.

For dynamic analysis, the system is assumed to consist of four rigid bodies, as indicated in Fig. 4.17, by the encircled numbers. The inertial parameters are now given as follows:

the mass of each wheel hub,	$m_w = 2.0$ kg,
the mass of the platform,	$m = 32.0$ kg.

The inertia tensor for each wheel in the $\mathbf{e}_i$-$\mathbf{f}_i$-$\mathbf{k}$ frame, for $i = 1, 2, 3$, is given by

$$\mathbf{I}_i = \begin{bmatrix} 0.01 & 0 & 0 \\ 0 & 0.00515 & 0 \\ 0 & 0 & 0.00515 \end{bmatrix} \text{kgm}^2$$

The inertia tensor $\mathbf{I}_4$ of the platform, in the **i**-**j**-**k** frame, is

$$\mathbf{I}_4 = \begin{bmatrix} 1.0888 & 0 & 0 \\ 0 & 1.0888 & 0 \\ 0 & 0 & 1.7067 \end{bmatrix} \text{kgm}^2$$

Here, all the three wheels of the vehicle are considered actuated. The kinematics results obtained from Levels 1 and 2, along with the actuated joint torques to move the vehicle in the specified paths that are calculated from Level 3, are shown in Figs. 4.20–4.25.

Wheel, i	α_i (deg)	β_i (deg)	δ_i (deg)	d_i (m)
1	90.0	90.0	90.0	0.3
2	90.0	210.0	210.0	0.3
3	90.0	330.0	330.0	0.3

The radius of the wheel hubs, $r = 0.1$ m and
the radius of the rollers, $r_r = 0.01$ m.

Table 4.1 Architecture of a 3-wheeled 3-DOF AGV.

Wheel, i	α_i (deg)	β_i (deg)	δ_i (deg)	d_i (m)
1	45.0	0.0	56.3	0.36
2	135.0	180.0	123.7	0.36
3	45.0	180.0	236.3	0.36
4	135.0	0.0	303.7	0.36

The radius of the wheel hubs, $r = 0.1$ m and
the radius of the rollers, $r_r = 0.01$ m.

Table 4.2 Architecture of a 4-wheeled 3-DOF AGV.

4.6.3 A Four-Wheeled AGV

A 4-wheeled 3-DOF AGV is shown in Fig. 4.18, whose architecture is given in Table 4.2. The vehicle consists of five rigid bodies. The inertial parameters of the wheels are those given for the wheels of the 3-wheeled vehicle. The mass m and the inertia tensor $\mathbf{I}_5$ of the platform, in the **i-j-k** frame, are as follows:

$$m = 37.0 \text{ kg}, \qquad \mathbf{I}_5 = \begin{bmatrix} 1.2333 & 0 & 0 \\ 0 & 0.6167 & 0 \\ 0 & 0 & 1.6033 \end{bmatrix} \text{kgm}^2$$

Two cases of a 4-wheeled 3-DOF AGV are considered. In the first case, three wheels are actuated. For example, wheels 1, 2 and 3, as denoted in Fig. 4.18 by the encircled numbers, are considered to be the actuated wheels. In the other case, all four wheels are actuated.

4.6.3.1 Three Wheels are Actuated

The kinematic and dynamic models obtained are based on eq.(4.84), where the total number of wheels is greater than the number of actuated wheels. It is to be noted here that the software reads two different input data files containing the

geometrical and inertial parameters, where the values for all the actuated wheels must be specified in a sequential order at the beginning of the data files. Thus, the geometrical and inertial parameters for wheel 1 are given first, then for the second and next for the third wheel. No order is necessary for the other wheels, but the geometrical and inertial parameters of the two data files must correspond to each other. The kinematics results are the same as those obtained in §4.6.3.2 for the case of all actuated wheels. The required torques to move the vehicle along Paths 1 and 3 are shown in Figs. 4.26(a) and (b), respectively.

4.6.3.2 All Four Wheels are Actuated

In the case of an AGV with four actuated wheels, the system is redundantly actuated. Thus, the dynamic analysis is done through torque optimization. The results are shown in Figs. 4.27 to 4.31. Note that, to move along a path parallel to vector **i** fixed to the vehicle, i.e., to move sideways, the wheels 1 and 2 should supply torques in opposite directions. The same is true for wheels 3 and 4. Due to the definitions of the unit vectors in Fig. 4.18, the required joint motions and torques to move sideways have the same sign, as evidenced in Fig. 4.28, which shows that the joint variables for wheels 1 and 3 are actually in the opposite direction to those for wheels 2 and 4, respectively. When the vehicle moves along Path 1, the required joint angles and rates for the active rollers, i.e., the rollers which are in contact with the floor, are zero. The joint angles and rates for the active roller, to move along Paths 2 and 3, are shown in Figs. 4.29(a)–(b) and 4.31(a)–(b), respectively. Note that the comparison between Figs. 4.26(b) and 4.30(d) shows that the maximum required motor torques at wheels 1, 2 and 3 are less when four wheels of the AGV are actuated. Since a torque minimization scheme is used in obtaining the required torques at the four actuated wheels of the vehicle, the maximum torque requirements are smaller than the maximum required torques at the three actuated wheels of the 4-wheeled vehicle. The inverse dynamics results are also obtained by considering the torque limitations. For instance, the plots shown in Fig. 4.33(a) are obtained by

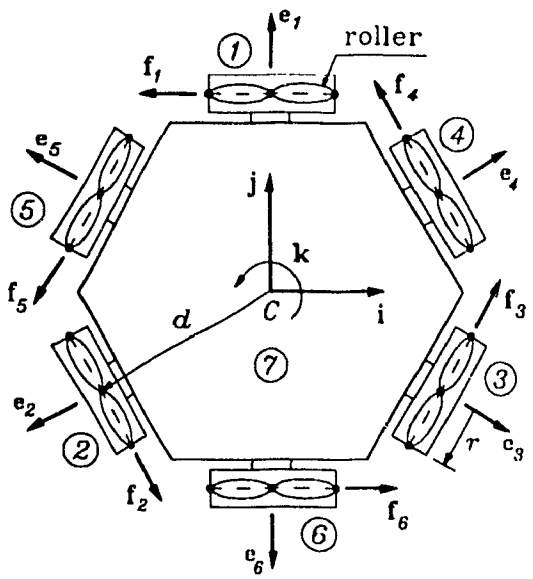

Fig. 4.19 A 6-wheeled 3-DOF AGV.

considering that the maximum allowable torque at the motor of wheel 4 is 0.01 Nm along the whole trajectory. From Fig. 4.33(a), it might appear that there is also a torque limitation on wheels 1 and 3 during the movement of the straight line segments, P_2P_3 and P_0P_1 of Fig. 4.6, respectively, which is not true. Actually, to move along a straight path parallel to **j** fixed to the vehicle, the magnitudes of the joint variables at the two front or rear wheels, 1 and 2, and 3 and 4, respectively, should be the same. On the other hand, to move along a straight path parallel to **i** fixed to the vehicle, the magnitudes of the joint variables at the two side wheels, 1 and 4, and 2 and 3, should be the same. Thus, when the vehicle first moves along the straight path, i.e., segment P_0P_1 of Fig. 4.6, the joint torque at wheel 3 is the same as that at wheel 4. Similarly, when the vehicle moves along segment P_2P_3 of Fig. 4.6, where the orientation of the **i-j-k** frame fixed to the platform is at 90° with the inertial frame, i.e., the vehicle moves along a path parallel to **i**, then the magnitudes of the torques at wheels 1 and 4 are equal. However, during the movement along segment P_1P_2, there is a torque limit only on wheel 4, whereas the variations of the other joint torques are such that these compensate for the limit on wheel 4. Note that the AGVs under study have 3-DOF. Thus, the required torques at motors of the vehicle with three actuated wheels are unique and no torque restriction is possible

Wheel, i	α_i (deg)	β_i (deg)	δ_i (deg)	d_i (m)
1	90.0	90.0	90.0	0.3
2	90.0	210.0	210.0	0.3
3	90.0	330.0	330.0	0.3
4	90.0	30.0	30.0	0.3
5	90.0	150.0	150.0	0.3
6	90.0	270.0	270.0	0.3

The radius of the wheel hubs, $r = 0.1$ m and
the radius of the rollers, $r_r = 0.01$ m.

Table 4.3 Architecture of a 6-wheeled 3-DOF AGV.

On the other hand, if more than three wheels are actuated then any arbitrary limits can be placed on the rest of the motors. In fact, specifying zero limits on the rest of the wheels, which is equivalent to a vehicle consisting of more than three actuated wheels, leads to a solution. For more than three actuated wheels, limits on the number of motors can be specified as long as the compensations by the other motors are possible. Otherwise, OMNI returns an error message that says, "There is no solution."

4.6.4 A Six-Wheeled AGV

The 6-wheeled vehicle shown in Fig. 4.19 is considered using the geometrical parameters given in Table 4.3. The system at hand consists of seven rigid bodies. The inertial parameters for each wheel and the platform are the same as in the case of the 3-wheeled vehicle.

4.6.4.1 Three Wheels are Actuated

Wheels 1, 2 and 3 are assumed to be actuated. Thus, the kinematic structure of the 6-wheeled AGV is the same as that of the 3-wheeled AGV of Fig. 4.17, and hence, the kinematics results are the same. The required torques to traverse the path of two lines connected by a curve are shown in Fig. 4.32(a). It is evident from Fig. 4.32(a) that, due to the three additional wheels, the required joint torques at the three actuated wheels of the 6-wheeled AGV are higher than those of the 3-wheeled

vehicle, as shown in Fig. 4.24(d).

4.6.4.2 Four Wheels are Actuated

Here, wheels 2, 3, 4 and 5, as in Fig. 4.19, are actuated. In order to use the OMNI software, the geometrical and inertial parameters of these four wheels should be given in a sequential order at the beginning of the data files. Results from inverse dynamics are obtained by torque optimization. The required joint torques at the actuated wheels to traverse Path 3 are given in Fig. 4.32(b). The required joint torques to move along Path 3 are also obtained by specifying a limit of 0.01 Nm on the maximum allowable torque of wheel 2 of the vehicle, which is shown in Fig. 4.33(b).

4.6.4.3 All Six Wheels are Actuated

The required actuated joint torques are shown in Figs. 4.32(c) (d), while the 6-wheeled vehicle traverses a path consisting of two straight lines connected by a smooth curve. Since the torque minimization scheme is used to find the six actuator torques of the vehicle, the maximum torques at wheels 1, 2 and 3, as shown in Fig. 4.32(c), are less than the maximum required torques at wheels 1, 2 and 3 of the 3-wheeled vehicle, as shown in Fig. 4.24(d). The results are also obtained by placing limits on the maximum allowable motor torques of wheels 2 and 6, which are 0.01 Nm and 0.025 Nm, respectively. The results are shown in Fig. 4.34.

4.7 Simulation Results for Three-DOF AGVs Using the OMNI Software

Simulations for 3-DOF AGVs were done by considering different vehicles moving in Paths 1, 2 and 3. In all the cases, the simulation errors are very small and the simulated path cannot be distinguished from the planned one when the step size and tolerance are taken as 0.3 s and 0.001, respectively. One set of simulation results

for the 6-wheeled vehicle with all actuated wheels is shown in Fig. 4.35, where the history of input torques is obtained from the inverse dynamics results of the AGV in the presence of inequality constraints, as given in Figs. 4.34(a)-(b).

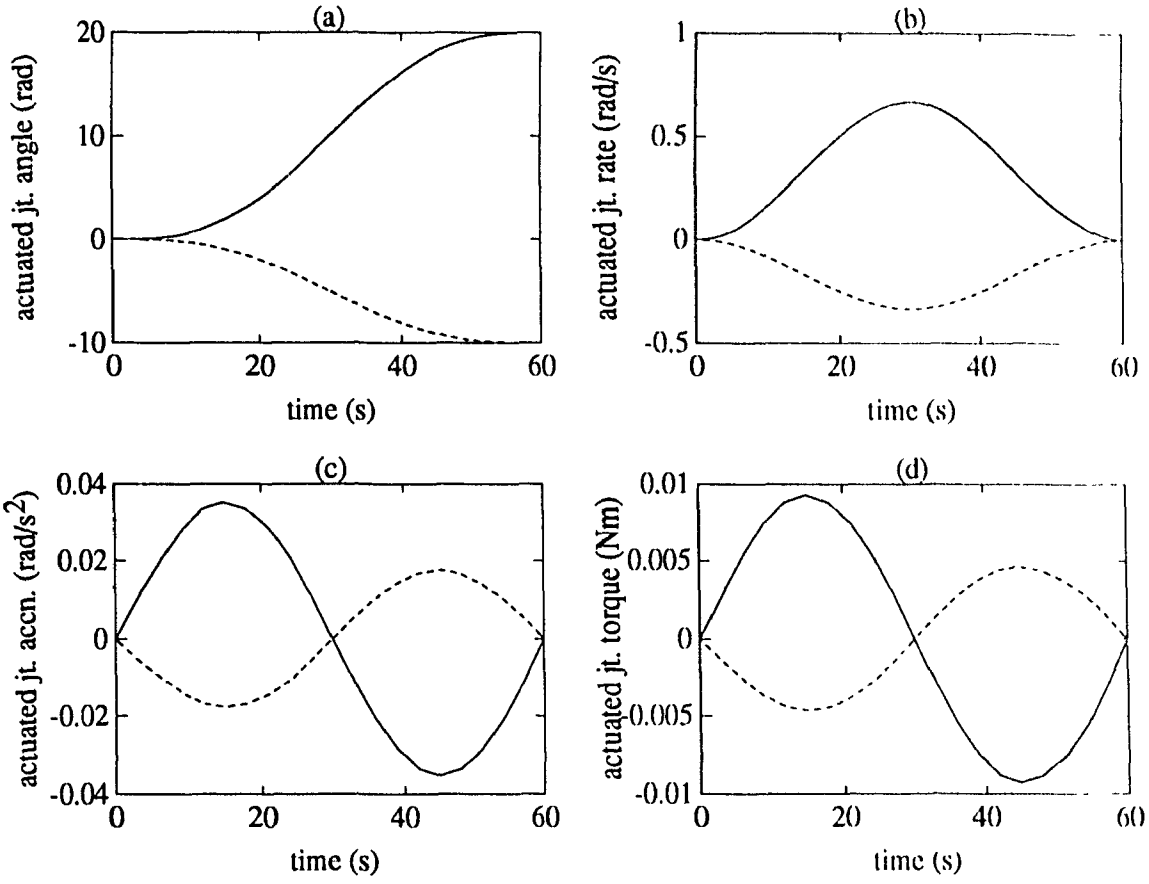

wheels — 1, - - 2 and 3.

Fig. 4.20 Required actuated joint (a) angles, (b) rates, (c) accelerations and (d) torques for the 3-wheeled AGV to traverse a straight path parallel to vector **i** fixed to the vehicle (Path 1).

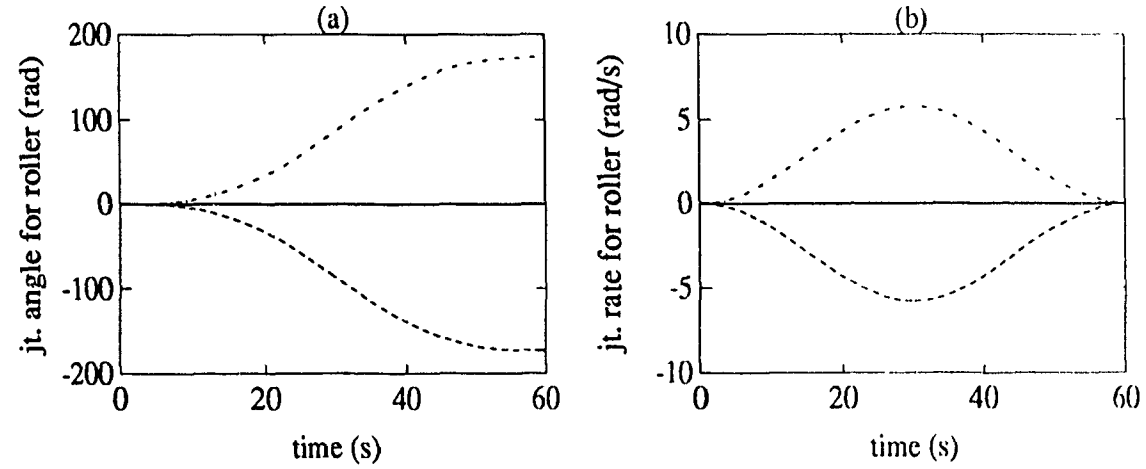

active rollers of wheels - · 1, - - 2, - · - 3.

Fig. 4.21 Required joint (a) angles and (b) rates for the active rollers of the 3-wheeled AGV to traverse a straight path parallel to vector **i** fixed to the vehicle (Path 1).

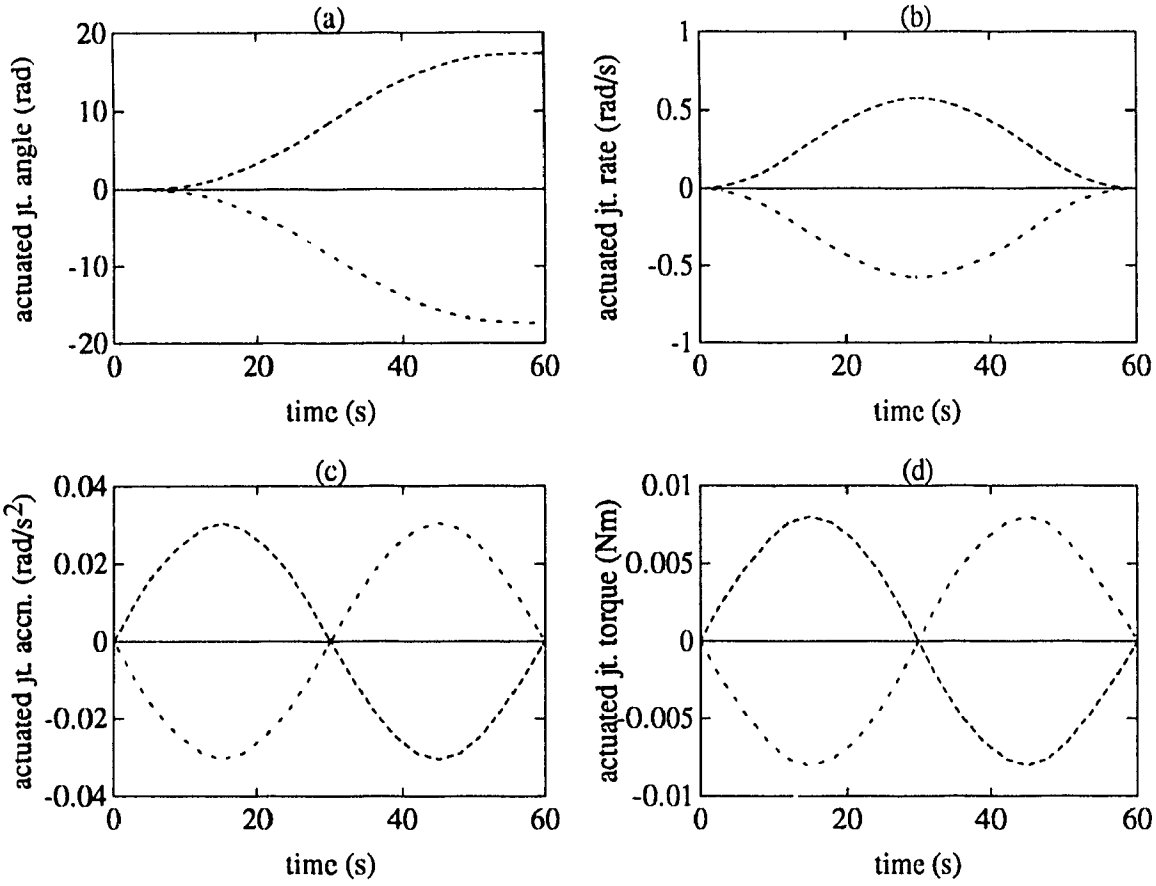

wheels — 1, - - 2, - · - 3.

Fig. 4.22 Required actuated joint (a) angles, (b) rates, (c) accelerations and (d) torques for the 3-wheeled AGV to traverse a path parallel to vector **j** fixed to the vehicle (Path 2).

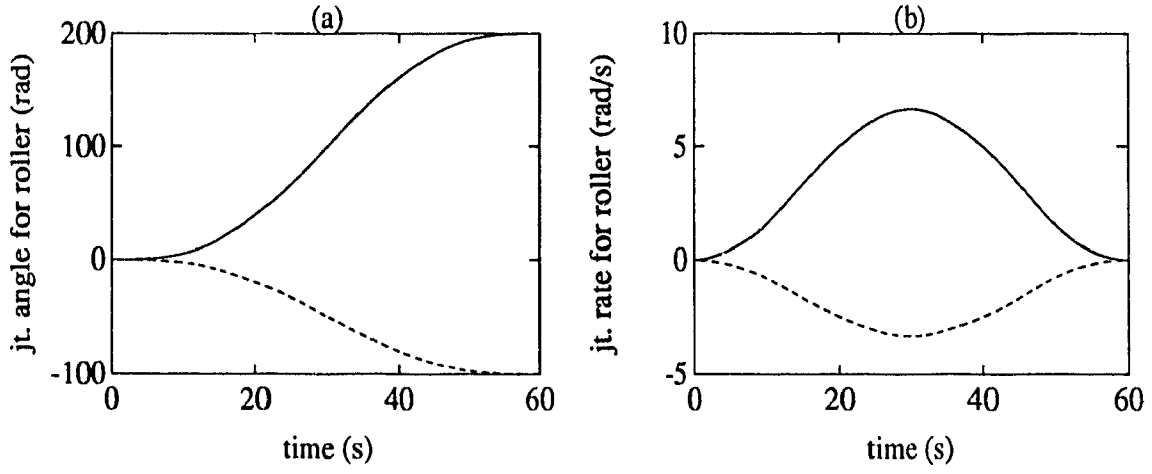

active rollers of wheels — 1, - - 2 and 3.

Fig. 4.23 Required joint (a) angles and (b) rates for the active rollers of the 3-wheeled AGV to traverse a path parallel to vector **j** fixed to the vehicle (Path 2).

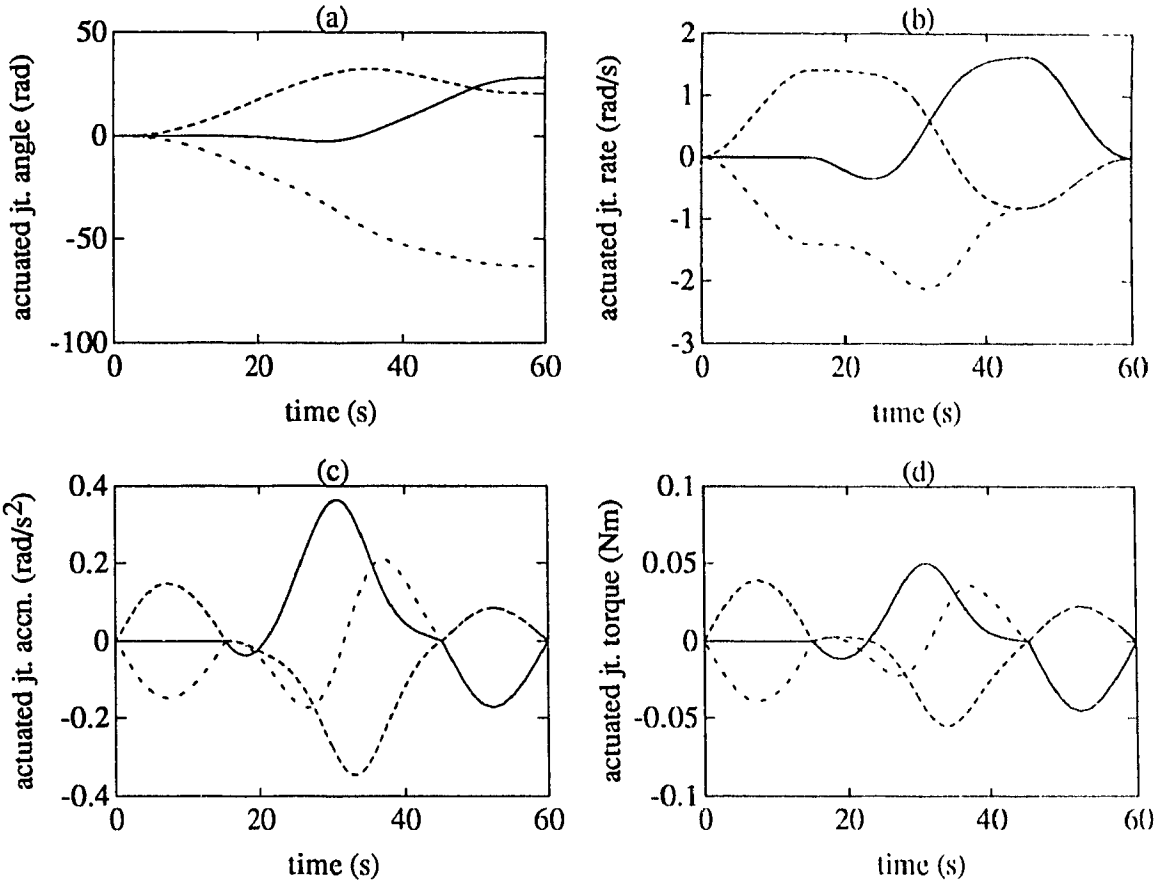

wheels — 1, - - 2, - · - 3.

Fig. 4.24 Required actuated joint (a) angles, (b) rates, (c) accelerations and (d) torques for the 3-wheeled AGV to traverse a path consisting of two straight lines connected by a smooth curve (Path 3).

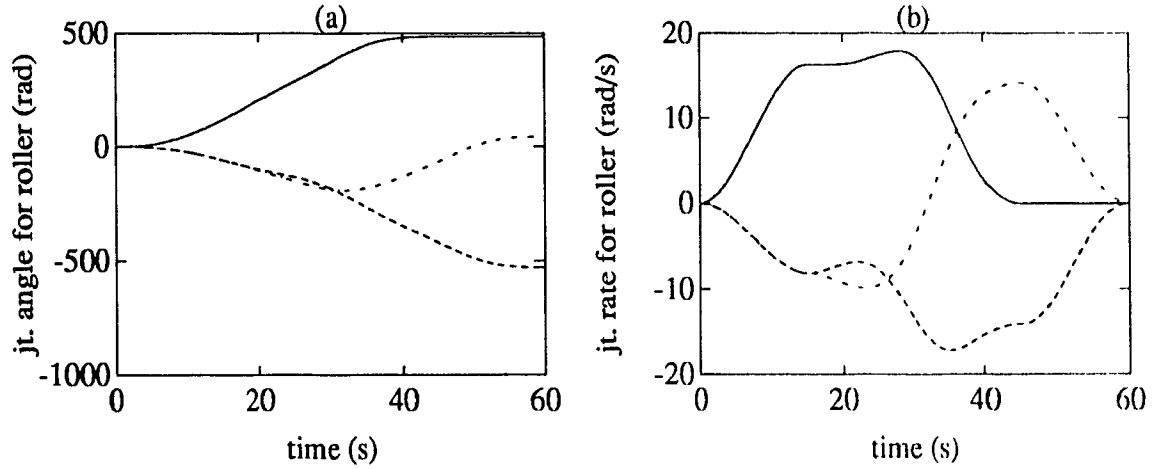

active rollers of wheels - 1, - - 2, - · - 3.

Fig. 4.25 Required joint (a) angles and (b) rates for the active rollers of the 3-wheeled AGV to traverse a path consisting of two straight lines connected by a smooth curve (Path 3).

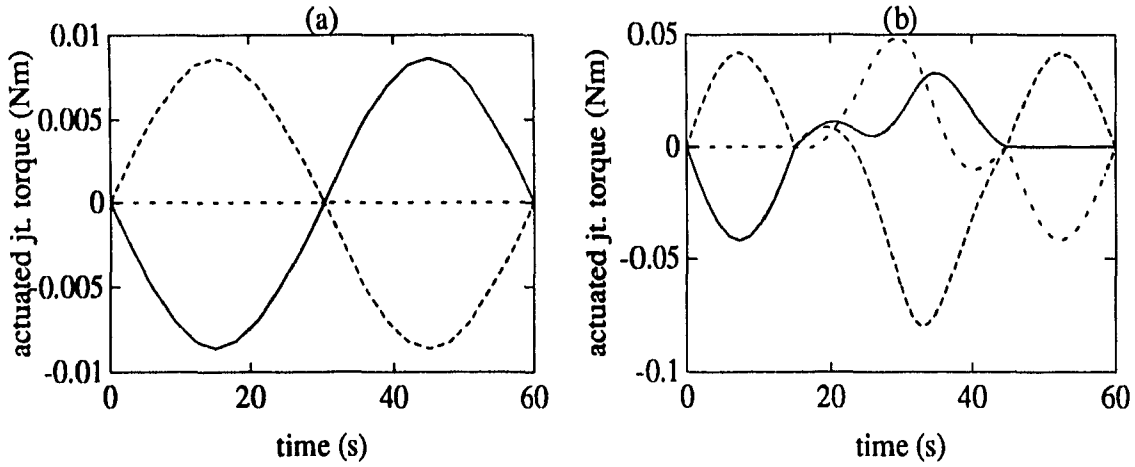

wheels — 1, - - 2, · · · 3.

Fig. 4.26 Required joint torques at the three actuated joints of the 4-wheeled AGV to traverse (a) a path parallel to vector **j** fixed to the vehicle (Path 1) and (b) a path consisting of two straight lines connected by a smooth curve (Path 3).

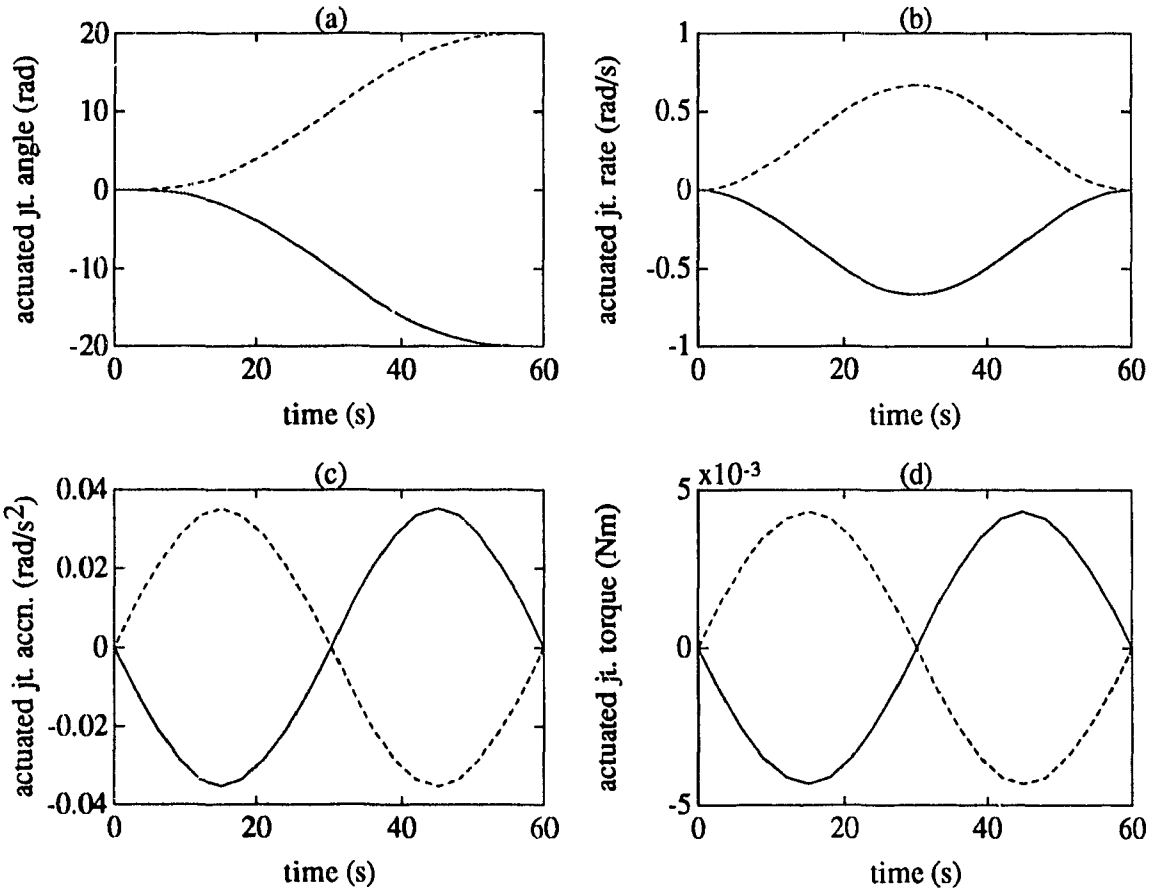

wheels — 1 and 4, - - 2 and 3.
joint angles and rates for active rollers are zero.

Fig. 4.27 Required actuated joint (a) angles, (b) rates, (c) accelerations and (d) torques of all the actuated wheels of the 4-wheeled AGV to traverse a straight path parallel to vector **j** fixed to the vehicle (Path 1).

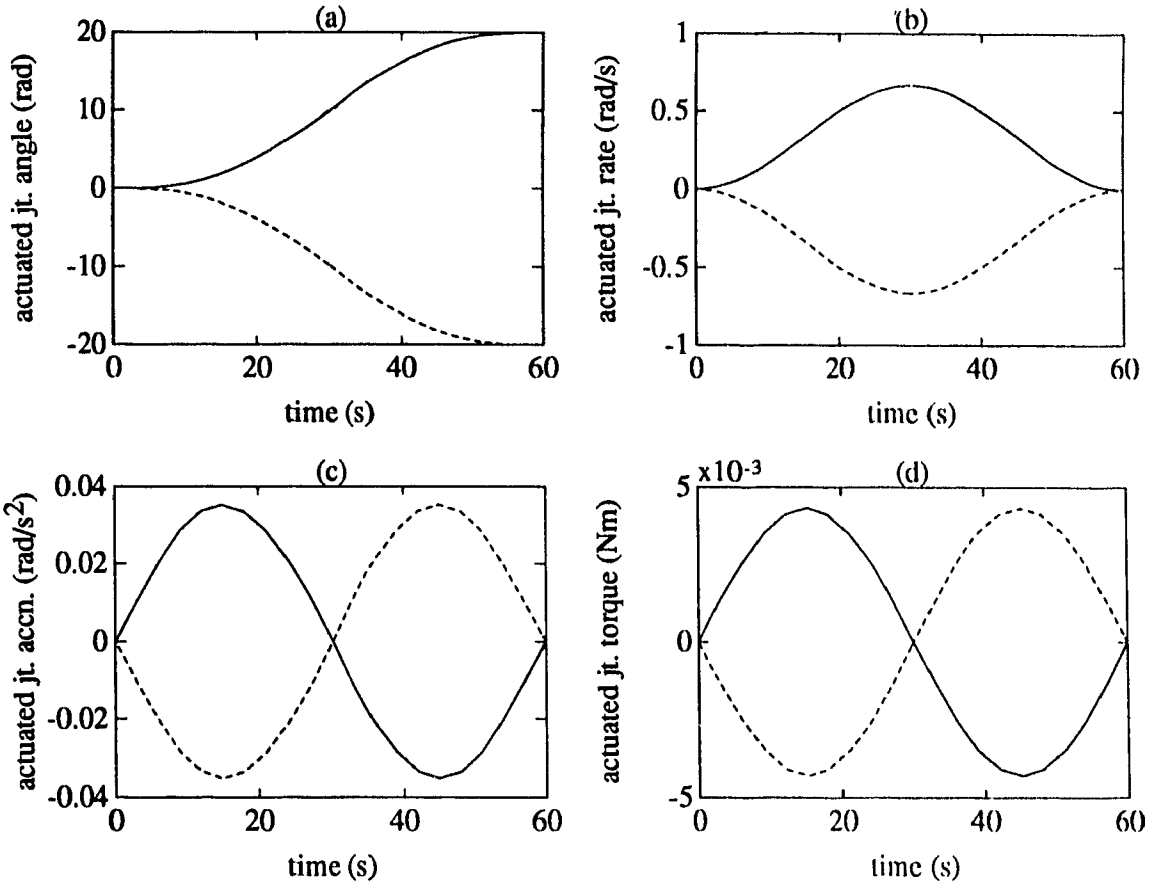

wheels — 1 and 2, - - 3 and 4.

Fig. 4.28 Required actuated joint (a) angles, (b) rates, (c) accelerations and (d) torques for the 4-wheeled AGV to traverse a path parallel to vector **i** fixed to the vehicle (Path 2).

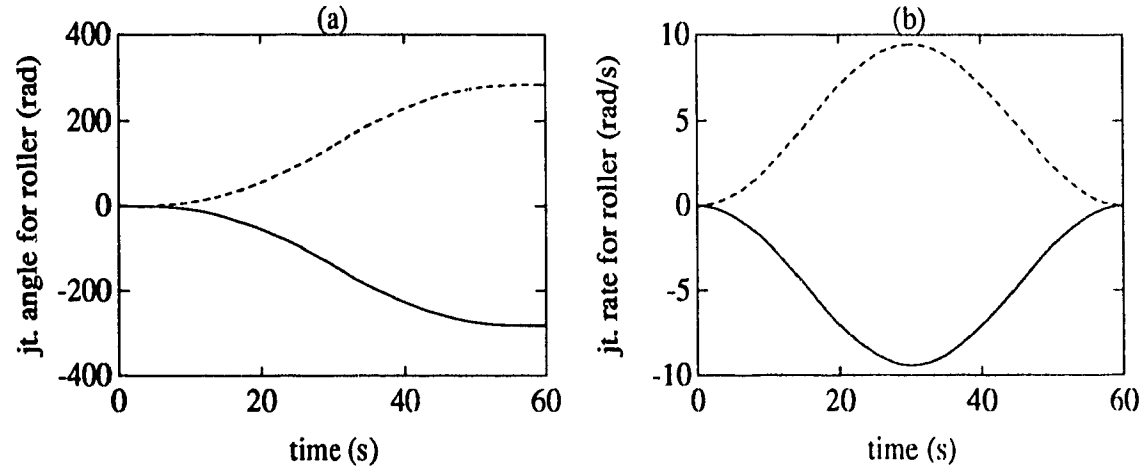

active rollers of wheels — 1 and 4, - - 2 and 3.

Fig. 4.29 Required joint (a) angles and (b) rates for the active rollers of the 4-wheeled AGV to traverse a path parallel to vector **i** fixed to the vehicle (Path 2).

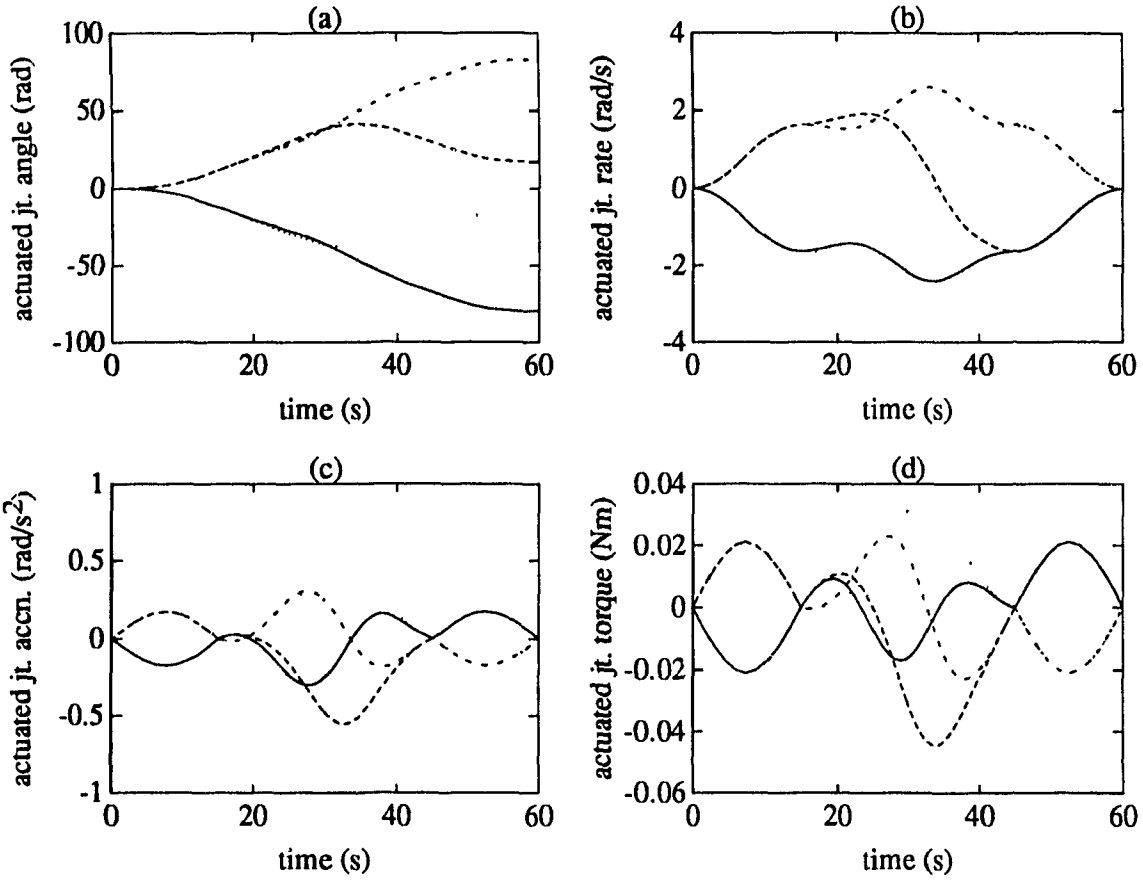

wheels — 1, - - 2, - · - 3, ··· 4.

Fig. 4.30 Required actuated joint (a) angles, (b) rates, (c) accelerations and (d) torques for the 4-wheeled AGV to traverse a path consisting of two straight lines connected by a smooth curve (Path 3).

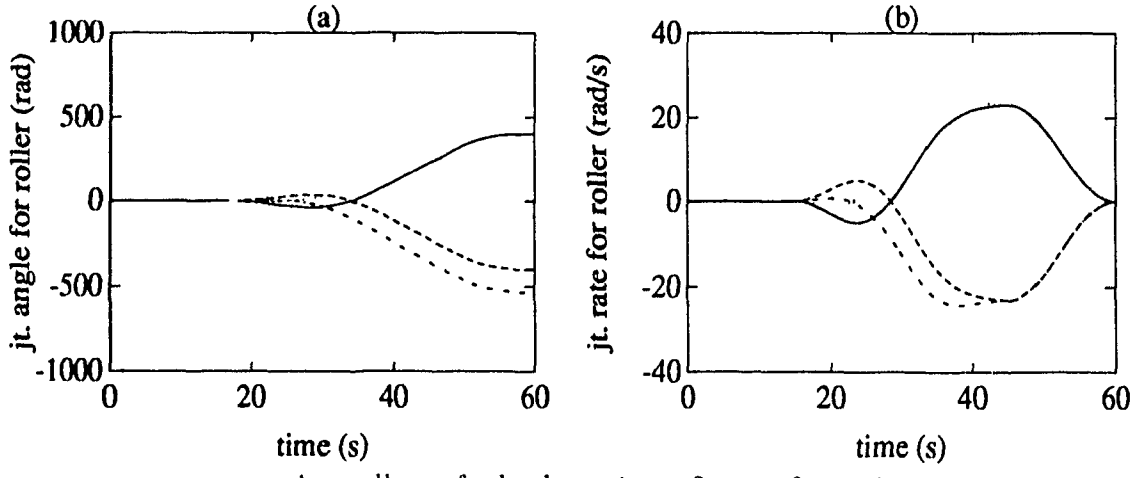

active rollers of wheels — 1, - - 2, - · - 3, ··· 4.

Fig. 4.31 Required joint (a) angles and (b) rates for the active rollers of the 4-wheeled AGV to traverse Path 3.

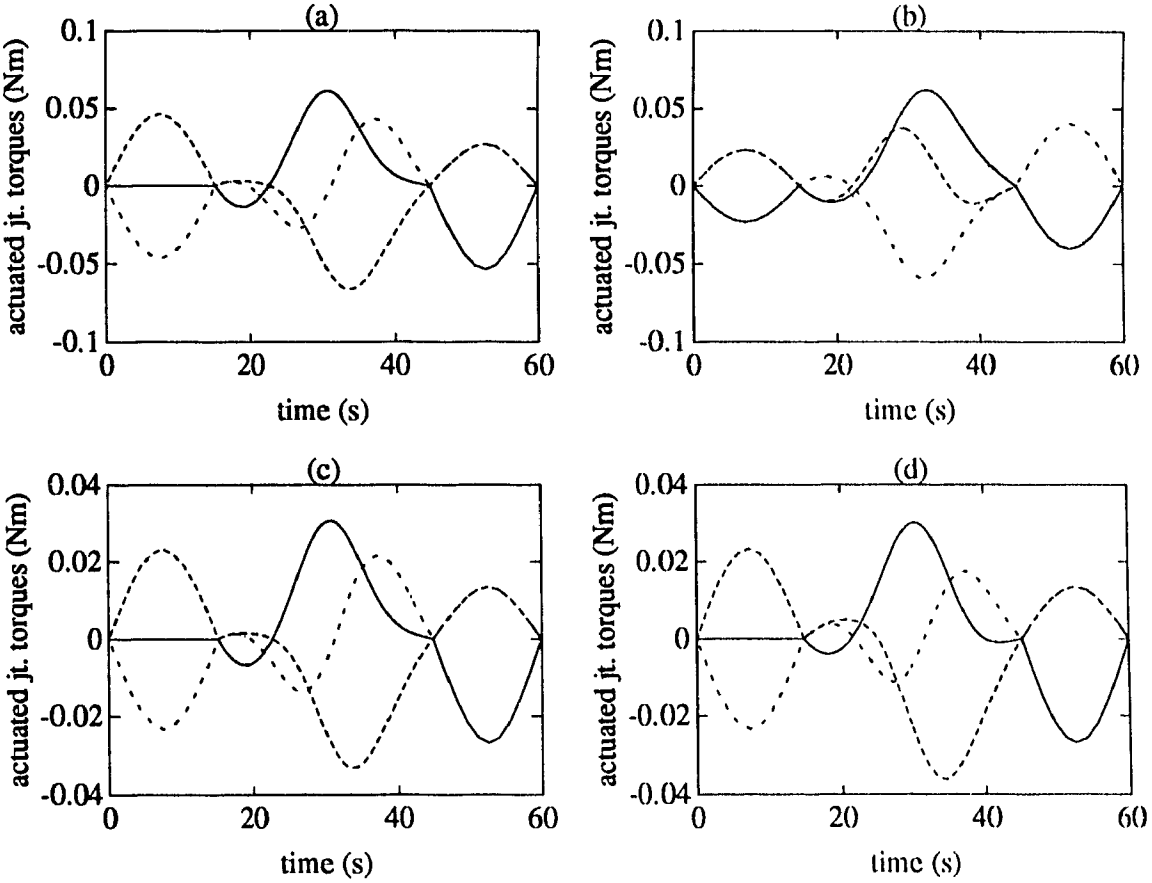

wheels (a)–(c) — 1, - - 2, - · - 3, · · · 4;
(d) — 4, - - 5, - · - 6.

Fig. 4.32 Required joint torques at the (a) three, (b) four and (c) & (d) six actuated joints of the 6-wheeled AGV while moving in a path consisting of two straight lines connected by a smooth curve (Path 3).

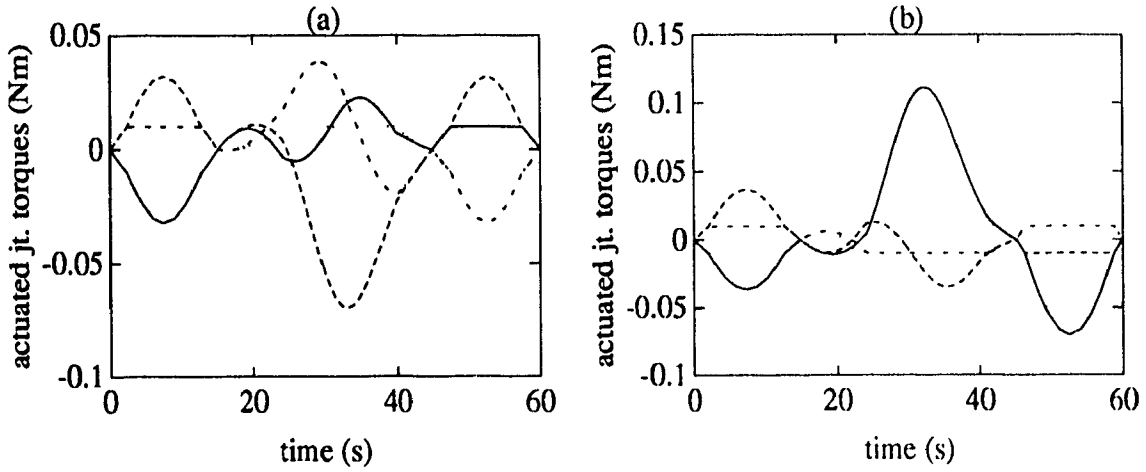

wheels (a) — 1, - - 2, - · - 3, · · · 4;
(b) - · - 2, · · · 3, — 4, - - 5.

Fig. 4.33 Required joint torques at the four actuated joints of the (a) 4-wheeled and (b) 6-wheeled vehicle with torque restrictions while moving in Path 3.

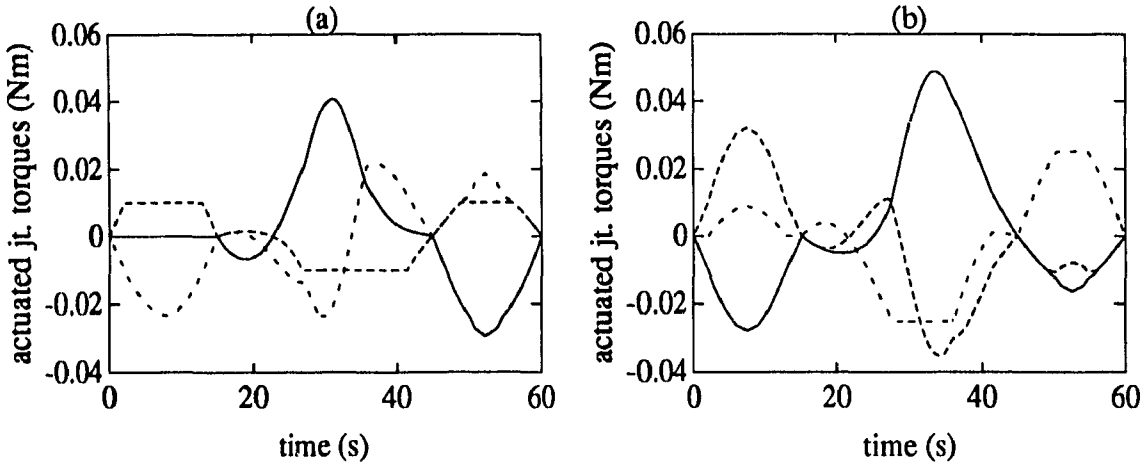

wheels (a) — 1, - - 2, - · - 3; (b) — 4, - - 5, - · - 6.

Fig. 4.34 Required joint torques at the six actuated joints of the 6-wheeled vehicle with torque restrictions while moving in Path 3.

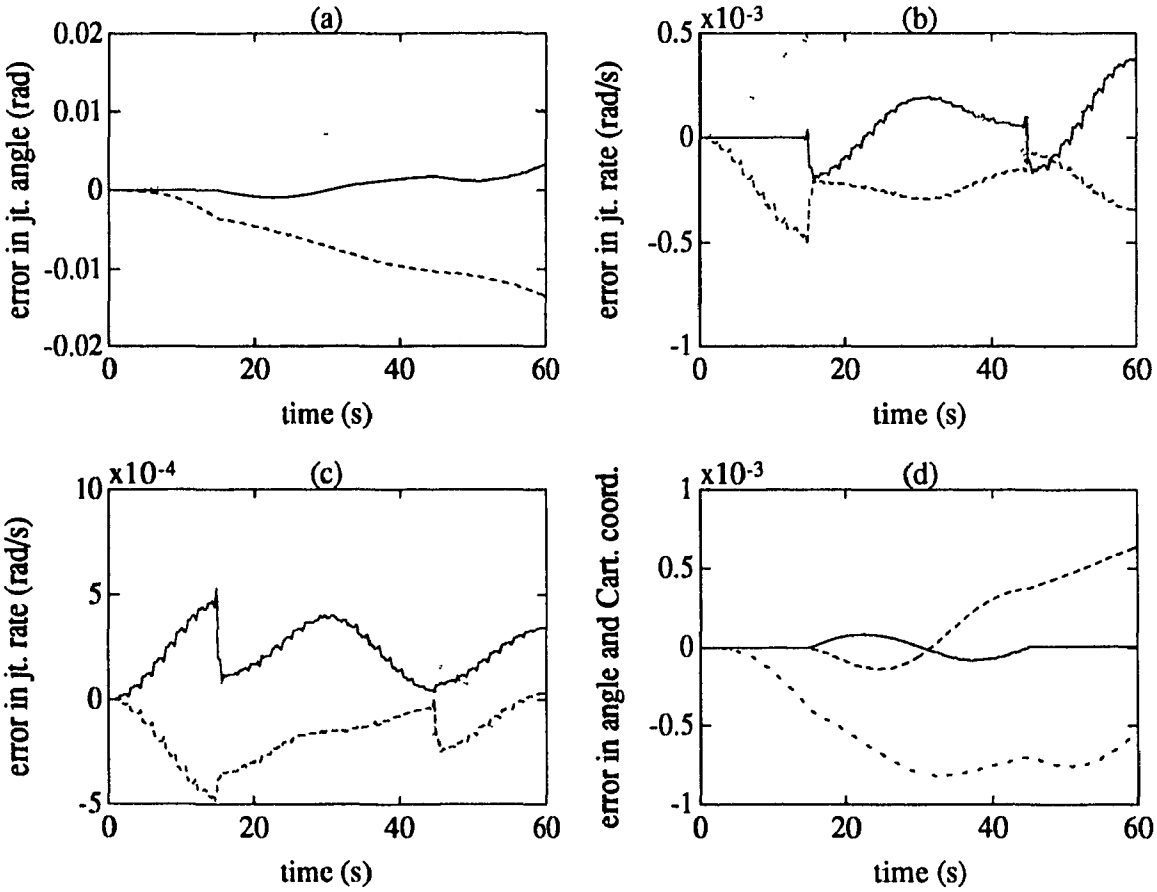

wheels (a) & (b) — 1, - - 2, - · - 3; (c) — 4, - - 5, - · - 6;
(d) error in — ψ (rad), - - x_c (m), - · - y_c (m).

Fig. 4.35 Simulation errors in (a) joint angles of the first three actuated wheels, (b) & (c) actuated joint rates of all the six wheels and (d) Cartesian space while the 6-wheeled AGV is moving in a path consisting of two straight lines connected by a smooth curve (Path 3).

Chapter 5

Kinematic Design of Three-DOF AGVs

Several issues regarding the design of omnidirectional wheels for 3-DOF AGVs warrant a deep study. The orientations of the wheel hubs relative to the platform, the roller orientation with respect to the wheel hub, the number of rollers in a wheel and the roller profiles, are only a few issues that are worth mentioning. Moreover, for autonomous behaviour of the vehicles, it is necessary to have an efficient control algorithm for on-line computations of the joint parameters. The effect of kinematics on the performance of the vehicles is studied in the section below, and then, a design is suggested based on the transformation matrices relating the joint angles with the twist of the platform.

5.1 Effects of Kinematics on the Performance of AGVs

The accuracy of the inverse and direct kinematics results of robotic mechanical systems depends on the condition number of the associated matrices, whose inverses are required in calculating the controller setpoints. For instance, if an AGV is assigned to move in a desired trajectory, its joint variables and their time derivatives are calculated from inverse kinematics. These variables are later used to obtain the

joint torques. The latter are set by the controller to move the vehicle along the specified path. The condition number of a matrix is a measure of the relative roundoff error amplification of the computed results with respect to the relative roundoff error of the input data, upon solving a system of equations associated with that matrix (Golub and Van Loan, 1983). Hence, the accuracy of the kinematics results depends on the condition number of the matrices whose inverses are needed. Matrices with small condition numbers produce accurate results. In fact, a condition number equal to unity, which does not introduce any roundoff error amplification in the solution, is the best that can be achieved. Thus, robustness of the kinematic control is ensured. Matrices with a condition number of unity are called isotropic.

5.2 Design Criteria

Referring to eq.(4.62), the inversion of matrix $\mathbf{\Theta}_i$ is required in determining the actuated as well as the unactuated joint rates, as in eq.(4.68). However, the matrix is singular at $\alpha_i = j\pi$, with j being an integer, i.e., an omnidirectional wheel is equivalent to a conventional wheel when $\alpha_i = 0, \pi, 2\pi, \cdots$ for $j = 0, 1, 2, \cdots$, respectively. Moreover, in direct kinematics, where the twist of the platform is calculated from the actuated joint rates, the solution for $\mathbf{t}'_C$, as in eq.(4.77), is required, which is given by eqs.(4.79) or (4.80), i.e., the evaluation of $\mathbf{L}_A^{-1}$ or $\mathbf{L}_A^I$ is needed. It is clear from eq.(4.77), where $\mathbf{L}_A$ is obtained using eq.(4.73), that if $\gamma_i - \delta_i = j\pi$, or $\gamma_i = j\pi$ or $(2j+1)\pi/2$, for $i = 1, \cdots, \mu$, with j and μ being an integer and the number of actuated wheels, respectively, then $\mathbf{L}_A$ is rank deficient. Since $\gamma_i \equiv \alpha_i + \beta_i$ and δ_i are not configuration-dependent, but rather architecture-dependent, rank deficiency of $\mathbf{L}_A$ results in a singular design of the vehicle.

5.3 Condition Number and Isotropic Design

Let $\mathbf{K}$ denote a $k \times k$ matrix. The condition number of $\mathbf{K}$ (Stewart, 1973; Golub and Van Loan, 1983), $\kappa(\mathbf{K})$, is defined as

$$\kappa(\mathbf{K}) \equiv ||\mathbf{K}||||\mathbf{K}^{-1}|| \tag{5.1}$$

where $||\cdot||$ denotes the norm of its matrix argument $(\cdot)$. If the Euclidean norm is adopted, which is invariant under isometric transformations, and hence under reflections or rotations of the k-dimensional configuration space at hand, then a frame-invariant condition number is derived. The definition of the condition number given in eq.(5.1) can be used with *any* matrix norm. For the Euclidean or Frobenius norm, the norm of matrix $\mathbf{K}$ is defined by

$$||\mathbf{K}|| \equiv \sqrt{\mathrm{tr}(\mathbf{K}^T\mathbf{N}\mathbf{K})} \tag{5.2}$$

in which $\mathbf{N}$ is a positive-definite $k \times k$ matrix that serves for normalization purposes. For instance, if $\mathbf{N}$ is defined as $(1/k)\mathbf{1}$, with $\mathbf{1}$ being the $k \times k$ identity matrix, then the Euclidean norm of the identity matrix turns out to be unity. Clearly, the definition of $\mathbf{N}$ does not affect the resulting condition number. Moreover, from the definition of the norm of a matrix, as given in eq.(5.2), the best conditioned matrices are those that are multiples of an orthogonal matrix. Thus, matrix $\mathbf{K}$ has a minimum condition number when the following holds:

$$\mathbf{K}^T\mathbf{K} = \sigma^2\mathbf{1} \tag{5.3}$$

where σ is a scalar. Note that, since the inverse of a rectangular matrix is not defined the condition number of a $\mu \times k$ $(\mu > k)$ matrix $\mathbf{K}$ cannot be given by eq.(5.1). Other definitions of the condition number, also applicable to rectangular matrices, for instance, the ratio between the maximum and minimum singular values of a matrix can be used. Moreover, in the presence of linearly independent columns, the square of the condition number of the $\mu \times k$ matrix $\mathbf{K}$ is equal to the condition number of $\mathbf{K}^T\mathbf{K}$ (Stewart, 1973). Thus, the condition number of the $\mu \times k$ matrix $\mathbf{K}$ is unity

if eq.(5.3) holds. Matrix $\mathbf{K}$ that satisfies eq.(5.3) is termed *isotropic*. Furthermore, from eq.(5.3), the inverse of a square $\mathbf{K}$ is simply $(1/\sigma^2)\mathbf{K}^T$. Likewise, the generalized inverse of a rectangular isotropic $\mathbf{K}$ is simply $(1/\sigma^2)\mathbf{K}^T$. Equation (5.3) is the *isotropy condition* for matrix $\mathbf{K}$. This condition will be used presently to attempt isotropic designs of 3-DOF AGVs.

5.4 Non-Existence of Isotropic Design for Inverse Kinematics

To verify the existence of an isotropic design for inverse kinematics, matrix $\mathbf{\Theta}_i$, given in eq.(4.63), is written as

$$\mathbf{\Theta}_i = r \begin{bmatrix} s\beta_i & \rho s\gamma_i \\ -c\beta_i & -\rho c\gamma_i \end{bmatrix} \tag{5.4}$$

where $\gamma_i \equiv \alpha_i + \beta_i$. Angles α_i, β_i and the radius r of the wheel hubs are shown in Fig. 4.14 and the ratio ρ is given by $\rho = r_r/r$. Now, $\mathbf{\Theta}_i^T\mathbf{\Theta}_i$ is evaluated as

$$\mathbf{\Theta}_i^T\mathbf{\Theta}_i = r^2 \begin{bmatrix} 1 & \rho\, c\alpha_i \\ \rho\, c\alpha_i & \rho^2 \end{bmatrix} \tag{5.5}$$

which is a symmetric and positive-definite 2×2 matrix. To derive eq.(5.5), γ_i is replaced by $\alpha_i + \beta_i$, which has been used in eqs.(4.61a) and (4.61b). It is clear from eq.(5.5) that for $\mathbf{\Theta}_i$ to be isotropic, the diagonal entries of matrix $\mathbf{\Theta}_i^T\mathbf{\Theta}_i$ must be identical, whereas the off-diagonal element must be zero. The off-diagonal element of $\mathbf{\Theta}_i^T\mathbf{\Theta}_i$ is zero when $\alpha_i = (2j+1)\pi/2$ for $j = 0, 1, 2, \cdots$ etc. The diagonal entries are identical if the ratio $1/\rho^2$ is equal to unity. Since a value of $\rho = 1$ implies that the radius of the wheel hubs is equal to the radius of the rollers, this is not practically feasible. Thus, an isotropic design for inverse kinematics is ruled out.

5.5 Isotropic Design for Direct Kinematics

Since for 3-DOF AGVs with μ actuated wheels, the $\mu \times 3$ matrix $\mathbf{L}_A$ of eq.(4.77) is not dimensionally homogeneous, different algebraic manipulations with the elements of the matrix may lead to meaningless operations. For example, in order to

find $\mathbf{L}_A\mathbf{L}_A^T$, the first element of the first column of the matrix product is obtained from the inner product of vector $\mathbf{l}_1$, defined as the first row of matrix $\mathbf{L}_A$, by itself, i.e., $\mathbf{l}_1^T\mathbf{l}_1$. Vector $\mathbf{l}_1$ can be written from eq.(4.73) as

$$\mathbf{l}_1 \equiv \eta_1[d_1 \;\; s\xi_1, \;\; c\gamma_1, \;\; s\gamma_1]^T \tag{5.6}$$

where ξ_1 has been substituted for $\gamma_1 - \delta_1$. The first component of $\mathbf{l}_1$ is dimensionless, whereas the other two components both have units of m^{-1}. Now, the inner product of $\mathbf{l}_1$ by itself leads to the addition of numbers of different dimensions. Moreover, matrix $\mathbf{L}_A^T\mathbf{L}_A$ contains entries of different dimensions and the use of its elements as the components of an objective function that can be minimized for the minimum condition number of matrix $\mathbf{L}_A$, as suggested at the end of this chapter, leads to algebraic operations between dimensionally nonhomogeneous parameters. Thus, a previous normalization of matrix $\mathbf{L}_A$ is needed. To this end, the first column of this matrix is divided by a characteristic length L, which can be achieved with a suitably defined matrix $\mathbf{N}$, as indicated in eq.(5.2). The normalization matrix can be given as

$$\mathbf{N} = \begin{bmatrix} 1/L^2 & 0 & 0 \\ 0 & 1 & 0 \\ 0 & 0 & 1 \end{bmatrix}$$

The $\mu \times 3$ matrix $\mathbf{L}_A$ is obtained after normalization as

$$\mathbf{L}_A = \begin{bmatrix} \epsilon_1 \; s\xi_1 & \eta_1 \; c\gamma_1 & \eta_1 \; s\gamma_1 \\ \vdots & \vdots & \vdots \\ \epsilon_\mu \; s\xi_\mu & \eta_\mu \; c\gamma_\mu & \eta_\mu \; s\gamma_\mu \end{bmatrix} \tag{5.7}$$

where $\epsilon_i = \eta_i\zeta_i$, $\eta_i = -1/(r \;\; s\alpha_i)$ and $\zeta_i = d_i/L$ for $i = 1, \cdots, \mu$. The left-hand side of eq.(5.3) for matrix $\mathbf{L}_A$ is now derived as the 3×3 symmetric and positive-definite matrix, namely,

$$\mathbf{R} \equiv \mathbf{L}_A^T\mathbf{L}_A = \begin{bmatrix} R_1 & R_2 & R_3 \\ R_2 & R_4 & R_5 \\ R_3 & R_5 & R_6 \end{bmatrix} \tag{5.8}$$

where

$$R_1 \equiv \epsilon_1^2 \; s^2\xi_1 + \cdots + \epsilon_\mu^2 \; s^2\xi_\mu \tag{5.9a}$$

$$R_2 \equiv \epsilon_1\eta_1 \; s\xi_1 c\gamma_1 + \cdots + \epsilon_\mu\eta_\mu \; s\xi_\mu c\gamma_\mu \tag{5.9b}$$

$$R_3 \equiv \epsilon_1\eta_1\ s\xi_1 s\gamma_1 + \cdots + \epsilon_\mu\eta_\mu\ s\xi_\mu s\gamma_\mu \tag{5.9c}$$

$$R_4 \equiv \eta_1^2\ c^2\gamma_1 + \cdots + \eta_\mu^2\ c^2\gamma_\mu \tag{5.9d}$$

$$R_5 \equiv \frac{1}{2}[\eta_1^2\ s2\gamma_1 + \cdots + \eta_\mu^2\ s2\gamma_\mu] \tag{5.9e}$$

$$R_6 \equiv \eta_1^2\ s^2\gamma_1 + \cdots + \eta_\mu^2\ s^2\gamma_\mu \tag{5.9f}$$

Now, from eq.(5.3), an isotropic design for direct kinematics of the AGVs is achieved if the conditions below are satisfied:

$$R_1 = \sigma^2,\quad R_2 = 0,\quad R_3 = 0,\quad R_4 = \sigma^2,\quad R_5 = 0,\quad R_6 = \sigma^2 \tag{5.10}$$

Using the isotropy conditions given in eq.(5.10), 3-, 4- and 6-wheeled 3-DOF AGVs are designed where all the wheels of the vehicles are actuated.

5.5.1 A Three-Wheeled AGV

A plausible assumption is made here, namely, that the design has the following symmetries, i.e.,

$$\alpha_i = \alpha \quad \text{and} \quad d_i = d, \quad \text{for} \quad i = 1,2,3 \tag{5.11}$$

Further assumptions are made by considering that the three axes of the hubs, $\mathbf{e}_i$ for $i = 1,2,3$, are symmetrically distributed, i.e.,

$$\beta_1 = \beta,\quad \beta_2 = \frac{2\pi}{3} + \beta \quad \text{and} \quad \beta_3 = \frac{4\pi}{3} + \beta$$

Also, the positions of the mass centres of the wheels are placed at the vertices of an equilateral triangle that inscribes a circle of radius d. With the above assumptions, six entries of $\mathbf{R}$, as in eqs.(5.9a)-(5.9f), are calculated as

$$R_1 = 3\epsilon^2\ s^2\xi \tag{5.12a}$$

$$R_2 = \epsilon\eta[s\xi c\gamma + s\xi c(\frac{2\pi}{3} + \gamma) + s\xi c(\frac{4\pi}{3} + \gamma)] \tag{5.12b}$$

$$R_3 = \epsilon\eta[s\xi s\gamma + s\xi s(\frac{2\pi}{3} + \gamma) + s\xi s(\frac{4\pi}{3} + \gamma)] \tag{5.12c}$$

$$R_4 = \eta^2[c^2\gamma + c^2(\frac{2\pi}{3} + \gamma) + c^2(\frac{4\pi}{3} + \gamma)] \tag{5.12d}$$

$$R_5 = \frac{1}{2}\eta^2[s2\gamma + s2(\frac{2\pi}{3} + \gamma) + s2(\frac{4\pi}{3} + \gamma)] \tag{5.12e}$$

$$R_6 = \eta^2[s^2\gamma + s^2(\frac{2\pi}{3} + \gamma) + s^2(\frac{4\pi}{3} + \gamma)] \tag{5.12f}$$

where

$$\epsilon = \eta\zeta,\ \eta = -\frac{1}{r\ s\alpha},\ \zeta = \frac{d}{L} \quad \text{and} \quad \gamma \equiv \alpha + \beta \tag{5.13}$$

From eqs.(5.12a)–(5.12f), R_2, R_3 and R_5 vanish, and R_4 and R_6 are found as $(3/2)\eta^2$. Thus, from eqs.(5.10) and (5.12a),

$$3\epsilon^2\ s^2\xi = \frac{3}{2}\eta^2 = \sigma^2 \tag{5.14}$$

which leads to

$$\sigma^2 = \frac{3}{2}\eta^2 = \frac{1.5}{r^2\ s^2\alpha} \tag{5.15}$$

and

$$s^2\xi = \frac{\sigma^2}{3\epsilon^2} = \frac{1}{2\zeta^2} \tag{5.16}$$

Hence, $c^2\xi$ is derived as

$$c^2\xi = \frac{2\zeta^2 - 1}{2\zeta^2} \tag{5.17}$$

and angle ξ being given by

$$\xi \equiv \alpha + \beta - \delta = \tan^{-1}\frac{1}{\sqrt{2\zeta^2 - 1}} \tag{5.18}$$

Thus, for a real solution ξ,

$$\zeta \geq \frac{1}{\sqrt{2}} \tag{5.19}$$

It is now evident from eq.(5.18) that, if $\beta = \delta$ and $\zeta = 1/\sqrt{2}$, the roller orientation with respect to the wheel hub is found to be $(2j+1)\pi/2$. For $j = 0$, $\alpha = \pi/2$ which has been used in the previous chapter in analysing the 3-wheeled AGV. Moreover, with $d = 0.3$ m and $r = 0.1$ m, as shown in Fig. 4.17, for the 3-wheeled vehicle, the characteristic length L and the value of σ are calculated from eqs.(5.13) and (5.15) as 0.42426 m and 12.25 m^{-1} , respectively.

5.5.2 A Four-Wheeled AGV

For 4-wheeled AGVs with all actuated wheels, the following assumptions are made:

$$\delta_1 = \delta,\ \ \delta_2 = \frac{\pi}{2} + \delta,\ \ \delta_3 = \pi + \delta \quad \text{and} \quad \delta_4 = \frac{3\pi}{2} + \delta \tag{5.20a}$$

$$\beta_1 = \beta,\ \ \beta_2 = \frac{\pi}{2} + \beta,\ \ \beta_3 = \pi + \beta \quad \text{and} \quad \beta_4 = \frac{3\pi}{2} + \beta \tag{5.20b}$$

Using eqs.(5.20a) and (5.20b), R_i for $i = 1, \cdots, 6$ of eq.(5.8) are obtained as

$$R_1 = \epsilon_1^2\ s^2\xi_1 + \epsilon_2^2\ s^2\xi_2 + \epsilon_3^2\ s^2\xi_3 + \epsilon_4^2\ s^2\xi_4 \tag{5.21a}$$

$$R_2 = \epsilon_1\eta_1\ s\xi_1 c\gamma_1 + \epsilon_2\eta_2\ s\xi_2 c\gamma_2 + \epsilon_3\eta_3\ s\xi_3 c\gamma_3 + \epsilon_4\eta_4\ s\xi_4 c\gamma_4 \tag{5.21b}$$

$$R_3 = \epsilon_1\eta_1\ s\xi_1 s\gamma_1 + \epsilon_2\eta_2\ s\xi_2 s\gamma_2 + \epsilon_3\eta_3\ s\xi_3 s\gamma_3 + \epsilon_4\eta_4\ s\xi_4 s\gamma_4 \tag{5.21c}$$

$$R_4 = \eta_1^2\ c^2\gamma_1 + \eta_2^2\ c^2\gamma_2 + \eta_3^2\ c^2\gamma_3 + \eta_4^2\ c^2\gamma_4 \tag{5.21d}$$

$$R_5 = \frac{1}{2}[\eta_1^2\ s2\gamma_1 + \eta_2^2\ s2\gamma_2 + \eta_3^2\ s2\gamma_3 + \eta_4^2\ s2\gamma_4] \tag{5.21e}$$

$$R_6 = \eta_1^2\ s^2\gamma_1 + \eta_2^2\ s^2\gamma_2 + \eta_s^2\ c^2\gamma_3 + \eta_4^2\ s^2\gamma_4 \tag{5.21f}$$

where ϵ_i and η_i for $i = 1, \cdots, 4$ were defined before, as in eq.(5.7), whereas ξ_i and γ_i of eqs.(5.21a)–(5.21f) are, respectively, $\alpha_i + \beta - \delta$ and $\alpha_i + \beta + (k-1)\pi/2$ for $k = 1, \cdots, 4$. Note that, according to the isotropy conditions given in eq.(5.10), $R_2 = R_3 = 0$, thus, from eqs.(5.21b) and (5.21c), R_2 and R_3 are equal when

$$s\gamma_1 = c\gamma_1, \quad s\gamma_2 = c\gamma_2, \quad s\gamma_3 = c\gamma_3, \quad s\gamma_4 = c\gamma_4 \tag{5.22}$$

In order to satisfy the above relations, eq.(5.22), the following must hold:

$$\gamma_1 \equiv \alpha_1 + \beta = (2j_1 + 1)\frac{\pi}{4} \tag{5.23a}$$

$$\gamma_2 \equiv \alpha_2 + \beta + \frac{\pi}{2} = (2j_2 + 1)\frac{\pi}{4} \tag{5.23b}$$

$$\gamma_3 \equiv \alpha_3 + \beta + \pi = (2j_3 + 1)\frac{\pi}{4} \tag{5.23c}$$

$$\gamma_4 \equiv \alpha_4 + \beta + \frac{3\pi}{2} = (2j_4 + 1)\frac{\pi}{4} \tag{5.23d}$$

where j_i for $i = 1, \cdots, 4$ are integers. Now, it can be shown that if all j_i of eqs.(5.23a)–(5.23d) are set to zero then no isotropic design is possible. However, with $j_1 = j_3 = 0$ and $j_2 = j_4 = 1$ an isotropic design can be achieved. To this end, a set of relations is derived from eqs.(5.23a)–(5.23d) using $\alpha_1 = \alpha$ and $\eta_1 = \eta$, namely,

$$\alpha_2 = \alpha, \quad \alpha_3 = \alpha_4 = \alpha - \pi \quad \text{and} \quad \eta_2 = \eta, \quad \eta_3 = \eta_4 = -\eta \tag{5.24}$$

Using eq.(5.24), the expressions for R_i, for $i = 1, \cdots, 6$, are rewritten, from eqs.(5.21a)–(5.21f), as

$$R_1 = 2c^2[s^2\xi + s^2(\xi - \pi)] \tag{5.25a}$$

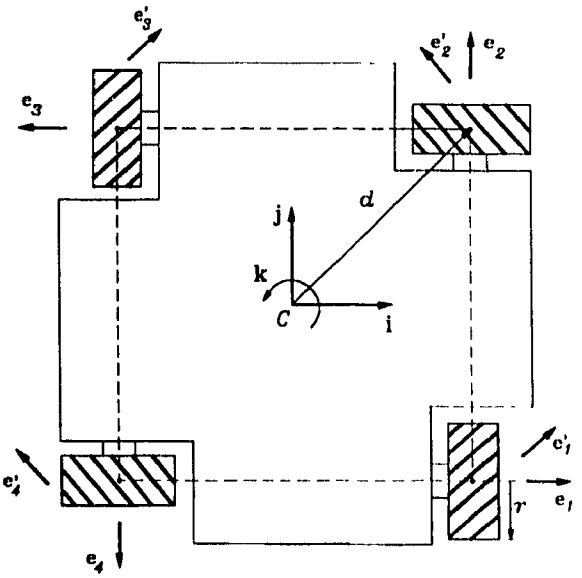

Fig. 5.1 An isotropic 4-wheeled 3-DOF AGV.

$$R_2 = \epsilon\eta[s\xi c\gamma + s\xi c(\gamma + \frac{\pi}{2}) + s(\xi - \pi)c\gamma + s(\xi - \pi)c(\gamma + \frac{\pi}{2})] \quad (5.25b)$$

$$R_2 = \epsilon\eta[s\xi s\gamma + s\xi s(\gamma + \frac{\pi}{2}) + s(\xi - \pi)s\gamma + s(\xi - \pi)s(\gamma + \frac{\pi}{2})] \quad (5.25c)$$

$$R_4 = 2\eta[c^2\gamma + c^2(\gamma + \frac{\pi}{2})] \quad (5.25d)$$

$$R_5 = \eta^2[s2\gamma + s2(\gamma + \frac{\pi}{2})] \quad (5.25e)$$

$$R_6 = 2\eta^2[s^2\gamma + s^2(\gamma + \frac{\pi}{2})] \quad (5.25f)$$

where $\epsilon = \eta\zeta$, $\eta = -1/(r\ s\alpha)$, $\zeta = d/L$ and $\gamma \equiv \alpha + \beta$. Now, from eqs.(5.25a) (5.25f), the off-diagonal entries of $\mathbf{L}_A^T\mathbf{L}_A$ for the 4-wheeled vehicles vanish. Moreover, the diagonal elements are equated with σ^2. Then, a relation similar to eq.(5.15) is obtained as

$$\sigma^2 = \frac{2}{r^2\ s^2\alpha} \quad (5.26)$$

Again, the isotropy conditions, eq.(5.10), of the 4-wheeled AGVs lead to $\zeta \geq 1/\sqrt{2}$ for real solutions of ξ. Angle ξ is given by eq.(5.18). Now, with $\zeta = 1/\sqrt{2}$ and $\beta = 0$, an isotropic vehicle architecture is obtained which is shown in Fig. 5.1, the geometrical parameters being given in Table 5.1. The values for σ and L are calculated as $2/r$ and $\sqrt{2}d$, respectively, with the radius of the wheels r, and d as shown in Fig. 5.1

Wheel, i	α_i (deg)	β_i (deg)	δ_i (deg)	d_i (m)
1	45	0	−45	d
2	45	90	45	d
3	−135	180	135	d
4	−135	270	225	d

Table 5.1 Architecture of an isotropic 4-wheeled 3-DOF AGV.

5.5.3 A Six-Wheeled AGV

In addition to the assumptions of eq.(5.11) the following symmetries are considered:

$$\beta_1 = \beta,\ \ \beta_2 = \frac{2\pi}{3} + \beta,\ \ \beta_3 = \frac{4\pi}{3} + \beta,\ \ \beta_4 = \frac{5\pi}{3} + \beta,\ \ \beta_5 = \frac{\pi}{3} + \beta \text{ and } \beta_6 = \pi + \beta$$

Then, the isotropic design of the 6-wheeled vehicles is done in exactly the same way as for the 3-wheeled AGVs. The design analysis for 6-wheeled AGVs leads to

$$\sigma^2 = \frac{3}{r^2\ s^2\alpha}$$

Angle ξ and the ratio ζ are given by eqs.(5.18) and (5.19), respectively.

In summary, isotropic designs for direct kinematics of 3-, 4- and 6-wheeled AGVs are obtained based on the isotropic conditions which are given in eq.(5.10). For a real solution of angle ξ, the isotropic conditions lead to $\zeta \geq 1/\sqrt{2}$ for all vehicles under study. Moreover, eq.(5.18) provides a relation for the angles associated with the AGVs. Furthermore, when an isotropic design does not exist for 3-DOF AGVs, design variables can be chosen in such a way that the condition number of matrix $\mathbf{L}_A$ is minimum. This may be achieved by minimizing a norm of a vector $\mathbf{f}$ defined by $\mathbf{f} \equiv [R_1 - \sigma^2,\ R_2,\ R_3,\ R_4 - \sigma^2,\ R_5,\ R_6 - \sigma^2]^T$. Finally, once the homogeneous matrix $\mathbf{L}_A$ has been used to obtain the direct kinematics results, the substitutions that were made to normalize the different elements of matrix $\mathbf{L}_A$ may be used in obtaining the actual physical dimensions.

Chapter 6

Motion Animation of Nonholonomic Systems. A Case Study

With the advent of fast processors and, more recently, with the development of powerful graphics hardware and software, the on-line animation of the motion of dynamic systems has become possible. Motion animation can find applications in the design and control of mechanical systems. In design, before a system is actually set in operation, its performance can be assessed on a computer monitor with the help of an animation tool coupled with a simulation program. In control, motion animation allows one to predict the behaviour of an existing system, in real time, before the system is in action, which is important for cases whereby a system is designed to work in a dangerous or inaccessible environment. Therefore, it is essential to have an efficient algorithm that will lead to a realistic animation of the system under study. Moreover, accuracy is another aspect of the animation and simulation, without which an efficient algorithm is meaningless. Furthermore, besides a methodology for the dynamic modelling of a mechanical system, a set of generalized coordinates and one coordinate frame are necessary to describe and render graphically the motion of the system. The choice of generalized coordinates, of course, depends on various issues, e.g., ease of sensing for feedback control, or simplicity of representation of the equations of motion for fast simulation purposes. Also, using a certain coordinate

frame to represent the dynamic equations of motion might lead to a faster or more accurate algorithm than using others. Since there can be many coordinate systems that are suitable for the representation of the dynamic model, one has to be chosen among them, based on certain selection criteria. These criteria will be discussed in this chapter. Other issues to be addressed in the realm of motion animation are rigid-body attitude representation, both holonomic and nonholonomic kinematic constraints and computational complexity. A suitable procedure, based on the NOC, described in Chapter 3, allows the systematic modelling of a mechanical system in any reference frame with any set of generalized coordinates. Various attitude representations and coordinate frames are compared with regard to computational complexity. The procedure is illustrated with a case study of a nonholonomic system, namely, a disk rolling on a plane.

6.1 Dynamic Model of a Disk Rolling on a Plane Using the NOC

The method of the NOC is used here to derive the equations of motion of a disk rolling on a plane, as shown in Fig. 1.1, as is described below: The velocity $\dot{\mathbf{c}}$ of the mass centre C of the disk, which is assumed to coincide with its centroid, is related to the angular velocity of the disk $\boldsymbol{\omega}$, namely,

$$\dot{\mathbf{c}} = \boldsymbol{\omega} \times (\mathbf{c} - \mathbf{q}) \tag{6.1}$$

where $\mathbf{q}$ and $\mathbf{c}$ are the position vectors of the point of contact, Q, and the centroid of the disk, C, respectively. Denoting vector $\mathbf{c} - \mathbf{q}$ by $\mathbf{r}$, eq.(6.1) is rewritten as:

$$\dot{\mathbf{c}} = \boldsymbol{\omega} \times \mathbf{r} \tag{6.2}$$

The kinematic constraint equations in the form of eq.(3.18) are written from eq.(6.2) as

$$\mathbf{A}\mathbf{t} = \mathbf{0}$$

where $\mathbf{A}$ is a 3×6 matrix, namely,

$$\mathbf{A} \equiv [\mathbf{R} \quad \mathbf{1}]$$

and $\mathbf{R}$ is the cross-product tensor associated with $\mathbf{r}$. The angular velocity $\boldsymbol{\omega}$ of the disk is now chosen as the 3-dimensional vector of independent generalized speeds, which is plausible because the degree of freedom of the system is three. Thus, the twist of the disk, $\mathbf{t}$, can be expressed as a linear transformation of $\boldsymbol{\omega}$, namely,

$$\mathbf{t} = \mathbf{T}\boldsymbol{\omega} \tag{6.3}$$

with the 6×3 matrix $\mathbf{T}$ defined as

$$\mathbf{T} \equiv \begin{bmatrix} \mathbf{1} \\ -\mathbf{R} \end{bmatrix}$$

It can be readily proven that matrix $\mathbf{T}$ is an orthogonal complement of $\mathbf{A}$ by noting that

$$\mathbf{AT} = \mathbf{O}$$

Matrix $\dot{\mathbf{T}}$ is now calculated as

$$\dot{\mathbf{T}} = \begin{bmatrix} \mathbf{O} \\ \dot{\mathbf{R}} \end{bmatrix}$$

Then, the equations of motion of the disk rolling on a plane are readily derived, which are given by

$$\mathbf{I}\dot{\boldsymbol{\omega}} = \mathbf{C}\boldsymbol{\omega} + \boldsymbol{\gamma} + \boldsymbol{\delta} \tag{6.4}$$

where the 3×3 generalized inertia matrix $\mathbf{I}$, the matrix of convective inertia terms $\mathbf{C}$ and the 3-dimensional vectors of generalized force due to gravity $\boldsymbol{\gamma}$ and of generalized dissipative force $\boldsymbol{\delta}$ are expressed as

$$\mathbf{I} \equiv \mathbf{T}^T\mathbf{M}\mathbf{T} = \mathbf{I}_C + m(\mathbf{r}^T\mathbf{r}\mathbf{1} - \mathbf{r} \otimes \mathbf{r}) \tag{6.5}$$

$$\mathbf{C} \equiv -\mathbf{T}^T[(\dot{\mathbf{M}} + \mathbf{W}\mathbf{M})\mathbf{T} + \mathbf{M}\dot{\mathbf{T}}] = -\dot{\mathbf{I}}_C - \boldsymbol{\sigma} \times \mathbf{I}_C + m(\dot{\mathbf{r}} \otimes \mathbf{r} - \boldsymbol{\sigma}^T\mathbf{r}\mathbf{R}) \tag{6.6}$$

$$\boldsymbol{\gamma} \equiv \mathbf{T}^T\mathbf{w}^G = m\mathbf{R}\mathbf{g} \tag{6.7}$$

$$\boldsymbol{\delta} \equiv \mathbf{T}^T\mathbf{w}^D = \mathbf{n}_d + \mathbf{R}\mathbf{f}_d \tag{6.8}$$

where $\boldsymbol{\sigma}$ is the angular velocity of the coordinate frame in which the equations of motion of the disk are represented, m is the mass of the disk and $\mathbf{I}_C$ is the 3×3 inertia tensor of the disk about its centroid C. Moreover, the sign $\otimes$ denotes the *tensor product* of the two vectors beside it. Furthermore, vectors $\mathbf{g}$, $\mathbf{n}_d$ and $\mathbf{f}_d$ are, respectively, the 3-dimensional vectors of acceleration due to gravity, of Cartesian—as opposed to generalized—moment and of Cartesian force acting at the mass centre of the disk, the last two items arising from dissipation in the system.

Note that eq.(6.5) has a physical interpretation, namely, the generalized inertia matrix $\mathbf{I}$ is nothing but the mass moment of inertia of the disk about the contact point Q. Furthermore, $\boldsymbol{\gamma}$ is the moment of the gravity force about the contact point Q. Equation (6.4) is used for the simulation of the disk motion. Dissipation is not considered in order to assess the accuracy of the various schemes which will be discussed in §6.3.

6.2 Orientation Representation

It is a common practice in dynamics to denote the orientation of a rigid body using Euler angles. This representation, although not invariant, is amongst the simplest because of its minimal set of variables. Its use is not recommended in cases where bodies attain arbitrary orientations. In these cases, Euler angles lead to frequent algorithmic singularities. The representation of rigid-body orientation using *linear* and *quadratic* invariants, as proposed in Angeles (1988), as well as the use of the orientation matrix itself, along with a matrix-differential equation, are recommended as alternate approaches to the orientation representation by Euler angles. The performances, i.e., speed and accuracy, of two orientation representations are compared to the orientation representation by Euler angles. These are the orientation representations based on quadratic invariants, best known as Euler-Rodrigues parameters, and the full orientation matrix and its differential equation. Note that, as indicated in §6.2.1, in contrast with the representation of an orthogonal matrix

by its quadratic invariants, the use of linear invariants leads to higher computational complexity and algorithmic singularities, and hence, the latter has been avoided.

6.2.1 Alternate Orientation Representations

Let $\mathbf{Q}$ be the matrix denoting the orientation of the coordinate frame attached to the disk with respect to the inertial frame, which is assumed to be a continuous and differentiable function of time. Then, the time derivative of the orientation matrix $\mathbf{Q}$, $\dot{\mathbf{Q}}$, is given as in Angeles (1988), by

$$\dot{\mathbf{Q}} = \boldsymbol{\Omega}\mathbf{Q} \tag{6.9}$$

where $\boldsymbol{\Omega}$ is defined, similar to eq.(2.7), as the cross-product tensor associated with the angular velocity $\boldsymbol{\sigma}$ of the coordinate frame in use. Note that, in this chapter, the notation that has already been introduced in eq.(4.81) will be used in representing vectors and matrices in a coordinate frame $\mathcal{C}$, i.e., vector components and matrix entries are included in a vector or, correspondingly, in a matrix array with a subscript $\mathcal{C}$, namely, as $[\,\cdot\,]_{\mathcal{C}}$, where $(\cdot)$ indicates the vector or matrix at hand. Now, if the coordinate frame used to express $\boldsymbol{\Omega}$ is different from that of $\mathbf{Q}$, e.g., if $\mathbf{Q}$ is expressed in an inertial frame denoted by $\mathcal{I}$ and $\boldsymbol{\Omega}$ is represented in any moving coordinate frame $\mathcal{M}$, then eq.(6.9) is modified as

$$[\dot{\mathbf{Q}}]_{\mathcal{I}} = [\mathbf{Q}]_{\mathcal{I}}[\boldsymbol{\Omega}]_{\mathcal{M}} \tag{6.10}$$

Integration of the equations of motion, eq.(6.4), will give the angular velocity of the disk, $\boldsymbol{\omega}$, which is necessary to calculate the angular velocity of the coordinate frame, $\boldsymbol{\sigma}$. Now, the time derivative of the orientation matrix, eq.(6.9) or eq.(6.10), can be readily obtained and the integration of these equations will give the orientation matrix. It can be noticed that the matrix differential equation, either eq.(6.9) or eq.(6.10), comprises nine scalar differential equations, which may affect the efficiency of the simulation algorithm. Alternatively, one can use the linear or the quadratic invariants of the rotation matrix $\mathbf{Q}$ (Angeles, 1988). However, if the linear invariants

are used, algorithmic singularities will occur whenever the disk attitude amounts to a rotation of 180^o from its reference orientation. This problem can be avoided if the quadratic invariants are used instead. Moreover, it can be shown that the calculation of the orientation matrix $\mathbf{Q}$ requires less computations when, instead of the linear invariants, the quadratic invariants are used. The quadratic invariants, better known as Euler-Rodrigues parameters, of matrix $\mathbf{Q}$, are defined as

$$\mathbf{s} \equiv \mathbf{e}\sin(\frac{\beta}{2}) \quad \text{and} \quad s_0 \equiv \cos(\frac{\beta}{2})$$

where $\mathbf{e}$ is the unit eigenvector of $\mathbf{Q}$ associated with its real eigenvalue $+1$ and β is defined, according to Euler's Theorem (Euler, 1776), as the *angle of rotation.* Now, the orthogonal matrix $\mathbf{Q}$ is given as

$$\mathbf{Q} = (2s_0^2 - 1)\mathbf{1} + 2\mathbf{s} \otimes \mathbf{s} + 2s_0\mathbf{s} \times \mathbf{1} \tag{6.11}$$

Introducing a 4-dimensional vector $\boldsymbol{\eta}$, which is defined as $[\mathbf{s}^T, \ s_0]^T$, the time derivative of the quadratic invariants is written as

$$\dot{\boldsymbol{\eta}} = \boldsymbol{\Sigma}\boldsymbol{\sigma} \tag{6.12}$$

where $\dot{\boldsymbol{\eta}} = [\dot{\mathbf{s}}^T, \ \dot{s}_0]^T$ and $\boldsymbol{\Sigma}$ is given by

$$\boldsymbol{\Sigma} \equiv \frac{1}{2}\begin{bmatrix} s_0\mathbf{1} - \mathbf{S} \\ -\mathbf{s}^T \end{bmatrix} \tag{6.13}$$

with $\mathbf{S}$ being the cross-product tensor associated with vector $\mathbf{s}$. As is apparent from eq.(6.10), if $\boldsymbol{\eta}$ is represented in the $\mathcal{I}$-frame and $\boldsymbol{\sigma}$ is expressed in the $\mathcal{M}$-frame, then the relation appearing in eq.(6.12) is modified as

$$[\dot{\boldsymbol{\eta}}]_{\mathcal{I}} = [\boldsymbol{\Sigma}']_{\mathcal{I}}[\boldsymbol{\sigma}]_{\mathcal{M}} \tag{6.14}$$

where

$$[\boldsymbol{\Sigma}']_{\mathcal{I}} \equiv \frac{1}{2}\begin{bmatrix} s_0\mathbf{1} + [\mathbf{S}]_{\mathcal{I}} \\ -[\mathbf{s}]_{\mathcal{I}}^T \end{bmatrix}$$

The orientation matrix, besides its representation by Euler angles, will be evaluated in two ways for comparison purposes: (i) by integrating the matrix-differential equation, eq.(6.9) or eq.(6.10), (ii) by integrating the differential equations of the quadratic invariants, as given either in eq.(6.12) or in eq.(6.14).

6.3 Equations of Motion of a Rolling Disk in Different Coordinate Frames

The equations of motion of the disk, eq (6.4), are derived in three different coordinate frames, namely, $\mathcal{F}$, a disk-following frame defined as a coordinate frame that follows the disk without being attached to it; $\mathcal{D}$, a disk-fixed frame, rigidly attached to the disk and $\mathcal{I}$, an inertial frame. The dynamic equations of motion in frame $\mathcal{F}$ are derived next, whereas the dynamic models of the system in the $\mathcal{D}$- and $\mathcal{I}$-frames are given in Appendix B. The simulation schemes for finding the orientation and position of the disk using $\mathcal{F}$-, $\mathcal{D}$- and $\mathcal{I}$-frames are outlined in §6.4.

6.3.1 A Disk-Following Frame

The $\mathcal{F}$-frame is defined as a coordinate frame following the disk without being attached to it, its origin being located at the centroid of the disk and its vector $\mathbf{v}$ coinciding with the disk spin axis, as shown in Fig. 1.1. The difference in motion between $\mathcal{F}$ and the disk is that $\mathcal{F}$ remains with its origin fixed at the disk centre and its two unit vectors $\mathbf{f}_1$ and $\mathbf{f}_2$ remain in the plane of the disk, but do not spin with the latter. The unit vectors $\mathbf{v}$, $\mathbf{f}_1$ and $\mathbf{f}_2$ are defined below:

- $\mathbf{v}$ is a unit vector parallel to the spin axis of the disk, which is perpendicular to the plane of the disk.
- $\mathbf{f}_2$ is defined as a unit vector directed from the contact point of the disk with the plane, Q, to the centroid, C. This vector lies in the plane of the disk and is perpendicular to $\mathbf{v}$.
- $\mathbf{f}_1$ is defined as a unit vector such that

$$\mathbf{f}_1 = \mathbf{f}_2 \times \mathbf{v}$$

Now, vector $\mathbf{r}$ is equal to $r\mathbf{f}_2$, which can be written in the $\mathcal{F}$-frame as

$$[\mathbf{r}]_{\mathcal{F}} = r[\mathbf{f}_2]_{\mathcal{F}} \tag{6.15}$$

where r is the radius of the disk and $[\mathbf{f}_2]_{\mathcal{F}} = [0,\ 1,\ 0]^T$. Substituting $[\mathbf{r}]_{\mathcal{F}}$ in eq.(6.5), the inertia matrix in the $\mathcal{F}$-frame can be expressed as

$$[\mathbf{I}]_{\mathcal{F}} = [\mathbf{I}_C]_{\mathcal{F}} + mr^2(\mathbf{1} - [\mathbf{f}_2]_{\mathcal{F}} \otimes [\mathbf{f}_2]_{\mathcal{F}}) \tag{6.16}$$

To evaluate the matrix of convective inertia terms in the $\mathcal{F}$-frame, as in eq.(6.6), it is noted that both vector $\dot{\mathbf{r}}$ and matrix $\dot{\mathbf{I}}_C$ vanish when represented in the $\mathcal{F}$-frame. Moreover, if $\dot{\psi}$ denotes the disk spin, then the angular velocity vector of the $\mathcal{F}$-frame, $\boldsymbol{\sigma}$, is equal to $\boldsymbol{\omega} - \dot{\psi}\mathbf{v}$, which can be understood from the motion of the disk, as illustrated in Fig. 1.1. Furthermore, $[\boldsymbol{\sigma}]_{\mathcal{F}}$ is written as

$$[\boldsymbol{\sigma}]_{\mathcal{F}} = [\boldsymbol{\omega}]_{\mathcal{F}} - \dot{\psi}[\mathbf{v}]_{\mathcal{F}} \tag{6.17}$$

where $[\mathbf{v}]_{\mathcal{F}} = [0,\ 0,\ 1]^T$. Then, matrix $[\mathbf{C}]_{\mathcal{F}}$ is computed as

$$[\mathbf{C}]_{\mathcal{F}} = -[\boldsymbol{\sigma}]_{\mathcal{F}} \times [\mathbf{I}_C]_{\mathcal{F}} - mr^2[\boldsymbol{\sigma}]_{\mathcal{F}}^T[\mathbf{f}_2]_{\mathcal{F}}([\mathbf{f}_2]_{\mathcal{F}} \times \mathbf{1}) \tag{6.18}$$

and

$$[\boldsymbol{\gamma}]_{\mathcal{F}} = mr[\mathbf{f}_2]_{\mathcal{F}} \times [\mathbf{g}]_{\mathcal{F}} \tag{6.19}$$

where

$$[\mathbf{g}]_{\mathcal{F}} = [\mathbf{F}]_{\mathcal{I}}^T[\mathbf{g}]_{\mathcal{I}}$$

with $[\mathbf{F}]_{\mathcal{I}}$ and $[\mathbf{g}]_{\mathcal{I}} = [0,\ 0,\ -g]^T$ being the matrix that denotes the orientation of the $\mathcal{F}$-frame with respect to the inertial frame and the acceleration vector due to gravity, respectively, both represented in the $\mathcal{I}$-frame, whereas the scalar g is the gravity acceleration.

Note that it is a common practice in the dynamics literature to use the Euler angles, θ, ϕ and ψ, indicated in Fig. 1.1, as the generalized coordinates of the disk, while their time derivatives $\dot{\theta}$, $\dot{\phi}$ and $\dot{\psi}$, play the role of the independent generalized speeds. Then, $[\boldsymbol{\omega}]_{\mathcal{F}}$ can be written as

$$[\boldsymbol{\omega}]_{\mathcal{F}} = [-\dot{\theta},\quad \dot{\phi}\cos\theta,\quad \dot{\psi} + \dot{\phi}\sin\theta]^T \tag{6.20}$$

Using eq.(6.20), along with eqs.(6.16), (6.18) and (6.19), the equations of motion in the $\mathcal{F}$-frame are derived as

$$[\mathbf{I}']_{\mathcal{F}}\ddot{\boldsymbol{\xi}} = [\mathbf{C}']_{\mathcal{F}}\,\dot{\boldsymbol{\xi}} + [\gamma]_{\mathcal{F}} \tag{6.21}$$

where

$$[\mathbf{I}']_{\mathcal{F}} = -\frac{mr^2}{4}\begin{bmatrix} 5 & 0 & 0 \\ 0 & 1+5s^2\theta & 6s\theta \\ 0 & 6s\theta & 6 \end{bmatrix}, \qquad [\mathbf{C}']_{\mathcal{F}} = \frac{mr^2}{4}\begin{bmatrix} 0 & -5\dot{\phi}s\theta c\theta & -6\dot{\phi}c\theta \\ 4\dot{\phi}s\theta c\theta & 6\dot{\theta}s\theta c\theta & 2\dot{\theta}c\theta \\ 5\dot{\phi}c\theta & 5\dot{\theta}c\theta & 0 \end{bmatrix}$$

and

$$[\gamma]_{\mathcal{F}} = -mgr\sin\theta[1,\ \ 0,\ \ 0]^T$$

Moreover, $\dot{\boldsymbol{\xi}} \equiv [\dot{\theta},\ \ \dot{\phi},\ \ \dot{\psi}]^T$ and vector $\ddot{\boldsymbol{\xi}}$ is the time derivative of $\dot{\boldsymbol{\xi}}$, while $s(\cdot)$ and $c(\cdot)$ represent the sine and cosine of $(\cdot)$, respectively. Furthermore, note that the inertia matrix in eq.(6.16) and the matrix of convective inertia terms in eq.(6.18) are different from those appearing in eq.(6.21), because the vectors of independent generalized speeds, $[\boldsymbol{\omega}]_{\mathcal{F}}$ and $\dot{\boldsymbol{\xi}}$, are different. In fact, $[\boldsymbol{\omega}]_{\mathcal{F}} = [\mathbf{U}]_{\mathcal{F}}\dot{\boldsymbol{\xi}}$, where

$$[\mathbf{U}]_{\mathcal{F}} = \begin{bmatrix} -1 & 0 & 0 \\ 0 & c\theta & 0 \\ 0 & s\theta & 1 \end{bmatrix}$$

Equation (6.21) is that reported in the literature on nonholonomic systems (Passerello and Huston, 1973).

In simulation, it is necessary to know the position and orientation of the disk in an inertial frame. The position will be obtained from integration of the velocity expression for the mass centre of the disk in the inertial frame, which is obtained as

$$[\dot{\mathbf{c}}]_{\mathcal{I}} = [\mathbf{F}]_{\mathcal{I}}[\dot{\mathbf{c}}]_{\mathcal{F}} \tag{6.22}$$

where $[\dot{\mathbf{c}}]_{\mathcal{F}}$ is determined by writing eq.(6.2) in the $\mathcal{F}$-frame as

$$[\dot{\mathbf{c}}]_{\mathcal{F}} = [\boldsymbol{\omega}]_{\mathcal{F}} \times [\mathbf{r}]_{\mathcal{F}} = r[\boldsymbol{\omega}]_{\mathcal{F}} \times [\mathbf{f}_2]_{\mathcal{F}} \tag{6.23}$$

Now, using Euler angles as generalized coordinates, matrix $[\mathbf{F}]_{\mathcal{I}}$ can be written as

$$[\mathbf{F}]_{\mathcal{I}} = \begin{bmatrix} c\phi & -s\theta s\phi & c\theta s\phi \\ s\phi & s\theta c\phi & -c\theta c\phi \\ 0 & c\theta & s\theta \end{bmatrix} \tag{6.24}$$

Alternatively, the orientation matrix $[\mathbf{F}]_{\mathcal{I}}$ can be computed by integrating the expressions for the time rate of change of the orientation matrix, $[\dot{\mathbf{F}}]_{\mathcal{I}}$, or for the time rate of change of the quadratic invariants, $[\dot{\boldsymbol{\eta}}]_{\mathcal{I}}$, which are given below,

$$[\dot{\mathbf{F}}]_{\mathcal{I}} = [\mathbf{F}]_{\mathcal{I}}[\boldsymbol{\Omega}]_{\mathcal{F}} \quad \text{or} \quad [\dot{\boldsymbol{\eta}}]_{\mathcal{I}} = [\boldsymbol{\Sigma}']_{\mathcal{I}}[\boldsymbol{\sigma}]_{\mathcal{F}} \tag{6.25}$$

Note that, when Euler angles are not used as generalized coordinates, the angular rate $\dot{\psi}$, appearing in eq.(6.17), is obtained by first solving for $[\boldsymbol{\omega}]_{\mathcal{F}}$ from the dynamic equations of motion, eq.(6.4), expressed in the $\mathcal{F}$-frame. Then, the expression for $\dot{\psi}$ is written as

$$\dot{\psi} = ([\mathbf{v}]_{\mathcal{F}} - [\mathbf{f}_2]_{\mathcal{F}} \tan\theta)^T [\boldsymbol{\omega}]_{\mathcal{F}} \tag{6.26}$$

Equation (6.26) can also be derived from eq.(6.20). Now, angle θ appearing in eq.(6.26) can in turn be calculated in two ways, namely,

- From Fig. 1.1,

$$\sin\theta = \mathbf{k}^T\mathbf{v} \quad \text{and} \quad \cos\theta = \mathbf{k}^T\mathbf{f}_2 \tag{6.27}$$

  where $\mathbf{k}$ is the unit vector parallel to the z_c-axis. Then, angle θ can be determined from eq.(6.27) by expressing the associated vectors in the $\mathcal{I}$-frame, which are readily recognized as: $[\mathbf{k}]_{\mathcal{I}} = [0,\ 0,\ 1]^T$, $[\mathbf{f}_2]_{\mathcal{I}}$ and $[\mathbf{v}]_{\mathcal{I}}$ being the second and third columns of matrix $[\mathbf{F}]_{\mathcal{I}}$, respectively.

- Another approach is to solve a differential equation in θ, which is the negative of the first component of $[\boldsymbol{\omega}]_{\mathcal{F}}$, as in eq.(6.20), namely,

$$\dot{\theta} = -[\mathbf{f}_1]_{\mathcal{F}}^T [\boldsymbol{\omega}]_{\mathcal{F}} \tag{6.28}$$

  where $[\mathbf{f}_1]_{\mathcal{F}} = [1,\ 0,\ 0]^T$.

6.4 Simulation Schemes

Simulation schemes are given based on the equations of motion, the orientation and position representation of the disk using the $\mathcal{F}$-, $\mathcal{D}$- and $\mathcal{I}$-frames.

6.4.1 Using Frame $\mathcal{F}$

Given the initial conditions, i.e., the initial position, orientation matrix and angular velocity of the disk, the simulation can be implemented in one of five different ways, namely,

(F1) Equation (6.21) is integrated to obtain Euler angles and their time derivatives. The constraint equation, which is the expression for the velocity of the mass centre of the disk, eq.(6.22), is obtained using eqs.(6.15), (6.20), (6.23) and (6.24). However, only the first two scalar equations of eq.(6.22) need to be integrated, because the third component of $\dot{\mathbf{c}}$ has a closed-form integral, namely, $r\cos\theta$. Therefore, eight scalar first-order differential equations are to be integrated.

(F2) When Euler angles are not used as generalized coordinates, an alternate approach is employed which consists of solving eq.(6.4) in the $\mathcal{F}$-frame to obtain the generalized speed $[\boldsymbol{\omega}]_{\mathcal{F}}$. Then, the velocity of the mass centre can be obtained from eqs.(6.15), (6.22) and (6.23), where the orientation matrix $[\mathbf{F}]_I$ is obtained by integrating the vector differential equation for $[\boldsymbol{\eta}]_I$ of eq.(6.25) and using the relation in eq.(6.11). Finally, eqs.(6.26) and (6.27) are used to calculate $\dot{\psi}$ and θ, respectively. This approach will give nine equations to integrate.

(F3) Alternatively, instead of using the geometrical relations of eq.(6.27), eq.(6.28) is utilised to evaluate θ. Therefore, there will be one additional differential equation, thereby deriving ten scalar ordinary differential equations.

(F4) The time derivative of matrix $[\mathbf{F}]_I$, $[\dot{\mathbf{F}}]_I$ in eq.(6.25), eq.(6.26) and eq.(6.27) are used to obtain the orientation matrix, $\dot{\psi}$ and θ, respectively. Thus, fourteen first-order differential equations are to be integrated with this approach to obtain the simulation results.

(F5) Similar to F4, but eq.(6.28) is used instead of eq.(6.27).

6.4.2 Using Frame $\mathcal{D}$

With the initial conditions, that is, the initial position, orientation matrix and angular velocity of the disk, the simulation can be implemented using the equations of motion, the expressions associated with the orientation and position representation of the disk in the $\mathcal{D}$-frame, as derived in §B.1. Similar to the case of the $\mathcal{F}$-frame, any one of the schemes given below can be used:

(D1) Using eq.(B.7) and the first two components of $[\dot{\mathbf{c}}]_{\mathcal{I}}$, as given in eq.(B.8), which will lead to eight first-order differential equations.

(D2) Using nine scalar differential equations, three from the equations of motion, eq.(6.4), expressed in the $\mathcal{D}$-frame, four from the time rate of change of the quadratic invariants, eq.(B.9), and two components of $[\dot{\mathbf{c}}]_{\mathcal{I}}$. Equations (B.11) and (B.12) are then used to calculate ψ and θ, respectively.

(D3) Instead of using geometrical relations, differential equations are used to calculate ψ and θ, eqs.(B.10) and (B.13), respectively, which will make a total of eleven first-order differential equations to integrate.

(D4) Alternatively, the matrix-differential equation for $[\mathbf{D}]_{\mathcal{I}}$, as in eq.(B.9), is used to calculate the orientation matrix. This approach is similar to D2.

(D5) Differential equations, eqs.(B.10) and (B.13), are used as in D4 to find ψ and θ, respectively. This will lead to sixteen differential equations.

6.4.3 Using Frame $\mathcal{I}$

The simulation results are obtained from one of the following schemes:

(I1) First, vectors $[\mathbf{r}]_{\mathcal{I}}$ and $[\dot{\mathbf{r}}]_{\mathcal{I}}$ are calculated as $r[\mathbf{f}_2]_{\mathcal{I}}$ and $r[\dot{\mathbf{f}}_2]_{\mathcal{I}}$, respectively. Then, the equations of motion in the $\mathcal{I}$-frame are solved for the angular velocity of the disk, $[\boldsymbol{\omega}]_{\mathcal{I}}$. The expression for $[\dot{\boldsymbol{\eta}}]_{\mathcal{I}}$, eq.(B.21), is used to find the orientation matrix. Here, nine first-order differential equations need to be solved.

$\phi = \psi$=0.0 deg, $\dot{\theta}$=0.0 deg/s

Case	θ (deg)	$\dot{\phi}$ (deg/s)	$\dot{\psi}$ (deg/s)
A	0.217633	57.295780	−28.647890
B	1.004186	103.132405	−74.481515
C	6.099778	240.642278	−211.994388
D	23.465159	550.039493	−521.391602

Table 6.1 Initial conditions.

(I2) Alternatively, the time derivative of matrix $[\mathbf{D}]_I$ in eq.(B.21) is utilised to derive the orientation matrix, which results in six more differential equations for simulation.

6.5 Simulation Results

Twelve simulation algorithms for animation were developed, as described in the previous section, in order to test their accuracy and speed. Simulation results for a time period of 3.5 s, shown in Figs. 6.1 to 6.5, were obtained by integrating the differential equations with the help of the DVERK[1] subroutine of the IMSL package (IMSL, 1980), which solves first-order differential equations by the Runge-Kutta 5th/6th order method. The integration was performed with a tolerance of 10^{-5}. The tolerance that is used by the DVERK subroutine has no units. The reasons are the same as those that have been given in §4.1.4 for the DIVPRK subroutine of the IMSL package (IMSL, 1990b). The results, shown in Figs. 6.1 to 6.3 and 6.4(a), were obtained with a step size of 0.007 s. To study the effect of the step size, a smaller step of 0.00175 s was taken, the corresponding simulation results being shown in Fig. 6.4(b).

To test the performance of the computer animation software, i.e., whether the animation is a true representation of the real motion of the disk, a set of initial conditions from Table 6.1, which corresponds to the steady states, e.g., circular motions of

[1]DVERK is another version of the DIVPRK subroutine of the IMSL (1990b) package that has been used in the previous chapters

the disk, are supplied to the simulation programs. For that purpose, a steady-state analysis is done in §A.6 using the equations of motion in the $\mathcal{F}$-frame, eq.(6.21), where Euler angles are the generalized coordinates, as in scheme F1. Henceforth, F1 to F5, D1 to D5. and I1 and I2 will be understood as the simulation schemes mentioned in §6.4.1, §6.4.2 and §6.4.3, respectively. Initial positions, velocities and orientation matrices for the simulation programs, based on the schemes F2–F5, D1–D5 and I1–I2, are similarly obtained, which also correspond to the circular motions of the disk. It is pointed out here that no different steady-state analyses were done, but Euler angles and their time derivatives in Table 6.1 were transformed to the initial conditions, which are compatible with the other routines to generate circular trajectories on the horizontal plane. Simulation results from the different schemes are given based on accuracy and speed.

6.5.1 Accuracy

The deviation of the plots of the y_c- vs. x_c-coordinates of the centroid of the disk, Figs. 6.2 (a)–(d) for the initial condition A of Table 6.1, from the circular trajectories, i.e., from a steady state, reflects the instability of the system under study. Similar responses were observed in the cases of the initial conditions B and C of Table 6.1 and, finally, in D, a limit cycle is observed, as in Fig. 6.4(a), which is in agreement with the initial conditions. In fact, with all the schemes, a delay in the growth of instability is observed as one goes from initial condition A to B and from B to C, but with initial condition D no deviation is noticed even for a simulation time of 70 s. The instability can be attributed to both the physics of the system and numerical errors. Since it is very difficult to input the exact values for the initial conditions corresponding to the steady states, the given values can be considered as perturbed values and the system may deviate from the circular trajectories due to its intrinsic instabilities. To detect the nature of the instability, an analysis, based on the principle of conservation of energy, was done when the disk was rolling on a plane in the absence of external and dissipative forces. The total energy at any

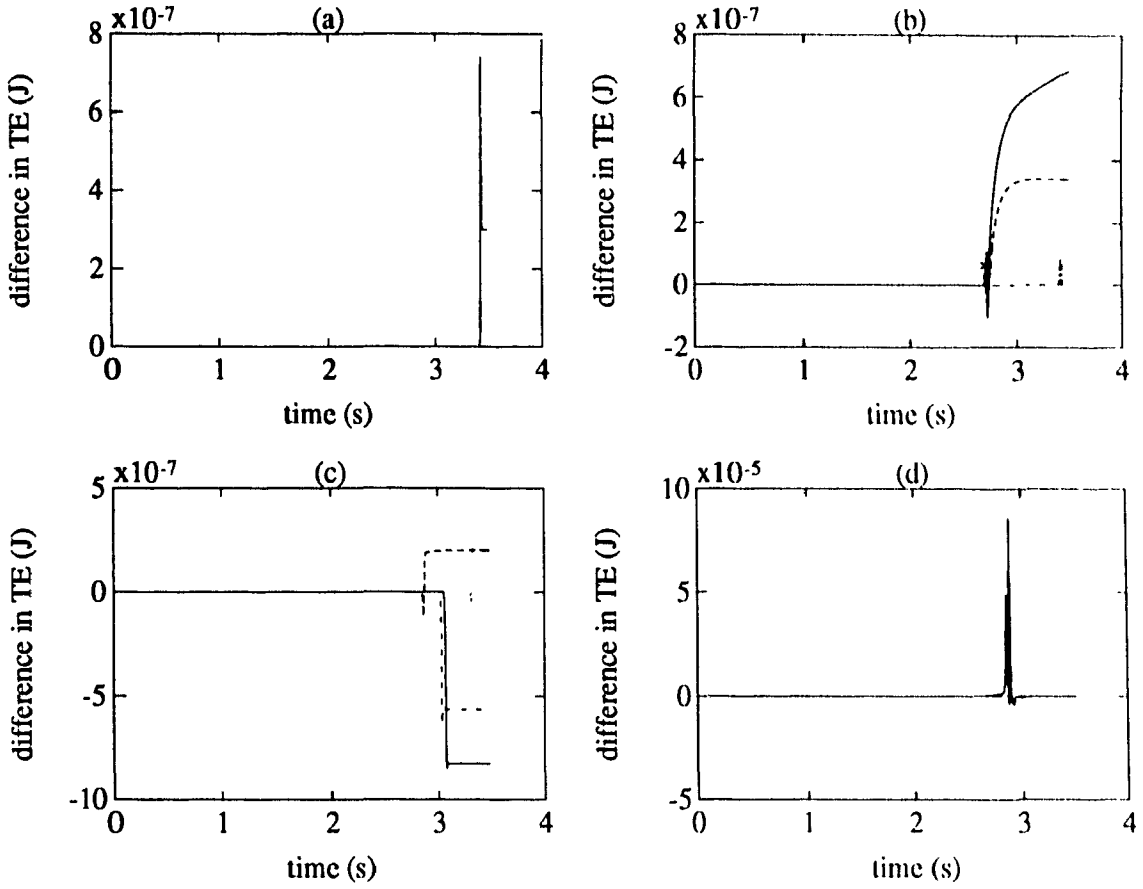

(a) — F1, D1; (b) — F2, - - F3, - · - F4, F5; (c) - D2, - - D3, - · - D4, · · · D5, (d) — I1, TE=0 for I2.

Fig. 6.1 Plots of the difference in total energy (TE) vs. time for the initial condition A with step size of 0.007 s and initial total energy of 0.0098254 J.

instant is compared with the initial total energy and the difference in energy, in Joules, is plotted against time, in seconds. Moreover, when the total energy remains constant but the motion of the disk deviates from its steady state, instability due to the dynamic behaviour of the system is detected On the other hand, if the total energy changes as the disk deviates from its circular motion, then the numerical instability is confirmed. Furthermore, if the total energy of the disk, which, for given inertial properties of the disk, depends on its position and velocity, is higher, then the system is less sensitive to the inaccuracies in the initial conditions, which is evident from Figs. 6.1 to 6.4. For example, in Figs. 6.1(b) and 6.3(b) the differences in total energy at time $t = 2.653$ s (marked '*') are 1.31758×10^{-11} J and 7.60834×10^{-9} J,

respectively, for scheme F2. Note that, in both the cases, the difference in total energy is very small, however, the y_c- vs. x_c-coordinates in Fig. 6.2(b) for scheme F2 at $t = 2.653$ s (marked '*') do not correspond to the circular trajectory—it is unnecessary to derive the equation of a circle from the given initial conditions in order to comment on the Cartesian position of the mass centre of the disk in the $x_c - y_c$-plane, as the figure is self-explanatory— , whereas Fig. 6.4(a) shows a stable motion of the disk at the point marked '*'. A similar explanation can be provided for the delay in the growth of the instability when the error in the total energy is sufficiently small, i.e , within some tolerance. However, a lower step size improves the simulation results, which can be noticed from Fig. 6 4(b), in contrast to Fig. 6.2(a), showing that the growth of the instability has been delayed.

6.5.2 Speed

To comment on the speed of the algorithms F1–F5, D1–D5 and I1–I2, as described in §6.4, a study of CPU times was done. In some cases, after a certain time of simulation, the total energy suddenly changes its value, indicating the initiation of numerical instability, which depends on the initial conditions, as can be seen in Figs. 6.1 and 6.2. Furthermore, it can be readily understood that, if simulation is continued beyond the jump in the total energy, the execution time not only depends on the complexity of the algorithm, but also on its numerical sensitivity. Therefore, in order to comment on the complexity of the algorithm, a simulation time, e.g., 2.1 s, is chosen so that the disk motion is stable, i.e., it follows a circular trajectory in all cases. However, the CPU time needed to execute a program is different at different times, because this time depends on the load of the computer system. So, data were taken at night when the computer system was assumed to be under constant load and by using double-precision on a SUN 3/75 workstation. To ensure correct data, the repeatability of the results was considered. The data were taken until at least five CPU times fell within a small error range, e.g., 3.5%. Finally, the CPU times were calculated as the average of the five readings mentioned above. The

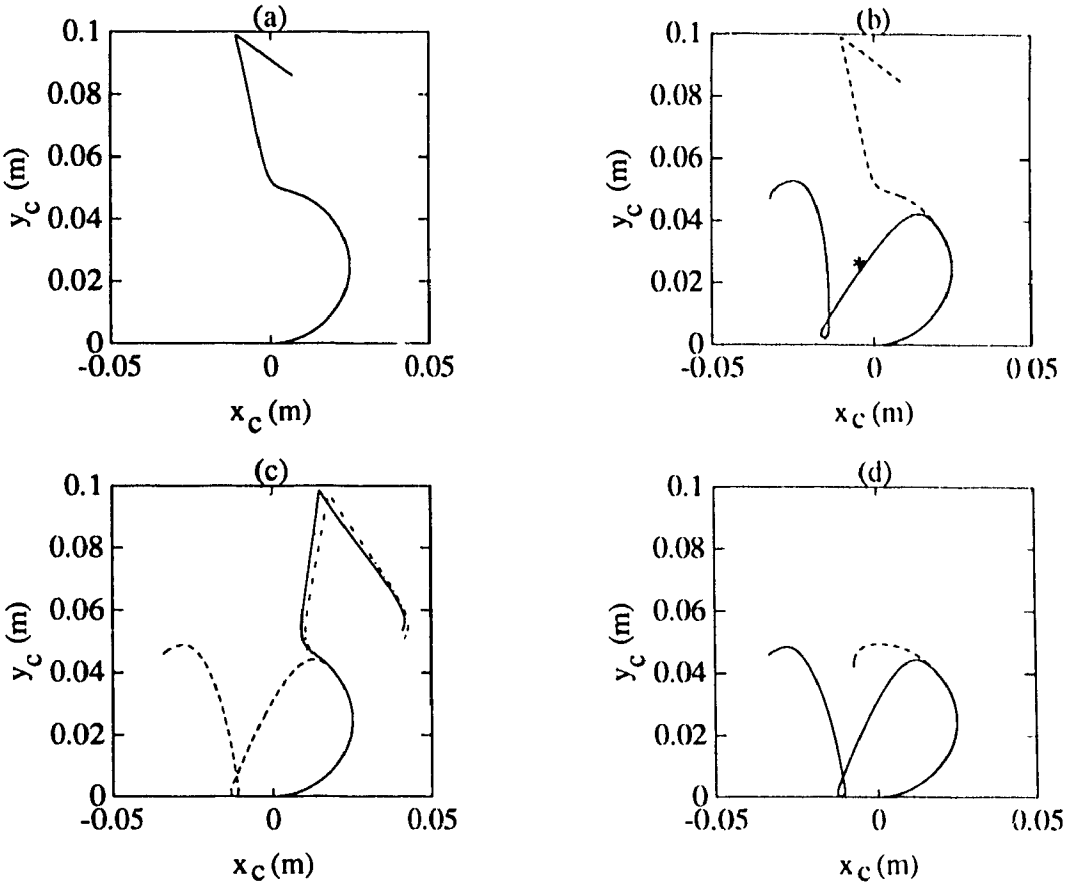

(a) — F1, D1; (b) — F2, F3, - - F4, F5; (c) · D2, - · D3, - - D4, · · · D5, (d) — I1, - - I2.

Fig. 6.2 Plots of y_c vs. x_c for the initial condition A with step size of 0.007 s and initial total energy of 0.0098254 J.

results of the comparative study of the CPU times with the initial condition A are shown in Fig. 6.5. It was noticed that the different initial conditions under study do not significantly affect the CPU time. Also, with lower step sizes the required CPU times increase by the factor of the decrement of the step size.

6.6 Analysis of the Results

The classical problem of a rigid disk rolling on a horizontal plane was used as a case study highlighting the methodology underlying computer animation. Algorithm accuracy was measured as the time between the start of the simulation and the

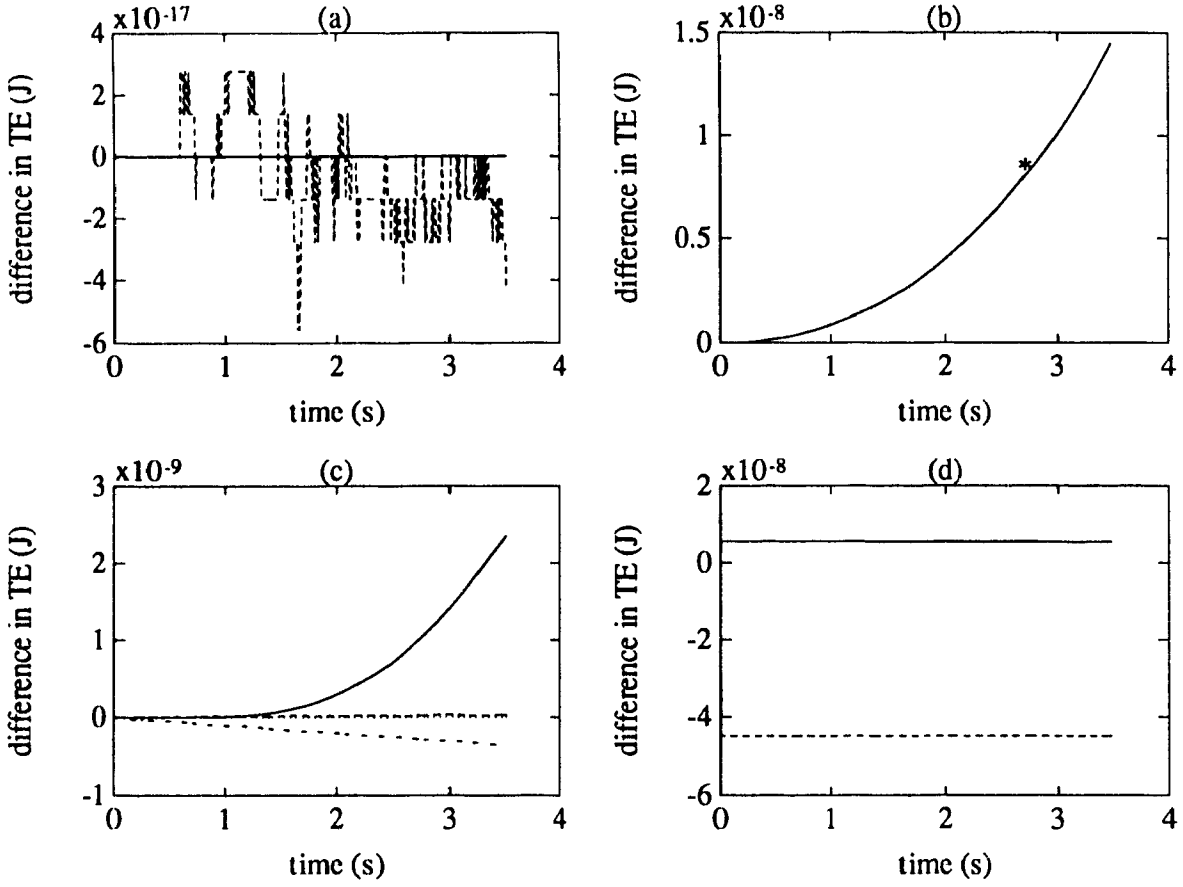

(a) — F1, - - D1; (b) — F2, F3, TE=0 for F4 and F5;
(c) — D2, - - D3, - · - D4, · · · D5; (d) — I1, - - I2.

Fig. 6.3 Plots of the difference in total energy (TE) vs. time for the initial condition D with step size of 0.007 s and initial total energy of 0.0105278 J.

growth of the instability beyond a certain bound. This instability was detected using a set of initial conditions leading to a circular trajectory of the mass centre of the disk under study on the horizontal surface. Thus, the instability occurs when the disk deviates from its circular path. Furthermore, algorithm efficiency was defined as the CPU time taken by the algorithm to complete the simulation for a certain time of the stable disk motion. In the present case this time is 2.1 s from the beginning of the disk motion corresponding to a circular path. Animation algorithms were then compared regarding their accuracy and speed for different independent generalized coordinates and different frames. The accuracy of the simulation algorithms, based on schemes F1 and D1, corresponding to the initial conditions A, B, C and D of

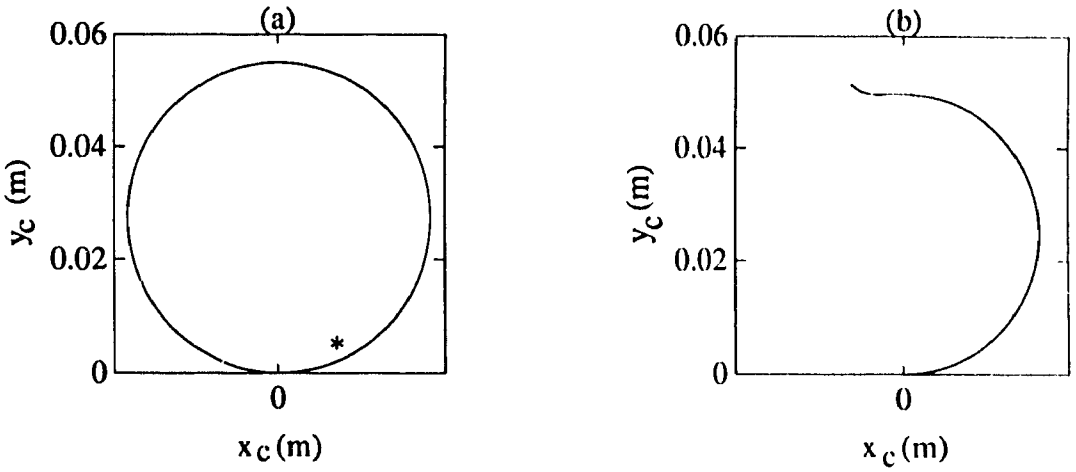

(a) — all schemes; (b) F1, D1.

Fig. 6.4 Plots of y_c vs. x_c for (a) the initial condition D with step size of 0.007 s and initial total energy of 0.0105278 J, (b) the initial condition A with step size of 0.00175 s and initial total energy of 0.0098254 J.

Table 6.1, is the same, which is evident from the fact that they have the same set of scalar differential equations. Simulation results with extreme initial conditions, i.e., A and D, are shown in Figs. 6.1 and 6.2, and Figs 6.3 and 6.4, respectively. The results for the initial conditions B and C of Table 6.1 are similar, but there are delays in the initiation of instability, as mentioned in §6.5.1. However, there is a difference in their speed, as shown in Fig. 6.5 for the initial condition A of Table 6.1. This difference results from the computation of the orientation matrix $[\mathbf{D}]_I$, which requires more operations than calculating matrix $[\mathbf{F}]_I$. Moreover, for a realistic animation, it is recommended to use the $\mathcal{D}$-frame, because the effect of the spin action of the disk will be clear using the orientation matrix $[\mathbf{D}]_I$. On the contrary, if the $\mathcal{F}$-frame is used, matrix $[\mathbf{F}]_I$ should be postmultiplied by matrix $[\mathbf{P}]_D^I$, matrix $\mathbf{P}$ being defined in eq.(B.1), to obtain the same effect. In fact, the resulting matrix, after multiplication, leads to matrix $[\mathbf{D}]_I$. The comparative results, based on accuracy, for F2–F5, are shown in Figs. 6.1(b) and 6.2(b) for the initial conditions A and in Figs. 6.3(b) and 6.4(a) for the initial conditions D. Moreover, the results for the algorithms based on schemes D2–D5 are shown in Figs. 6.1(c), 6.2(c), 6.3(c) and 6.4(a) and in Figs. 6.1(d), 6.2(d), 6.3(d) and 6.4(a) for those based on schemes I1–I2. Apart from schemes F1 and D1, schemes F4, D5 and I2 lead to the most

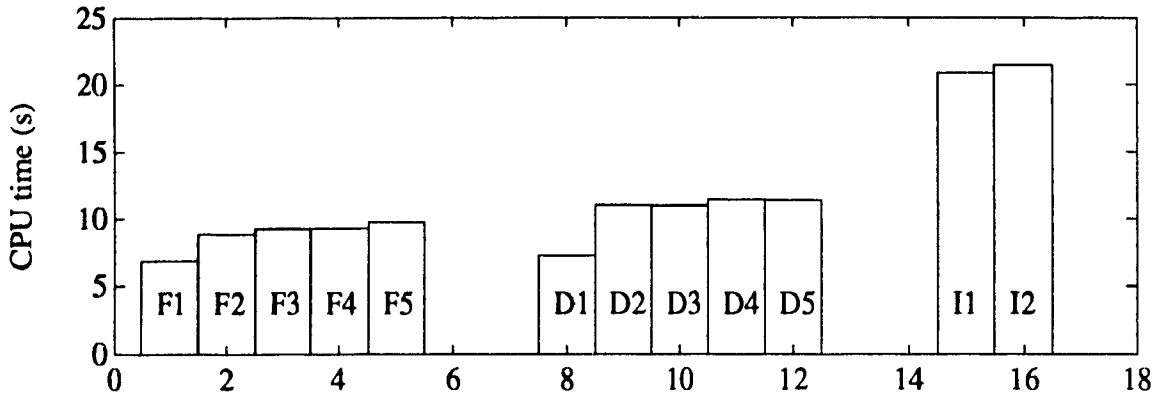

Fig. 6.5 CPU time in seconds for the initial condition A using the schemes shown inside the bars.

accurate simulation results in the $\mathcal{F}$-, $\mathcal{D}$- and $\mathcal{I}$-frames, respectively. It is noted that scheme D5, which uses differential equations instead of geometrical relations to evaluate angles ψ and θ, results in a more accurate simulation algorithm, which is surprising because the use of differential equations involves integration resulting in cumulative errors On the contrary, the use of geometrical relations does not involve any such errors. This unexpected result can be explained as follows: Angles ψ and θ are computed in scheme D4 from cumbersome expressions, eqs.(B.11) and (B.12), which require vector dot and cross products, and the evaluation of norms of vectors. Vectors $\mathbf{d}_1$, $\mathbf{d}_2$ and $\mathbf{v}$, appearing in the geometrical relations, in the $\mathcal{I}$-frame, are the first, second and third columns of matrix $[\mathbf{D}]_{\mathcal{I}}$, respectively, which are obtained from the integration of the matrix-differential equation. On the other hand, expressions for $\dot{\psi}$ and $\dot{\theta}$, eqs.(B.10) and (B.13), respectively, require less cumbersome computations, while vectors $\mathbf{f}_1$, $\mathbf{f}_2$ and $\mathbf{v}$ in the $\mathcal{F}$-frame, as proposed in scheme D5, do not require any integration and have very simple forms, namely, $[1, 0, 0]^T$, $[0, 1, 0]^T$ and $[0, 0, 1]^T$, respectively. Therefore, scheme D4, which requires the integration of nine scalar differential equations, three for each column vector of matrix $[\mathbf{D}]_{\mathcal{I}}$, produces more numerical errors than scheme D5, which needs simpler operations to evaluate $\dot{\psi}$ and $\dot{\theta}$, in addition to the integration of the latter two differential equations. Further comparisons between the results based on schemes F4, D5, I2,

F1 and D1 show that the last two schemes, where the equations of motion are in terms of Euler angles, are better than the others. A comparative study on the CPU times shows that the simulation software based on scheme F1 is the fastest algorithm for simulation purposes and in the case of an animation program to be coupled with a simulation scheme, scheme D1 should be considered as the most efficient algorithm. However, as pointed out in §6.2, the use of Euler angles in representing the orientation of a body is not suitable in many applications. Choosing the components of the angular velocity of the disk as the independent generalized speeds and writing down the equations of motion in a suitable coordinate frame provides one with different means for obtaining dynamic models of mechanical systems. In addition, alternate orientation representations were introduced in §6.2.1, which have been utilised to implement the simulation of the disk motion, as in schemes F2–F5, D2–D5 and I1–I2. Furthermore, before selecting an algorithm for animation, it is always wise to perform a comparative study, as indicated above, in order to decide on the fastest, the most accurate and the most practically feasible simulation scheme. For that, the method of the NOC is suitable to express the dynamic equations of motion in any coordinate system using an arbitrary set of generalized coordinates, as is made evident in §6.1, §6.3 and Appendix B. Moreover, it has been noticed that schemes F4, D5 and I2, which integrate nine scalar differential equations to obtain the orientation matrix, lead to more accurate results than schemes F2, F3, D2, D3 and I1, which require only four differential equations to be integrated and some additional computations, as in eq.(6.11). Furthermore, scheme D5 produced more accurate results than scheme D4. In fact, from Fig. 6.5, it is clear that the use of redundant differential equations does not lead to a significant increase in the CPU time. Hence, it is recommended not to always discard the integration of differential equations over algebraic or geometrical solutions.

Chapter 7

Conclusions and Suggestions for Further Research

The thesis is concluded with a brief summary of the completed work as well as the practical use of the results. Suggestions for further research are also outlined.

7.1 Discussion

A review of classification of mechanical systems based on kinematic constraints is given in Chapter 1 in order to clearly understand the terminology and the discussion in connection with the kinematic and dynamic analyses of nonholonomic robotic mechanical systems containing both holonomic and nonholonomic couplings. Robotic mechanical systems, i.e., mechanical systems under computer control, are classified based on the kinematic constraints which arise from the kinematic couplings. Thus, a class of robotic systems, termed nonholonomic robotic mechanical systems (NHRMS), is defined. Chapter 2 gives an overall review of different formulations for dynamic modelling of nonholonomic mechanical systems. The review has been given with merits and demerits of different dynamic modelling techniques.

A new method for the dynamic modelling of mechanical systems is introduced in Chapter 3 as a six-step method. The method is based on a novel formulation of kinematic constraints. In the adopted kinematic formulations, two lemmas are given

in connection with the holonomicity of kinematic constraints. Dynamic models of nonholonomic mechanical systems are then developed using the natural orthogonal complement (NOC) of the kinematic constraint matrix, which is formulated in §3.1. The dynamic modelling technique developed here, termed the method of the NOC, was suitably used for the dynamic modelling of mechanical systems with multiple kinematic loops. Moreover, mechanical systems with redundant actuation can also be modelled with the aid of the NOC in conjunction with an optimization technique. Thus, a complete modelling technique is introduced in this thesis, which is capable of modelling a broad class of robotic mechanical systems composed of rigid bodies and both holonomic and nonholonomic constraints.

The method of the NOC is then used to model different NHRMS, as in Chapter 4 for dynamic simulations. However, as pointed out in Step 5 of §3.2, the model thus developed can be exploited for the design of mechanical systems (Saha and Angeles, 1991d). The performance of AGVs was tested using the kinematic and dynamic models derived here while following different paths. In order to avoid discontinuous motions of the vehicles, which are harmful to the driving motors, proper path planning was done, whereby the system always started and stopped with zero velocity and acceleration.

Since dissipation leads to damping of the built-up error upon integration of the ordinary differential equations of motion, it becomes difficult to assess the accuracy of the various schemes that are developed for simulation purposes. On the other hand, it is intuitively easy to judge the validity of the simulation results with no dissipation, because, if the dynamic model of a system includes dissipation, then deviations from the intuitive results cannot be exactly ascertained either due to the characteristics of the dissipative model or due to the dynamic model itself, since nothing is known about the nature of the tool developed here. Thus, in spite of the ability of the method of the NOC to account for dissipation, as done in Cyril et al. (1989), using the 3-wheeled 2-DOF AGV of §4.2, dissipation models are not included in this thesis for the simulation of the NHRMS under study.

With regard to 3-DOF AGVs, a software package, OMNI, is developed for AGVs consisting of any number of omnidirectional wheels, which analyses a vehicle in four different levels. OMNI may help a designer in selecting an AGV for a particular application. The design of 3-DOF AGVs based on the isotropic kinematic transformation matrix for direct kinematics is done in Chapter 5. The design aims at providing robust direct kinematic control with respect to manufacturing and measurement errors. Note that the design of the 4-wheeled 3-DOF AGV, as shown in Fig. 5.1, is novel in that, as opposed to existing designs, the wheel axes are not parallel. On the other hand, designs with three driven wheels exist whose architectural parameters are similar to those obtained here. Note that the conditions of isotropic design for direct kinematics of 3-DOF AGVs are general, in a sense that eq.(5.10) can be used for isotropic design of AGVs consisting of an arbitrary number of omnidirectional wheels.

Finally, some issues associated with computer animation are discussed in Chapter 6. It is well-known that fast and accurate animation and simulation programs are needed to produce a realistic representation of a moving system. It has been pointed out that a coordinate frame used in representing the dynamic equations of motion affects the simulation algorithm. Moreover, alternative approaches for representing the orientation of a rigid body for fast simulation are introduced.

7.2 Suggestions for Further Research

The author would like to suggest further research work to extend that reported here, namely,

(i) Consideration of different types of dissipation models in simulation.

(ii) The extension of the kinematic formulation and the dynamic modelling technique, introduced in this thesis, to nonholonomic systems with rubber tyred wheels.

(iii) The developed tool for dynamic modelling of mechanical systems has potential in solving for constraint moments and forces arising due to the constraints at the joints. Thus, the method can be extended to design complex mechanical systems like AGVs, whose simulation models are developed in this thesis.

(iii) The number of rollers in a wheel and the profile of the rollers can be designed optimally.

(iv) Finally, with regard to the simulation of the systems, a performance criterion may be established in deciding upon the best reference frame to represent the equations of motion.

References

Adams, R., 1984, "Omnidirectional vehicle," *Robotics Age*, Feb., pp. 21–22.

Agulló, J., Cardona, S., and Vivancos, J., 1987, "Kinematic of vehicles with directional sliding wheels," *Mechanism and Machine Theory*, Vol. 22, No. 4, pp. 295 301.

Agulló, J., Cardona, S., and Vivancos, J., 1989, "Dynamics of vehicles with directionally sliding wheels," *Mechanism and Machine Theory*, Vol. 24, No. 1, pp. 53–60.

Alexander, J. C., and Maddocks, J. H., 1989, "On the kinematics of wheeled mobile robots," *Int. J. of Robotics Research*, Vol. 8, No. 5, pp. 15–27.

Andrews, G. C., and Kesavan, H. K., 1975, "The vector network model: a new approach to vector dynamics," *Mechanism and Machine Theory*, Vol. 10, No. 1, pp. 57 75.

Angeles, J., 1988, *Rational Kinematics*, Springer-Verlag. New York.

Angeles, J., and Gosselin, C., 1988, "Détermination du degré de liberté des chaînes cinématiques simples et complexes (On the determination of the degree of freedom of simple and complex kinematic chains)," *Trans. of the Canadian Soc. of Mech. Eng.*, Vol. 12, No. 4, pp. 219-226.

Angeles, J., and Lee, S., 1988, "The formulation of dynamical equations of holonomic mechanical systems using a natural orthogonal complement," *Trans. of the ASME, J of Applied Mechanics*, Vol. 55, March, pp. 243–244.

Angeles, J., and Lee, S., 1989, "The modelling of holonomic mechanical systems using a natural orthogonal complement," *Trans. of the Canadian Soc. of Mech. Eng.*, Vol. 13, No. 4, pp. 81-89.

Angeles, J., and Ma, O., 1988, "Dynamic simulation of n-axis serial robotic manipulators using a natural orthogonal complement," *Int. J. of Robotics Research*, Vol. 7, No. 5, pp. 32 47.

Appell, P., 1899, "Sur une forme nouvelle des équations de la dynamique," *C. R.*

Acad. Sci., Paris, Vol. 129, pp. 459–460.

Balafoutis, C. A., Misra, P., and Patel, R. V., 1988, " A Cartesian tensor approach for fast computation of manipulator dynamics," *Proc. of the IEEE Conf. on Robotics & Automation*, Philadelphia, Pennsylvania, April 24–29, Vol. 3, pp. 1348 1353.

Baker, J. E , 1981, "On mobility and relative freedoms in multiloop linkages and structures," *Mechanism and Machine Theory*, Vol. 16, No. 6, pp. 583 597.

Boegli, P., 1985, "A comparative evaluation of AGV navigation techniques," *Proc. of the 3rd Int. Conf. on Automated Guided Vehicles*, Stockholm, Sweden, Oct. 15 17, pp. 169–177.

Borenstein, J., and Koren, Y., 1985, "A mobile platform for nursing robots," *IEEE Trans. on Industrial Electronics*, Vol. 32, No. 2, May, pp. 158 165.

Bortz, B. B., 1984, "Moravec's mobile robots," *Robotics Age*, Sept., pp. 25 31.

Carlisle, B., 1984, "An omni-directional mobile robot," *Development in Robotics*, IFS Publications, Ltd., England, pp. 79–87.

Chace, M. A., and Sheth, P. N., 1973, "Adaptation of computer techniques to the design of mechanical dynamic machinery," *ASME Paper* 73-DET-58.

Chen, F. Y., 1982, *Mechanics and Design of Cam Mechanisms*, Pergamon Press, New York.

Cheng, R. M. H., and Rajagopalan, R., 1988, "Kinematics of an automatic guided vehicle with an inclined steering column," *Proc. of the ASME Conf. on Computers in Eng.*, July 31–Aug. 4, San Francisco, California, pp. 259-265.

Cheng, R. M. H , Rajagopalan, R. and Sankar, T. S., 1989, "System architecture of an automatic guided vehicle (AGV)," *Proc. of the 4th Int. Conf. on CAD/CAM, Robotics and Factories of the Future*, Dec. 19-22, New Delhi, India, Vol. 2, pp. 254–263.

Crosheck, J., and Ford, M., 1988, "Simulation takes three-wheeler for a spin," *Mechanical Engineering*, Nov., pp. 48–51.

Culley, G., and Baldur, R., 1988, "A free wheel approach to AGV navigation," *Proc. of the ASME Conf. on Computers in Eng.*, San Francisco, California, July 31 Aug. 4, pp. 267–274.

Cyril, X., Angeles, J. and Misra, A. K., 1989, "Flexible-link robotic manipulator dynamics," *Proc. of the 1989 American Control Conference*, Pittsburgh, Pennsylvania, June 21–23, pp. 2346–2351.

Cyril, X., Cheng, R. M. H., and Sankar, T. S., 1989, "Dynamics of wheeled mobile

robots (AGVs)," *Proc. of the 4th Int. Conf. on CAD/CAM, Robotics and Factories of the Future*, Dec. 19-22, New Delhi, India, Vol. 2, pp. 264-273.

d'Andréa-Novel, B., Bastin, G., and Campion, G., 1991, "Modelling and control of nonholonomic wheeled mobile robots," *Proc. of the IEEE Conf. on Robotics & Automation*, Sacramento, California, Vol. 2, pp. 1130–1135.

Daniel, J. D., Krogh, B. H., and Friedman, M. B., 1985, "Kinematic and open-loop control of an ilonator-based mobile platform," *Proc. of the IEEE Conf. on Robotics & Automation*, St. Louis, Missouri, Vol. 1, pp. 346–351.

Darcovich, J., 1991, *Dynamics of Single-loop Mechanical Systems with Flexible Links*, April, an M. Eng. thesis submitted to the Dept. of Mech. Eng., McGill University, Montreal, Canada.

Davies, T. H., 1981, "Kirchhoff's circulation law applied to multi-loop kinematic chains," *Mechanism and Machine Theory*, Vol. 16, pp. 171–183

Desloge, E. A., 1986a, "A comparison of Kane's equations of motion and the Gibbs-Appell equations of motion," *American J. of Physics*, Vol. 54, No. 5, pp. 470–472.

Desloge, E. A., 1986b, "Relationship between Kane's equations and the Gibbs-Appell equations," *J. Guidance, Control, and Dynamics*, Vol. 10, No. 1, pp. 120–122.

Dillmann, R., and Rembold, U., 1985, "Autonomous robot of the University of Karlsruhe," *Proc. of the 15th Int. Sym· on Industrial Robots*, Tokyo, Japan, Sept. 11 13, Vol. 1, pp. 91–102.

Dix, R. C., and Lehman, T. J., 1: "Simulation of the dynamics of machinery," *Trans. of the ASME, J. of Eng · for Industry*, May, pp. 433–438.

Dobrjanskyj, L., and Freudenstein, F., 1967, "Some applications of graph theory to the structural analysis of mechanisms," *Trans of the ASME, J. of Engineering for Industry*, Vol. 89, No 1, pp. 153–158.

Dolapchiev, B., 1969, "Reduction of Neilsen's equations for nonholonomic systems to Čaplygin's equation," *J. of Applied Mathematics and Mechanics*, Vol. 33, No. 5, pp. 916 917.

Euler, L., 1776, "Nova methodus motum corporum rigidorum determinandi," *Novi Comentarii Academiæ Scientiarum Petropolitanæ*, 20 (1775) 1776, pp. 208–238; *Opera Omnia*, Vol. 2, No. 9, pp 99–125.

Gear, C W., and Petzold, L. R., 1984, "ODE methods for the solution of differential/algebraic systems," *SIAM J. of Numerical Analysis*, Vol. 21, No. 4, pp. 716 728.

Gibbs, J. W., 1879, "On the fundamental formulae of dynamics," *American J of Mathematics*, Vol. II, pp. 49–64.

Gibbs, J. W., 1961, *The Scientific Papers of J.W. Gibbs*, Dover Publications, Inc., New York.

Gill, P., Murray, W., and Wright, M., 1981, *Practical Optimization*, Academic Press, Inc., New York.

Ginsberg, J. H., 1988, *Advanced Engineering Dynamics*, Harper & Row, Publishers, New York.

Goldfarb, D., and Idnani, A., 1983, "A numerically stable dual method for solving strictly convex quadratic programs," *Mathematical Programming*, Vol. 27, pp. 1–33

Golub, G. H., and Van Loan, C. F., 1983, *Matrix Computations*, John Hopkins University Press, Baltimore.

Gosselin, C., 1988, *Kinematic Analysis, Optimization and Programming of Parallel Robotic Manipulators*, June, a Ph.D thesis submitted to the Dept of Mech. Eng., McGill University, Montreal, Canada

Greenwood, D. T., 1977, *Classical Dynamics*, Prentice-Hall, Inc., New Jersey

Hammond, G., 1986, *AGVS at Work*, IFS Ltd., UK and Springer-Verlag, New York

Harary, F., 1969, *Graph Theory*, Addison-Wesley Publishing Co., Inc., New York

Hemami, H., and Weimer, F. C., 1981, "Modeling of nonholonomic dynamic systems with applications," *Trans. of the ASME, J. of Applied Mechanics*, Vol. 48, March, pp. 177–182.

Hiller, M., and Schmitz, T., 1990, "Kinematics and dynamics of the combined wheeled and legged vehicle RoboTRAC," *Canadian Soc of Mech. Eng. Forum*, Toronto, Canada, June, pp. 387–392.

Hirose, S., and Morishima, A., 1990, "Design and control of a mobile robot with an articulated body," *Int J. of Robotics Research*, Vol. 9, No. 2, pp. 99–114.

Huston, R. L., and Passerello, C. E., 1974, "On constraint equations – a new approach," *Trans. of the ASME*, Vol. 96, *ASME J. of Applied Mechanics*, Vol. 41, pp. 1130–1131.

Huston, R. L., Passerello, C. E., and Harlow, M. W., 1978, "Dynamics of multirigid-body systems," *Trans. of the ASME, J. of Applied Mechanics*, Vol. 45, Dec., pp. 889–894.

Huston, R. L., and Passerello, C. E., 1979, "On multi-rigid-body system dynamics,"

Computers & Structures, Vol. 10, No. 3, pp. 439–446.

Huston, R. L., and Passerello, C. E., 1980, "Multibody structural dynamics including translation between the bodies," *Computers & Structures*, Vol. 12, No. 5, pp. 713–720.

Iijima, J., Yuta, S., and Kanayama, Y., 1981, "Elementary functions of a self-contained robot YAMABICO 3.1," *Proc. of the 11th Int. Symp. on Industrial Robots*, Tokyo, Japan, Oct. 7-9, pp. 211–218.

IMSL, 1980, *User's Manual: IMSL Math Library*, IMSL, Inc., Houston, Texas.

IMSL, 1990a, *User's Manual: IMSL Math Library*, Vol. 3, IMSL, Inc., Houston, Texas.

IMSL, 1990b, *User's Manual: IMSL Math Library*, Vol. 2, IMSL, Inc., Houston, Texas.

Ince, E.L., 1956, *Ordinary Differential Equations*, Dover Publication, Inc., New York.

Isidori, A., 1985, *Nonlinear Control Systems: An Introduction.* Lecture notes in control and information sciences, Springer-Verlag, New York.

Jonsson, S, 1985, "New AGV with revolutionary movement," *Proc. of the 3rd Int. Conf. on Automated Guided Vehicles*, Stockholm, Sweden, Oct. 15–17, pp. 135–144.

Kailath, T., 1980, *Linear Systems*, Prentice-Hall, Inc., New Jersey.

Kajiwara, T., Yamaguchi, J., Kanayama, Y., Yuta, S., Iijima, J., Imasato, K., and Uehara, T., 1985, "Development of a mobile robot for security guard," *Proc. of the 15th Int. Symp. on Industrial Robots*, Tokyo, Japan, Sept. 11–13, Vol. 1, pp. 271–278.

Kamman, J. W., and Huston, R. L., 1984, "Dynamics of constrained multibody systems," *Trans. of the ASME, J. of Applied Mechanics*, Vol. 51, Dec., pp. 899–903.

Kane, T. R., 1961, "Dynamics of nonholonomic systems," *Trans. of the ASME*, Vol. 83, *ASME J. of Applied Mechanics*, Vol. 28, pp. 574–578.

Kane, T. R., and Wang, C. F., 1965, "On the derivation of equations of motion," *J. of the SIAM*, Vol. 13, No. 2, pp. 487–492.

Kane, T. R., 1968, *Dynamics*, Holt, Rinehart and Winston, New York.

Kane, T. R., 1983, "Formulation of dynamical equations of motion," *American Journal of Physics*, Vol. 51, No. 11, pp. 974-977.

Kane, T. R., and Levinson, D. A., 1983, "The use of Kane's dynamical equations in robotics," *Int. J. of Robotics Research*, Vol. 2, No. 3, pp 3 21.

Kane, T. R., and Levinson, D. A., 1985, *Dynamics: Theory and Applications*, McGraw-Hill, New York.

Kangari, R., and Yoshida, T., 1990, "Automation in construction," *Robotics and Autonomous Systems*, Vol. 6, No. 4, pp 327 335.

Khalil, W., Kleinfinger, J. F., and Gauter, M., 1986, "Reducing the computational burden of the dynamic models of robots," *Proc. of the IEEE Conf on Robotics & Automation*, San Francisco, Calfornia, April 7 10, Vol. 1, pp. 525 531

Kim, S. S., and Vanderploeg, M. J., 1986, "QR decomposition for state space representation of constrained mechanical dynamic systems," *Trans of the ASME, J of Mechanisms, Transmissions, and Automation in Design*, Vol 108, June, pp 183 188.

Lee, C. S. G., and Chang, P. R., 1986, "Efficient parallel algorithm for robot inverse dynamics computation," *Proc. of the IEEE Conf. on Robotics & Automation*, San Francisco, Calfornia, April 7 10, Vol. 2, pp. 525 531.

Levinson, D. A., 1987, "Comment on relationship between Kane's equations and the Gibbs-Appell equations," *J. of Guidence, Control and Dynamics*, Vol. 1, No. 1, p 593.

Liang, C. G., and Lance, G. M., 1987, "A differentiable null space method for constrained dynamic analysis," *Trans. of the ASME, J. of Mechanisms, Transmissions, and Automation in Design*, Vol. 109, Sept., pp. 105 111.

Lindauer, B., and Hill, J. D., 1985, "Military robotics: an overview," *Robotics Age*, Nov., pp. 16-21.

Luh, J. Y. S., Walker, M. W., and Paul, R. P. C., 1980, "On-line computational scheme for mechanical manipulators," *Trans. of the ASME, J. of Dynamic Systems, Measurement, and Control*, Vol. 102, June, pp. 69 767.

Ma, O., and Angeles, J., 1989, "Direct kinematics and dynamics of a planar three-dof parallel manipulator," *Advances in Design Automation, Proc. of the 15th Design Automation Conf*, Montreal, Canada, Sept., pp. 313 320.

MACSYMA, 1983, *Reference Manual*, Vol. 1, MIT, Cambridge, Massachusetts.

Maggi, G. A., 1901, "Di alcune nuove forme delle equazioni della dinamica, applicabili ai sistemi anolonomi," *Atti Accad. Naz. Lincei Rend Cl. Fis. Mat. Nat.*, Vol. 10, No. 5, pp. 287-291.

Maki, H., 1985, "The concept of the advanced robot for nuclear power plants," *Proc. of the Int. Conf. on Advanced Robotics*, Tokyo, Japan, Sept. 9-10, pp. 497-505.

Mani, N. K., Haug, E. J., and Atkinson, K. E., 1985, "Application of singular value decomposition for analysis of mechanical system dynamics," *Trans. of the ASME. J. of Applied Mechanics*, Vol. 107, March, pp. 82-87.

Meieran, H. B., and Gelhaus, F. E., 1986, "Mobile robots designed for hazardous environments," *Robotics Engineering*, March, pp. 10-16.

Meirovitch, L., 1970, *Methods of Analytical Dynamics*, McGraw-Hill, New York.

Moravec, H. P., 1983, "The Stanford cart and the CMU rover," *Proc. of the IEEE*, Vol. 71, No. 7, pp. 872-884.

Muir, P. F., and Neuman, C. P., 1987a, "Kinematic modeling of wheeled mobile robots," *J. of Robotic Systems*, Vol. 4, No. 2, pp. 281-340.

Muir, P. F., and Neuman, C. P., 1987b, "Kinematic modeling for feedback control of an omnidirectional wheeled mobile robot," *Proc. of the IEEE Conf. on Robotics & Automation*, Raleigh, North Carolina, March 31-April 3, Vol. 3, pp. 1772-1778.

Muir, P. F., and Neuman, C. P., 1988, "Dynamic modeling of multibody robotic mechanisms. incorporating closed-chains, friction, higher-pair joints, and unactuated and unsensed joints," *Proc. of the IEEE Conf. on Robotics & Automation*, Philadelphia, Pennsylvania, April 24-29, Vol. 3, pp. 1546-1551.

Nahon, M., 1990, *Optimization of Force Distribution in Redundantly-Actuated Robotic Systems*, Dec., a Ph D thesis submitted to the Dept. of Mech. Eng., McGill University, Montreal, Canada.

Nakamura, Y., and Mukherjee, R., 1990, "Nonholonomic path planning of space robots via bi-directional approach," *Proc. of the IEEE Conf. on Robotics & Automation*, Cincinnati, Ohio, May 13-18, Vol. 3, pp. 1764-1769.

Nakano, E. Arai, T., Yamaba, K., Hashino, S., Ono, T., and Ozaki, S., 1981, "First approach to the development of the patient care robot," *Proc. of the 11th Int. Symp. on Industrial Robots*, Tokyo, Japan, Oct. 7-9, pp. 87-94.

Neĭmark, Ju. I., and Fufaev, N. A., 1967, *Dynamics of Nonholonomic Systems* (in Russian), Translated version in English, 1972, American Mathematical Society, Providence, Rhode Island.

Papastavridis, J. G., 1988, "On the nonlinear Appell's equations and the determination of generalized reaction forces," *Int. J. of Engineering Science*, Vol. 26, No. 6, pp. 609-625.

Papastavridis, J. G., 1990, "Maggi's equations of motion and the determination of constraint reactions," *J. Guidance, Control, and Dynamics*, Vol. 13, No. 2, pp 213-220.

Park, T. W., and Haug, E. J., 1986, "A hybrid numerical integration method for machine dynamic simulation," *Trans. of the ASME, J. of Mechanisms, Transmissions, and Automation in Design*, Vol. 108, June, pp 211-216

Passerello, C. E., and Huston, R. L., 1973, "Another look at nonholonomic systems," *Trans. of the ASME, J. of Applied Mechanics*, March, pp. 101-104.

Poole, H. H., 1989, *Fundamentals of Robotics Engineering*, Van Nostrand Reinhold, New York.

Premi, S. K., and Besant, C. B., 1983, "A review of various vehicle guidance techniques that can be used by mobile robots or AGVS," *Proc. of the 2nd Int. Conf. on Automated Guided Vehicles*, Stuttgart, Germany, June 7-9, pp. 195-209

Rajagopalan, R., and Huard, G., 1989, "System report on CONCIC-2 AGV: design, control and theory of operation," *Internal Report No. CIC-0024*, Centre for Industrial Control, Concordia University, Montreal, Canada

Rao, C. R., and Mitra, S. K., 1971, *Generalized Inverse of Matrices and Its Application*, John Wiley & Sons Inc., New York.

Rothbart, H. A., 1956, *CAMS: Design, Dynamics, and Accuracy*, John Wiley & Sons, Inc., New York.

Rudin, W., 1976, *Principles of Mathematical Analysis*, McGraw-Hill, Inc., New York

Saha, S. K., and Angeles, J., 1989, "Kinematics and dynamics of 3-wheeled 2-DOF AGV," *Proc. of the IEEE Conf. on Robotics & Automation*, Scottsdale, Arizona, May 14-19, Vol. 3, pp. 1572-1577

Saha, S. K., and Angeles, J., 1991a "Dynamics of nonholonomic mechanical systems using a natural orthogonal complement," *Trans. of the ASME, J. of Applied Mechanics*, Vol. 58, March, pp. 238-243.

Saha, S. K., and Angeles, J., 1991b, "The mathematics of motion simulation, a case study," to appear in the *Int. J. of Mathematical & Computer Modelling*

Saha, S. K., and Angeles, J., 1991c, "On the formulation of linear homogeneous velocity constraints in mechanical systems," *Proc. of the 13th Canadian Congress of Applied Mechanics*, University of Manitoba, Winnipeg, Canada, June 2-6, Vol. 2, pp. 658-659.

Saha, S.K., and Angeles, J., 1991d, "The formulation of kinematic constraints in

design-oriented machine dynamics," to appear in the *Proc. of ASME Conf. on Design Automation*, Miami, Florida, Sept. 22–25.

Samson, C., and Ait-Abderrahim, K., 1991, "Feedback control of a nonholonomic wheeled cart in Cartesian space," *Proc. of the IEEE Conf. on Robotics & Automation*, Sacramento, California, Vol. 2, pp. 1136–1141.

Saito, M., Tanaka, N., Arai, K., and Banno, K., 1985, "The development of a mobile robot for concrete slab finishing," *Proc. of the 15th Int. Symp on Industrial Robots*, Tokyo, Japan, Sept. 11-13, Vol 1, pp. 71–78.

Schaechter, D. B., Levinson, D. A., and Kane, T.R., 1988, *AUTOLEV User's manual*, OnLine Dynamics, Inc., Sunnyvale, California.

Sheth, P. N., and Uicker, J. J Jr., 1972, "IMP (Integrated mechanisms program): a computer-aided design analysis system for mechanisms and linkages," *Trans. of the ASME, J. of Engineering for Industry*, May, pp 454-464

Singh, R. P., and Likins, P. W., 1985, "Singular value decompositions for constrained dynamical systems," *Trans. of the ASME, J. of Applied Mechanics*, Vol. 52, Dec., pp. 943-948.

Spiegel, N R., 1985, *Applied Differential Equations*, Prentice-Hall, Inc., New Jersey.

Stewart, G. E , 1973, *Introduction to Matrix Computations*, Academic Press, Inc., New York.

Tachi, S., Komoriya K., Tanie, K., Ohno, T., and Abe, M., 1981, "Guide dog robot—feasibility experiments with MELDOG MARK III," *Proc of the 11th Int. Symp. on Industrial Robots*, Tokyo, Japan, Oct. 7 9, pp. 95-102

Tanaka, N., 1985, "The concept of the advanced robot for support of offshore oil exploration," *Proc. of the Int. Conf. on Advanced Robotics*, Tokyo. Japan, Sept. 9-10, pp. 507-511.

Tsumura, T., 1986, "Survey of automated guided vehicle in Japanese factory," *Proc. of the IEEE Conf. on Robotics & Automation*, San Francisco, California, April 7–10, Vol. 2, pp. 1329-1334.

Vidyasagar, M., 1978, *Nonlinear Systems Analysis*, Prentice-Hall, Inc., New Jersey.

Volterra, V., 1898, "Sopra una classe di equazione dinamiche," *Atti Accad. Sci. Torino*, Vol. 33, pp. 451–475, errata, ibid. Vol. 35 (1899), p. 118.

Voronec, P. V., 1901, "On the equations of motion for nonholonomic systems" (in Russian), *Mat. Sb.*, Vol. 22, pp. 659–686.

Walker, M. W., and Orin, D. E., 1982, "Efficient dynamic computer simulation of

robotic mechanisms," *Trans. of the ASME, J. of Dynamic Systems, Measurement, and Control*, Vol. 104, Sept., pp. 205–211.

Waldron, K. J., 1985, "Mobility and controllability characteristics of mobile robotic platforms," *Proc. of the IEEE Conf. on Robotics & Automation*, St. Louis, Missouri, Vol. 1, pp. 237–243.

Wehage, R. A., and Haug, E. J., 1982, "Generalized coordinate partitioning for dimension reduction in analysis of constrained dynamic systems," *Trans. of the ASME, J. of Mechanical Design*, Vol. 104, Jan., pp. 247–255.

Appendix A

Basic Derivations

A.1 Reduction of Matrix $\mathbf{A}_h$

From eq.(3.8), matrix $\mathbf{A}_h$ is given as

$$\mathbf{A}_h = \begin{bmatrix} \mathbf{E}_t & \mathbf{O} & -\mathbf{E}_t & \mathbf{O} \\ \mathbf{R}_t & \mathbf{1} & \mathbf{B}_{t-1} & -\mathbf{1} \end{bmatrix} \tag{A.1}$$

Now, obvious elementary operations are performed on matrix $\mathbf{A}_h$ that do not perturb its rank, i.e.,

$$\text{rank}\left(\begin{bmatrix} \mathbf{E}_t & \mathbf{O} & -\mathbf{E}_t & \mathbf{O} \\ \mathbf{R}_t & \mathbf{1} & \mathbf{B}_{t-1} & -\mathbf{1} \end{bmatrix}\right) = \text{rank}\left(\begin{bmatrix} \mathbf{E}_t & \mathbf{O} & -\mathbf{E}_t & \mathbf{O} \\ \mathbf{R}_t & \mathbf{1} & \mathbf{B}_{t-1} & \mathbf{O} \end{bmatrix}\right) = \tag{A.2}$$

$$\text{rank}\left(\begin{bmatrix} \mathbf{E}_t & \mathbf{O} & \mathbf{O} & \mathbf{O} \\ \mathbf{R}_t & \mathbf{1} & \mathbf{B}_{t-1}+\mathbf{R}_t & \mathbf{O} \end{bmatrix}\right) = \text{rank}\left(\begin{bmatrix} \mathbf{E}_t & \mathbf{O} & \mathbf{O} & \mathbf{O} \\ \mathbf{R}_t & \mathbf{1} & \mathbf{O} & \mathbf{O} \end{bmatrix}\right) = \tag{A.3}$$

$$\text{rank}\left(\begin{bmatrix} \mathbf{E}_t & \mathbf{O} & \mathbf{O} & \mathbf{O} \\ \mathbf{O} & \mathbf{1} & \mathbf{O} & \mathbf{O} \end{bmatrix}\right) \tag{A.4}$$

and hence, the rank of matrix $\mathbf{A}_h$ is equal to the rank of the 6×6 matrix $\mathbf{A}_h^r$, as obtained from eq.(A.4), namely,

$$\mathbf{A}_h^r = \begin{bmatrix} \mathbf{E}_t & \mathbf{O} \\ \mathbf{O} & \mathbf{1} \end{bmatrix} \tag{A.5}$$

A.2 Reduction of Matrix $\mathbf{A}_n$

From eq.(3.10), matrix $\mathbf{A}_n$ is given by

$$\mathbf{A}_n = [\mathbf{R}_i \quad \mathbf{1} \quad \mathbf{B}_{i-1} \quad -\mathbf{1}] \tag{A.6}$$

Elementary operations are performed on matrix $\mathbf{A}_n$ as

$$\begin{aligned} \text{rank}([\mathbf{R}_i \quad \mathbf{1} \quad \mathbf{B}_{i-1} \quad -\mathbf{1}]) = \text{rank}([\mathbf{R}_i \quad \mathbf{1} \quad \mathbf{B}_{i-1} \quad \mathbf{O}]) = \\ \text{rank}([\mathbf{R}_i \quad \mathbf{1} \quad \mathbf{O} \quad \mathbf{O}]) = \text{rank}([\mathbf{O} \quad \mathbf{1} \quad \mathbf{O} \quad \mathbf{O}]) \end{aligned} \tag{A.7}$$

and hence, the rank of matrix $\mathbf{A}_n$ is equal to the rank of the 3×3 identity matrix $\mathbf{1}$.

A.3 Eigenvalues of tensor $\mathbf{E}_i$

First, the cross-product tensor $\mathbf{E}_i$, associated with a unit vector $\mathbf{e}_i$ is defined by

$$\mathbf{E}_i \equiv \frac{\partial(\mathbf{e}_i \times \mathbf{x})}{\partial \mathbf{x}} \equiv \mathbf{e}_i \times \mathbf{1} \tag{A.8}$$

for an arbitrary 3-dimensional vector $\mathbf{x}$. Then, a proof of $\mathbf{E}_i^3 = -\mathbf{E}_i$, is given, which will be used to calculate the eigenvalues of $\mathbf{E}_i$.

Proof: Referring to the definition of $\mathbf{E}_i$, eq.(A.8), for an arbitrary 3-dimensional vector $\mathbf{x}$,

$$\begin{aligned} \mathbf{E}_i^2\mathbf{x} &\equiv (\mathbf{e}_i \times \mathbf{1})[(\mathbf{e}_i \times \mathbf{1})\mathbf{x}] \\ &\equiv (\mathbf{e}_i \times \mathbf{1})(\mathbf{e}_i \times \mathbf{x}) \\ &\equiv \mathbf{e}_i \times (\mathbf{e}_i \times \mathbf{x}) \end{aligned} \tag{A.9}$$

Furthermore, eq.(A.9) can be written as

$$\begin{aligned} \mathbf{E}_i^2\mathbf{x} &\equiv \mathbf{e}_i \times (\mathbf{e}_i \times \mathbf{x}) \\ &\equiv (\mathbf{e}_i^T\mathbf{x})\mathbf{e}_i - (\mathbf{e}_i^T\mathbf{e}_i)\mathbf{x} \\ &\equiv (\mathbf{e}_i \otimes \mathbf{e}_i)\mathbf{x} - \mathbf{x} \\ &\equiv -(\mathbf{1} - \mathbf{e}_i \otimes \mathbf{e}_i)\mathbf{x} \end{aligned} \tag{A.10}$$

where $\oslash$ denotes the *tensor product* of the two vectors beside it, which can also be expressed as

$$\mathbf{e}_i \oslash \mathbf{e}_i \equiv \mathbf{e}_i\mathbf{e}_i^T$$

Now, the tensor $\mathbf{E}_i^3$ is obtained as follows:

$$\begin{aligned}\mathbf{E}_i^3 &\equiv \mathbf{E}_i^2\mathbf{E}_i \\ &\equiv -(\mathbf{1} - \mathbf{e}_i \otimes \mathbf{e}_i)(e_i \times \mathbf{1}) \\ &\equiv -\mathbf{e}_i \times \mathbf{1} + (\mathbf{e}_i \oslash \mathbf{e}_i)(\mathbf{e}_i \times \mathbf{1})\end{aligned} \tag{A.11}$$

For any arbitrary vector $\mathbf{x}$, the expression $(\mathbf{e}_i \otimes \mathbf{e}_i)(\mathbf{e}_i \times \mathbf{1})\mathbf{x}$ is given by

$$(\mathbf{e}_i \otimes \mathbf{e}_i)(\mathbf{e}_i \times \mathbf{1})\mathbf{x} \equiv (\mathbf{e}_i \otimes \mathbf{e}_i)(\mathbf{e}_i \times \mathbf{x}) \equiv \mathbf{e}_i\mathbf{e}_i^T(\mathbf{e}_i \times \mathbf{x}) \tag{A.12}$$

According to the definition of vector cross product, vector $(\mathbf{e}_i \times \mathbf{x})$ is orthogonal to vector $\mathbf{e}_i$, and hence, $(\mathbf{e}_i \otimes \mathbf{e}_i)(\mathbf{e}_i \times \mathbf{x})$ vanishes. Thus, since $\mathbf{x}$ is arbitrary $(\mathbf{e}_i \otimes \mathbf{e}_i)(\mathbf{e}_i \times \mathbf{1})$ vanishes and eq.(A.11) then reduces to

$$\mathbf{E}_i^3 = -\mathbf{e}_i \times \mathbf{1} = -\mathbf{E}_i \tag{A.13}$$

To obtain the eigenvalues of $\mathbf{E}_i$, let λ and $\mathbf{y} \neq \mathbf{0}$ be an eigenvalue and the associated eigenvector of $\mathbf{E}_i$, respectively, i.e.,

$$\mathbf{E}_i\mathbf{y} = \lambda\mathbf{y} \tag{A.14}$$

Premultiplying both sides of eq.(A.14) by $\mathbf{E}_i$ yields

$$\mathbf{E}_i^2\mathbf{y} = \lambda\mathbf{E}_i\mathbf{y} = \lambda^2\mathbf{y} \tag{A.15}$$

Repeating the same operation gives

$$\mathbf{E}_i^3\mathbf{y} = \lambda\mathbf{E}_i^2\mathbf{y} = \lambda^3\mathbf{y} \tag{A.16}$$

From eq.(A.13), $\mathbf{E}_i^3 = -\mathbf{E}_i$, and hence, the left-hand side of eq.(A.16) can be substituted by $-\mathbf{E}_i\mathbf{y}$ which results in

$$-\mathbf{E}_i\mathbf{y} = \lambda^3\mathbf{y} \tag{A.17}$$

Using eq.(A.14), eq.(A.17) is rewritten as

$$-\lambda \mathbf{y} = \lambda^3 \mathbf{y}$$

or

$$\lambda(\lambda^2 + 1)\mathbf{y} = \mathbf{0} \tag{A.18}$$

and, since $\mathbf{y} \neq \mathbf{0}$, eq.(A.18) leads to

$$\lambda(\lambda^2 + 1) = 0$$

which thus produces the three eigenvalues of tensor $\mathbf{E}_i$, namely,

$$\lambda = 0, \quad \sqrt{-1} \quad \text{and} \quad -\sqrt{-1} \tag{A.19}$$

A.4 Kane's Equations of Motion of a Two-Wheeled Mechanical System

Let two independent generalized coordinates be θ_1 and θ_2, as shown in Fig. 4.1. According to the methodology described in §2.2.6, matrix $\mathbf{U}_q$ and vector $\mathbf{q}'$ are assumed to be the 2×2 identity matrix and the 2-dimensional zero vector, respectively. Thus, $\dot{\mathbf{q}} = \dot{\boldsymbol{\theta}}_I$. The angular velocity and the velocity of the mass centre of the left wheel, i.e., body 1, are given in eq.(4.25) which yields

$$\mathbf{V}_1^{\omega} = [\mathbf{i} + \eta\mathbf{k} \quad -\eta\mathbf{k}] \quad \text{and} \quad \mathbf{V}_1^{c} = [-r\mathbf{j} \quad \mathbf{0}] \tag{A.20}$$

where $\boldsymbol{V}_1^{\omega}$ and $\boldsymbol{V}_1^{c}$ are the 3×2 matrices consisting of partial angular velocities and partial velocities of body 1, respectively. Similar expressions for the right wheel and the axle can be found which, when combined with eq.(A.20), lead to,

$$\mathbf{V} = \begin{bmatrix} \mathbf{i} + \eta\mathbf{k} & -\eta\mathbf{k} \\ -r\mathbf{j} & \mathbf{0} \\ \eta\mathbf{k} & \mathbf{i} - \eta\mathbf{k} \\ \mathbf{0} & -r\mathbf{j} \\ \eta\mathbf{k} & -\eta\mathbf{k} \\ -(r/2)\mathbf{j} & -(r/2)\mathbf{j} \end{bmatrix} \tag{A.21}$$

Note that matrix $\mathbf{V}$ of eq.(A.21) is the same as the NOC matrix of the system, i.e., $\mathbf{T}$ of eq.(4.28), which is due to the definition of the twist of the rigid body in Kane's

formulation, as in eq.(2.39) where $\mathbf{v}_t = \mathbf{0}$. Now, according to the definition of the generalized active and inertia forces of Kane's equations, eq.(2.41), the generalized active force is the same as the left-hand side of eq.(3.17), whereas the generalized inertia force is nothing but the right-hand side of eq.(3.17).

A.5 Symbolic Derivations of Inertia Terms

The symbolic equations of motion of a 3-wheeled 2-DOF AGV are derived using MACSYMA, symbolic manipulation software. The mass of the fork (body 4) connecting the caster wheel assembly with the platform is assumed to be negligible. Moreover, the platform is considered as a thin plate in the form of an equilateral triangle whose vertices are at a distance b from the centroid. Matrices $\mathbf{I}$ and $\mathbf{C}$ are now calculated based on the scheme given in §3.3, namely,

$$\mathbf{I} \equiv \begin{bmatrix} I_{11} & I_{12} \\ I_{21} & I_{22} \end{bmatrix} \quad \text{and} \quad \mathbf{C} \equiv \begin{bmatrix} C_{11} & C_{12} \\ C_{21} & C_{22} \end{bmatrix} \tag{A.22}$$

One of the simplest elements of matrix $\mathbf{I}$, I_{11}, is as follows:

$$\begin{aligned} I_{11} = {} & \frac{m_w[lr\sin 2\theta_4 - 4(a+b)r\sin^2\theta_4]^2}{16l^2} + \frac{m_w[(a+b)r\sin 2\theta_4 - lr\cos^2\theta_4]^2}{4l^2} \\ & + \frac{m_w r^2(1+\sin^2\theta_4)[l\sin 2\theta_4 - 4(a+b)\sin^2\theta_4]^2}{64l^2} \\ & + \frac{m_w r^2(1+\cos^2\theta_4)[(a+b)\sin 2\theta_4 - l\cos^2\theta_4]^2}{16l^2} \\ & - \frac{m_w r^2\sin 2\theta_4\sin^2\theta_4(a+b)[l\sin 2\theta_4 - 4(a+b)\sin^2\theta_4]}{32l^2} \\ & + \frac{m_w r^2[-lr\sin\theta_4 - 2(a+b)r\cos\theta_4]^2}{16d^2l^2} \\ & + \frac{m_w r^4}{2l^2} + \frac{mb^2r^2}{4l^2} + \frac{ma^2r^2}{l^2} + \frac{mr^2}{4} + \frac{3m_w r^2}{2} \end{aligned} \tag{A.23}$$

and one of the simplest elements of matrix $\mathbf{C}$, C_{12}, is

$$\begin{aligned} C_{12} = {} & -mr^3[l\sin\theta_4 + 2(a+b)\cos\theta_4]\{\frac{\dot\theta_3[l\sin 2\theta_4 + 4(a+b)\sin^2\theta_4]}{32l^2d} \\ & + \frac{r(\dot\theta_4+\dot\psi)[-2(a+b)\sin\theta_4 - l\cos\theta_4]}{16l^2d^2} + \frac{r\cos\theta_4[l\dot\psi - 2d(\dot\theta_4+\dot\psi)\sin\theta_4]}{16l^2d^2} \\ & + \frac{r\sin[d(\dot\theta_4+\dot\psi)\cos\theta_4 + \dot\psi(a+b)]}{8l^2d^2}\} + mr^2[l\sin 2\theta_4 - 4(a+b)\sin^2\theta_4] \end{aligned}$$

$$
\begin{aligned}
&\{\frac{r\dot{\theta}_3[l\sin\theta_4-2(a+b)\cos\theta_4]}{32l^2d}+\frac{r\sin^2\theta_4[l\dot{\psi}-2d(\dot{\theta}_4+\dot{\psi})\sin\theta_4]}{32l^2r}\\
&-\frac{\sin\theta_4\cos\theta_4[d(\dot{\theta}_4+\dot{\psi})\cos\theta_4+(a+b)\dot{\psi}]}{16l^2}\\
&-\frac{(\dot{\theta}_4+\dot{\psi})\sin\theta_4[l\sin\theta_4-2(a+b)\cos\theta_4-2d]}{32l^2}\\
&+\frac{(\dot{\theta}_4+\dot{\psi})\cos\theta_4[2(a+b)\sin\theta_4+l\cos\theta_4]}{32l^2}+\frac{(\dot{\theta}_4+\dot{\psi})[(a+b)\sin 2\theta_4+l\cos^2\theta_4]}{16l^2}\}\\
&-mr^2[(a+b)\sin 2\theta_4-l\cos^2\theta_4]\{\frac{r\sin\theta_4\cos\theta_4[l\dot{\psi}-2d(\dot{\theta}_4+\dot{\psi})\sin\theta_4]}{8l^2r}\\
&-\frac{\cos^2\theta_4[d(\dot{\theta}_4+\dot{\psi})\cos\theta_4+(a+b)\dot{\psi}]}{4l^2}\\
&-\frac{(\dot{\theta}_4+\dot{\psi})\cos\theta_4[l\sin\theta_4-2(a+b)\cos\theta_4-2d]}{8l^2}\\
&-\frac{(\dot{\theta}_4+\dot{\psi})\sin\theta_4[2(a+b)\sin\theta_4+l\cos\theta_4]}{8l^2}\\
&-\frac{(\dot{\theta}_4+\dot{\psi})[l\sin 2\theta_4+4(a+b)\sin^2\theta_4]}{32l^2}\}\\
&+m_wr^2[l\sin 2\theta_4-4(a+b)\sin^2\theta_4]\{\frac{\sin^2\theta_4[l\dot{\psi}-2d(\dot{\theta}_4+\dot{\psi})\sin\theta_4]}{8l^2r}\\
&-\frac{\sin\theta_4\cos\theta_4[d(\dot{\theta}_4+\dot{\psi})\cos\theta_4+(a+b)\dot{\psi}]}{4l^2}\\
&-\frac{(\dot{\theta}_4+\dot{\psi})\sin\theta_4[l\sin\theta_4-2(a+b)\cos\theta_4-2d]}{8l^2}\\
&+\frac{(\dot{\theta}_4+\dot{\psi})\cos\theta_4[2(a+b)\sin\theta_4+l\cos\theta_4]}{8l^2}\}+m_wr^2[(a+b)\sin 2\theta_4-l\cos^2\theta_4]\\
&\{\frac{-\cos\theta_4\sin\theta_4[l\dot{\psi}-2d(\dot{\theta}_4+\dot{\psi})\sin\theta_4]}{4l^2}+\frac{\cos^2\theta_4[d(\dot{\theta}_4+\dot{\psi})\cos\theta_4+(a+b)\dot{\psi}]}{2l^2}\\
&+\frac{(\dot{\theta}_4+\dot{\psi})\cos\theta_4[l\sin\theta_4-2(a+b)\cos\theta_4-2d]}{4l^2}\\
&+\frac{(\dot{\theta}_4+\dot{\psi})\sin\theta_4[2(a+b)\sin\theta_4+l\cos\theta_4]}{4l^2}\}-\frac{ma\dot{\psi}r^2}{l}
\end{aligned}
\tag{A.24}
$$

where the radius of the wheels r, l, a, b and d are shown in Fig. 4.5. Parameters m_w and m are the mass of each wheel and of the platform, respectively.

A.6 Steady-State Analysis of a Disk Rolling on a Plane

A steady state of a system is defined either as a constant state or as a periodic state, as time approaches infinity. In the case of a disk rolling on a plane, a steady state can be a circular motion of the disk, i.e., given certain initial conditions, the mass centre of the disk will trace a circle.

Thus, when the disk rolls in a circular trajectory, the generalized coordinates, Euler angles, and their time derivatives can be specified as

$$\begin{aligned} \theta &= \theta_s, \quad \dot{\theta} = 0, \quad \ddot{\theta} = 0 \\ \phi &= \dot{\phi}_0 t, \quad \dot{\phi} = \dot{\phi}_0, \quad \ddot{\phi} = 0 \\ \psi &= \dot{\psi}_0 t \quad \dot{\psi} = \dot{\psi}_0, \quad \ddot{\psi} = 0 \end{aligned} \tag{A.25}$$

where $\dot{\phi}_0$ and $\dot{\psi}_0$ are constant angular rates, which are specified in the initial conditions, whereas t denotes time. Now, the conditions in eq.(A.25) are substituted into the equations of motion, eq.(6.21). The last two scalar equations in eq.(6.21) are identically zero, while the first scalar equation gives

$$5\dot{\phi}_0^2 \sin\theta_s \cos\theta_s + 6\dot{\phi}_0\dot{\psi}_0 \cos\theta_s + \frac{4g}{r}\sin\theta_s = 0 \tag{A.26}$$

To solve the above equation for θ_s, the usual trigonometric identities are introduced, namely,

$$\sin\theta_s = \frac{2x}{1+x^2}, \quad \cos\theta_s = \frac{1-x^2}{1+x^2} \quad \text{and} \quad x = \tan\frac{\theta_s}{2}$$

Substituting for $\sin\theta_s$ and $\cos\theta_s$ into eq.(A.26), a quartic equation in x is obtained, namely,

$$x^4 + \gamma x^3 - \delta x - 1 = 0 \tag{A.27}$$

where

$$\gamma = \frac{5\dot{\phi}_0}{3\dot{\psi}_0} - \frac{4g}{3\dot{\phi}_0\dot{\psi}_0 r}, \qquad \delta = \frac{5\dot{\phi}_0}{3\dot{\psi}_0} + \frac{4g}{3\dot{\phi}_0\dot{\psi}_0 r}$$

Equation (A.27) was solved numerically resorting to the ZPOLR subroutine of the IMSL package which computes the zeros of a polynomial with real coefficients by Laguerre's method. Given the dimensions of the disk and the initial angular rates $\dot{\phi}_0$ and $\dot{\psi}_0$, eq.(A.27) is found to have two complex and two real roots Complex roots do not correspond to any physically attainable state θ_s, and hence, they are discarded. One of the two real roots led to an angle which was less than $-90°$, and was discarded as unfeasible. So, only one meaningful angle, θ_s, corresponding to the only remaining root x_s was considered for the steady-state analysis. Finally, θ_s was evaluated as

$$\theta_s = 2\tan^{-1} x_s$$

Solving for θ_s, the complete set of initial conditions for the steady state was obtained.

Appendix B

Dynamic Model of a Rolling Disk in Two Different Coordinate Frames

The equations of motion of a disk rolling on a plane are derived in the $\mathcal{D}$- and $\mathcal{I}$-frames that were introduced in Chapter 6. The orientation representation and the calculation of the position of the mass centre of the disk in the $\mathcal{D}$- and $\mathcal{I}$-frames are also discussed in this appendix.

B.1 A Disk-Fixed Frame

The $\mathcal{D}$-frame is defined as a coordinate frame which is rigidly attached to the disk, its origin being located at the centroid of the disk. Unlike the $\mathcal{F}$-frame, the $\mathcal{D}$-frame spins with the disk. Thus, the coordinate system $\mathcal{D}$ and the disk move with the same angular velocity. The unit vectors $\mathbf{d}_1$, $\mathbf{d}_2$ and $\mathbf{v}$, associated with this frame, shown in Fig. 1.1, are defined below:

- $\mathbf{d}_2$ is a unit vector rigidly fixed to the plane of the disk, directed from the centroid, C, of the disk to its periphery and is perpendicular to $\mathbf{v}$, as defined in §6.3.1.

- $\mathbf{d}_1$ is defined as the unit vector given below

$$\mathbf{d}_1 = \mathbf{d}_2 \times \mathbf{v}$$

If matrix $\mathbf{P}$ denotes the orientation of vector $\mathbf{r}$ in the $\mathcal{D}$-frame, i.e., if $\mathbf{P}$ denotes the relative orientation between the $\mathcal{F}$- and $\mathcal{D}$-frames, represented in the $\mathcal{D}$-frame, then $\mathbf{f}_2$ in the $\mathcal{D}$-frame is written as

$$[\mathbf{f}_2]_{\mathcal{D}} = [\mathbf{P}]_{\mathcal{D}}[\mathbf{f}_2]_{\mathcal{F}} \tag{B.1}$$

where $[\mathbf{P}]_{\mathcal{D}}$ is given as

$$[\mathbf{P}]_{\mathcal{D}} = \begin{bmatrix} c\psi & s\psi & 0 \\ -s\psi & c\psi & 0 \\ 0 & 0 & 1 \end{bmatrix} \tag{B.2}$$

Now, vector $\mathbf{r}$ in the $\mathcal{D}$-frame is

$$[\mathbf{r}]_{\mathcal{D}} = r[\mathbf{f}_2]_{\mathcal{D}} \tag{B.3}$$

It is to be noted that, due to the inertial axial symmetry of the disk, $\mathbf{I}_C$ has the same representation in the $\mathcal{F}$- and $\mathcal{D}$-frames, i.e., $[\mathbf{I}_C]_{\mathcal{D}} = [\mathbf{I}_C]_{\mathcal{F}}$. Therefore, matrix $\mathbf{I}$ in this frame can be obtained from eq.(6.5) as

$$[\mathbf{I}]_{\mathcal{D}} = [\mathbf{I}_C]_{\mathcal{F}} + mr^2(\mathbf{1} - [\mathbf{f}_2]_{\mathcal{D}} \otimes [\mathbf{f}_2]_{\mathcal{D}}) \tag{B.4}$$

In this frame the angular velocity of the coordinate frame is the same as the angular velocity of the disk, i.e., $[\boldsymbol{\sigma}]_{\mathcal{D}} = [\boldsymbol{\omega}]_{\mathcal{D}}$. Moreover, from Fig. 1.1 it is clear that $\dot{\psi}$ is the relative angular speed of $\mathcal{D}$ with respect to $\mathcal{F}$. Hence,

$$[\dot{\mathbf{r}}]_{\mathcal{D}} = -\dot{\psi}[\mathbf{v}]_{\mathcal{D}} \times [\mathbf{r}]_{\mathcal{D}} = -r\dot{\psi}[\mathbf{v}]_{\mathcal{F}} \times [\mathbf{f}_2]_{\mathcal{D}} \tag{B.5}$$

In the above expression, the identity $[\mathbf{v}]_{\mathcal{D}} = [\mathbf{v}]_{\mathcal{F}}$ is used, which is clear from Fig. 1.1. Moreover, $[\dot{\mathbf{I}}_C]_{\mathcal{D}} = [\dot{\mathbf{I}}_C]_{\mathcal{F}} = \mathbf{O}$, where $\mathbf{O}$ has been defined before as the 3×3 zero matrix. Using eqs.(B.3) and (B.5), matrix $[\mathbf{C}]_{\mathcal{D}}$ is given as

$$[\mathbf{C}]_{\mathcal{D}} = -[\boldsymbol{\omega}]_{\mathcal{D}} \times [\mathbf{I}_C]_{\mathcal{F}} + mr^2\{\dot{\psi}([\mathbf{v}]_{\mathcal{F}} \times [\mathbf{f}_2]_{\mathcal{D}}) \otimes [\mathbf{f}_2]_{\mathcal{D}} + [\boldsymbol{\omega}]_{\mathcal{D}}^T[\mathbf{f}_2]_{\mathcal{D}}([\mathbf{f}_2]_{\mathcal{D}} \times \mathbf{1})\} \tag{B.6}$$

whereas $\boldsymbol{\gamma}$ in the $\mathcal{D}$-frame is

$$[\boldsymbol{\gamma}]_{\mathcal{D}} = mr[\mathbf{f}_2]_{\mathcal{D}} \times ([\mathbf{D}]_{\mathcal{I}}^T[\mathbf{g}]_{\mathcal{I}})$$

where $[\mathbf{D}]_{\mathcal{I}}$ is the matrix representing the orientation of the $\mathcal{D}$-frame with respect to the inertial $\mathcal{I}$-frame, in the $\mathcal{I}$-frame.

Now, if Euler angles are taken as the generalized coordinates, then the dynamic equations appearing below are obtained:

$$[\mathbf{I}']_{\mathcal{D}}\ddot{\boldsymbol{\xi}} = [\mathbf{C}']_{\mathcal{D}}\dot{\boldsymbol{\xi}} + [\boldsymbol{\gamma}]_{\mathcal{D}} \tag{B.7}$$

where $[\mathbf{I}']_{\mathcal{D}} = [\mathbf{I}']_{\mathcal{F}}$, $[\mathbf{C}']_{\mathcal{D}} = [\mathbf{C}']_{\mathcal{F}}$ and $[\boldsymbol{\gamma}]_{\mathcal{D}} = [\boldsymbol{\gamma}]_{\mathcal{F}}$. Note that the generalized coordinates θ, ϕ and ψ are defined in such a way that their values do not depend on any choice of the coordinate frames. Hence, the equations of motion derived using Euler angles as the generalized coordinates are the same in both the $\mathcal{F}$- and $\mathcal{D}$-frames.

For animation purposes, the velocity of the centroid in the inertial frame $\mathcal{I}$ can be written as

$$[\dot{\mathbf{c}}]_{\mathcal{I}} = [\mathbf{D}]_{\mathcal{I}}[\dot{\mathbf{c}}]_{\mathcal{D}} \tag{B.8}$$

where

$$[\dot{\mathbf{c}}]_{\mathcal{D}} = [\boldsymbol{\omega}]_{\mathcal{D}} \times [\mathbf{r}]_{\mathcal{D}} = r[\boldsymbol{\omega}]_{\mathcal{D}} \times [\mathbf{f}_2]_{\mathcal{D}}$$

with matrix $[\mathbf{D}]_{\mathcal{I}}$ in terms of Euler angles being given by

$$[\mathbf{D}]_{\mathcal{I}} = \begin{bmatrix} c\phi c\psi - s\theta s\phi s\psi & -c\phi s\psi - s\theta s\phi c\psi & c\theta s\phi \\ s\phi c\psi + s\theta c\phi s\psi & -s\phi s\psi + s\theta c\phi c\psi & -c\theta c\phi \\ c\theta s\psi & c\theta c\psi & s\theta \end{bmatrix}$$

By virtue of the definition of Euler angles, as in Fig. 1.1, the expression in eq.(B.8) has the same form as that appearing in eq.(6.22). Alternatively, to obtain the orientation matrix $[\mathbf{D}]_{\mathcal{I}}$, either of the two differential equations can be integrated, namely,

$$[\dot{\mathbf{D}}]_{\mathcal{I}} = [\mathbf{D}]_{\mathcal{I}}[\boldsymbol{\Omega}]_{\mathcal{D}} \quad \text{or} \quad [\dot{\boldsymbol{\eta}}]_{\mathcal{I}} = [\boldsymbol{\Sigma}']_{\mathcal{I}}[\boldsymbol{\omega}]_{\mathcal{D}} \tag{B.9}$$

where $[\boldsymbol{\Omega}]_{\mathcal{D}}$ is $\boldsymbol{\Omega}$ represented in the $\mathcal{D}$-frame and $[\boldsymbol{\Sigma}']_{\mathcal{I}}$ is evaluated from the quadratic invariants of $[\mathbf{D}]_{\mathcal{I}}$. Furthermore, once $[\boldsymbol{\omega}]_{\mathcal{D}}$ is obtained by integrating eq.(6.4) in the

$\mathcal{D}$-frame, the term $\dot{\psi}$ appearing in eq.(B.6) is readily evaluated by writing eq.(6.26) in the $\mathcal{D}$-frame as

$$\dot{\psi} = ([\mathbf{v}]_{\mathcal{D}} - [\mathbf{f}_2]_{\mathcal{D}} \tan\theta)^T [\boldsymbol{\omega}]_{\mathcal{D}} = ([\mathbf{v}]_{\mathcal{F}} - [\mathbf{f}_2]_{\mathcal{D}} \tan\theta)^T [\boldsymbol{\omega}]_{\mathcal{D}} \tag{B.10}$$

Angles ψ and θ, as appearing in eqs.(B.2) and (B.10), respectively, can be computed geometrically or by integration of the differential equations, as indicated below:

- From Fig. 1.1,

$$\sin\psi = \frac{\mathbf{d}_2^T(\mathbf{k}\times\mathbf{v})}{||\mathbf{k}\times\mathbf{v}||} \quad \text{and} \quad \cos\psi = \frac{\mathbf{d}_1^T(\mathbf{k}\times\mathbf{v})}{||\mathbf{k}\times\mathbf{v}||} \tag{B.11}$$

  Also,

$$\sin\theta = \mathbf{k}^T\mathbf{v} \quad \text{and} \quad \cos\theta = \frac{\mathbf{k}^T[\mathbf{v}\times(\mathbf{k}\times\mathbf{v})]}{||\mathbf{v}\times(\mathbf{k}\times\mathbf{v})||} \tag{B.12}$$

  It is convenient to express the vectors of the above expressions, eqs.(B.11) and (B.12), in the $\mathcal{I}$-frame, where they have simple forms, as explained in §6.3.1.

- The differential equation for ψ appears in eq.(B.10), whereas the differential equation for θ is given below, i.e.,

$$\dot{\theta} = -[\mathbf{f}_1]_{\mathcal{D}}^T [\boldsymbol{\omega}]_{\mathcal{D}} \tag{B.13}$$

  where

$$[\mathbf{f}_1]_{\mathcal{D}} = [\mathbf{P}]_{\mathcal{D}} [\mathbf{f}_1]_{\mathcal{F}}$$

B.2 An Inertial Frame

As shown in Fig. 1.1, $\mathbf{i}, \mathbf{j}$ and $\mathbf{k}$ are defined as three unit vectors, parallel to the x_c, y_c and z_c axes, respectively. The evaluation of the expression for vectors $\mathbf{r}$ and $\dot{\mathbf{r}}$ in this frame is not as straightforward as in the $\mathcal{F}$- and $\mathcal{D}$-frames. It is described below how to obtain $\mathbf{r}$ and $\dot{\mathbf{r}}$: First, vector $\mathbf{f}_2$ is defined as

$$\mathbf{f}_2 \equiv \frac{\mathbf{v}\times(\mathbf{v}\times\mathbf{k})}{||\mathbf{v}\times(\mathbf{v}\times\mathbf{k})||} = \mathbf{B}\mathbf{v} \tag{B.14}$$

where $\mathbf{B}$ is the 3×3 matrix defined as

$$\mathbf{B} \equiv \frac{(\mathbf{v}^T\mathbf{k})\mathbf{1} - \mathbf{k} \otimes \mathbf{v}}{\sqrt{1 - (\mathbf{v}^T\mathbf{k})^2}} \tag{B.15}$$

while vectors $\mathbf{r}$ and $\dot{\mathbf{r}}$ are $r\mathbf{f}_2$ and $r\dot{\mathbf{f}}_2$, respectively. Upon differentiation of $\mathbf{f}_2$, eq.(B.14), we obtain

$$\dot{\mathbf{f}}_2 = \mathbf{N}\dot{\mathbf{v}} \tag{B.16}$$

with $\mathbf{N}$ given by

$$\mathbf{N} \equiv \frac{1}{\sqrt{1 - (\mathbf{v}^T\mathbf{k})^2}}[\mathbf{v} \otimes \mathbf{k} + (\mathbf{v}^T\mathbf{k})\mathbf{1} + \frac{(\mathbf{v}^T\mathbf{k})^2\mathbf{v} \otimes \mathbf{k} - (\mathbf{v}^T\mathbf{k})\mathbf{k} \otimes \mathbf{k}}{1 - (\mathbf{v}^T\mathbf{k})^2}] \tag{B.17}$$

Equations (B.14) and (B.16) can be readily obtained in the $\mathcal{I}$-frame by noting that $[\mathbf{k}]_\mathcal{I} = [0,\ 0,\ 1]^T$ and $[\mathbf{v}]_\mathcal{I}$ is the third column of the associated orthogonal matrix representing the orientation of the disk in the inertial frame, which is nothing but the orientation matrix $[\mathbf{D}]_\mathcal{I}$, as introduced in §B.1.

It is clear from eqs.(B.15) and (B.17) that matrices $\mathbf{B}$ and $\mathbf{N}$ are undefined when vectors $\mathbf{v}$ and $\mathbf{k}$ are parallel. It is also clear from Fig. 1.1 that vector $\mathbf{v}$ can be parallel to vector $\mathbf{k}$ only when the flat surface of the disk touches the plane on which the disk rolls, i.e., when the disk is no longer in its rolling motion. In this situation, the motion can be described as the disk moving on the plane. Now, it is straightforward to calculate $[\mathbf{r}]_\mathcal{I}$ and $[\dot{\mathbf{r}}]_\mathcal{I}$, required for the derivation of matrices $[\mathbf{I}]_\mathcal{I}$ and $[\mathbf{C}]_\mathcal{I}$, by writing eqs.(B.14) and (B.16) in the $\mathcal{I}$-frame and, hence, the inertia matrix is given as

$$[\mathbf{I}]_\mathcal{I} = [\mathbf{I}_C]_\mathcal{I} + mr^2(\mathbf{1} - [\mathbf{f}_2]_\mathcal{I} \otimes [\mathbf{f}_2]_\mathcal{I}) \tag{B.18}$$

where $[\mathbf{I}_C]_\mathcal{I}$ is $[\mathbf{D}]_\mathcal{I}[\mathbf{I}_C]_\mathcal{F}[\mathbf{D}]_\mathcal{I}^T$. Notice that, in the expression for $\dot{\mathbf{C}}$ in eq.(6.6), $[\boldsymbol{\sigma}]_\mathcal{I}$ vanishes, whereas $[\dot{\mathbf{I}}_C]_\mathcal{I}$ is $[\boldsymbol{\omega}]_\mathcal{I} \times [\mathbf{I}_C]_\mathcal{I}$. Therefore, matrix $[\mathbf{C}]_\mathcal{I}$ is obtained as

$$[\mathbf{C}]_\mathcal{I} = -[\boldsymbol{\omega}]_\mathcal{I} \times [\mathbf{I}_C]_\mathcal{I} + mr^2([\dot{\mathbf{f}}_2]_\mathcal{I} \otimes [\mathbf{f}_2]_\mathcal{I}) \tag{B.19}$$

and $[\boldsymbol{\gamma}]_\mathcal{I}$ is

$$[\boldsymbol{\gamma}]_\mathcal{I} = mr[\mathbf{f}_2]_\mathcal{I} \times [\mathbf{g}]_\mathcal{I} \tag{B.20}$$

With eqs.(B.18), (B.19) and (B.20), the equations of motion in the $\mathcal{I}$-frame are complete.

For animation purposes, the velocity of the centroid is given as

$$[\dot{\mathbf{c}}]_{\mathcal{I}} = r[\boldsymbol{\omega}]_{\mathcal{I}} \times [\mathbf{f}_2]_{\mathcal{I}}$$

and the orientation matrix is obtained either from the matrix-differential equation or from the 4-dimensional vector differential equation in the Euler-Rodrigues parameters, namely,

$$[\dot{\mathbf{D}}]_{\mathcal{I}} = [\Omega]_{\mathcal{I}}[\mathbf{D}]_{\mathcal{I}} \quad \text{or} \quad [\dot{\eta}]_{\mathcal{I}} = [\Sigma]_{\mathcal{I}}[\omega]_{\mathcal{I}} \tag{B.21}$$

Equation (B.21) is nothing but eqs.(6.9) and eq.(6.12) in the $\mathcal{I}$-frame.